DNA Conjugation and DNA Directed Self-Assembly of Quantum Dots for Nanophotonic Applications

by

Anirban Samanta

A Dissertation Presented in Partial Fulfillment
of the Requirements for the Degree
Doctor of Philosophy

Approved April 2014 by the
Graduate Supervisory Committee:

Hao Yan, Co-Chair
Yan Liu, Co-Chair
Daniel Buttry
Ian Gould

ARIZONA STATE UNIVERSITY

May 2014

ABSTRACT

Colloidal quantum dots (QDs) or semiconductor nanocrystals are often used to describe 2–20 nm solution processed nanoparticles of various semiconductor materials that display quantum confinement effects. Compared to traditional fluorescent organic dyes, QDs provide many advantages. For biological applications it is necessary to develop reliable methods to functionalize QDs with hydrophilic biomolecules so that they may maintain their stability and functionality in physiological conditions. DNA, a molecule that encodes genetic information, is arguably the smartest molecule that nature has ever produced and one of the most explored bio-macromolecules. QDs that are functionalized with DNA can potentially be organized with nanometer precision by DNA directed self-assembly, and the resulting arrangements may facilitate the display of novel optical properties. The goal of this dissertation was to achieve a robust reliable yet simple strategy to link DNA to QDs so that they can be used for DNA directed self assembly by which we can engineer their optical properties.

Presented here is a series of studies to achieve this goal. First we demonstrate the aqueous synthesis of colloidal nanocrystal heterostructures consisting of the CdTe core encapsulated by CdS/ZnS or CdSe/ZnS shells using glutathione (GSH), a tripeptide, as the capping ligand. We next employed this shell synthesis strategy to conjugate PS-PO chimeric DNA to QDs at the time of shell synthesis. We synthesized a library of DNA linked QDs emitting from UV to near IR that are very stable in high salt concentrations. These DNA functionalized QDs were further site-specifically organized on DNA origami in desired patterns directed by DNA self-assembly. We further extended our capability to functionalize DNA to real IR emitting $Cd_xPb_{1-x}Te$ alloyed QDs, and demonstrated their

stability by self-assembling them on DNA origami. The photo-physical properties of the QDs were further engineered by attaching a QD and a gold nanoparticle in controlled distances on the same DNA origami, which revealed a much longer range quenching effect than usual Förster Resonance Energy Transfer. We are currently engaged in enhancing the photoluminescence intensity of the QDs by bringing them in the plasmonic hot spots generated by a cluster of larger plasmonic nanoparticles.

ACKNOWLEDGMENTS

Firstly I want express my sincere gratitude to The Almighty God for leading and guiding me through the journey of life to fulfill my dream and complete my research successfully. I would like to take this opportunity to express my sincere thank to my advisor Prof. Hao Yan and Prof. Yan Liu for helping me to expand the frontiers of my knowledge. Past five years have been an extraordinary educational journey with both of you. You have given me a firm grounding in the process of scientific research from the very first day in this lab. You uninterruptedly provided nourishments for fresh ideas and encouraged my independent thinking, which will always help me in my future career. Dedication and hard work, how important they are, I have learned from you. Thank you again.

My mother, thank you for everything. I know it has been extremely tough for you to live alone years after years in a lonely house. You are the best mom in this world. I can't express my love in words here. I thank my sisters for standing beside our mother always. I would also like to thank my friends here in United States and in India for their continuous love and support. It was not easy to relocate in a country half globe away from my little home. Without those non-scientific supports my scientific journey would not have been possible. I am indebted to my flat mate Mr. Palash Dutta for the past five years for being with me. I'll miss the delicious food you cooked. My other friends, Debkumar, Raju, Suva, Amit, Anjan; thank you for those countless laugh, arguments, love and support over the phone and skype.

Finally I want to thank all the past and present graduate and undergraduate students, post docs, research professionals, and technicians in the Yan lab. My special thanks go to Dr. Zhengtao Deng for unraveling the beautiful world of quantum dots to me. I would also

like to thank my committee member Prof. Daniel Buttry and Prof. Ian Gould for their advices and guidance.

TABLE OF CONTENTS

Page

CHAPTER Page

CHAPTER Page

LIST OF TABLES

Table Page

LIST OF FIGURES

Figure Page

Figure Page

Figure Page

CHAPTER 1

QUANTUM DOTS (QDS) AND THEIR DNA DIRECTED SELF ASSEMBLY

1.1.Introduction to Quantum Dots and their synthesis

Colloidal quantum dots (QDs) or semiconductor nanocrystals are often used to describe 2-20 nm solution processed nanoparticles of various semiconductor materials that display quantum confinement effect. The tiny size is responsible for the three dimensional quantum confinements, which give rise to the unique electronic band structure that allows only specific energy states to be occupied by electrons. Electron can be excited to the conduction band from the valence band by supplying the amount of energy in the form of light that surpass the band gap. Recombination of the excited electron with the 'left behind' hole triggers the emission of photon that we call fluorescence. The wavelength of this emitted light is dependent on the size of the particles, which is considered as striking feature of QDs than other available fluorphores.

Notably, the past two decades have witnessed the emergence and development of QDs as novel fluorophores. Compared to the traditional fluorescent organic dyes, QDs provide many advantages such as, high quantum yield, high molar extinction coefficients, broad absorption with narrow symmetric photoluminescence (PL) spectra spanning the UV to near-infrared (NIR), high multi-photon cross sections, and high resistance to photo-bleaching and chemical degradation.

Tracing back to 1993, Murray et al. first developed a synthetic route to make nearly mono-dispersed CdSe QDs by injecting organometallic reagents into a hot organic solvent that acted as the surface encapsulating molecule[1]. This method had been followed

as a general route to make QDs. The QDs are capped with hydrophobic organic molecules as surface ligands, which render them not soluble in water.

For biological applications it is necessary to develop reliable methods to functionalize QDs with hydrophilic biomolecules, so that they may maintain their stability and functionality in physiological conditions. The requirements is not limited to making them water soluble, retaining the monodispersity and strong fluorescence, but also linking them to biomolecules that bear biological information and stabilizing them at high salt concentrations and resistant to other oxidizing and reducing environment.

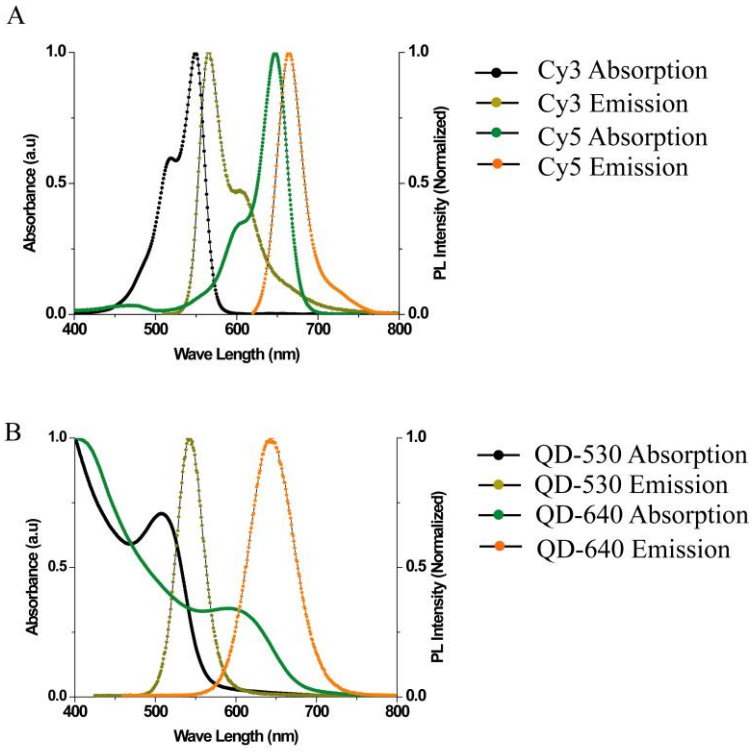

***Figure 1.1*:** Comparison of the absorption and emission of organic dyes and quantum dots. The uppermost figure (A) shows the narrow absorption and emission of a very well known Cy3-Cy5 FRET pair. The figure bellow (B) depicts the typical broad absorption

but narrow symmetric emission of QD-530 (means the emission maxima comes at 530nm) and QD 640. Both of the QD would be able to emit if excited somewhere bellow 500nm

A. Hydrophilic Quantum Dots

Today, quantum dots find their applications both in material and in biological science. The early works came up with the employment of quantum dots in microelectronics and optoelectronics, making LED[2, 3], solar cell[4] etc. But a vast area was waiting to be explored in biological systems, which finally turned out to be one of the major applications of these nanoparticles in bioimaging, biolabeling and tracking. But hydrophobic quantum dots were absolutely inapplicable for that purpose.

Investigation began from many directions to get QDs compatible with the biological system Still an active area of research, the approach to synthesize water soluble QDs came primarily from three directions: (a) Replacement of the hydrophobic ligand with water friendly ones by means of ligand exchange; (b) Creating a shell of hydrophilic materials over the core particle; (c) Synthesizing them directly in water.

Still heavily used, ligand exchange has been a very popular method for making water soluble QDs by replacing organic ligands such as trioctylphosphine oxide (TOPO), Trioctylphosphine (TOP), oleic acid, dodecyl amine, etc., with hydrophilic bifunctional ligands[5]. The latter ones have a common characteristic of having a thiol group at one end and a hydrophilic group, for example, acid or hydroxyl at the other end. From small molecules like mercaptopropionic acid (MPA)[6-8], cysteine[9], dihydrolipoic acid[10] to complex large molecules, for example, oligomeric phosphine[11], dendrons[12], peptides[13] have been used as the replacing ligands. However, ligand exchange does not have a jovial

relationship with the photoluminescence efficiency of the particles. Due to strong polar nature of water, the existing equilibriums in the hydrophobic medium get disturbed that generate severe surface defects on the QDs, which is detrimental to the efficacy of photoluminescence of the particles. In spite of the narrow size distribution and nearly perfect crystal structure of QDs synthesized in organic media at high temperature, the ligand exchange process to produce water soluble QDs seems inadequate.

To generate hydrophilic shell around the hydrophobic particle, amphiphilic polymer[14], or phospholipid that can form micelle like structures[15] or even inorganic shell[16] have been used. Hydrophilization with the micelle technology was claimed to be better than the ligand exchange process in terms of retention of photoluminescence. It does not interrupt the binding of primary ligand on the surface of the QDs. Building a shell of silicates around QD is also a popular approach. There are couple of advantages that silicates have over other materials, such as, its chemical inertness, non-toxicity, robustness, protracted stability and wide range of available modifications (which is also a very powerful tool to chemically conjugate biomolecules to them)[17]. But an inorganic or polymer shell markedly increases the size of the QDs, which restricts their application for some specific purpose where fine control over the distance necessitates, for example Fluorescence Resonance Energy Transfer (FRET).

Growing good quality QDs directly in water is still an active area of research. Mercaptopropionic acid, 2 mercaptoethanol, 1-thioglycerol, L-cysteine, glutathione, thioglycolic acid are often used to make CdTe[18-20], CdS[21], ZnS[22], HgTe[23] etc. in water. In this way QDs can be synthesized at moderate temperatures (100°C to 120°C) as well as in microwave or in autoclave by hydrothermal method. Broad size distribution and low

photoluminescence quantum yield (PLQY) are some of the major problems in these processes; however, constructing additional shell of semiconductor material with hydrophilic capping ligand has been developed recently to circumvent these drawbacks[24,25].

B. Bioconjugation

Making quantum dot water-soluble is unarguably the major leap towards their use in biological and biomedical field. Metallic[26] and magnetic particles[27] are the predecessor in this vast arena but with limited scope. But Quantum Dot has fluorescence, which is an immensely powerful tool that opens up the door of microscopic world to be seen easily. Organic Dye molecules are doing this job for years but with several tight restrictions[28]. Here QDs came up as a potential contender to throw off the bowline. The most astounding property of QDs makes them special from the crowd is their broad absorption and narrow nearly Gaussian emission and that is also tunable with their size. They can be excited anywhere lower than their emission peak without any change in the peak position. This is brilliant because this allows us to use them as a multiplexing agent, exciting at a single wavelength yet getting all kind of colors, which was inconceivable with organic dyes. Starting from the very fast paper from Warren et al[6], with no wonder, myriad of reports can be found in literature conjugating QDs with various kinds of biomolecules and use them for real purpose. From small biomolecule like biotin, serotonin or small peptides to sophisticated proteins, nucleic acid has been conjugated to QDs effectively. There are some nice reviews published covering this topic of bioconjugation and biolabeling of QDs[29-31]. However, we will focus on a special area, DNA conjugation of QDs, strategies, development, current status and future aspects of this new biomaterial.

C. DNA conjugation to Quantum Dots and the existing methods

The carrier of our genetic information, DNA, is one of the smartest molecules that nature has ever produced and one of the most precisely explored biomacromolecule. Since the discovery of its double helical structure, DNA has been the focus of research in bioscience and now in nanotechnology, material science and medicine. Double helical DNA has a diameter of ~2 nm and the repetitive helical unit consisting approximately 10.5 base pairs that is about 3.5 nm in length. Single stranded DNA can recognize another strand with complimentary sequence by the highly predictable Watson-Crick base pairing. The powerful self assembly of DNA have made the simplest double stranded DNA to sophisticated 2D and 3D nano-objects [32]. By functionalizing QDs with DNA, one can bring selectivity and visibility together. Potentially this could pave the way of ordered fabrication of QDs with nanometer precision, which is another unachieved goal of nanotechnology.

How this can be done is the inevitable next question. Chemistry of attaching oligonucleotide on Gold (Au) nanoparticles showed some directions here. After the early paper of Chad Markin and Paul Alivasatos showing that thiol modified DNA can be used to derivatize AuNPs of various sizes[33, 34], now it is a common practice as we see in the literature

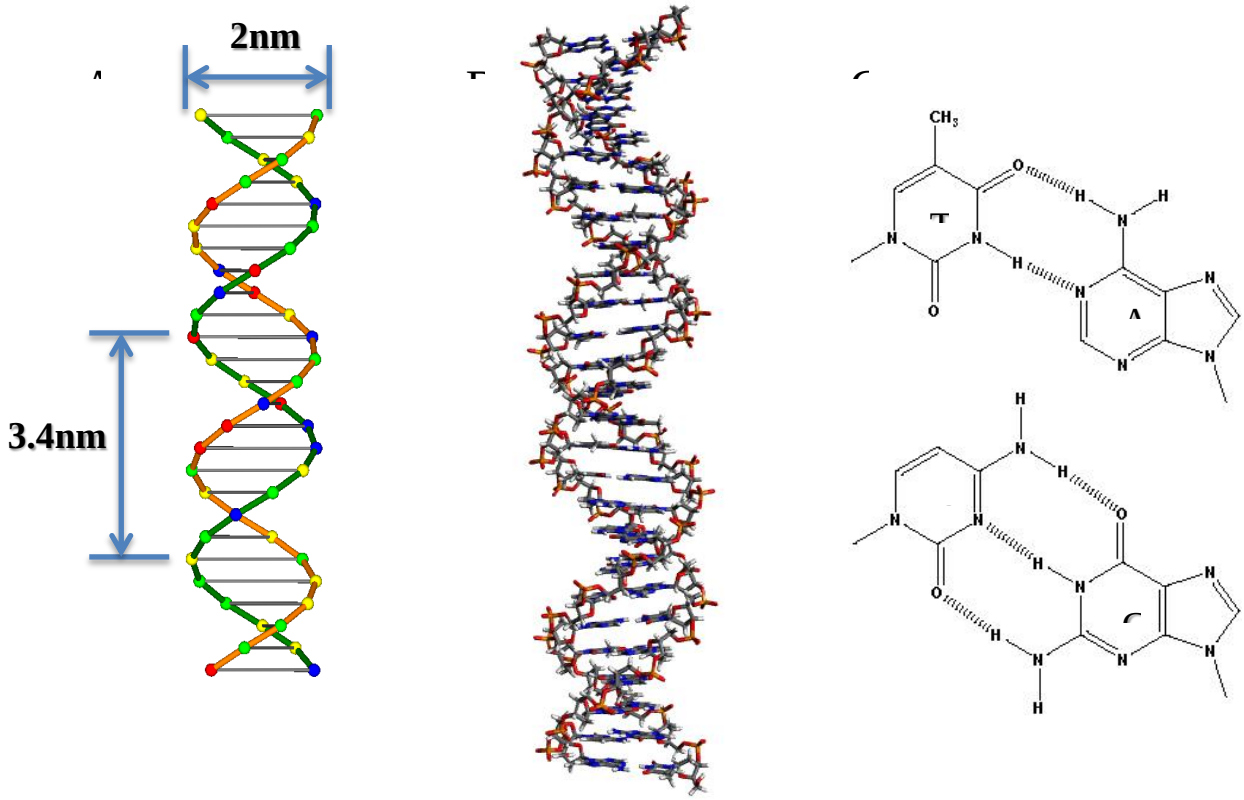

Figure 1.2: (A) Double stranded structure of B DNA with helical turn per 10.5 bases on average which is approximately 3.4nm in length. The width of the double helix is 2nm (B) The same double helix in stick frame displaying the 3D orientation of the sugar-phosphate back bone carrying the nucleobases that are lying horizontally between two spiral strands. (C) The detail hydrogen bonding of Watson-Crick base pairs (top) Thymine and Adenine (bottom) Cytosine and Guanine

Two dimensional to three dimensional self assembled structures of AuNPs have been constructed using that technique[35]. However, the case of QDs is slightly different. QDs are made of semiconductor materials containing metal elements such as Cd or Zn. The binding energy of Cd-S or Zn-S is much weaker than that of Au-S bond. (ΔH_{Au-S} = 418

kJ/mol, $\Delta H_{Cd\text{-}S}$ = 208 kJ/mol, $\Delta H_{Zn\text{-}S}$ = 205 kJ/mol). Due to this intrinsic difficulty, several attempts in the last decade from various directions have been made, but with limited success. Although there are reports on DNA templated growth of semiconductor nanoparticles[36-38], the approaches to functionalize QDs with DNA of specific sequence can be classified into three categories: 1) Attachment of thiol modified DNA or poly-Histidine modified DNA to the surface of the QDs in a ligand exchange step; 2) Covalent conjugation of DNA to preexisting capping ligands on the QD surface; 3) Incorporation of DNA ligands during QDs synthesis.

i. Surface ligand exchange using modified DNA with an affinity to the QD surface

(A) Thiolated DNA

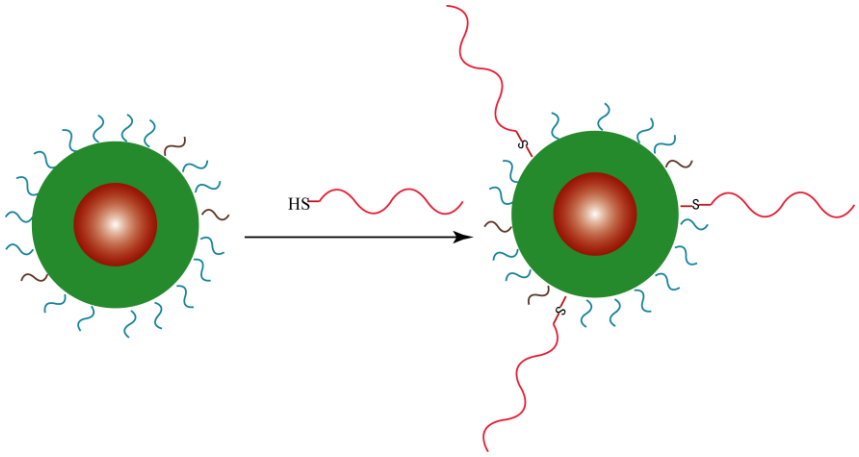

Figure 1.3: Attachment of thiolated DNA to core/shell QDs (represented by the red ball surrounded by a green shell) that have been rendered water-soluble by capping with MPA (represented by short blue curves). A ligand exchange results in the partial replacement of MPA with thiolated DNA (long red curves) on the QD surface.[39]

(B) Polyhistidine DNA

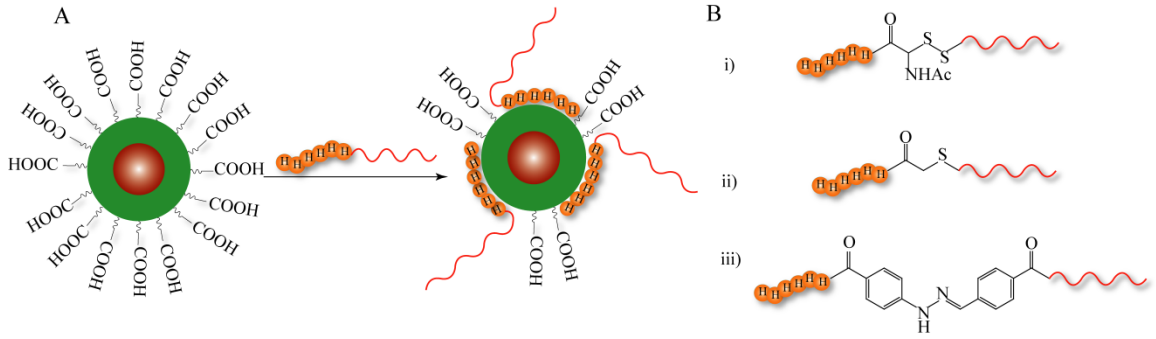

Figure 1.4: **A**. Schematic depicting the attachment of DNA carrying a small peptide containing 6 histidine residues to the surface of water soluble CdSe/ZnS QDs capped with MPA or DHLA. **B.** Examples of functional linkers between the peptide and DNA. i) coupling through difulfide bond via reaction between cysteine and thiol group on DNA, ii) coupling through reaction between iodoacetyl group on peptide and thiol group on DNA, iii) coupling through hydrazone linkage.[29, 40]

ii. Covalent coupling of DNA to QD surface ligands

(A) EDC coupling

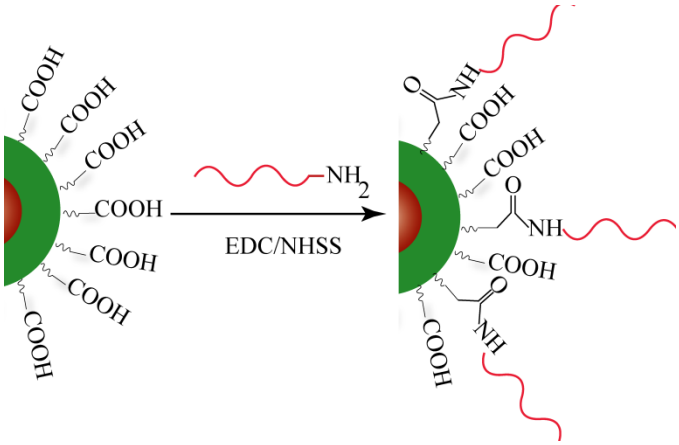

Figure 1.5: Chemical conjugation of QDs to DNA via EDC coupling. The carboxyl group of the capping ligands pre-existing on the QD surface is first activated by EDC/NHSS and subsequently reacted with primary amine modified DNA. This process results in amide linkages between the capping ligand and the DNA.[41-44]

(B) Miscellaneous covalent conjugation method

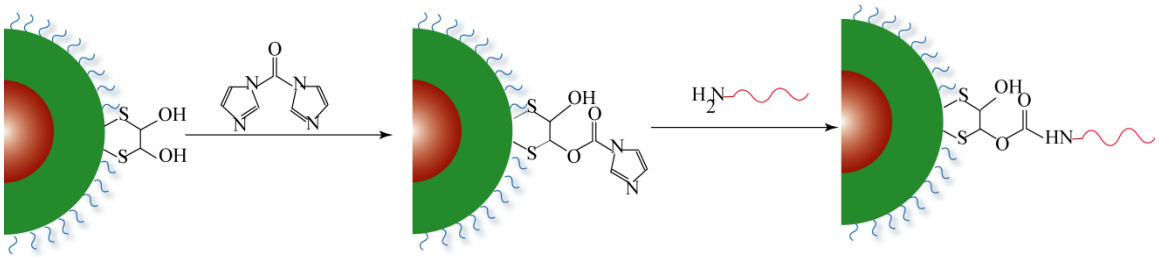

Figure 1.6: Schematic depicting dithiothreitol functionalized QDs activated by CDI to create imidazole carbamate groups at the surface. The second step reaction with amine modified DNA removes the amidazole group.[45]

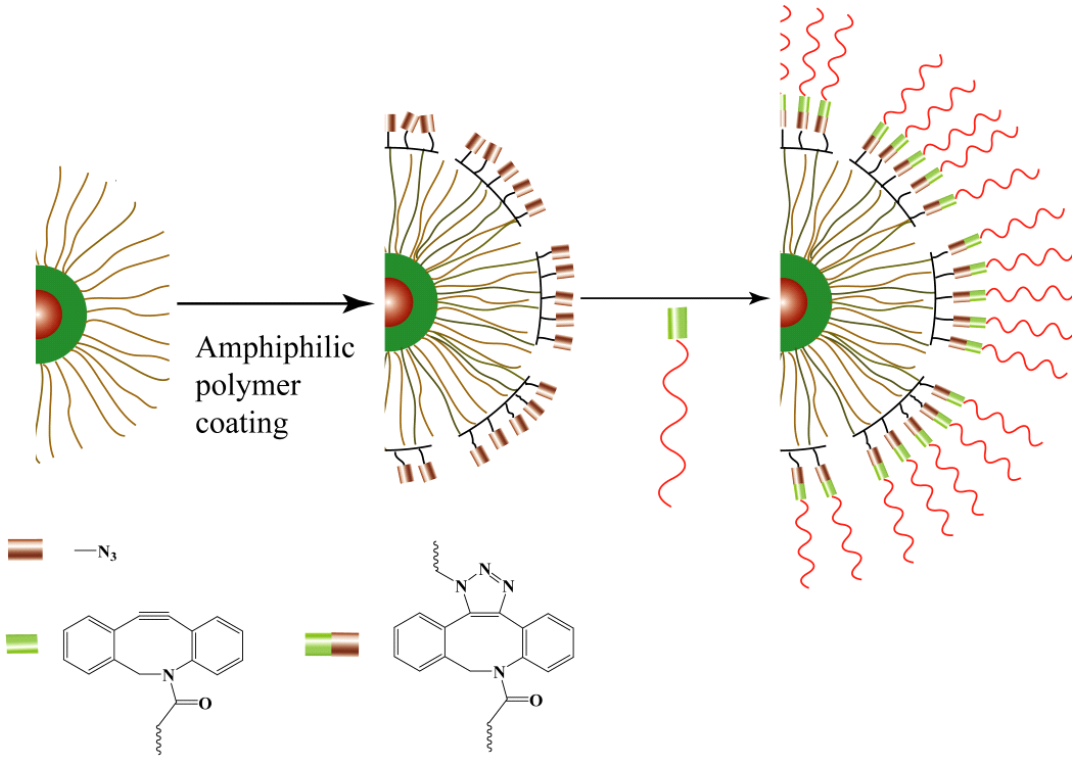

Figure 1.7: In the first step CdSe/ZnS QDs with oleylamine capping ligand is encapsulated with amphiphilic polymer. The long alkyl chains on the polymer are inserted into the pre-existing layer of the hydrophobic ligand. The hydrophilic azide groups protrude out making the QDs water soluble. In the second step the strained octyne ring modified DNA is linked with the amphiphilic polymer layer by azide-alkyne click chemistry.[46]

(C) SMCC coupling

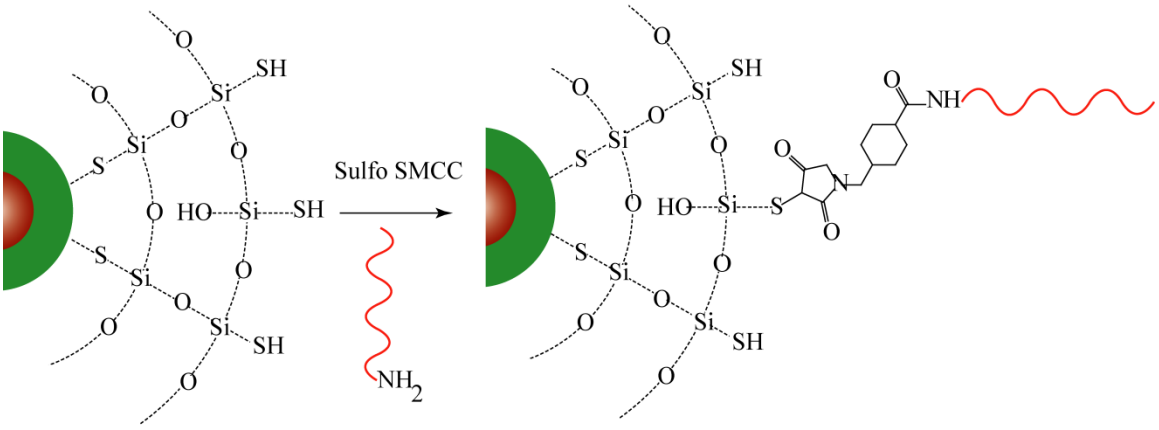

Figure 1.8: Schematic depicting thiol functionalized silica coated CdSe/ZnS QDs that are conjugated to amine modified DNA by means of the hetero bifunctional cross linker sulfo-SMCC.[47]

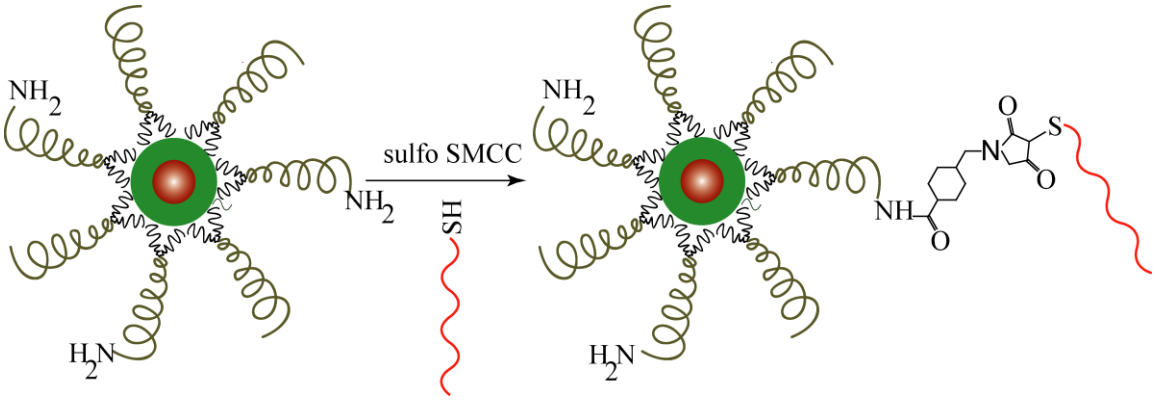

Figure 1.9*:* Phospholipid block-copolymer micelle encapsulated CdSe/ZnS QDs are linked to DNA by the hetero-bifunctional cross linker sulfo-SMCC. Amino-PEG-PE molecules were introduced to display amine functionality on the outer surface of the micelle. Sulfo-SMCC facilitates the linkage between the amine modified QDs and thiol modified ssDNA.[15]

iii. DNA conjugation during QD synthesis

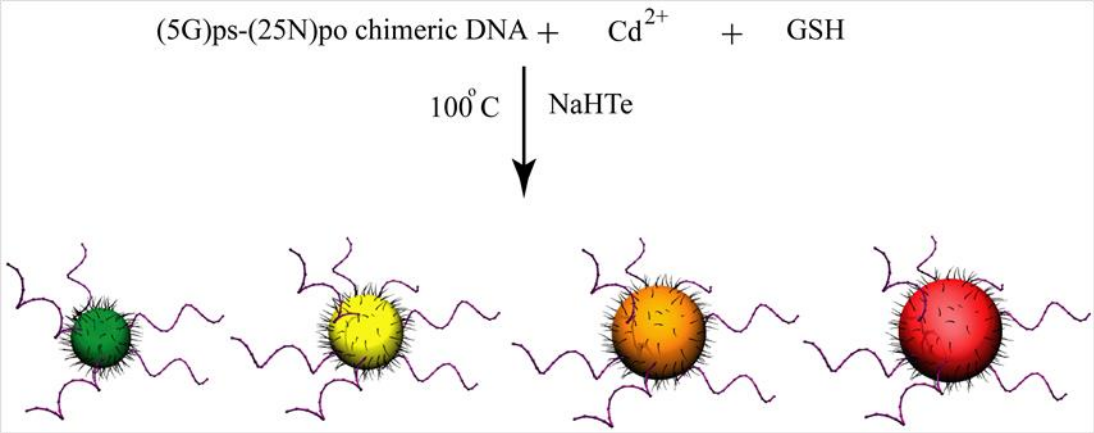

Figure 1.10: Schematic illustrating one-pot synthesis of DNA conjugated CdTe QDs. Mixing all the necessary components with phosphorothiolated DNA at 100°C in water results in the formation of the desired DNA-QD conjugates. Varying the time of the reaction allows researchers to control the color of the resulting particle; longer times produce larger QDs with red shifted emissions.[48]

1.2.DNA nanotechnology

A. DNA directed assembly of assembly of Nanomaterials

DNA has two standard base pairs; Adenine (A) binds with Thymine (T) and Guanine (G) binds with Cytosine(C). In the presence of salt, single stranded DNA can recognize another strand with complimentary sequence by Watson-Crick base pairing which is highly predictable. This is the simplest form of DNA based spontaneous self assembly.

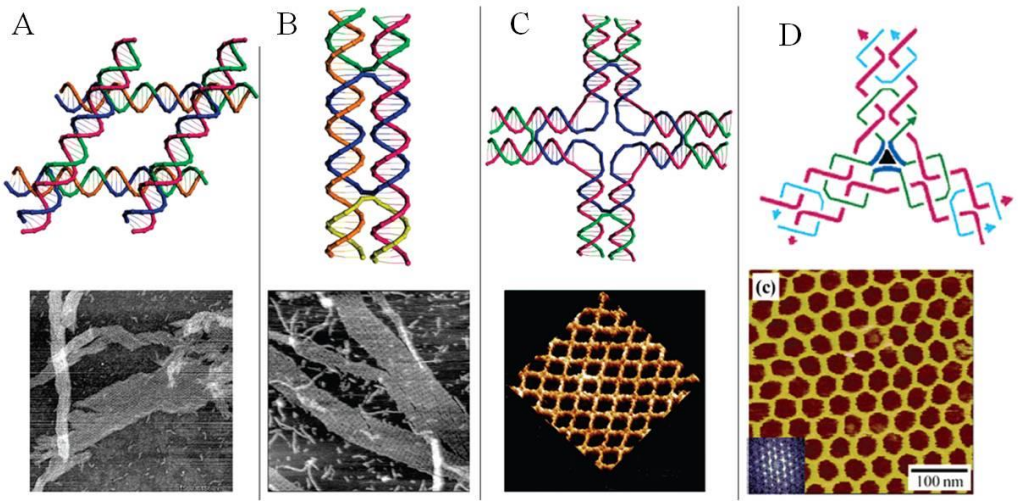

Figure 1.11: Computer generated models of some representative DNA tiles. (A) Parallelogram DNA tile constructed by four Holliday junctions. (B) Double crossover (DX) tile. (C) 4 way junction motif. (D) Three point star motif. AFM image bellow of each model represents the self-assembled 2D structure. [49, 50]

More sophisticated structure can also be found in nature. Holiday junction is one example. It is a four arm junction, first discovered in fungi at the time of gene recombination. This branched DNA motif was the inspiration of Prof. Nadrian Seeman, which led to the proposal in 1982 that this kind of motifs can be artificially designed and be combined together if the sticky ends of the arms have complimentary sequences to one another. Later this was experimentally proved by forming a 2D array of four arm junction motifs bearing sticky ends with designated base pairing. Seeman's dream was to extend this infinitely grown 2D array to 3rd dimension, which can lead to 3D crystals that can serve as templates to crystallize proteins. Although protein crystallization has not been achieved yet following this method, DNA tiles have been crystallized successfully.[51]

Past decade has witnessed an aggressive growth of the periodic 2D array of DNA tiles with various geometries and topologies.[49] The scenario is so rich, it can safely be concluded that any kind of imaginable 2D pattern is possible to make today. In the past few years 3D motif with precise geometry has also emerged radically.[52] A series of DNA tetrahedra, octahedra, other polyhedra, and bucky balls have been synthesized with high yield. The newest addition to this field is DNA origami. It was first introduce by Paul Rothemund in 2006.[53] It is a special technique of creating discrete DNA nanostructure by folding a long single stranded scaffold strand by numerous short 'staple' strands into closed packed anti-parallel helices. He demonstrated the power of this technique by forming arbitrary geometry, from simple triangle or rectangle to smiley faces or the map of the American continent. The great addressability of this was evident since it acted like a molecular peg-board with pixel size of 6 nm. For organizing DNA conjugated nanomaterials or biomolecules this proved to be excellent in controlling distance between them. With no surprise, it was readily picked up by scientific community and now the pioneered paper has nearly 2000 citations till today. Shih's group and Yan's group recently took it to another dimension by creating 3D nanostructures and curved shapes.[54] It is evident that DNA nanotechnology has contributed significantly in the world of nanoscience and a lot more to come.

It has been repeatedly proved that self assembled DNA nanoarchitectures are excellent scaffold for organizing nanomaterial and biomolecules. One of the major advantages that it offers is the ability to control the distance between multiple components. This is very useful for fundamental studies related to distance dependency

of some properties of certain nanoparticles. This is also applicable in the area of biosensing or drug delivery.

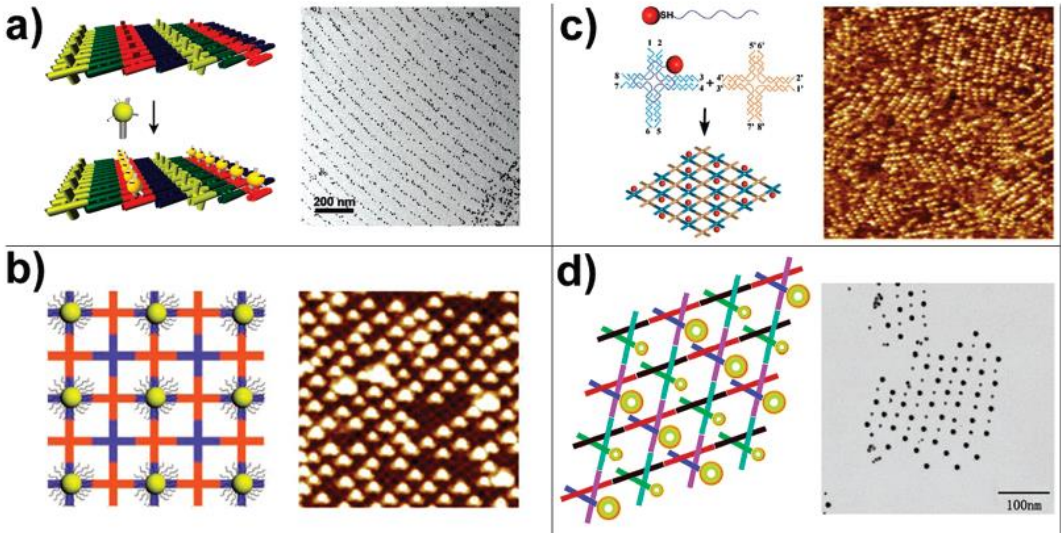

Figure 1.12: DNA directed periodic assembly of plasmonic nanoparticles. (a) Organization of 5nm gold nanoparticles on DNA DX polymeric array. (b) Periodic 5nm AuNP arrays with controlled interparticle distance. (c) Single DNA modified 5nm AuNPs are self assembled into periodic array in one step. (d) Single DNA modified 5 and 10nm AuNPs are self assembled into 2D periodic array. [49]

Functionalization of the DNA nanostructures has been done in two ways mainly. One is chemical conjugation where pre-engineered specific functional group displaying from the surface of the nanostructure covalently gets attached to biomolecules. Other one is the extension of a participating DNA strand with a sequence that is complimentary to the DNA displaying on the specific target. Using both of this two methods inorganic nanomaertials (metallic[55-59] and semiconducting nanoparticles[59]) and biomolecules (proteins, antibodies, aptamers)[60-62] has been successfully patterned on DNA platform.

Figure 1.12 depicts some of these assemblies in a periodic fashion on DNA tile based array. However, the boundary of such 2D arrays is not well defined.

To attach discrete number of nanoparticles at specific locations with nanometer precision, DNA origami technology is more reliable. A variety of nanoelements have been organized on DNA origami of different shapes, which includes gold nanoparticles[63], silver nanoparticles[64], quantum dots[65], carbon nanotubes[66], virus capsids[67], and various proteins[68]. By controlling the distance between two interacting nanoobjects, their properties can be tuned with highly controlled fashion. Because of the biocompatibility and finite dimension and great addressability it holds great promise in the future biological applications of nanoscience.

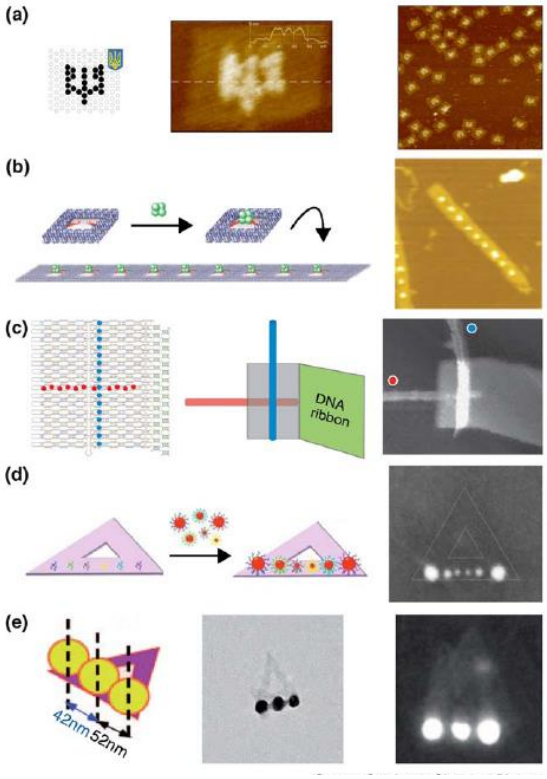

***Figure 1.13*:** Organization of nanomaterials on DNA origami. (a) Streptavidin proteins are organized in a specific pattern on rectangular DNA origami. Corresponding zoom in

and zoom out images is shown at the right. (b) Streptavidin protein is being captured by a tape like origami (c) DNA functionalized single walled carbon nanotube is organized in a cross hair fashion on rectangular origami (d) DNA conjugated gold nanoparticle is organized on a triangle shape DNA origami like self similar chain. (e) Three DNA capped Silver nanoparticles are organized in a line on a triangular DNA origami.

B. DNA directed higher order organization of QDs

Spatially arrange metallic nanoparticles into well-defined geometric configurations with nanometer precision will facilitate the emergence of novel optoelectronic properties. DNA conjugated AuNPs have been directed by DNA nanostructures into more complicated 3D DNA structures[69, 70] and well-defined crystalline lattices.[71, 72] However, there are only a few reports of the self-assembly of DNA functionalized QDs. Streptavidin coated QDs were reportedly organized on DNA scaffolds in periodic patterns.[59] Bui et al. reported the assembly of streptavidin coated CdSe/ZnS QDs on discrete, DNA origami tubes.[65] Discrete self-assembly of QDs and AuNPs has been described before, but at that time it was only used to confirm that the DNA linkage on the QDs was present.[73, 74] Fu et al. reported the preparation of DNA conjugated QDs with controllable valency, which they verified by TEM images that showed 1, 2, 3 or 4 AuNPs surrounding a central QD.[73] When DNA conjugated QDs were hybridized to AuNPs carrying the complimentary DNA sequence, quenching of QD fluorescence was observed. This was reported as a 'new approach for biosensing" by Dyadyusha et al.[41] Besides AuNP-QD heteromers, DNA conjugated CdTe QDs with controllable discrete valencies have been self-assembled into molecule like structures.[48] The controlled distance, geometry and stoichiometry between the QDs will enable precise studies of

energy transfer behaviors between different colored QDs, e.g. energy can be transferred unidirectionally from green to yellow to red QDs. This series of energy transfers were made possible because of the programmability of DNA molecules. One of the most fascinating aspects of DNA directed self-assembly of QDs is that various color QDs can be organized on the same platform by assigning unique sequences to the DNA displayed from the different QDs, and to the complementary capture probes projecting from the DNA scaffold. It can be envisioned that different combinations of QDs with unique emission wavelengths can be used to produce color barcodes that can potentially be used for multiplex imaging of cellular components. Beyond imaging, the convergence of plasmonic materials and semiconductor nanoparticles on DNA scaffolds may reveal new and interesting properties including plasmonic quenching or enhancement of fluorescence. It may also be possible to engineer the lifetime of the fluorescent particles or even a non-linear optical response.

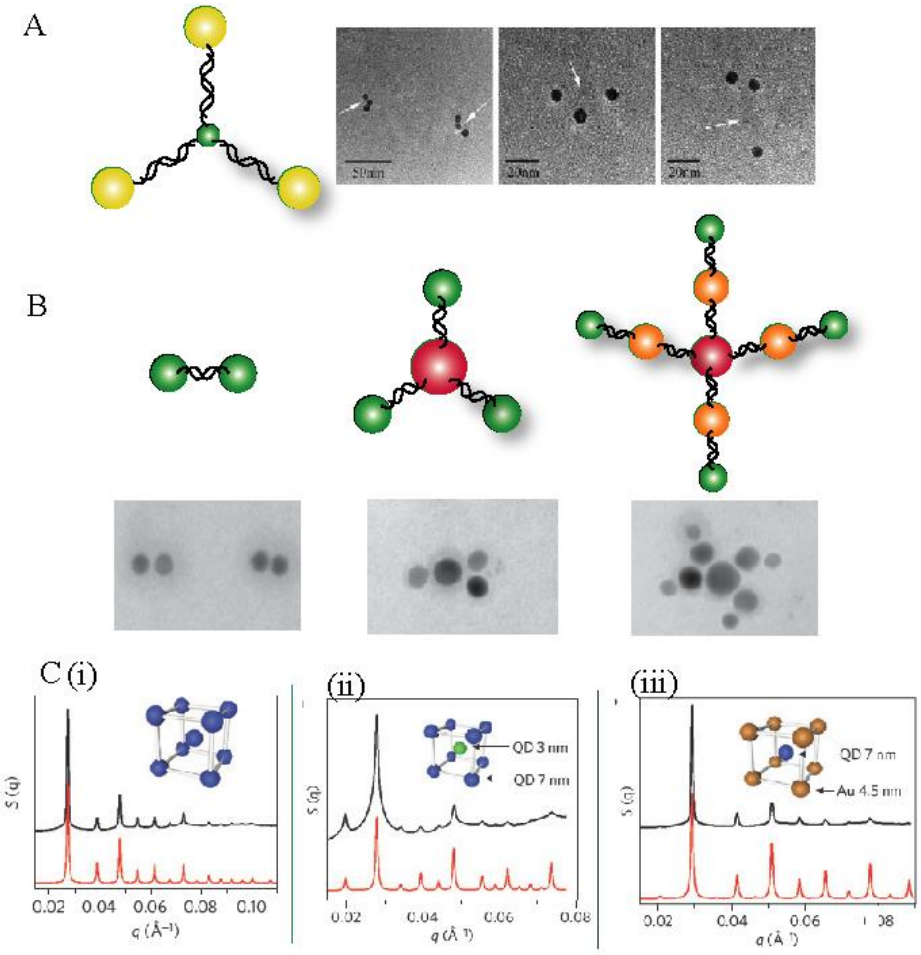

Figure 1.14 : DNA-directed self-assembly of QDs with other nanomaterials. (a) Self-assembly of discrete AuNP–QD constructs with three AuNPs around one QD (b) Controlled self-assembly of QD–QD dimers, red and green QD heteromers and more complex heteromers. Control over the valency of linkages allows the formation of molecule-like nano-constructs. (c) DNA-directed assembly of nanoparticles into body centered cubic lattice arrangements: (1) QDs, (2) 3 nm and 7 nm QDs and (3) 7 nm QD and 4.5 nm AuNPs.

1.3.Overview of the projects in the thesis:

A. Aqueous Synthesis of Glutathione-Capped CdTe/CdS/ZnS and CdTe/CdSe/ZnS Core/Shell/Shell Nanocrystal Heterostructures

Here we demonstrate the aqueous synthesis of colloidal nanocrystal heterostructures consisting of a CdTe core encapsulated by two CdS/ZnS or CdSe/ZnS shells, using glutathione (GSH), a tri-peptide, as the capping ligand. By tuning the diameter of the core and the thickness of each shell, a broad range of high QY (up to 45%) nanocrystal heterostructures with emissions ranging from visible to NIR wavelengths (500-730 nm) were obtained.

B. Robust DNA functionalized quantum dots compatible with DNA directed self-assembly

In this project we have developed a method that facilitates the synthesis of stable core/shell (1 to 20 monolayers) QD-DNA conjugates by 'embedding' the end part (5-10 nucleotides) of the phosphorothiolated oligonucleotides within the outer shell of the QDs. These reliable QD-DNA conjugates exhibit excellent chemical and photonic stability, colloidal stability over a wide pH range (4-12) and high salt (>100 mM Na^{+} or Mg^{2+}) conditions, bright fluorescence emission with quantum yield up to 70%, and broad spectra tunability with emission ranging from ultraviolet to near infrared.

C. IR Emitting QDs: DNA Conjugation and DNA origami directed self assembly

We have produced $Cd_xPb_{1-x}Te$ alloyed QDs capped with hydrophilic ligands and DNA that emit above 1000nm which can be very useful to circumvent the limitation

imposed by visible light emitting QDs. Interestingly we have found a ligand dependent emission in our synthesized QDs. In the presence of Mercaptopropionic acid (MPA) as the primary capping ligand, the DNA conjugated particle shows emission maxima at ~1300 nm while in case of Glutathione (GSH) it is ~1200nm. The DNA directed assembly of the particles onto DNA nano structures further ensures that the particle can withstand in high salt concentration which is crucial as far as biological application is concerned.

D. Controlled engineering of the photophysical properties of QDs by plasmonic nano particle.

Using DNA origami we have successfully constructed hybrid nano structure containing a QD and a gold nano particle where we have altered the distance between them with nano meter precision. We have noticed fluorescence quenching of a QD with emission maxima at 645nm by the 30nm gold nano particle over a distance as far as 50nm. We have constructed a moleculer ruler where fluorescence intensity or the life time has been engineered which can be seen as a new generation moleculer ruler beyond standard FRET.

1.4.References

1. Murray, C. B.; Norris, D. J.; Bawendi, M. G., Synthesis and characterization of nearly monodisperse CdE (E = S, Se, Te) semiconductor nanocrystallites. *J. Am. Chem. Soc.* **1993**, 115, 8706-8715.

2. Colvin, V. L.; Schlamp, M. C.; Alivisatos, A. P., Light-emitting-diodes made from cadmium selenide nanocrystals and a semiconducting polymer. *Nature* **1994**, 370, 354-357.

3. Schlamp, M. C.; Peng, X. G.; Alivisatos, A. P., Improved efficiencies in light emitting diodes made with CdSe(CdS) core/shell type nanocrystals and a semiconducting polymer. *J. Appl. Phys.***1997**, 82, 5837-5842.

4. Schaller, R. D.; Klimov, V. I., High efficiency carrier multiplication in PbSe nanocrystals: Implications for solar energy conversion. *Phys. Rev. Lett.* **2004**, 92.

5. Brichkin, S. B.; Chernykh, E. V., Hydrophilic semiconductor quantum dots. *High Energ. Chem.* **2011**, 45, 1-12.

6. Chan, W. C. W.; Nie, S. M., Quantum dot bioconjugates for ultrasensitive nonisotopic detection. *Science* **1998**, 281, 2016-2018.

7. Pradhan, N.; Battaglia, D. M.; Liu, Y.; Peng, X., Efficient, stable, small, and water-soluble doped ZnSe nanocrystal emitters as non-cadmium biomedical labels. *Nano Lett.* **2007**, 7, 312-317.

8. Wuister, S. F.; Swart, I.; van Driel, F.; Hickey, S. G.; Donega, C. D., Highly luminescent water-soluble CdTe quantum dots. *Nano Lett.s* **2003**, 3, 503-507.

9. Liu, W.; Choi, H. S.; Zimmer, J. P.; Tanaka, E.; Frangioni, J. V.; Bawendi, M., Compact cysteine-coated CdSe(ZnCdS) quantum dots for in vivo applications. *J. Am. Chem. Soc.* **2007**, 129, 14530-14531.

10. Algar, W. R.; Krull, U. J., Multidentate surface ligand exchange for the immobilization of CdSe/ZnS quantum dots and surface quantum dot-oligonucleotide conjugates. *Langmuir* **2008**, 24, 5514-5520.

11. Kim, S.; Bawendi, M. G., Oligomeric Ligands for luminescent and stable nanocrystal quantum dots. *J. Am. Chem. Soc.* **2003**, 125, 14652-14653.

12. Wang, Y. A.; Li, J. J.; Chen, H. Y.; Peng, X. G., Stabilization of inorganic nanocrystals by organic dendrons. *J. Am. Chem. Soc.* **2002**, 124, 2293-2298.

13. Pinaud, F.; King, D.; Moore, H. P.; Weiss, S., Bioactivation and cell targeting of semiconductor CdSe/ZnS nanocrystals with phytochelatin-related peptides. *J. Am. Chem. Soc.* **2004**, 126, 6115-6123.

14. Wu, X. Y.; Liu, H. J.; Liu, J. Q.; Haley, K. N.; Treadway, J. A.; Larson, J. P.; Ge, N. F.; Peale, F.; Bruchez, M. P., Immunofluorescent labeling of cancer marker Her2 and other cellular targets with semiconductor quantum dots. *Nat. Biotechnol.* **2003**, 21, 41-46.

15. Dubertret, B.; Skourides, P.; Norris, D. J.; Noireaux, V.; Brivanlou, A. H.; Libchaber, A., In vivo imaging of quantum dots encapsulated in phospholipid micelles. *Science* **2002**, 298, 1759-1762.

16. Gerion, D.; Pinaud, F.; Williams, S. C.; Parak, W. J.; Zanchet, D.; Weiss, S.; Alivisatos, A. P., Synthesis and properties of biocompatible water-soluble silica-coated CdSe/ZnS semiconductor quantum dots. *J. Phys. Chem. B* **2001**, 105, 8861-8871.

17. Selvan, S. T.; Tan, T. T.; Ying, J. Y., Robust, non-cytotoxic, silica-coated CdSe quantum dots with efficient photoluminescence. *Adv. Mater.* **2005**, 17, 1620-1625.

18. Rogach, A. L.; Franzl, T.; Klar, T. A.; Feldmann, J.; Gaponik, N.; Lesnyak, V.; Shavel, A.; Eychmueller, A.; Rakovich, Y. P.; Donegan, J. F., Aqueous synthesis of thiol-capped CdTe nanocrystals: State-of-the-art. *J. Phys. Chem. C* **2007**, 111, 14628-14637.

19. Bao, H. F.; Wang, E. K.; Dong, S. J., One-pot synthesis of CdTe nanocrystals and shape control of luminescent CdTe-cystine nanocomposites. *Small* **2006**, 2, 476-480.

20. Qian, H. F.; Dong, C. Q.; Weng, J. F.; Ren, J. C., Facile one-pot synthesis of luminescent, water-soluble, and biocompatible glutathione-coated CdTe nanocrystals. *Small* **2006**, 2, 747-751.

21. Zhang, Z. H.; Chin, W. S.; Vittal, J. J., Water-soluble CdS quantum dots prepared from a refluxing single precursor in aqueous solution. *J. Phys. Chem. B* **2004**, 108, 18569-18574.

22. Kho, R.; Torres-Martinez, C. L.; Mehra, R. K., A simple colloidal synthesis for gram-quantity production of water-soluble ZnS nanocrystal powders. *J. Colloid. Interface Sci.* **2000**, 227, 561-566.

23. Rogach, A.; Kershaw, S.; Burt, M.; Harrison, M.; Kornowski, A.; Eychmuller, A.; Weller, H., Colloidally prepared HgTe nanocrystals with strong room-temperature infrared luminescence. *Adv. Mater.* **1999**, 11, 552-555.

24. He, Y.; Lu, H.-T.; Sai, L.-M.; Su, Y.-Y.; Hu, M.; Fan, C.-H.; Huang, W.; Wang, L.-H., Microwave synthesis of water-dispersed CdTe/CdS/ZnS core-shell-shell quantum dots with excellent photostability and biocompatibility. *Adv. Mater.* **2008**, 20, 3416-3421.

25. Samanta, A.; Deng, Z.; Liu, Y., Aqueous Synthesis of Glutathione-Capped CdTe/CdS/ZnS and CdTe/CdSe/ZnS Core/Shell/Shell Nanocrystal Heterostructures. *Langmuir* **2012**, 28, 8205-8215.

26. Murphy, C. J.; Gole, A. M.; Stone, J. W.; Sisco, P. N.; Alkilany, A. M.; Goldsmith, E. C.; Baxter, S. C., Gold Nanoparticles in Biology: Beyond Toxicity to Cellular Imaging. *Acc. Chem. Res.* **2008**, 41, 1721-1730.

27. Pankhurst, Q. A.; Connolly, J.; Jones, S. K.; Dobson, J., Applications of magnetic nanoparticles in biomedicine. *J. Phys. D: Appl. Phys.* **2003**, 36, R167-R181.

28. Resch-Genger, U.; Grabolle, M.; Cavaliere-Jaricot, S.; Nitschke, R.; Nann, T., Quantum dots versus organic dyes as fluorescent labels. *Nat. Methods* **2008**, 5, 763-775.

29. Medintz, I. L.; Uyeda, H. T.; Goldman, E. R.; Mattoussi, H., Quantum dot bioconjugates for imaging, labelling and sensing. *Nat. Mater.* **2005**, 4, 435-446.

30. Michalet, X.; Pinaud, F. F.; Bentolila, L. A.; Tsay, J. M.; Doose, S.; Li, J. J.; Sundaresan, G.; Wu, A. M.; Gambhir, S. S.; Weiss, S., Quantum dots for live cells, in vivo imaging, and diagnostics. *Science* **2005**, 307, 538-544.

31. Xing, Y.; Chaudry, Q.; Shen, C.; Kong, K. Y.; Zhau, H. E.; Wchung, L.; Petros, J. A.; O'Regan, R. M.; Yezhelyev, M. V.; Simons, J. W.; Wang, M. D.; Nie, S., Bioconjugated quantum dots for multiplexed and quantitative immunohistochemistry. *Nat. Protoc.* **2007**, 2, 1152-1165.

32. Pinheiro, A. V.; Han, D.; Shih, W. M.; Yan, H., Challenges and opportunities for structural DNA nanotechnology. *Nat.e Nanotechnol.* **2011**, 6, 763-772.

33. Alivisatos, A. P.; Johnsson, K. P.; Peng, X. G.; Wilson, T. E.; Loweth, C. J.; Bruchez, M. P.; Schultz, P. G., Organization of 'nanocrystal molecules' using DNA. *Nature* **1996**, 382, 609-611.

34. Mirkin, C. A.; Letsinger, R. L.; Mucic, R. C.; Storhoff, J. J., A DNA-based method for rationally assembling nanoparticles into macroscopic materials. *Nature* **1996**, 382, 607-609.

35. Tan, S. J.; Campolongo, M. J.; Luo, D.; Cheng, W., Building plasmonic nanostructures with DNA. *Nat. Nanotechnol.* **2011**, 6, 268-276.

36. Torimoto, T.; Yamashita, M.; Kuwabata, S.; Sakata, T.; Mori, H.; Yoneyama, H., Fabrication of CdS nanoparticle chains along DNA double strands. *J. Phys. Chem. B* **1999**, 103, 8799-8803.

37. Levina, L.; Sukhovatkin, W.; Musikhin, S.; Cauchi, S.; Nisman, R.; Bazett-Jones, D. P.; Sargent, E. H., Efficient infrared-emitting PbS quantum dots grown on DNA and stable in aqueous solution and blood plasma. *Adv. Mater.* **2005**, 17, 1854-1857.

38. Coffer, J. L.; Bigham, S. R.; Li, X.; Pinizzotto, R. F.; Rho, Y. G.; Pirtle, R. M.; Pirtle, I. L., Dictation of the shape of mesoscale semiconductor nanoparticle assemblies by plasmid DNA. *Appl. Phys. Lett.* **1996**, 69, 3851-3853.

39. Mitchell, G. P.; Mirkin, C. A.; Letsinger, R. L., Programmed assembly of DNA functionalized quantum dots. *J. Am. Chem. Soc.* **1999**, 121, 8122-8123.

40. Boeneman, K.; Prasuhn, D. E.; Blanco-Canosa, J. B.; Dawson, P. E.; Melinger, J. S.; Ancona, M.; Stewart, M. H.; Susumu, K.; Huston, A.; Medintz, I. L., Self-Assembled Quantum Dot-Sensitized Multivalent DNA Photonic Wires. *J. Am. Chem. Soc.* **2010**, 132, 18177-18190.

41. Dyadyusha, L.; Yin, H.; Jaiswal, S.; Brown, T.; Baumberg, J. J.; Booy, F. P.; Melvin, T., Quenching of CdSe quantum dot emission, a new approach for biosensing. *Chem. Commun.* **2005**, 3201-3203.

42. Algar, W. R.; Krull, U. J., Adsorption and hybridization of oligonucleotides on mercaptoacetic acid-capped CdSe/ZnS quantum dots and quantum dot-oligonucleotide conjugates. *Langmuir* **2006**, 22, 11346-11352.

43. He, S.; Huang, B.-H.; Tan, J.; Luo, Q.-Y.; Lin, Y.; Li, J.; Hu, Y.; Zhang, L.; Yan, S.; Zhang, Q.; Pang, D.-W.; Li, L., One-to-one quantum dot-labeled single long DNA probes. *Biomaterials* **2011**, 32, 5471-5477.

44. Zhou, D.; Ying, L.; Hong, X.; Hall, E. A.; Abell, C.; Klenerman, D., A compact functional quantum dot-DNA conjugate: Preparation, hybridization, and specific label-free DNA detection. *Langmuir* **2008**, 24, 1659-1664.

45. Pathak, S.; Choi, S. K.; Arnheim, N.; Thompson, M. E., Hydroxylated quantum dots as luminescent probes for in situ hybridization. *J. Am. Chem. Soc.* **2001**, 123, 4103-4104.

46. Zhang, C.; Macfarlane, R. J.; Young, K. L.; Choi, C. H. J.; Hao, L.; Auyeung, E.; Liu, G.; Zhou, X.; Mirkin, C. A., A General Approach to DNa-programmable atom equivalents. *Nat.e Mater.* **2013**, 12, 741-746.

47. Parak, W. J.; Gerion, D.; Zanchet, D.; Woerz, A. S.; Pellegrino, T.; Micheel, C.; Williams, S. C.; Seitz, M.; Bruehl, R. E.; Bryant, Z.; Bustamante, C.; Bertozzi, C. R.; Alivisatos, A. P., Conjugation of DNA to silanized colloidal semiconductor nanocrystalline quantum dots. *Chem. .Mater.* **2002**, 14, 2113-2119.

48. Tikhomirov, G.; Hoogland, S.; Lee, P. E.; Fischer, A.; Sargent, E. H.; Kelley, S. O., DNA-based programming of quantum dot valency, self-assembly and luminescence. *Nat.e Nanotechnol.* **2011**, 6, 485-490.

49. Lin, C.; Liu, Y.; Yan, H., Designer DNA Nanoarchitectures. *Biochemistry* **2009**, 48, 1663-1674.

50. He, Y.; Chen, Y.; Liu, H. P.; Ribbe, A. E.; Mao, C. D., Self-assembly of hexagonal DNA two-dimensional (2D) arrays. *J. Am. Chem. Soc.* **2005**, 127, 12202-12203.

51. Zheng, J.; Birktoft, J. J.; Chen, Y.; Wang, T.; Sha, R.; Constantinou, P. E.; Ginell, S. L.; Mao, C.; Seeman, N. C., From molecular to macroscopic via the rational design of a self-assembled 3D DNA crystal. *Nature* **2009**, 461, 74-77.

52. He, Y.; Ye, T.; Su, M.; Zhang, C.; Ribbe, A. E.; Jiang, W.; Mao, C., Hierarchical self-assembly of DNA into symmetric supramolecular polyhedra. *Nature* **2008**, 452, 198-201.

53. Rothemund, P. W. K., Folding DNA to create nanoscale shapes and patterns. *Nature* **2006**, 440, 297-302.

54. Han, D. R.; Pal, S.; Nangreave, J.; Deng, Z. T.; Liu, Y.; Yan, H., DNA Origami with Complex Curvatures in Three-Dimensional Space. *Science* **2011**, 332, 342-346.

55. Le, J. D.; Pinto, Y.; Seeman, N. C.; Musier-Forsyth, K.; Taton, T. A.; Kiehl, R. A., DNA-templated self-assembly of metallic nanocomponent arrays on a surface. *Nano Lett.* **2004**, 4, 2343-2347.

56. Zhang, J. P.; Liu, Y.; Ke, Y. G.; Yan, H., Periodic square-like gold nanoparticle arrays templated by self-assembled 2D DNA nanogrids on a surface. *Nano Lett.s* **2006**, 6, 248-251.

57. Sharma, J.; Chhabra, R.; Liu, Y.; Ke, Y. G.; Yan, H., DNA-templated self-assembly of two-dimensional and periodical gold nanoparticle arrays. *Angew. Chem. Int. Ed.* **2006**, 45, 730-735.

58. Zheng, J.; Constantinou, P. E.; Micheel, C.; Alivisatos, A. P.; Kiehl, R. A.; Seeman, N. C., Two-dimensional nanoparticle arrays show the organizational power of robust DNA motifs. *Nano Lett.* **2006**, 6, 1502-1504.

59. Sharma, J.; Ke, Y. G.; Lin, C. X.; Chhabra, R.; Wang, Q. B.; Nangreave, J.; Liu, Y.; Yan, H., DNA-tile-directed self-assembly of quantum dots into two-dimensional nanopatterns. *Angew. Chem. Int. Ed.* **2008**, 47, 5157-5159.

60. Park, S. H.; Yin, P.; Liu, Y.; Reif, J. H.; LaBean, T. H.; Yan, H., Programmable DNA self-assemblies for nanoscale organization of ligands and proteins. *Nano Lett.* **2005**, 5, 729-733.

61. Liu, Y.; Lin, C. X.; Li, H. Y.; Yan, H., Protein nanoarrays - Aptamer-directed self-assembly of protein arrays on a DNA nanostructure. *Angew. Chem. Int. Ed.* **2005**, 44, 4333-4338.

62. Chhabra, R.; Sharma, J.; Ke, Y.; Liu, Y.; Rinker, S.; Lindsay, S.; Yan, H., Spatially addressable multiprotein nanoarrays templated by aptamer-tagged DNA nanoarchitectures. *J. Am. Chem. Soc.* **2007**, 129, 10304-10305.

63. Ding, B. Q.; Deng, Z. T.; Yan, H.; Cabrini, S.; Zuckermann, R. N.; Bokor, J., Gold Nanoparticle Self-Similar Chain Structure Organized by DNA Origami. *J. Am. Chem. Soc.* **2010**, 132, 3248-3249.

64. Pal, S.; Deng, Z. T.; Ding, B. Q.; Yan, H.; Liu, Y., DNA-Origami-Directed Self-Assembly of Discrete Silver-Nanoparticle Architectures. *Angew. Chem. Int. Ed.* **2010**, 49, 2700-2704.

65. Bui, H.; Onodera, C.; Kidwell, C.; Tan, Y.; Graugnard, E.; Kuang, W.; Lee, J.; Knowlton, W. B.; Yurke, B.; Hughes, W. L., Programmable Periodicity of Quantum Dot Arrays with DNA Origami Nanotubes. *Nano Lett.* **2010**, 10, 3367-3372.

66. Maune, H. T.; Han, S.-p.; Barish, R. D.; Bockrath, M.; Goddard, W. A., III; Rothemund, P. W. K.; Winfree, E., Self-assembly of carbon nanotubes into two-dimensional geometries using DNA origami templates. *Nat. Nanotechnol.* **2010**, 5, 61-66.

67. Stephanopoulos, N.; Liu, M.; Tong, G. J.; Li, Z.; Liu, Y.; Yan, H.; Francis, M. B., Immobilization and One-Dimensional Arrangement of Virus Capsids with Nanoscale Precision Using DNA Origami. *Nano Lett.* **2010**, 10, 2714-2720.

68. Kuzyk, A.; Laitinen, K. T.; Torma, P., DNA origami as a nanoscale template for protein assembly. *Nanotechnology* **2009**, 20.

69. Shen, X.; Song, C.; Wang, J.; Shi, D.; Wang, Z.; Liu, N.; Ding, B., Rolling Up Gold Nanoparticle-Dressed DNA Origami into Three-Dimensional Plasmonic Chiral Nanostructures. *J. Am. Chem. Soc.* **2012**, 134, 146-149.

70. Shen, X.; Asenjo-Garcia, A.; Liu, Q.; Jiang, Q.; Favier Garcia de Abajo, F.; Liu, N.; Ding, B., Three-Dimensional Plasmonic Chiral Tetramers Assembled by DNA Origami. *Nano Lett.* **2013**, 13, 2128-2133.

71. Maye, M. M.; Kumara, M. T.; Nykypanchuk, D.; Sherman, W. B.; Gang, O., Switching binary states of nanoparticle superlattices and dimer clusters by DNA strands. *Nat. Nanotechnol.* **2010**, 5, 116-120.

72. Macfarlane, R. J.; Lee, B.; Jones, M. R.; Harris, N.; Schatz, G. C.; Mirkin, C. A., Nanoparticle Superlattice Engineering with DNA. *Science* **2011**, 334, 204-208.

73. Fu, A. H.; Micheel, C. M.; Cha, J.; Chang, H.; Yang, H.; Alivisatos, A. P., Discrete nanostructures of quantum dots/Au with DNA. *J. Am. Chem. Soc.* **2004**, 126, 10832-10833.

74. Wang, Q.; Wang, H.; Lin, C.; Sharma, J.; Zou, S.; Liu, Y., Photonic interaction between quantum dots and gold nanoparticles in discrete nanostructures through DNA directed self-assembly. *Chem. Commun.* **2010**, 46, 240-242.

CHAPTER 2

AQUEOUS SYNTHESIS OF GLUTATHIONE CAPPED CdTe/CdS/ZnS AND CdTE/CdSe/ZnS CORE/SHELL/SHELL NANOCRYSTAL HETEROSTRUCTURES.

2.1. Abstract

Here we demonstrate the aqueous synthesis of colloidal nanocrystal heterostructures consisting of the CdTe core encapsulated by CdS/ZnS or CdSe/ZnS shells, using glutathione (GSH), a tri-peptide, as the capping ligand. The inner CdTe/CdS and CdTe/CdSe heterostructures have type-I, quasi type-II, or type-II band offsets depending on the core size and shell thickness, while the outer CdS/ZnS and CdSe/ZnS structures have type-I band offsets. The emission maxima of the assembled heterostructures were found to be dependent on the CdTe core size, with a wider range of spectral tunability observed for the smaller cores. Due to encapsulation effects, the formation of successive shells resulted in a considerable increase in the photoluminescence quantum yield, however, identifying optimal shell thicknesses was required to achieve maximum quantum yield. Photoluminescence lifetime measurements revealed that the decrease in the quantum yield of thick shell nanocrystals was caused by a substantial decrease in the radiative rate constant. By tuning the diameter of the core and the thickness of each shell, a broad range of high quantum yield (up to 45%) nanocrystal heterostructures with emissions ranging from visible to NIR wavelengths (500-730 nm) were obtained. This versatile route to engineer the optical properties of nanocrystal heterostructures will provide new opportunities for applications in bio-imaging and bio-labeling.

2.2. Introduction

Colloidal semiconductor nanocrystals, especially II-VI quantum dots (or nanocrystals), have immense potential for bio-labeling and bio-imaging applications, because of their size-dependent photoluminescence (PL), broad absorption and narrow emission spectra, and excellent physical and chemical stability.[1-4] For type-I core/shell nanocrystals, an arrow bandgap core is coated by a large band gap shell. In these nanocrystals, the bandgap of the core falls within the bandgap of the shell so that the exciton charge carriers are primarily confined to the core, limiting our ability to tailor the wavelength of emission. For quasi-type II nanocrystals, the electron is core-localized but the hole is delocalized over the entire nanocrystals, or the hole is shell-localized but the electron is delocalized over the entire nanocrystal.[5] For type-II core/shell nanocrystals, the band structures of the core and the shell are different, with the valence and conduction bands of the core offset (either higher or lower) from the band gap of the shell. This leads to spatial confinement of the excited electron and hole in the shell or the core separately[6-8] and results in indirect recombination of the excitons across the core-shell boundary. By varying the composition of the core and shell, and the size and thickness of the core and shell, respectively, type-II nanocrystals with a broad range of band edges can be engineered. Thus, the emission of type-II nanocrystals can be tuned from blue to near-infrared (NIR) wavelengths.[9] Another advantage of core/shell nanocrystals is that the heavy metal core elements can be encapsulated by chemically stable and biocompatible shell materials, which helps to prevent leaching of the toxic core to the surrounding medium.

Over the past few years, several research groups have reported the synthesis of a variety of highly fluorescent nanocrystal heterostructures, such as CdTe/CdSe[10-13], CdSe/CdTe[14-16], CdSe/ZnS[3,17,18], CdSe/CdS/ZnS[19], and CdTe/CdSe/ZnS[20]. Most of these nanocrystals were synthesized in organic media, typically in trioctylphosphine oxide (TOPO) and trioctylphosphine (TOP), using organometallic chemistry routes. Occasionally, ligand exchange was used to make the nanocrystals water-soluble; however, this generally results in a dramatic reduction in the photoluminescence quantum yield. An alternative strategy to generate water-soluble core/shell nanocrystals is to directly synthesize them in aqueous media by successive ion layer deposition.[21-26] For example, Green et. al. synthesized CdTe/CdSe/ZnSe[25] and CdTe/CdS/ZnS[26] quantum dots using mercaptoundecanoic acid (MUA) as the capping ligand. Despite these initial reports, a clear understanding of the formation of ternary nanocrystal heterostructures and their related photo-physical mechanisms is still lacking. Moreover, the most commonly used capping ligands, mercaptopropionic acid (MPA)[27,28] and MUA[29], are cytotoxic, limiting the number of potential bio-medical applications.[29-31] Thus, it was necessary to develop a new strategy to directly generate high quality, water-soluble nanocrystal heterostructures using a more bio-compatible capping ligand.

Here we report the synthesis of two series of core/shell/shell ternary heterostructures, CdTe/CdS/ZnS and CdTe/CdSe/ZnS, directly in aqueous medium using glutathione (GSH), a tri-peptide, as the capping ligand. To reduce the toxicity of the nanocrystals, the CdTe cores were coated by an inert ZnS outer shell and biocompatible GSH capping ligand. The crystal mismatch between ZnS and CdTe, ZnS and CdS, and ZnS and CdSe is 16%, 7%, and 11%, respectively. The sharp lattice mismatch can be

avoided by incorporating a CdS or CdSe shell between the CdTe core and the ZnS outer shell so that a more gradual two step interface is introduced, facilitating the crystal growth process. Variations in the composition and thickness of the inner shell, spectral tunability of the heterostructure nanocrystals, and ideal conditions for maximum quantum yield have been evaluated.

The relative band gaps of the core and the shell materials used in this study are shown in Figure 2.1. For CdTe/CdS core/inner shell structures, the junctions are either type-I or quasi type-II depending on the core size and shell thickness, while CdTe/CdSe core/inner shell structures are type-II only. The CdS/ZnS and CdSe/ZnS shell/shell junctions are both type-I due to the broad bandgap of ZnS. Different combinations of these semiconductor materials results in a range of nanocrystal emissions. Two methods of encapsulating the nanocrystal cores were employed: (1) all shell precursors were mixed with the pre-assembled core materials and various aliquots of the sample mixtures were collected at different reaction times, where the thickness of the shell increased with time; and (2) deliberate amounts of the shell precursors were injected in steps into a solution with the pre-assembled core materials, allowing the shell to form around the core one monolayer at a time. This method permits monitoring the quantum yield and shift in emission wavelength after the growth of each monolayer. The results reveal a strong dependence of the quantum yield and emission maxima of the heterostructure nanocrystals on the diameter of the CdTe core and the shell thicknesses. Presumably, as the thickness of the shell increases for small (less than Bohr radius) CdTe nanocrystals, the core/shell junction transitions from type-I to quasi type-II or type-II.

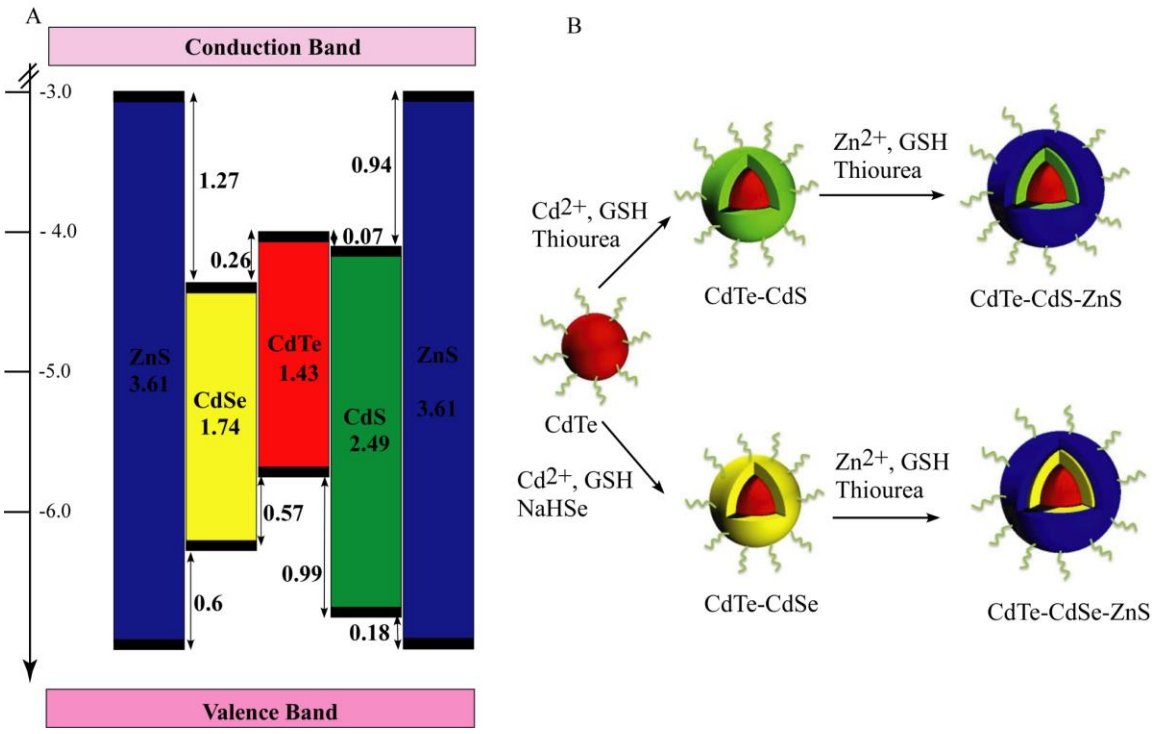

Figure 2.1. (A) Schematic illustrating the band offsets of CdTe, CdS, CdSe, and ZnS materials.[32] The energy levels of the band edges correspond to bulk materials, with units of eV. The band gap of each material is listed in the center of each bar, and the offset of conduction and valence band between each interface is specified by the arrows, with a value corresponding to the energy difference. (B) Schematic of the synthesis of CdTe/CdS/ZnS and CdTe/CdSe/ZnS Core/shell/shell nanocrystals. Both routes begin with a CdTe core, and are followed by the step-wise growth of inner and outer shells.

2.3. Materials and Methods

See APPENDIX-A

2.4. Result and Discussion

2.4.1. Structural Characterization

Transmission electron microscopy (TEM) images of representative CdTe core, CdTe/CdS core/shell and CdTe/CdS/ZnS core/shell/shell nanocrystals are shown in Figure 2.2A-F. The obvious lattice spacing observed in the HRTEM images confirms the high-quality crystallinity of all of the nanocrystals. The same CdTe and CdTe/CdS solutions were used for the preparation of the CdTe/CdS and CdTe/CdS/ZnS nanocrystals, thus, it is reasonable to estimate the core and core/shell sizes from the TEM images and subsequently determine the thicknesses of the CdS and ZnS shells from the measured size differences. The average diameters of this series of CdTe core, CdTe/CdS core/shell and CdTe/CdS/ZnS core/shell/shell nanocrystals are 3.0, 5.0 and 8.0 nm, respectively. Based on these results, the thicknesses of the inner CdS and the outer ZnS shells are estimated to be 1.0 nm and 1.5 nm, corresponding to approximately 3 monolayers of CdS and 5 monolayers of ZnS. It should be noted that these nanocrystals were prepared solely to characterize their crystallinity through TEM analysis, and demonstrate the narrow size distribution of the samples and the gradual increase of the nanocrystal size along the shell growth. They not necessarily represent nanocrystals with the maximum quantum yield.The corresponding elemental composition of the CdTe core, CdTe/CdS core/shell and CdTe/CdSe/ZnS core/shell/shell nanocrystals were determined by energy dispersive spectroscopy (EDS) (Figure 2.2G, I-III). Spectrum I illustrate the presence of Cd and Te without any traces of zinc, where a small S peak originates from the GSH capping ligands. In spectrum II, the ratio of S to Cd increases compared to spectrum I, supporting the proposed formation of a CdS shell. In spectrum III, the

appearance of a peak at 8.7 keV corresponds to the presence of Zn, with a decrease in the ratio of Te to Cd and an increase in the ratio of S to Cd compared to spectrum II. This result suggests the formation of an outer ZnS shell, although the possibility of alloy formation cannot be conclusively ruled out.

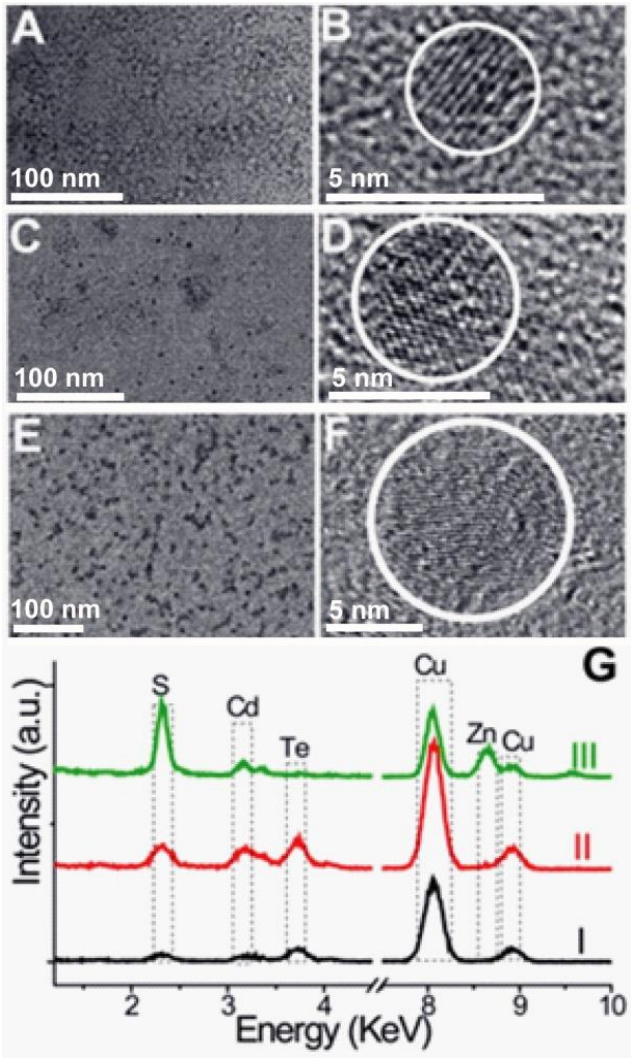

Figure 2.2. TEM and zoom in HRTEM images of the CdTe core (A, B), CdTe/CdS Core/Shell (C, D), and CdTe/CdS/ZnS Core/Shell/Shell (E, F); where the scale bars are 100 nm and 5 nm, respectively. (G) The corresponding EDS patterns. I: CdTe core; II:

CdTe/CdS; III: CdTe/CdS/ZnS. Note that after encapsulating the CdTe core with CdS and ZnS layers, the CdTe inner core will produce a weaker Te signal in the EDS spectra, thus the Te to Cd ratio drops from sample II to III.

Similarly, the TEM images of the representative CdTe core, CdTe/CdSe core/shell and CdTe/CdSe/ZnS core/shell/shell nanocrystals (shown in Figure 2.3A-F) confirm their synthesis. The average diameters of the core, core/shell and core/shell/shell nanocrystals are 3.0, 5.0 and 8.0 nm, respectively. Accordingly, the thicknesses of the inner CdSe shell and outer ZnS shell are estimated to be 1.0 and 1.5 nm, respectively. The elemental composition of the CdTe core, CdTe/CdSe core/shell and CdTe/CdSe/ZnS core/shell/shell nanocrystals were characterized by EDS (Figure 2.3G). The appearance of Se (1.4 keV) in spectra II and III provide evidence of the formation of an inner CdSe shell. The emergence of a Zn peak at 8.7 keV in spectrum III, in combination with the observed increase in the ratio of S to Cd in spectrum III compared to spectrum II, and minimal change in the ratio of Se to Cd in spectra II and III, all indicate the formation of the outer ZnS shell.

The core/shell and core/shell/shell structures were further confirmed by powder X-ray diffraction (PXRD) (Figure 4). The diffraction pattern of the CdTe core reveals three peaks that are assigned to the (111), (220) and (311) planes, consistent with the cubic phase of CdTe. The other nanocrystal heterostructures also exhibit the same cubic lattice. The broad diffraction peaks observed for each of the samples are due to the nanometer size of the nanometer crystals. The growth of consecutive CdS or ZnS shells shifts the diffraction peaks toward higher angles due to the small crystal constants for CdS and ZnS compared to CdTe. For example, in Figure 2.4A the scattering peaks for

CdTe/CdS nanocrystals are between those of bulk cubic CdTe and bulk CdS. The diffraction pattern of the CdTe/CdS/ZnS nanocrystals shifts to even higher angles due to the presence of a ZnS shell. The same patterns were observed for nanocrystals with a CdSe inner shell (Figure 2.4B). The scattering peaks become noticeably narrower with the formation of each successive layer, which can be explained by the increase in the crystalline domain size, providing additional evidence of epitaxial shell growth.

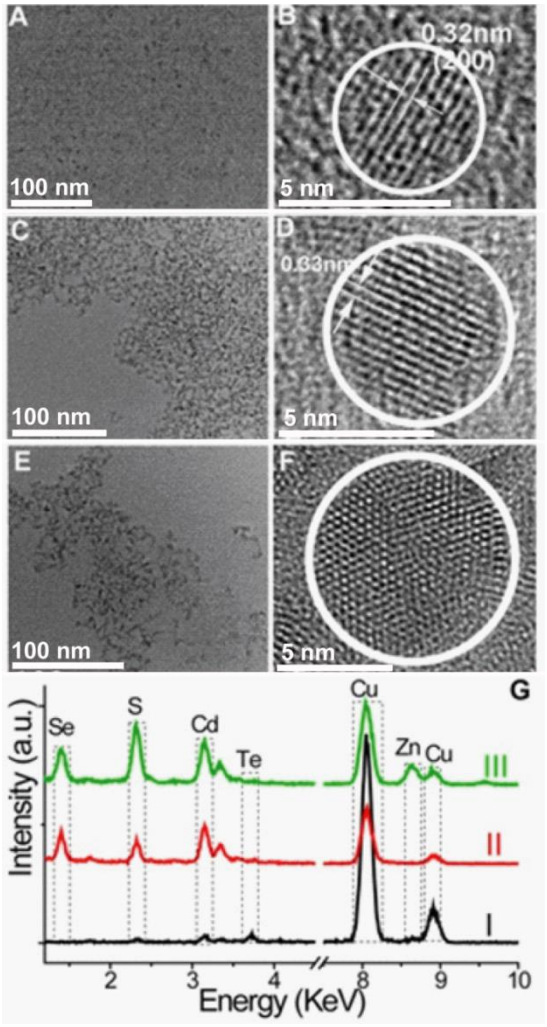

Figure 2.3. TEM and zoom-in HRTEM images of the CdTe core (A, B), CdTe/CdSe Core/Shell (C, D), and CdTe/CdSe/ZnS Core/Shell/Shell (E, F); (G) The corresponding EDS patterns. I: CdTe core; II: CdTe/CdSe; and III: CdTe/CdSe/ZnS. Note that after

deposition of the ZnS and CdS layers, the innermost CdTe core produces a weaker Te signal in the EDS spectra, thus, the Te to Cd ratio drops from samples II to III.

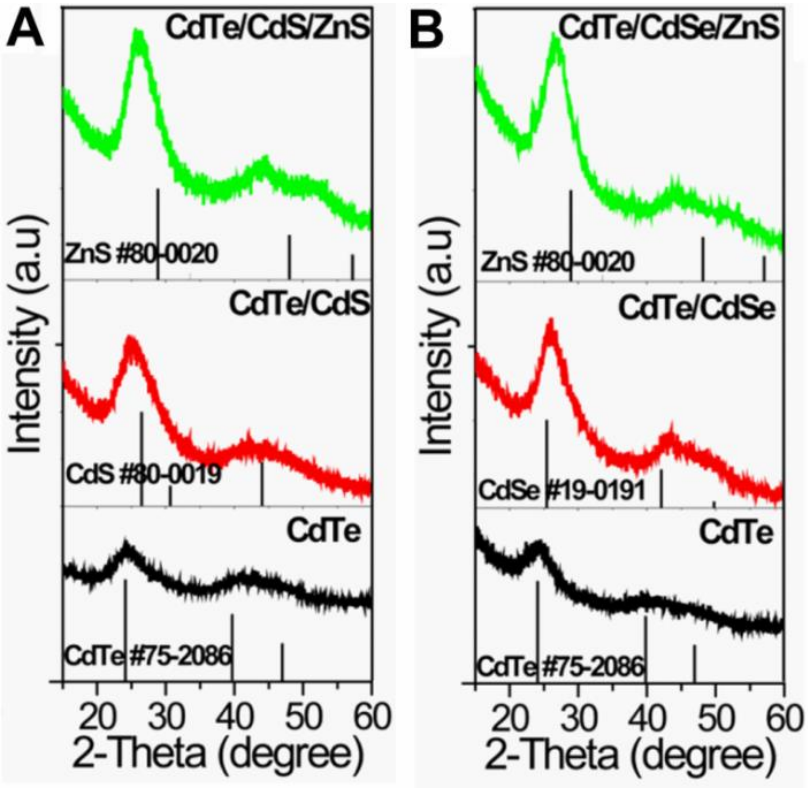

Figure 2.4. Powder XRD patterns of (A) CdTe (black), CdTe/CdSe (red), CdTe/CdSe/ZnS (green) and (B) CdTe (black), CdTe/CdS (red), CdTe/CdS/ZnS (green).The bulk XRD data of CdTe, CdS, CdSe and ZnS are also shown as vertical lines for comparison.

2.4.2. Photo-physical properties

a. CdTe core

UV-Vis absorption and PL emission spectra of GSH-capped CdTe core nanocrystals are shown in Figure 2.5A&B. As the size of the nanocrystal increases, the onset of absorption and emission maximum of the nanocrystals gradually shifts towards longer wavelengths due to quantum confinement effects. The narrow emission (full width at half maximum, FWHM are between 32 and 44 nm, see supporting information Page S4) and obvious absorption peaks indicate a small size distribution of the core nanocrystals. The PL emission band appears near the band edge, and as the reaction time and thus the size of the nanocrystals increased, a decrease in the quantum yield was observed (Figure 2.5C), possibly due to an increase in the number of surface defects per nanocrystal. "Surface defects" can affect the recombination of electrons and holes non-radiatively by acting as temporary "traps". This results in decrease of the quantum yield.

b. CdTe/CdS core/shell nanocrystals

A robust shell is required to impart chemical and physical stability to the nanocrystals and to increase the quantum yield of emission. However, lattice mismatches between core and shell materials creates excessive crystal strain at core/shell interfaces. CdS is a more suitable shell material for encapsulation of a CdTe core than ZnS because of better overlap between the lattice parameters. The full width at half maximum of each CdTe/CdS photoluminescence spectra are between 53 and 62 nm (see supporting information Page S4). CdTe/CdS and CdTe/CdS/ZnS nanocrystals are considerably more stable than the CdTe cores, as evidenced by very high (35-45%) quantum yields and PL emission that is stable for several months. As shown in Supporting Information Table 3,

after six freshly prepared samples were exposed to air for four months (4 ^{o}C, dark), they were still highly florescent with the PL quantum yield remained above 20%, and a minimal shift (< 5 nm) of the emission wavelength.

Figures 2.5D-E show the UV-Vis absorption and PL emission spectra corresponding to the CdTe/CdS core/shell nanocrystals. A CdTe core with green emission maximum at 540 nm and quantum yield of ~8.4% was selected for encapsulation by a CdS shell. As the thickness of the CdS shell increased, the maximum absorbance and emission peaks shifted toward longer wavelengths (red shift). It worth noting that the full width at half maximum (FWHM) of the CdTe/CdS nanocrystal samples continue to increase as the CdS shell grown thicker, possibly due to the increased polydispersity of the nanocrystals.

As illustrated in the schematic picture in Figure 2.1, we speculate that the band edge evolves from type-I to type-II as a CdS shell encapsulates the CdTe ore. This is due to the energy offset of the conduction bands of bulk CdTe and CdS are very close (0.07 eV), therefore, quantum confinement of the core and shell may result in the conduction band of the CdTe core lying above (type I) or below (type II) that of the CdS shell, depending on the core size and shell thickness. When a thin CdS layer encapsulates a specific size CdTe core, the conduction band of CdTe will lie below that of CdS due to stronger quantum confinement of the CdS shell than the CdTe core, forming a type I structure. As the thickness of the CdS layer continues to grow, the quantum confinement of the CdS shell will become weaker than that of the CdTe core, a transition from type I to type II structure is expected. [36,37]

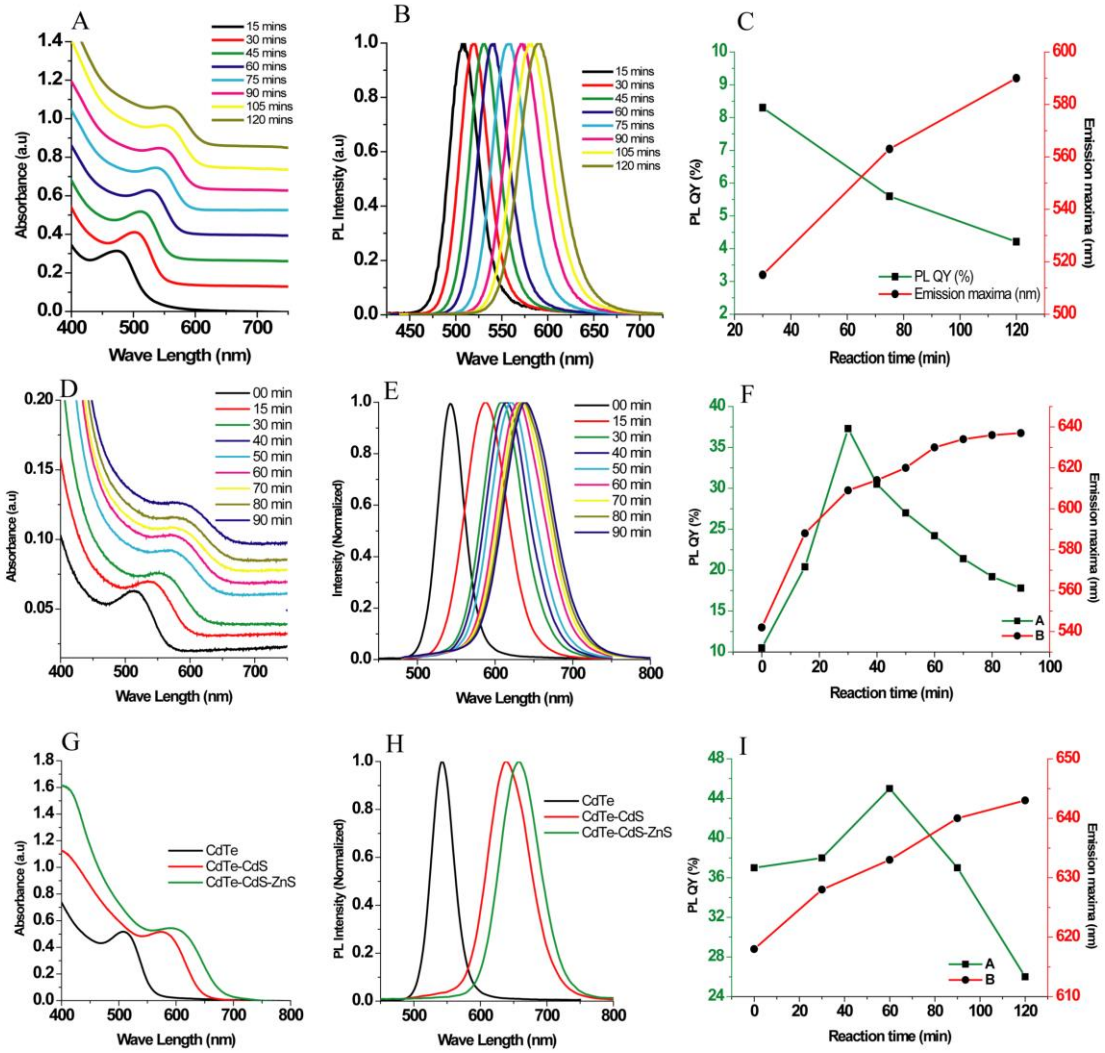

Figure 2.5. **A-B**, **D-E**, and **G-H** contain UV-Vis and PL spectra of the CdTe core, CdTe/CdS core/shell, and CdTe/CdS/ZnS nanocrystals, respectively. Both the absorption and emission maxima progressively shift toward longer wavelengths as the thicknesses of the CdS and ZnS shells around the CdTe core nanocrystals increase. **C**, **F**, **and I** show the evolution of the PL quantum yield and emission maxima of the CdTe, CdTe/CdS and CdTe/CdS/ZnS with reaction time. Increasing the thickness of the shell results in a continuous red shift of the emission maximum, however, the quantum yield exhibits a

maximum at a certain thickness and decreases with further shell growth. The CdTe core with the highest quantum yield (8.4%), corresponding to an emission maximum at 540 nm, was selected to for subsequent encapsulation by a CdS shell. The core/shell CdTe/CdS structure with the highest quantum yield (37%), corresponding to an emission maximum at 615nm, was chosen for encapsulation by a second ZnS shell.

We attribute the significant red shift of the absorption and emission maxima to epitaxial shell growth rather than alloying. Gurusinghe et al.[38] suggested that alloyed CdS_xTe_{1-x} nanocrystals exhibit pronounced optical bowing and their band gap is highly nonlinear with alloy composition, which will cause a significant red shift in the fluorescence of alloyed CdS_xTe_{1-x} nanocrystals compared to the emission wavelength of the parent binary CdS and CdTe compounds. However, the absorption profile of alloyed CdS_xTe_{1-x} nanocrystals is dominated by CdS, and is expected to show large Stokes shifts (up to 150 nm) for the emission. For the CdTe/CdS nanocrystals reported here, the absorption profile was dominated by CdTe, and only small Stokes shifts (20-30 nm) were observed, which behaves different from the alloyed nanocrystals. Nie et. al.[37] reported that epitaxial deposition of a ZnSe shell onto a CdTe core to form a lattice mismatched core/shell nanocrystal could be used to tune the emission across the visible and near-infrared part of the spectrum (500–1,050 nm), which was attributed to standard type-I nanocrystal behavior being replaced by type-II nanocrystal behavior as the shell grew thicker. This explanation is consistent with our observations. However, typical type II nanocrystals are expected to have a featureless absorption tail because they should behave like semiconductors with an indirect bandgap. The CdTe/CdS nanocrystals prepared here have distinctive peaks in the absorption spectra. Therefore they are not

typical a type II nanocrystal, but a quasi-type II nanocrystal, which means the electron is core-localized but the hole is delocalized over the entire nanocrystals.[5] Furthermore, it is known that ternary alloyed nanocrystals have shorter lifetimes than binary nanocrystals[39] and the formation of type II core/shell nanocrystals results in much longer lifetimes[37] because the electron or hole reside in the core or shell, respectively, and their recombination occurs across the core/shell boundary.[40] The lifetime measurements reveal that for the core/shell nanocrystals, the lifetime of PL emission gradually increases as the thickness of the shell increases (Supporting Information Figure S1), providing further evidence of the formation of quasi type-II nanocrystals rather than an alloyed structure. Overall, the red shift of the absorption and emission maxima, continuous smearing of the absorption spectra, and longer emission lifetimes that were observed as the thickness of the shell increased (Figure 2.5D), are consistent with formation of quasi type-II core/shell nanocrystals. The PL quantum yield steadily increases to a maximum value and then gradually decreases as the shell becomes thicker (Figure 2.5F). It seems that 1-2 monolayers of CdS are required to generate the maximum quantum yield for the quasi type-II core/shell nanocrystal heterostructures.

c. CdTe/CdS/ZnS core/shell/shell nanocrystals

To further increase the PL quantum yield and to reduce the toxicity of the exposed CdS layer, a ZnS shell was grown on the outer surface of the core/shell structure. The incorporation of a CdS layer between the CdTe core and outer ZnS shell facilitates a gradual change in the lattice parameters, increasing the stability and performance of the nanocrystals. The band gap of ZnS is larger than CdS (conduction band offset ~ 1eV),

thus, the confinement of the excitons is enhanced in the CdTe/CdS/ZnS system, with a significant reduction in the number of non-radiative surface or interface defects and increase in the PL quantum yield. The FWHM of each CdTe/CdS/ZnS photoluminescence spectra are between 54 and 63 nm (see supporting information Page S5).

To ensure maximum quantum yield in the final nanocrystal heterostructure, the CdTe/CdS core/shell nanocrystals with the highest quantum yield (37%) and emission maximum at 615 nm were selected for further encapsulation by a ZnS layer. Figure 2.5G&H compare the UV-Vis and PL spectra of the CdTe core, CdTe/CdS core/shell, and CdTe/CdS/ZnS core/shell/shell structures. Although growth of the CdS shell resulted in an obvious red shift (over a range of ~ 100 nm) in both the absorption and emission maxima (Figure 2.5F), the addition of outer ZnS shell produced a much smaller red shift, ~ 25 nm (Figure 2.5I). These shifts reflect the successful formation of distinct shells rather than alloyed nanocrystals that would exhibit a blue shift.

The band gap of ZnS is much larger than that of CdS, creating a type-I shell/shell boundary where the excitons remain confined to the core/shell inner structure and dominate the absorption and emission process. The small red shift that coincides with the emergence of the outer shell can be explained by the slightly reduced quantum confinement that is present within a type-I shell/shell junction, as the overall quantum size increases with the outer shell growth. Similar to the trend in the CdTe/CdS core/shell nanocrystals, for the ZnS outer shell, the quantum yield initially increases to 45%, and subsequently decreases as the shell becomes thicker (Figure 2.5I). The increase in quantum yield corresponds to a reduction in the number of surface defects as the

nanocrystal surface is encapsulated. The subsequent decrease in quantum yield may be attributed to a larger number of defects per nanocrystal as the overall size of the nanocrystal increases.

d. Effects of core size and shell thickness on the quantum yield and spectral tunability of emission

We selected several different CdTe cores (Figure 2.6A&B) to explore the effects of core size and shell thickness on the quantum yield and color tunability of core/shell heterostructures. The three CdTe nanocrystals that were chosen had emission maxima at 509 nm (green), 560 nm (yellow) and 590 nm (red), each with a relatively low quantum yield (~ 4-10%). The PL quantum yield increased significantly after encapsulation of the CdTe core by 1-2 CdS monolayers, reaching a maximum of 23% - 43%. Further coating of the core resulted in a gradual decrease in the quantum yield. The green CdTe core (with the smallest diameter) exhibited the largest increase in quantum yield with the formation of the first monolayer.

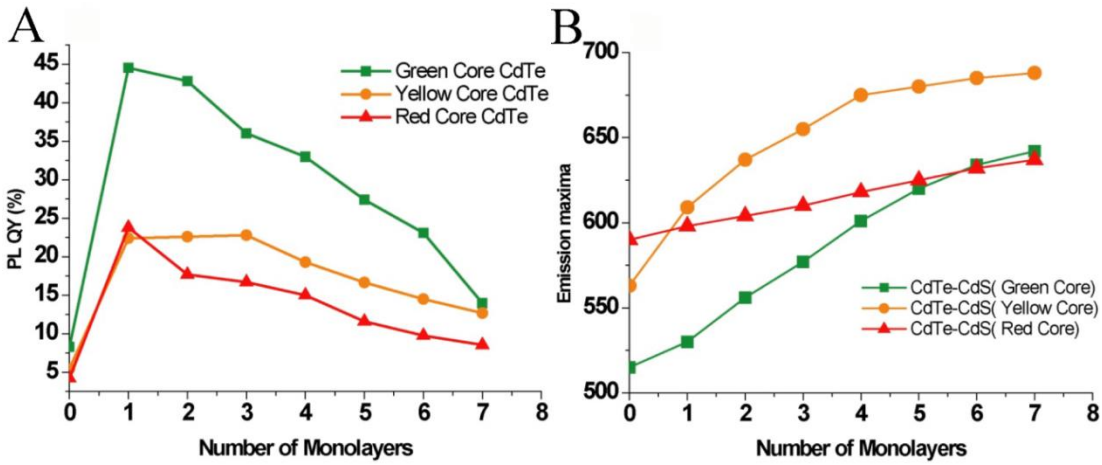

Figure 2.6. Individual CdS monolayers were deposited on green, orange, and red CdTe nanocrystal cores to determine the range of potential emission colors and conditions for

maximum PL quantum yield. Figures A and B illustrate the dependence of PL quantum yield and emission maxima, respectively, on the number of shell monolayers. Monolayers were deposited by precisely calculating the amount of reagents required for each layer, adding them to the reaction mixture in steps, and allowing sufficient time for the reaction to reach equilibrium at each step.

The initial increase in PL quantum yield that occurs is accompanied by a small red shift, indicating the formation of type-I nanocrystals. It is known that depositing a shell with a small lattice constant and wide band gap (such as CdS) on a CdTe nanocrystal core with a larger lattice constant causes significant structural strain on both of the core and the shell, altering the band edges of both.[37] For small cores (green CdTe nanocrystals), as the shell grows thicker the band gap decreases and causes the energy offset of the conduction bands of the core and shell to switch from a larger CdS offset to a larger CdTe offset. Therefore, the CdTe/CdS interface changes from type-I to quasi type-II as argued before, and the electron-hole pair recombination switches from direct transfer within the core to indirect transfer across the core/shell boundary. This leads to a decrease in the radiative rate constant (k_r), as evidenced by the significant increase in the decay lifetime of emission (Supporting Information Figures S1&S2) and a decrease in quantum yield (Figure 2.6A).

Increasing the thickness of the CdS shell causes a continuous red shift of the emission peak for all three sets of samples (Figure 2.6B). The ability to precisely tune the emission color was comparable for the green and orange cores, with a shift in the wavelength of emission of ~ 15 nm for each monolayer that was deposited, and a total range of > 110 nm. A much smaller shift of ~ 4 nm per monolayer was observed for the

red core; with a total range of ~ 30 nm. This can be attributed to the effect of size on the bandgap of both the core and the shell. The green and orange cores have smaller diameters and wider band gaps than the red core, thus they are more sensitive to changes in the size and structure of the shell, and are able to switch from type-I to quasi type-II with shell growth beyond the first monolayer. However, red CdTe cores have larger diameter and smaller band gaps, and the core/shell structures are unable to switch from type-I to type-II during the shell growth process, and the small spectral tunability observed is simply due to the overall increase in quantum size. The results show that small cores are more amenable to a wide range of color tunability.

e. CdTe/CdSe and CdTe/CdSe/ZnS nanocrystals

To further study the effect of shell material and thickness on the photo-physical behavior of core/shell/shell nanocrystals, we synthesized a CdTe/CdSe/ZnS core/shell/shell system (Figure 2.7), where the inner CdTe/CdSe core/shell is a true type-II nanocrystal (Figure 2.7A&B). Here, a green emitting (545 nm) CdTe core was encapsulated by a CdSe shell. The core/shell structure was subsequently coated by a ZnS outer layer. The FWHM of each CdTe/CdSe photoluminescence spectra are between 49 and 70 nm (see supporting information Page S4).

The CdTe core was coated by a CdSe shell in a monolayer by monolayer fashion. To ensure uniform growth of the CdSe shell, the NaHSe solution was added gradually, rather than in a single step. After each injection step, adequate time was given to allow complete monolayer formation. Figure 2.7 confirms that CdTe/CdSe core/shell and CdTe/CdSe/ZnS core/shell/shell nanocrystals were successfully synthesized in aqueous medium, exhibiting a clear red shift of the UV-Vis absorbance and PL emission spectra

(Figure 2.7). The FWHM of each CdTe/CdSe/ZnS photoluminescence spectra are between 60 and 68 nm (see supporting information Page S5). The broadening of the PL spectra for samples after the first monolayer shell growth (Figure 2.7B) may indicate a slightly larger size distribution of the core/shell nanocrystals. The smearing of the UV-Vis spectra as successive CdSe and ZnS shells form on the CdTe core (Figure 2.7A&D) is an accepted feature of type-II nanocrystals.

As shown in Figure 2.7C (green trace), the PL quantum yield of the CdTe/CdSe nanocrystals follows the same trend as that of CdTe/CdS nanocrystals with respect to the shell thickness. The quantum yield increases from an initial value of ~ 10% to a maximum of ~ 32%, followed by a decrease as the CdSe shell grows thicker. This is likely for the same reasons previously described, i.e. initial reduction in surface defects (increased quantum yield) that results in a significant reduction of the non-radiative rate constant, followed by a decrease in the radiative rate constant with the formation of a typical type-II structure as the shell grows thicker. This theory is supported by the lifetime measurements that show that the CdTe/CdSe core/shell nanocrystals have emission decay lifetimes three to five times longer than the CdTe core only (Supporting Information Figure S2).

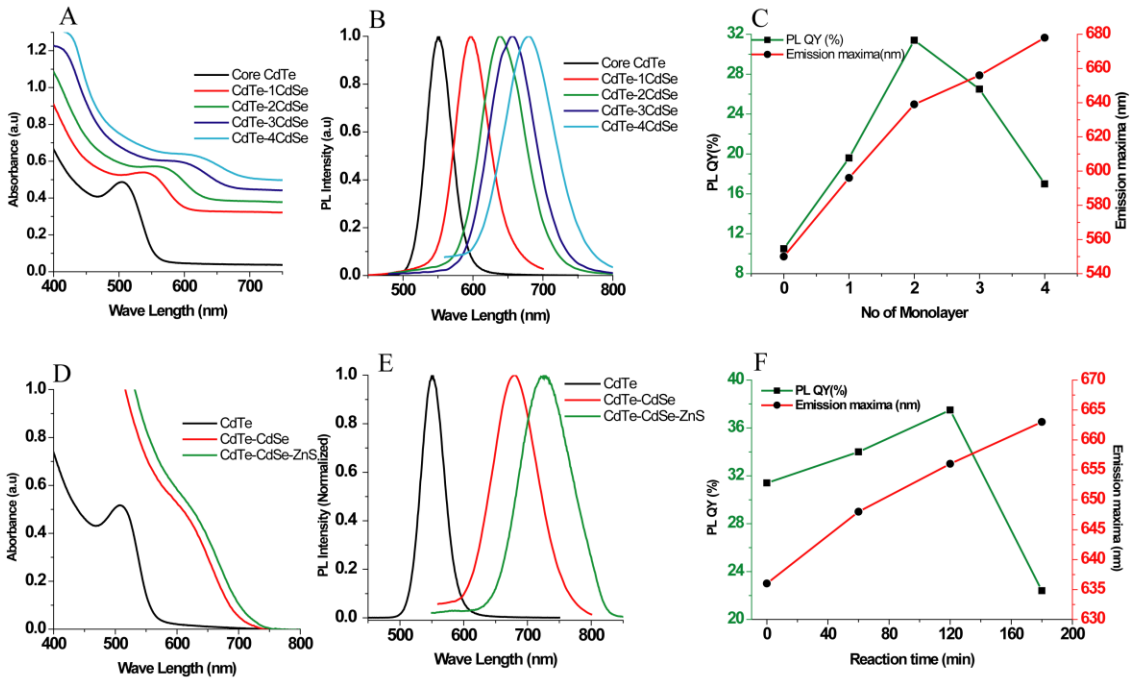

Figure 2.7. (A, B) UV-Vis and PL emission spectra of GSH capped CdTe/CdSe core/shell nanocrystals following the layer by layer shell growth. (C) Dependence of the PL quantum yield and emission maxima of CdTe/CdSe nanocrystals on number of monolayers of the shell. (D, E) Comparison of the UV-Vis spectra and PL spectra of CdTe, CdTe/CdSe, and CdTe/CdSe/ZnS nanocrystals. (F) Dependence of the PL quantum yield and emission maxima of CdTe/CdSe/ZnS nanocrystals following the ZnS shell growth.

We selected the CdTe/CdSe sample with two monolayers of CdSe shell and the highest quantum yield (32%) as the precursor upon which to grow an outer ZnS shell. The maximum quantum yield that was obtained for the CdTe/CdSe/ZnS heterostructures was ~ 37%, corresponding to a moderate ZnS shell thickness. Similar to the growth of the first shell, the initial increase in quantum yield upon deposition of the second shell can

also be attributed to a reduction in the number of surface defects that is manifested by a reduction in the non-radiative rate constant (Supporting Information Figure S2). Thicker ZnS shells result in a decrease in the quantum yield (Figure 2.7F, green trace), which can be attributed to structural strain and the higher probability of generating surface defects that non-radiatively quench the PL as the size of the nanocrystal increases.

The color tunability of the CdTe/CdSe/ZnS nanocrystals (Figure 2.7C&F) also follows a similar trend as the CdTe/CdS/ZnS system (Figure 2.5F&I), but with a wider range. Starting with a green emitting CdTe core, we observed a large red shift (>130 nm) upon deposition of the inner CdSe shell, followed by a small red shift (~40 nm) after encapsulation by the outer ZnS shell. Compared to the CdTe/CdS/ZnS nanocrystal system, the range of tunable wavelengths is larger for both steps (with similar core diameters). The broad range of spectral tunability is due to the small band gap of CdSe compared to CdS, which generates a larger band edge offset in CdTe/CdSe than in CdTe/CdS. These observations indicate the presence of a true type-II junction in the CdTe/CdSe nanocrystals, and a type-I junction in the CdSe/ZnS nanocrystals. The prepared CdTe/CdS/ZnS and CdTe/CdSe/ZnS core/shell/shell nanocrystal samples are stable after up to 6 months storage in 4 ^{o}C, showing no obvious precipitation and highly bright fluorescence with PL quantum yield large than 20% (see Supporting Information Figure S3) and minimal shift in the emission peak (< 5 nm).

f. Emission decay lifetime measurements

The layer-by-layer growth strategy was used to encapsulate CdTe nanocrystal cores (emission maximum at 509 nm) for all samples evaluated by lifetime experiments. To prepare each sample, between one and five monolayers of an inner shell, either CdS

or CdSe, were deposited on the core, followed by encapsulation with an outer ZnS shell. The green emitting CdTe core has a PL quantum yield of 8.5% and an average lifetime of 7.9 ns. Deposition of the first monolayer of the inner shell (for both the CdS and CdSe shells) resulted in a significant increase in the lifetime and the quantum yield of emission. As the size of the inner shell increased, the lifetime of emission continued to increase, while the quantum yield reached a maximum (two monolayers) in both cases.

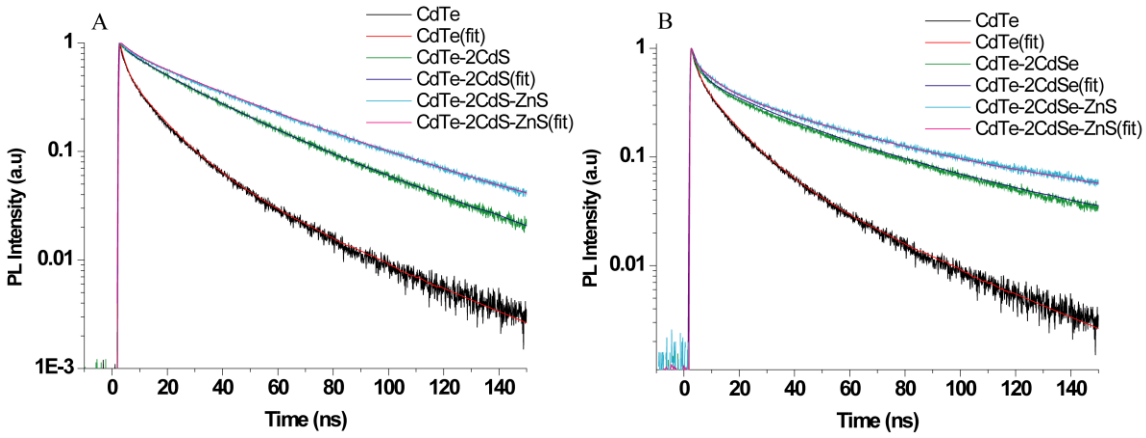

Figure 2.8. Emission decay measurements for (A) CdTe, CdTe/CdS and CdTe/CdS/ZnS samples, where the core/shell and core/shell/shell structures contain two monolayers of CdS, and (B) CdTe, CdTe/CdSe and CdTe/CdSe/ZnS samples, where the core/shell and core/shell/shell structures contain two monolayers of CdSe.

The quantum yield depends on the ratio of the radiative decay rate (k_r) to the sum of the radiative and non-radiative decay rates (k_{nr}):

$$QY = \frac{k_r}{k_r + k_{nr}} \qquad [1]$$

while the measured emission decay life time can be expressed as

$$\tau = \frac{1}{k_r + k_{nr}} \qquad [2]$$

Since multiple (three) exponentials were required to fit the decay data, the average decay lifetime was calculated by $\langle\tau\rangle = \sum_{i=1}^{3} A_i$, where A_i is the normalized amplitude of each component. Thus, k_r and k_{nr} are only loosely defined here. Although they cannot be assigned to any specific optical transition, their relative values help us to understand the contribution of the radiative and nonradiative processes in the exciton recombination process following each layer of shell growth.

From the quantum yield and lifetime measurements, k_r and k_{nr} can be calculated using equations [1] and [2]. The results reveal that after deposition of the initial layers of the inner shell, k_{nr} dramatically decreases with a corresponding increase in k_r and quantum yield. This is presumably due to a reduction in the number of interfacial defects between the core and shell boundary that occurs as the core is encapsulated. As the size of the shell increases and after it reaches a threshold thickness, a quasi or true type-II core/shell junction develops. Because of the indirect exciton recombination that occurs across a type-II core/shell boundary, k_r decreases significantly, while k_{nr} is relatively stable with a mild decrease as the shell thickness increases (Figure 2.8). Overall, these lead to a gradual decrease of the quantum yield and continuous increase of the lifetime. Comparing the quantum yield and lifetime data of the two types of core/shell nanocrystals, larger radiative (k_r) and similar nonradiative (k_{nr}) rate constants were observed for the CdTe/CdS samples than that of the CdTe/CdSe samples. This can be explained by the smaller band edge offset in CdTe/CdS nanocrystals, which leads to a faster radiative exciton recombination across the core/shell boundary.

Interestingly, encapsulation of the CdTe/CdS and CdTe/CdSe core/shell nanocrystal heterostructures (with two monolayers of the inner shell) by a moderately thick ZnS shell resulted in a further increase in both the quantum yield and lifetime of emission (labeled 'CSS' in FiguresS3A-D). The data reveals that both k_r and k_{nr} were reduced for the CSS sample compared to the corresponding core/shell structure (CS-2 data). This is most likely because of a larger quantum size that reduces k_r, and the surface encapsulation that further reduces interfacial defects. Overall, this results in higher quantum yield and longer emission lifetime when compared to the core/shell structure.

2.5. Conclusions

In summary, we have demonstrated the aqueous synthesis of CdTe/CdS/ZnS and CdTe/CdSe/ZnS core/shell/shell nanocrystal heterostructures that contain type-I, quasi type II, or type-II nanocrystal junctions, rather than the formation of alloyed nanocrystals. CdTe nanocrystal cores were protected by two inorganic shell layers (core/shell/shell), either CdS/ZnS or CdSe/ZnS, and glutathione was used as a capping ligand to reduce the toxicity of the nanocrystals. The synthesis of CdTe nanocrystals with several different shell materials and thicknesses are done in mild aqueous conditions. The study reveals that the size of the CdTe core has a very clear effect on the quantum yield and emission maxima of the heterostructure nanocrystals. In addition, the PL quantum yield increases significantly after deposition of one and two monolayers of CdS or CdSe on the CdTe core. By tuning the core size and thicknesses of the shell layers in CdTe/CdSe/ZnS nanocrystals, NIR emissions with peak wavelengths up to 730 nm were obtained. These series of core/shell/shell nanocrystals may find applications in bio-imaging, bio-labeling and display devices.

2.6. References

1. Michalet, X.; Pinaud, F. F.; Bentolila, L. A.; Tsay, J. M.; Doose, S.; Li, J. J.; Sundaresan, G.; Wu, A. M.; Gambhir, S. S.; Weiss, S., Quantum dots for live cells, in vivo imaging, and diagnostics. *Science* **2005**, *307*, 538-544.

2. Medintz, I. L.; Uyeda, H. T.; Goldman, E. R.; Mattoussi, H., Quantum dot bioconjugates for imaging, labelling and sensing. *Nature Mater.* **2005**, *4*, 435-446.

3. Dabbousi, B. O.; RodriguezViejo, J.; Mikulec, F. V.; Heine, J. R.; Mattoussi, H.; Ober, R.; Jensen, K. F.; Bawendi, M. G., (CdSe)ZnS core-shell quantum dots: Synthesis and characterization of a size series of highly luminescent nanocrystallites. *J. Phys. Chem. B* **1997**, *101*, 9463-9475.

4. Peng, X. G.; Schlamp, M. C.; Kadavanich, A. V.; Alivisatos, A. P., Epitaxial growth of highly luminescent CdSe/CdS core/shell nanocrystals with photostability and electronic accessibility. *J. Am. Chem. Soc.* **1997**, *119*, 7019-7029.

5. Piryatinski, A.; Ivanov, S. A.; Tretiak, S.; Klimov, V. I., Effect of quantum and dielectric confinement on the exciton-exciton interaction energy in type II core/shell semiconductor nanocrystals. *Nano Lett.* **2007**, *7*, 108-115.

6. Chen, C. Y.; Cheng, C. T.; Lai, C. W.; Hu, Y. H.; Chou, P. T.; Chou, Y. H.; Chiu, H. T., Type-II CdSe/CdTe/ZnTe (core-shell-shell) quantum dots with cascade band edges: The separation of electron (at CdSe) and hole (at ZnTe) by the CdTe layer. *Small* **2005**, *1*, 1215-1220.

7. Hatami, F.; Grundmann, M.; Ledentsov, N. N.; Heinrichsdorff, F.; Heitz, R.; Bohrer, J.; Bimberg, D.; Ruvimov, S. S.; Werner, P.; Ustinov, V. M.; Kop'ev, P. S.; Alferov, Z. I., Carrier dynamics in type-II GaSb/GaAs quantum dots. *Phys. Rev. B* **1998**, *57*, 4635-4641.

8. Yoffe, A. D., Semiconductor quantum dots and related systems: electronic, optical, luminescence and related properties of low dimensional systems. *Adv. Phys.* **2001**, *50*, 1-208.

9. Deng, Z. T.; Schulz, O.; Lin, S.; Ding, B. Q.; Liu, X. W.; Wei, X. X.; Ros, R.; Yan, H.; Liu, Y., Aqueous Synthesis of Zinc Blende CdTe/CdS Magic-Core/Thick-Shell Tetrahedral-Shaped Nanocrystals with Emission Tunable to Near-Infrared. *J. Am. Chem. Soc.* **2010**, *132*, 5592-5593.

10. Kim, S.; Fisher, B.; Eisler, H. J.; Bawendi, M., Type-II quantum dots: CdTe/CdSe(core/shell) and CdSe/ZinTe(core/shell) heterostructures. *J. Am. Chem. Soc.* **2003**, *125*, 11466-11467.

11. Yu, K.; Zaman, B.; Romanova, S.; Wang, D. S.; Ripmeester, J. A., Sequential synthesis of type II colloidal CdTe/CdSe core-shell nanocrystals. *Small* **2005**, *1*, 332-338.

12. Wang, C. H.; Chen, T. T.; Tan, K. W.; Chen, Y. F.; Cheng, C. T.; Chou, P. T., Photoluminescence properties of CdTe/CdSe core-shell type-II quantumdots. *J. Appl. Phys.* **2006**, *99*, 123521.

13. Chang, J. Y.; Wang, S. R.; Yang, C. H., Synthesis and characterization of CdTe/CdS and CdTe/CdSe core/shell type-II quantum dots in a noncoordinating solvent. *Nanotechnology* **2007**, *18*, 345602.

14. Blackman, B.; Battaglia, D. M.; Mishima, T. D.; Johnson, M. B.; Peng, X. G., Control of the morphology of complex semiconductor nanocrystals with a type II heterojunction, dots vs peanuts, by thermal cycling. *Chem. Mater.* **2007**, *19*, 3815-3821.

15. Blackman, B.; Battaglia, D.; Peng, X. G., Bright and water-soluble near IR-Emitting CdSe/CdTe/ZnSe Type-II/Type-I nanocrystals, tuning the efficiency and stability by growth. *Chem. Mater.* **2008**, *20*, 4847-4853.

16. Dooley, C. J.; Dimitrov, S. D.; Fiebig, T., Ultrafast electron transfer dynamics in CdSe/CdTe donor-acceptor nanorods. *J. Phys. Chem. C* **2008**, *112*, 12074-12076.

17. Mattoussi, H.; Mauro, J. M.; Goldman, E. R.; Anderson, G. P.; Sundar, V. C.; Mikulec, F. V.; Bawendi, M. G., Self-assembly of CdSe-ZnS quantum dot bioconjugates using an engineered recombinant protein. *J. Am. Chem. Soc.* **2000**, *122*, 12142-12150.

18. Talapin, D. V.; Rogach, A. L.; Kornowski, A.; Haase, M.; Weller, H., Highly luminescent monodisperse CdSe and CdSe/ZnS nanocrystals synthesized in a hexadecylamine-trioctylphosphine oxide-trioctylphospine mixture. *Nano Lett.* **2001**, *1*, 207-211.

19. Talapin, D. V.; Mekis, I.; Gotzinger, S.; Kornowski, A.; Benson, O.; Weller, H., CdSe/CdS/ZnS and CdSe/ZnSe/ZnS core-shell-shell nanocrystals. *J. Phys. Chem. B* **2004**, *108*, 18826-18831.

20. Zhang, W. J.; Chen, G. J.; Wang, J.; Ye, B. C.; Zhong, X. H., Design and Synthesis of Highly Luminescent Near-Infrared-Emitting Water-Soluble CdTe/CdSe/ZnS Core/Shell/Shell Quantum Dots. *Inorg. Chem.* **2009**, *48*, 9723-9731.

21. Gao, M. Y.; Kirstein, S.; Mohwald, H.; Rogach, A. L.; Kornowski, A.; Eychmuller, A.; Weller, H., Strongly photoluminescent CdTe nanocrystals by proper surface modification. *J. Phys. Chem. B* **1998**, *102*, 8360-8363.

22. He, Y.; Lu, H. T.; Sai, L. M.; Lai, W. Y.; Fan, Q. L.; Wang, L. H.; Huang, W., Microwave-assisted growth and characterization of water-dispersed CdTe/CdS core-shell nanocrystals with high photoluminescence. *J. Phys. Chem. B* **2006**, *110*, 13370-13374.

23. Wang, C. L.; Zhang, H.; Zhang, J. H.; Li, M. J.; Sun, H. Z.; Yang, B., Application of ultrasonic irradiation in aqueous synthesis of highly fluorescent CdTe/CdS core-shell nanocrystals. *J. Phys. Chem. C* **2007**, *111*, 2465-2469.

24. Zhang, W. H.; Yu, J. S., Synthesis and Characterization of High Fluorescence, Type-II Core/Shell CdTe/CdSe Quantum Dots in Aqueous Medium. *Chin. J. Inorg. Chem.* **2010**, *26*, 775-780.

25. Taniguchi, S.; Green, M.; Rizvi, S. B.; Seifalian, A., The one-pot synthesis of core/shell/shell CdTe/CdSe/ZnSe quantum dots in aqueous media for in vivo deep tissue imaging. *J. Mater. Chem.* **2011**, *21*, 2877-2882.

26. Green, M.; Williamson, P.; Samalova, M.; Davis, J.; Brovelli, S.; Dobson, P.; Cacialli, F., Synthesis of type II/type I CdTe/CdS/ZnS quantum dots and their use in cellular imaging. *J. Mater. Chem.* **2009**, *19*, 8341-8346.

27. Yan, C.; Tang, F.; Li, L.; Li, H.; Huang, X.; Chen, D.; Meng, X.; Ren, J., Synthesis of Aqueous CdTe/CdS/ZnS Core/shell/shell Quantum Dots by a Chemical Aerosol Flow Method. *Nanoscale Res. Lett.* **2010**, *5*, 189-194.

28. He, Y.; Lu, H.-T.; Sai, L.-M.; Su, Y.-Y.; Hu, M.; Fan, C.-H.; Huang, W.; Wang, L.-H., Microwave synthesis of water-dispersed CdTe/CdS/ZnS core-shell-shell quantum dots with excellent photostability and biocompatibility. *Adv. Mater.* **2008**, *20*, 3416-3419.

29. Hoshino, A.; Fujioka, K.; Oku, T.; Suga, M.; Sasaki, Y. F.; Ohta, T.; Yasuhara, M.; Suzuki, K.; Yamamoto, K., Physicochemical properties and cellular toxicity of nanocrystal quantum dots depend on their surface modification. *Nano Lett.* **2004**, *4*, 2163-2169.

30. Jamieson, T.; Bakhshi, R.; Petrova, D.; Pocock, R.; Imani, M.; Seifalian, A. M., Biological applications of quantum dots. *Biomaterials* **2007**, *28*, 4717-4732.

31. Kirchner, C.; Liedl, T.; Kudera, S.; Pellegrino, T.; Javier, A. M.; Gaub, H. E.; Stolzle, S.; Fertig, N.; Parak, W. J., Cytotoxicity of colloidal CdSe and CdSe/ZnS nanoparticles. *Nano Lett.* **2005**, *5*, 331-338.

32. Wei, S. H.; Zhang, S. B.; Zunger, A., First-principles calculation of band offsets, optical bowings, and defects in CdS, CdSe, CdTe, and their alloys. *J. Appl. Phys.* **2000**, *87*, 1304-1311.

33. Deng, Z. T.; Zhang, Y.; Yue, J. C.; Tang, F. Q.; Wei, Q., Green and orange CdTe quantum dots as effective pH-sensitive fluorescent probes for dual simultaneous and independent detection of viruses. *J. Phys. Chem. B* **2007**, *111*, 12024-12031.

34. Yu, W. W.; Qu, L. H.; Guo, W. Z.; Peng, X. G., Experimental determination of the extinction coefficient of CdTe, CdSe, and CdS nanocrystals. *Chem. Mater.* **2003**, *15*, 2854-2860.

35. Deng, Z. T.; Yan, H.; Liu, Y., Band Gap Engineering of Quaternary-Alloyed ZnCdSSe Quantum Dots via a Facile Phosphine-Free Colloidal Method. *J. Am. Chem. Soc.* **2009**, *131*, 17744-17745.

36. Zeng, Q. H.; Kong, X. G.; Sun, Y. J.; Zhang, Y. L.; Tu, L. P.; Zhao, J. L.; Zhang, H., Synthesis and optical properties of type IICdTe/CdS core/shell quantum dots in aqueous solution via successive ion layer adsorption and reaction. *J. Phys. Chem. C* **2008**, *112*, 8587-8593.

37. Smith, A. M.; Mohs, A. M.; Nie, S., Tuning the optical and electronic properties of colloidal nanocrystals by lattice strain. *Nature Nanotech.* **2009**, *4*, 56-63.

38. Gurusinghe, N. P.; Hewa-Kasakarage, N. N.; Zamkov, M., Composition-tunable properties of CdSxTe1-x alloy nanocrystals. *J. Phys. Chem. C* **2008**, *112*, 12795-12800.

39. Panda, S. K.; Hickey, S. G.; Waurisch, C.; Eychmuller, A., Gradated alloyed CdZnSe nanocrystals with high luminescence quantum yields and stability for optoelectronic and biological applications. *J. Mater. Chem.* **2011**, *21*, 11550-11555.

40. Smith, A. M.; Nie, S. M., Semiconductor Nanocrystals: Structure, Properties, and Band Gap Engineering. *Acc. Chem. Res.* **2010**, *43*, 190-200.

CHAPTER 3

DNA FUNCTIONALIZATION OF QUANTUM DOTS AND THEIR DNA DIRECTED SELF ASSEMBLY

3.1. Abstract:

The assembly and isolation of DNA oligonucleotide functionalized gold nanoparticles (AuNPs) has become a well-developed technology due to the strong bonding interactions between gold and thiolated DNA. However, achieving DNA functionalized semiconductor quantum dots (QDs) that are robust enough to withstand precipitation at high temperature and ionic strength through simple 'attachment' of modified DNA on the QD surface remains a challenge. In this chapter we report a method that facilitates the synthesis of stable core and core/shell (1- 20 monolayers) QD-DNA conjugates by 'embedding' the end part (5-10 nucleotides) of the phosphorothiolated oligonucleotides within the outer shell of the QDs or by simply attaching onto the surface. These reliable QD-DNA conjugates exhibit excellent chemical and photonic stability, colloidal stability over a wide pH range (4-12) and high salt (>100 mM Na^+ or Mg^{2+}) conditions, bright fluorescence emission with quantum yield up to 70%, and broad spectra tunability with emission ranging from ultraviolet to near infrared (360-800nm). We have also synthesized DNA functionalized alloyed QD that can emit in the IR range. The DNA conjugated QDs are further self assembled as discreet well defined architecture on the DNA origami. We also fabricated hetero dimeric or multi-meric structures containing different color QDs or QDs/gold nanoparticle with precise control over the distance between them.

3.2. Introduction

Organizing inorganic nanoparticles (NPs) with nanoscale precision is of great interest to energy, nanophotonics and nanobiotechnology applications.[1-3] One of the most promising approaches for the fully programmable self-assembly of NPs, DNA nanotechnology, relies on Watson-Crick base-pairing interactions between DNA functionalized NPs and underlying DNA nano-scaffolds.[4-6] DNA-directed self-assembly of oligonucleotide functionalized gold nanoparticles (AuNPs) was first introduced by Mirkin et al.[7] and Alivisatos et al.[8] in 1996. Since then, the process of attaching thiolated oligonucleotides on citrate-stabilized AuNPs through successive salt-aging has been well-developed.[9-11] These stable DNA-AuNP conjugates have made possible the DNA directed self-assembly of one-dimensional (1D) AuNP self-similar chain and arrays,[12, 13] two-dimensional (2D) AuNP superlattice sheets,[14] three-dimensional (3D) AuNP tubes,[15] AuNP superlattice crystals,[16] and even chiral plasmonic AuNP nanostructures with tailored optical responses.[17]

However, progress in organizing semiconductor nanoparticles or quantum dots (QDs) into architectures with interesting fluorescence properties has fallen behind that of metallic NPs. To facilitate DNA-directed assembly of semiconductor QDs and achieve reliable architectures, the QDs should exhibit the following properties: 1) High chemical and photonic stability - the QDs should be highly resistant to chemical degradation and to photo-bleaching during assembly of the underlying DNA nanoscaffolds, as the annealing process involves relatively high temperatures and ionic conditions. This property requires the use of core/shell QDs. 2) Strong binding affinity between the DNA oligonucleotides and the QDs - the chemically modified oligonucleotides should not detach from the QD

surface while in solution. As such, conventional thiolated oligonucleotide binding strategies are not adequate. 3) High colloidal stability over a wide range of buffer conditions - the chemically modified oligonucleotides should not precipitate or aggregate in high salt conditions (>100 mM Na^+ or Mg^{2+}), and also should be stable in a variety of pHs. 4) High fluorescence quantum efficiency (> 50%) – this is important for applications in which the QDs are used as fluorescent markers for molecular detection or monitoring biological processes at the single particle level. 5) High spectral tunability to achieve a wide range of QD emissions (UV-Vis-NIR) - this is critical to various applications including biolabelling, light manipulation and controlled energy transfer.

Recently, DNA-protein interactions have been used to arrange QDs on DNA tile arrays and origami. In 2008, our group used biotinylated DNA-tile arrays to direct the assembly of commercially available streptavidin-conjugated CdSe/ZnS core/shell QDs into well-defined periodic patterns.[18] In 2010, Bui et al. used biotinylated DNA origami nanotubes to assemble streptavidin-conjugated CdSe/ZnS QDs into arrays.[19] Even more recently, Ko et al. used biotinylated DNA origami structures to assembly of streptavidin-functionalized QDs.[20] Unfortunately, the complexity of structures that can be formed by this method is limited, as the biotin-streptavidin interaction is not an information bearing interface.

Alternatively, QD-DNA conjugates can be designed to bind directly to an underlying DNA nanostructure through sequence specific Watson-Crick base-pairing, making it is possible to significantly increase the level of structural complexity that can be achieved. Several conjugation strategies have been developed to attach DNA oligonucleotides to the surface of QDs. Mirkin et al,[21] reported the attachment of thiol

modified (3' propylthiol or 5' hexylthiol) single stranded DNA (ssDNA) to the surface of CdSe/ZnS QDs, similar to ssDNA-AuNP conjugates. Our group reported the attachment of thiol modified ssDNA to the surface of CdSe/ZnS core/shell QDs, where the conjugation occurred during a one-step core/shell formation process.[22] Recently, Kelley et al.[23, 24] reported a synthetic route to produce phosphorotiolated-phosphorodiester-DNA (ps-po-DNA) functionalized CdTe QDs, but these core only QDs without shells are not stable, with low quantum yield (<50%). However, these QD-DNA conjugates are not as stable as their AuNP-DNA counterparts in similar buffer conditions. This is because the Au-S (ΔH = 418 KJ/mole) bonds are much stronger that the Au-O (ΔH = 221.8 KJ/mole), so the thiolated DNA can kick out the original citrate ligand on the AuNPs surface to form stable Au-DNA conjugation. But the Cd-S (ΔH = 208.4 KJ/mole) and Zn-S (ΔH = 205 KJ/mole) bonds are similar to Cd-O (ΔH =235.6 KJ/mole) and Zn-O (ΔH =159 KJ/mole) energies. As a result, these thiol ligands on the QD surface are readily displaced by other ionic species present in the aqueous buffer.

3.3. Materials and Methods

See APPENDIX B

3.4. Result and Discussion

3.4.1. DNA functionalized core/shell Quantum Dots with fluorescent emission spreading from UV-Vis to near IR

Herein we report a new strategy to achieve robust DNA functionalized core/shell QDs that satisfy all of the five requirements for DNA-directed self-assembly. The schematic is shown in Figure 3.1. illustrates the overall process of QD functionalization and subsequent DNA-origami directed assembly of the QD-DNA conjugates. Our

strategy takes advantage of chimeric ps-po-ssDNA strands that are directly inserted within a QD shell (thick CdS or ZnS shell) during synthesis over the core. This synthetic route results in core/shell QD-DNA conjugates that are chemically, photonically and colloidally stable, and highly fluorescent (PL quantum yields up to 70%), for a wide range of semiconductor materials with tunable fluorescent emissions spanning from UV to NIR (360 to 800 nm). We further demonstrated the organization of these QD-DNA conjugates by complementary base pairing to triangle and rectangular shaped DNA origami structures.

The synthesis proceeded as follows: first, water-soluble, mercaptopropionic acid (MPA)-capped CdTe QDs cores were encapsulated by thick CdS shells in the presence of ps-po-ssDNA (details in the SI pages S3-S12 and Figures S1-S9). The magic size, MPA-capped CdTe nanocrystals (1.6 nm with PL peak at 480 nm) were synthesized following the methods outlined in our previous work.[25] In a typical reaction, an aliquot of CdTe core QDs was purified and re-dissolved in 100 μL of nanopure water. A prescribed amount of Cd^{2+}-MPA complex (serving as both the Cd and S precursors for CdS shell growth) and ps-po-ssDNA (the surface ligand) were added to the core mixture. The ps-po-ssDNA oligonucleotides (5'-G5-ps-T28-3') contain a stretch of five consecutive guanine residues, followed by five consecutive ps backbone modifications and 28 unmodified thymine residues linked by conventional phosphodiester bonds. The pH of the mixture was adjusted to 12 and subsequently heated at 90 ^{o}C for 70 minutes. During this time, the Cd^{2+}-MPA complex slowly decomposes and a CdS shell of particular thickness surrounds the CdTe core. The 5 sulfur atoms in the ps domain 'insert' into the CdS shell during its formation, while most (if not all) of the poly T domain extends away

from the surface of the shell making it available for hybridization to complementary DNA within the underlying DNA nanostructure. As we reported previously, at this relatively mild temperature the monolayer-by-monolayer formation of the CdS shell is fully controlled by the slow decomposition of the Cd^{2+}-MPA complex.[25] Here, the shell thickness is directed by the total reaction time. We observed that 7 CdS shell monolayers are formed in 70 minutes, thus, the estimated synthesis time is 10 minutes/monolayer. Considering the relatively slow rate of growth, the S atoms in the ps-domain of the oligonucleotides have ample opportunity to bond to the Cd atoms and are readily incorporated into the CdS shell. The numbers of the ssDNA on one QD are estimated to be 9, as calculated in the SI Figure S9 based on the UV-Vis absorption spectra.

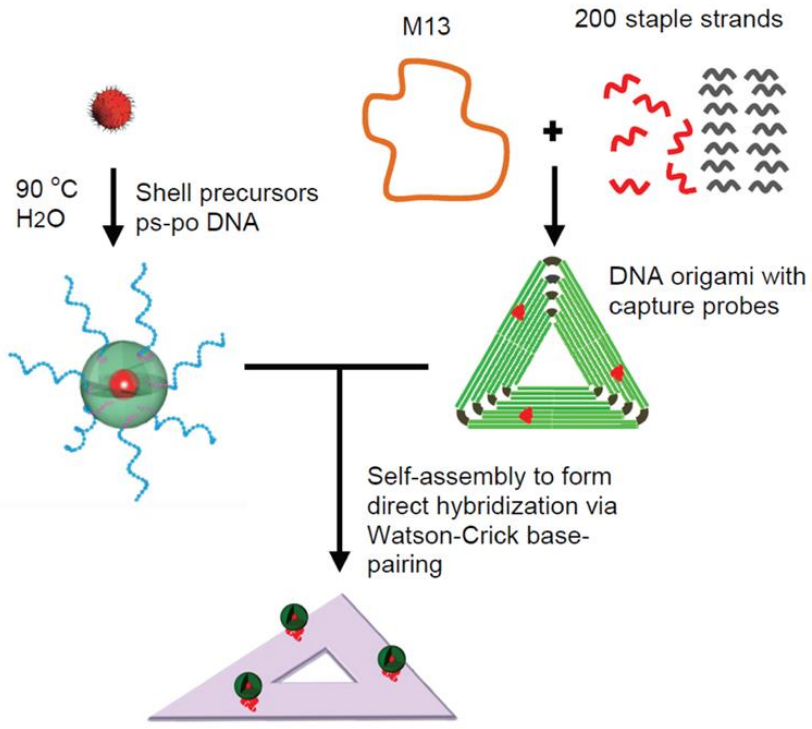

Figure 3.1. DNA functionalization of core/shell QDs and organization by self-assembled DNA origami. Core/shell QDs are functionalized with oligonucleotides during shell

growth in aqueous solution. The resulting core/thick-shell QDs are chemically, photonically, and colloidally stable, displaying PL quantum yield up to 70% and broad spectra tunability from UV to near infrared. In this novel method the shell growth temperature is held constant at 90 ^{o}C, with reaction times ranging from 20 to 120 min. The DNA oligonuclotides contain phosphorotiolated (ps) domains (5-10nucleotides) for 'nailing' (shown in violet color) the DNA into the outer QD shells, and for 'recognition' (shown in blue) by DNA capture probes within origami structures (containing a typical phosphodiester backbone). The QD core (shown in red) can be QDs synthesized in aqueous solution or organic solvent. The shells (shown in green) are CdS or ZnS. In the meantime, self-assembled DNA origami was synthesized by thermal annealing of M13 DNA with staple and capture strands. Finally, hybridization of the recognition domain of the QD-DNA conjugates to complementary capture strands (shown in red) displayed from the surface of the DNA origami yield higher order architectures

The resulting core/shell CdTe/CdS QD-DNA conjugates have an estimated diameter of 6.5 nm (7 CdS shell monolayers), with band-edge emission maxima at 672 nm and PL quantum yield of 70%. The observed about 200 nm red shift of the emission peak is assigned to quasi-type-II QDs.[12] The TEM and HRTEM images reveal that the QD-DNA conjugates are monodispersed, single crystalline particles (Figure 3.2a). The QD-DNA conjugates are synthesized and stabilized in solution with a pH of 12. The purified thick-shell QD-DNA conjugates are stable in a variety of buffer conditions, including 1X PBS buffer with a pH of 4.0, 7.0 and 10.0; 1X TAE-Mg^{2+} buffer; 1X TBE Mg^{2+} buffer; and 10 X TAE-Mg^{2+} buffer (125 mM of Mg^{2+}) (Figure 3.2c). Thus our QD-

DNA conjugates are colloidal stable over a wide pH range (4-12) and high salt (>100 mM Na^+ or Mg^{2+}) conditions.

These CdTe/7CdS QD-DNA conjugates were subsequently assembled at precise positions on DNA origami structures via hybridization to complementary poly A capture probes extended from the surface of the origami (3 capture probes/1 QD-DNA). We demonstrated the organization of two or three QD-DNA conjugates on triangular and rectangular DNA origami, as shown in Figure 3.2d-h. The self-assembled structures were evaluated by atomic force microscopy (AFM) and scanning transmission electron microscopy (STEM) imaging techniques. The images in Figure 3.2d-e confirm that over 95% of the triangle DNA origami structures display three QDs, one on each arm, as prescribed by the design (design details and additional images can be found in the SI Figures S24-S25, Page S27-S41). Meanwhile, 90% of the rectangular origami structures display two QD-DNA conjugates, one each at opposite corners, as directed by the design scheme (Figure 3.2f-g). The height profile of the AFM images reveals that the size of the QD-DNA conjugates fall into a narrow range (6-7 nm).

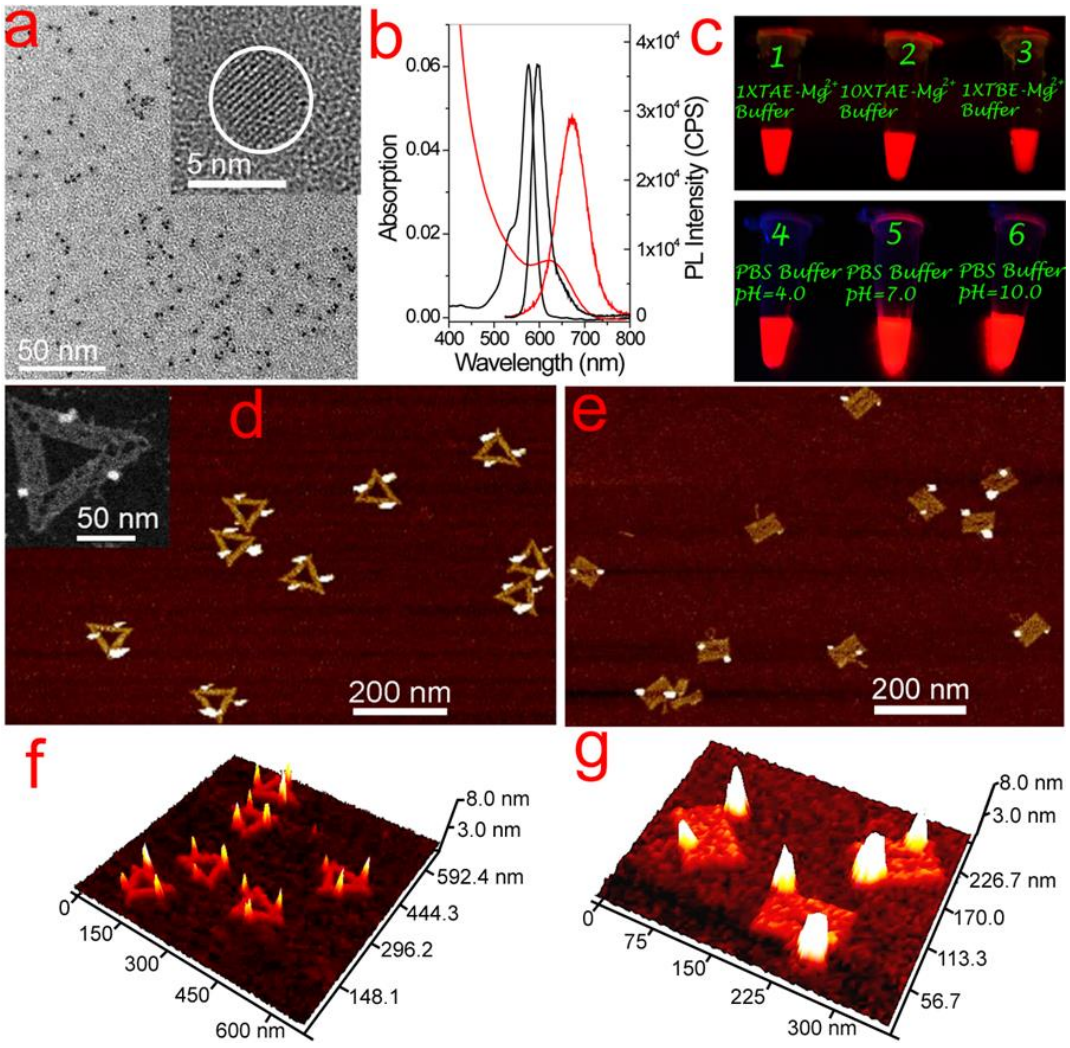

Figure 3.2. DNA functionalized core/shell CdTe/7 CdS QDs with MPA-capped magic-sized CdTe cores and emission at 672 nm. a, TEM and HRTEM images of the QD-DNA conjugates. b, The red traces correspond to the UV-Vis absorption and PL emission spectra of the conjugates, and the black traces correspond to the Rhodamine101 for PL quantum yield measurements. A comparison to the PL intensity of the reference dye reveals the QD-DNA conjugates display 70% QY. c, Photographs of the QDs illuminated by a 365 nm UV lamp in several different buffer conditions: 1-6: 1XTAE Mg^{2+}, 10X TAE-Mg^{2+}, 1X TBE-Mg^{2+}, PBS buffer with pH of 4, 7, 10. d,e,f,g, AFM images and

height profiles of the CdTe-CdS QDs organized by triangular (three QDs total - one QD/per arm) and rectangular (two QDs total in opposite corners) DNA origami structures. Inset in d, STEM image of CdSe/7CdS QD-DNA conjugates assembled on triangular DNA origami structures. Here the triangular shape of the DNA origami template is clearly visible after the sample was negatively stained using uranyl formate.

We further synthesized thick shell CdSe/CdS QD-DNA conjugates that contained 20 CdS monolayers. As reported by Hollingsworth et al.[26] and Dubertret et al.[27], "giant"-shell or thick-shell QDs are more chemically stable and exhibit reduced blinking behavior at the single particle level. Thick-shell QDs have been achieved by the successive ionic layer adsorption and reaction (SILAR) method which requires high temperatures (240 ^{o}C) and a tedious growth process in organic solvent. Here, we developed a new method to achieve thick-shell CdSe/20 CdS QDs at lower temperatures (90 ^{o}C) in aqueous solution. More significantly, we incorporated the ssDNA within the shell itself during the encapsulation process. First oleic acid (OLA) capped CdSe core QDs (6 nm diameter) were synthesized in paraffin liquid at 320 ^{o}C (Figure 3.3a&d and details in the SI pages S13-S21 and Figures S10-S17).[28] The oleic acid capped CdSe cores had a diameter of approximately 6.0 nm and fluorescence emission at 650 nm. Next, 9 CdS shell monolayers were deposited on the CdSe core in aqueous solution at 90 ^{o}C with MPA serving as the capping ligand. After the ligand exchange and CdS shell growth, the tetrahedral shaped MPA-capped QD exhibited emission at 660 nm. The approximate length of these tetrahedral shaped QDs was 12 nm (Figure 3.3b,e). Finally, the additional shells were incorporated on the QDs in the presence of ps-po-ssDNA. The resulting DNA oligonucleotide functionalized thick-shell CdSe/CdS QDs displayed emission at 663 nm.

The length of the QD-DNA conjugates increased to 18 nm (Figure 3.3c&f). The relatively small red shift in emission wavelength that occurred upon shell growth is because these core/shell QDs with large core size (6 nm diameter). When we encapsulated small CdSe core QDs (3 nm diameter) with a thick-shell, we observed a 70 nm PL red shift (from 565 to 635 nm see SI Figure S10). This may be due to a strain induced PL shift.[29]

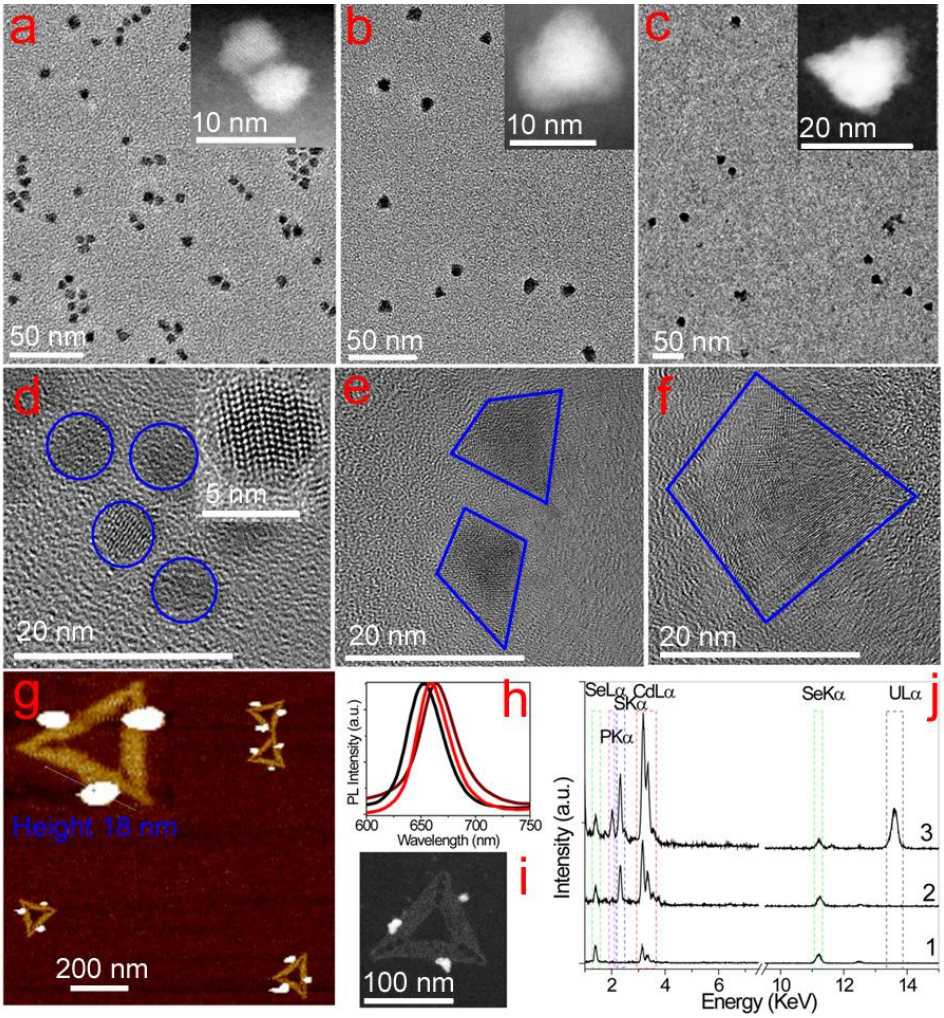

Figure 3.3. Characterization of various stages during the synthesis of CdSe/20 CdS QD-DNA conjugates. a-f TEM, HRTEM, and STEM images of the oleic-acid capped CdSe core QDs (a and d are spherical with 6 nm diameter), core/shell CdSe/9 CdS QDs (b and

e are tetrahedral with 12 nm length), and core/thick-shell CdSe/20 CdS QD-DNA conjugates (c, and f are tetrahedral with 18 nm length). Insets in a, b and c contain the STEM images. g, i AFM image, height profile (inset) and STEM image of CdTe/20 CdS QD-DNA conjugates organized by triangular DNA origami. h, j PL and EDS spectra of the samples. In h and j, the black and "1" curves are for CdSe, the red and "2" curves are for CdSe/9 CdS, and the wine and "3" curves are CdSe/20 CdS-DNA.

We demonstrated that these robust, thick shell QD-DNA conjugates are readily organized by addressable DNA origami structures to form, discrete, well-ordered nanoarchitectures. In addition, DNA origami are an ideal platform to confirm the successful DNA functionalization of the QDs, which is more straightforward and reliable than the previous QD-DNA-dye FRET method.[8b] As demonstrated in Figure 3.3j, energy dispersive X-ray spectroscopy (EDS) of the self-assembled origami nanostructures reveals the presence of cadmium, selenium, sulfur, phosphorus from the CdSe/20 CdS QD-DNA conjugates (Figure 3.3j).

We also wanted to show that this strategy is quite versatile and can be applied to QDs composed of other semiconductor materials. For example, we sought to demonstrate that a ZnS shell can be deposited on a variety of different core materials using the same strategy. Using a water-soluble ZnSe core,[30] we produced ZnSe/4 ZnS QD-DNA conjugates that displayed UV emission at 360 nm (Figure 3.4 and details in the SI pages S22-S27 and Figures S18-S23). Using oleic acid capped CdS or quaternary alloyed ZnCdSSe QD core materials,[31] we synthesized CdS/4 ZnS-DNA conjugates with blue emission at 425 nm and ZnCdSSe/4 ZnS QD-DNA conjugates with green emission at

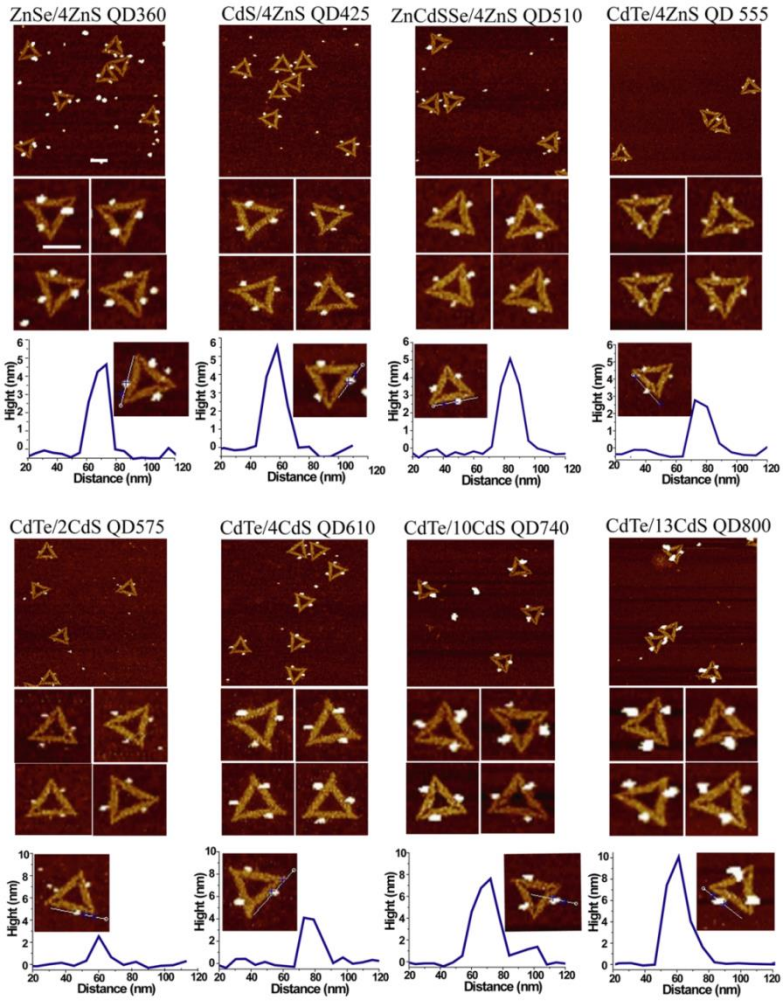

Figure 3.4. A series of DNA functionalized core/shell QDs with tunable fluorescence emission from UV to near infrared. Zoom out and in AFM images and corresponding height profiles of QD-DNA/DNA origami structures. The conjugates have the following emissions and compositions: UV-emitting (360 nm) ZnSe/4 ZnS QDs, blue-emitting (425 nm) ZnSe/4 ZnS QDs, green-emitting (510 nm) ZnCdSSe/4 ZnS QDs, yellow-emitting (555 nm) CdTe/2 ZnS QDs, yellow-emitting (575 nm) CdTe/2 CdS, orange-emitting (610 nm) CdTe/4 CdS, NIR-emitting (740 nm) CdTe/8 CdS, and NIR-emitting (800 nm) CdTe/13 CdS, respectively. The scale bars are 100 nm.

510 nm, respectively. Further, we produced CdTe/4 ZnS QD-DNA with yellow emission at 555 nm. Finally, we used magic-sized CdTe core QDs to synthesize a series of DNA functionalized QDs, including: CdTe/2 CdS, CdTe/ 4CdS, and thick-shell CdTe/10 or 13 CdS QDs in the orange, red, and near infrared with emission maxima at 575, 610, 740, and 800 nm, respectively. The organization of each of QD-DNA conjugates by DNA origami was demonstrated in Figure 3.4. The height profiles of the particles obtained from AFM cross-sections correspond well to the sizes measured using TEM imaging.

Given that CdS and ZnS are wide band gap semiconductor materials that are generally used in QD shells, it is reasonable to expect that many other core/shell QDs can be synthesized with various core compositions, such as binary PbS, InP, InAs QDs for IR emission, doped ZnSe:Mn QDs, ternary alloyed CuInSe or ZnCdSe QDs, and quaternary alloyed CuInSSe, etc, all of which should be compatible with the oligonucleotide functionalization strategy reported here.

3.4.2. DNA functionalized visible light emitting QDs with reduced blinking

Colloidal semiconductor Quantum Dots (QDs) have been the subject of great scientific and technological interest because of their unique size dependent properties and potential use in bioimaging applications and optoelectronic devices. One more advantage QDs offer is their resistance to bleaching which is a serious problem for organic fluorescent dye because it imposes a restriction on the duration of measurement. However, QDs are infamous for another significant drawback called blinking.[32-34] If a single Quantum Dot is observed under the microscope, a random fluctuation in its intensity will be noticed in pite of continuous excitation. This intermittency of fluorescence intensity is called blinking. This is problematic for their use as single

fluorophore and tracking tag and indeed there are very few reports on QDs used for single molecule spectroscopy.[35-37] Why this random switching between ON and OFF state is, is a long debated issue.[33, 38-53] A general consensus was the extra charge that builds up in the nanocrystal increases the probability of non-radiative decay.[54] When multiple excitons form inside a QD, due to their strong interaction, ejection of either an electron or a hole can results in a charged QD. When the very next exciton forms in a charged QD, it prefers to decay through non-radiative charge recombination pathway which creates an OFF state leaving again a charged QD. As long the QD is not neutralized by the external charge, it remains in the charged state. Recently Galland et al reported an extraordinary finding of another parallel mechanism of blinking.[55] They proposed some trap energy state which devours the "hot electrons" (The electrons that are excited above the lowest energy state of the conduction band) which finally comes back to the ground state without emitting any photon. Now there are several reports available in the literature to reduce the blinking.[56-60] They are mainly focused on modifying the structure of the QDs, for example, forming a thick shell. Thick shell can repair the defects on the surface of the core particle which are claimed to be potential trapping site. Mahler et al reported a CdSe/CdS core shell QD of diameter 13nm which has shown suppressed blinking.[27] Wang et al reported CdZnSe/ZnSe which has exhibited suppressed photoluminescence for hours.[56] In spite of this significant development in this area, bio-functionalized QDs with reduced or completely suppressed blinking is still unavailable to the best of our knowledge which is important as far as biological tracking is concerned.

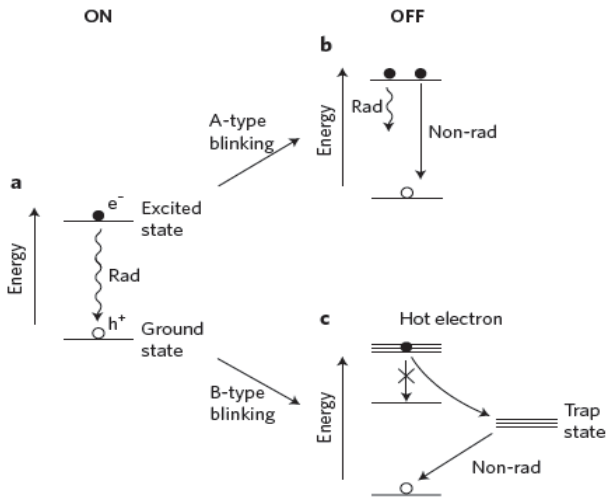

Figure 3.5. Schematic depicting the mechanism of blinking (a) ON state with normal exciton recombination emitting photons (b) OFF state that involves a charged state which enhance the decay of exciton in a nonradiative pathway. (c) OFF state involving trap state that devours the 'hot' electrons which finally comes back to the ground state without emitting photon. Reproduced with permission Krauss et al. *Nat. Mater*. **2012**, 11, 14-16,

Here we have reported CdSe/CdS QDs functionalized with DNA that has shown no blinking over the time frame of several minutes. DNA conjugated QDs allow us to incorporate any sequence on the surface which can be some cell specific aptamer or could bind other biomolecule. The detail synthetic procedure has been reported earlier. The DNA functionalization is proved by their site specific organization on the DNA origami. An AFM combined confocal that is capable of single molecule detection was used for the measurement. A normal CdTe QD was first tested. Due to its small size (~2nm) it could not sustain under the strong laser irradiation. A CdTe/CdS QDs with 6nm in diameter shows very strong blinking. DNA conjugated CdSe/CdS/ZnS QDs with diameter of 20nm showed great reduction in blinking probably due the thick layer of shell on the 6nm

core CdSe particles (10 mono-layers of CdS and 10 mono-layers of ZnS). The corresponding EDS spectrum shows the presence of Phosphorous along with other materials confirms the presence of DNA onto the particles.

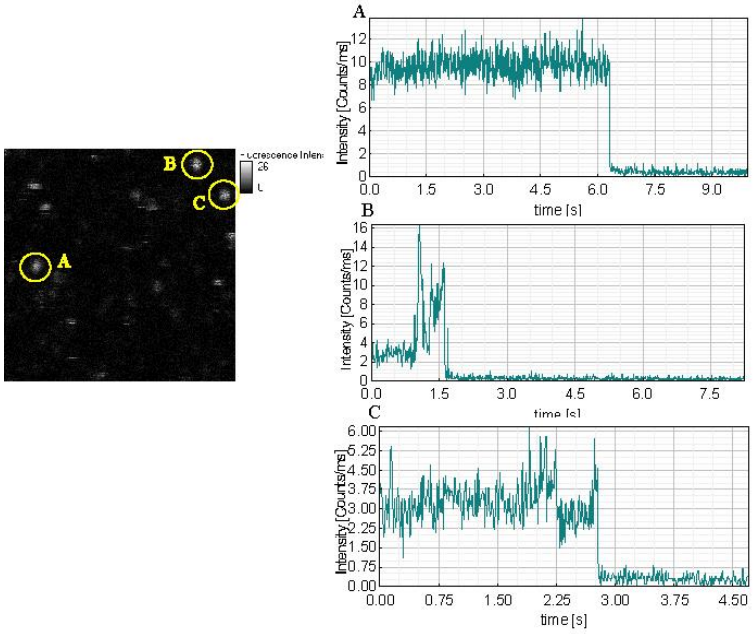

Figure 3.6. DNA functionalized CdTe QDs (Emission maxima 580nm) are being investigated in single molecule spectroscopy set up. Left: Fluorescence intensity (without AFM), moderate excitation. Right: time traces of the three bright spots after the scan.

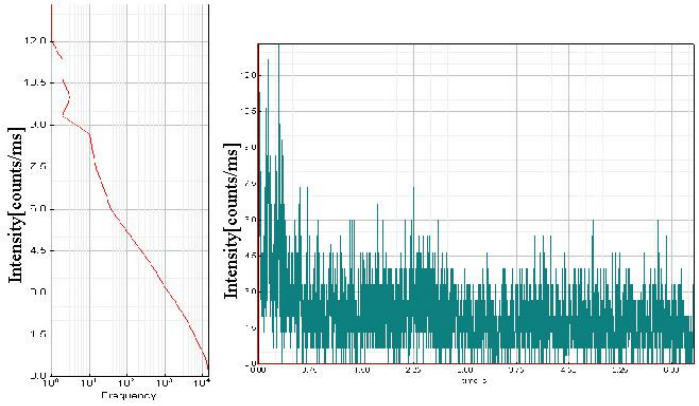

Figure 3.7. Left: DNA conjugated CdTe/CdS QDs with emission maxima at 610nm is being investigated under single molecule spectroscopy set up. Average photon count per millisecond. Right: Actual fluorescence intensity over the time period of 6 seconds. Strong blinking is evident**.**

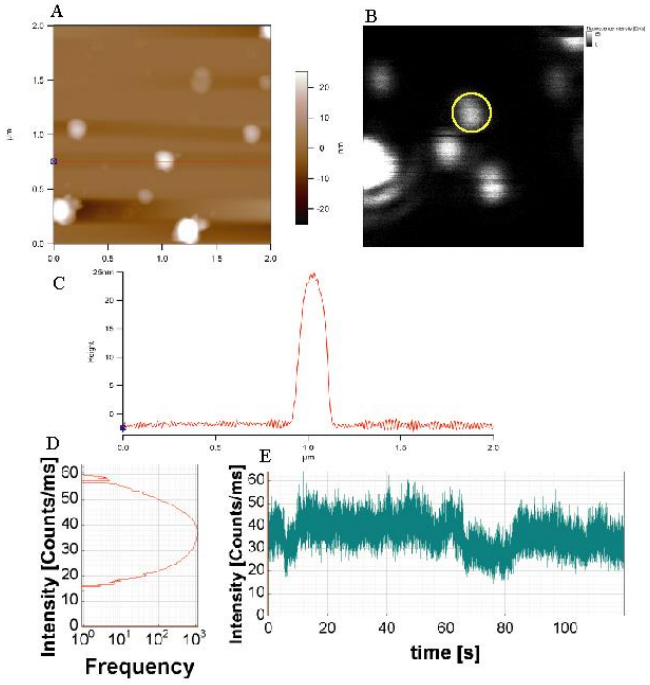

Figure 3.8. DNA conjugated CdSe/CdS QDs with emission maxima at 610nm is being investigated under single molecule spectroscopy set up (A) AFM image of the DNA

functionalized CdSe/CdS/ZnS QDs immobilized on DNA origami. (B) Corresponding confocal image. (C) AFM height profile. It shows the particle is 25nm in diameter. (D) Average photon count per millisecond (E) Actual fluorescence intensity over the time period of 4 minutes.

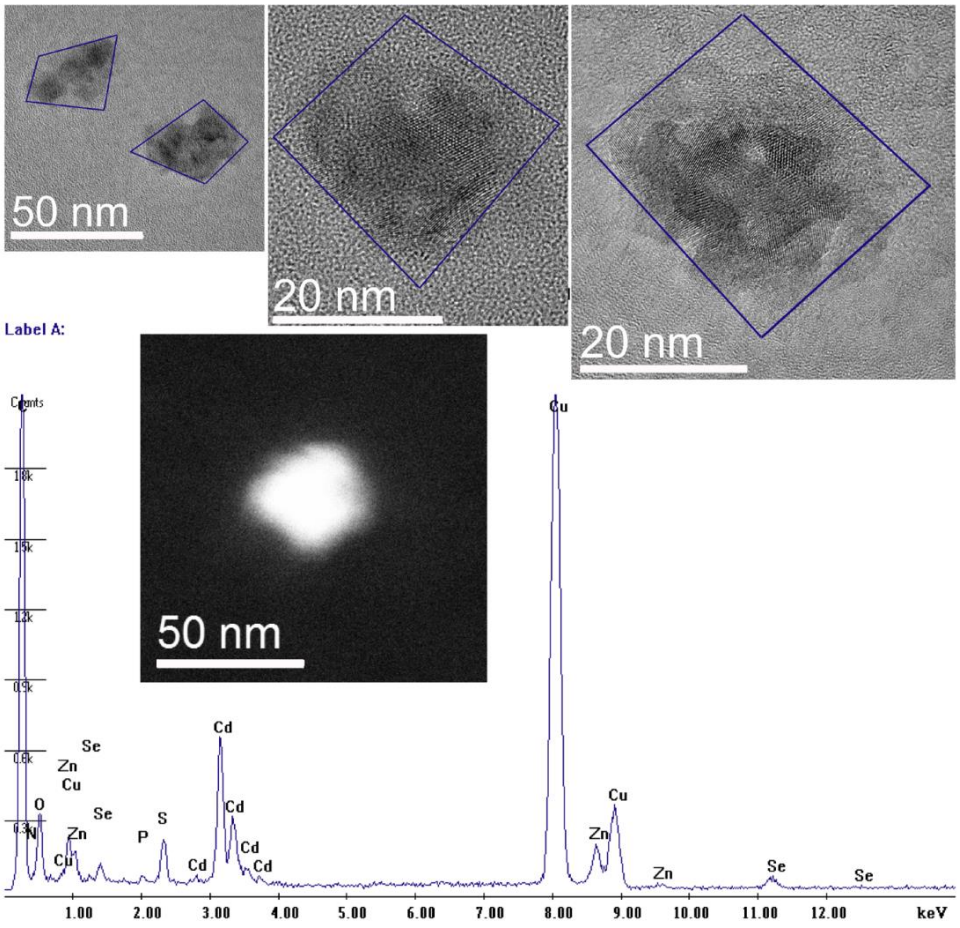

Figure 3.9. HRTEM image giant CdSe/CdS/ZnS Core/Shell/Shell QDs 6nm CdSe core, 6nm CdS inner shell and 6nm outer shell ZnS Shell. The EDS spectrum shows the presence every element along with S and P which is coming from the ligands and DNA respectively.

3.4.3 DNA based assembly of QDs with increased complexity

In the previous section we have demonstrated organization of QDs on triangular origami on its three arms or on the two corners of a rectangular origami. With the help of DNA nanotechnology we can create more sophisticated assembly of QDs. Here we have organized four QDs in close vicinity on an arm of the triangular origami. Overall yield of the desired structure was above 50%. The motivation behind making this structure was to create a Quantum rod from the bottom up self assembly of Quantum dots. We expected to see some sort of tunneling effect which would be reflected in the emission spectra. Unfortunately the intended effect was not observed. We speculated that the reason behind this is the presence of abundant amount of unbound QDs in the solution which submerged the effect. We could not develop any reliable method till today to purify this structure from the excess free QDs.

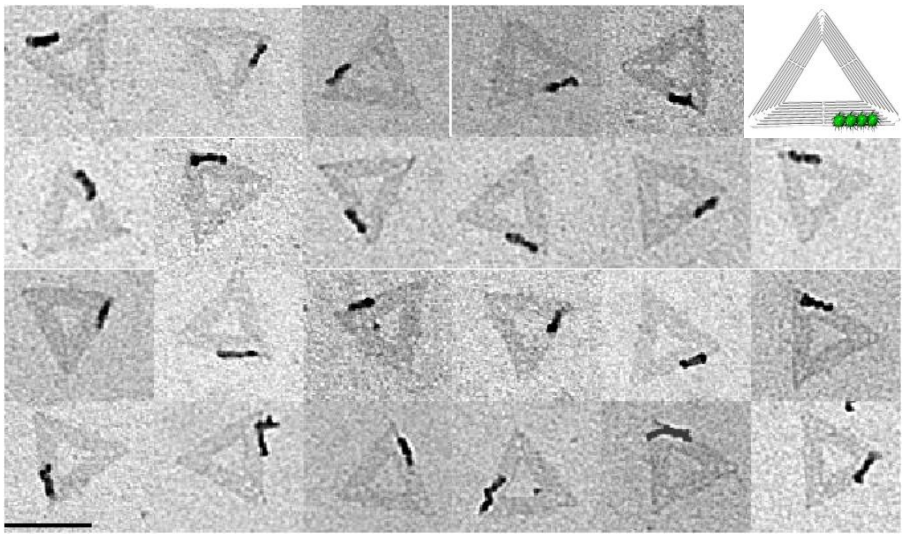

Figure 3.10. Zoom in TEM images of 4QDs assembled in close vicinity on one arm of the triangular origami.

So far I have discussed about the self-assembly where DNA origami has been used as scaffold for organizing QDs that emit same color photons, more or less if we ignore the inhomogeneity for a moment. But DNA nanotechnology offers much more than that. DNA tile based array has been used for periodic patterning of nanoparticles or biomolecules.[61] Sharma et al demonstrated periodic array of gold nanoparticles formed by self assembly of 4 arm junction tile.[62] Sharma et al in 2008 reported periodic array of streptavidin coated QDs on the self assembled 2D array of DX tiles.[18] In 2007, Chhabra et al created a multiprotein nanoarray by the self assembly of DX tiles bearing aptamer for the specific proteins.[63] Potentially DNA tile can be used for creating periodic array of two or little more than two types of nano-elements. But one major problem with DNA tile based array is the absence of a clear boundary. So its utilization for real application is always questioned. However, DNA origami can serve this purpose of creating multicomponent nanostructures. As I already mentioned previously they are discrete nanostructure with well-defined boundary, which is made by folding a circular single stranded 'scaffold strand' with numerous small synthetic 'staple strands'. Recently Lin et al. has reported a library of molecular bar code with sub micrometer dimension embedding some fluorescent molecule into an origami tube.[64] With the emergence of super resolution microscopy this kind of molecular bar code can be really useful for bio-medical imaging in the coming days. The two disadvantages of using organic dye is (a) Bleaching; which means they are not very stable under the exposure of strong laser irradiation for long time. (b) Different excitation light has to be used for exciting specific dye. QDs are excellent candidate to circumvent these two drawbacks. QDs are famous for their optical and chemical stability. And because of their broad absorption but narrow

emission spectra, they are perfect for multiplex imaging. For example, a green light emitting QD and a red light emitting QD can both be excited at 400nm. So for imaging different part of a cellular body they are unparalleled. Here we report the construction of different color QDs on the same DNA body. With streptavidin coated QDs these are difficult to achieve which requires multiple steps. Another problem associated with streptavidin coated QDs is their big size. They core QD is encapsulated with a cross-linked polymer and on the top of that the bulky proteins. To achieve this multicolor assembly, selected staple strands at specific location of the origami was extended with a DNA sequence that will be complimentary to the DNA displayed on the QD surface. For two colors assembly two different sequences were chosen. This is also been extended for three colors QDs where three different types of capture strands was used. The sequences of the capture strands and the DNA displayed on the QD surface can be found in supplementary information. To organize the QDs, first the DNA template was annealed and then purified. Annealing condition and method of purification has been described before. After that DNA functionalized QDs emitting different color was mixed with the DNA origami and annealed from 40°C to 4°C for 24hrs. The resulting hybrid structure was characterized under AFM (Figure 3.11 (a), (b), (c)). We have constructed three double colors construct, G-Y, G-O and G-R, where G, Y, O and R represents green, yellow, orange and red QDs. From the AFM height profile it shows green QD is ~3.5nm in diameter, yellow QD is ~4.5nm, orange QD is ~5.5nm and red QD is ~6.5nm. The height may not represent their actual size as the double stranded DNA can contribute something here. The statistical yield was obtained by counting more than 100 constructs. It shows the yield is best in case of G-Y and worst in case of G-R. Several other

combinations can potentially be achieved. We have extrapolated this double color to triple color system where green, yellow and red QDs have been organized on one arm of the origami. The zoom in AFM images and corresponding height profile has been shown in the figure bellow.(Figure 3.11 (d)) The yield of the desired structure was ~20%. Since we could not purify these structures, its applicability cannot be realized immediately. Apart from using them as spectroscopic bar code, these kind of system are suitable for understanding the energy transfer mechanism between two QDs. FRET like energy transfer between QD and organic dye has been investigated to great extent. DNA origami offers a rigid platform with excellent addressability which is very useful for stoichiometric control. We left an open question here.

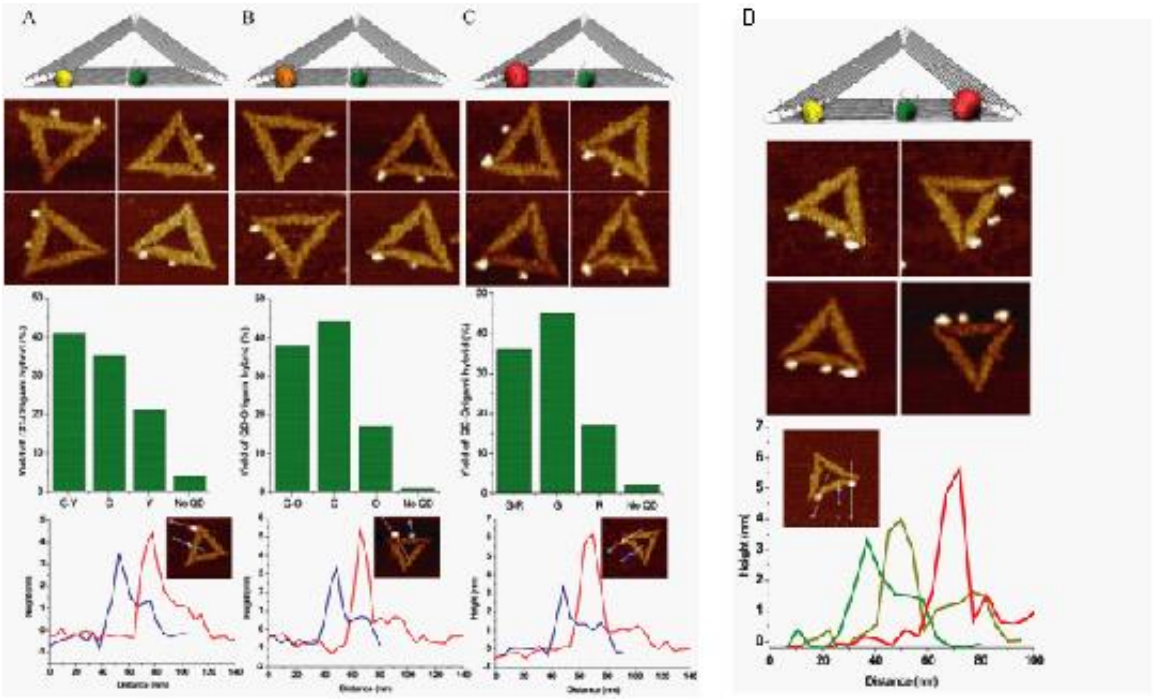

Figure 3.11. Left (A) (B) and (C) panel represent schematic drawing, zoom in AFM images, statistical yield, and height profile of G-Y, G-O and G-R respectively. Right (D)

yellow, green and red QDs are organized which can be easily seen in the attached AFM images.

We have taken the hybrid nanomaterials to a different level by putting together semiconductor and metallic nano particles on the same origami platform. Engineering distance between the constituent particles, novel optoelectronic properties can be achieved. We have chosen gold nanoparticles as the metallic part and QDs as the semiconductor. Gold nano particles are of special interest due their unique Surface Plasmon Resonance. This resonance condition depends on the size and shape of the particles as well as on the dielectric constant of the metal and surrounding media.[65] SPR is basically the collective oscillation of electrons in the conduction band of gold when irradiated with light. The absorption coefficient of the palsmon resonance is much higher than the traditional organic dyes which are very useful for detection purposes.[66] Also gold nanoparticles enhance electric field localized to its surface which can be used to enhance the raman or fluorescence signal.[67-70] Previous studies have shown that presence of proximal gold nano particles changes the fluorescence intensity. The change could be enhancement or quenching depending on the win of a competition between field enhancement and non-radiative energy transfer.[71, 72] Although, as mentioned, previous studies do exist, still control over the stoichiometry and distance is an area which requires improvement for better understanding of the mechanism. DNA origami technology offers both with an impressive record. It is the latest discovered molecular peg-board with a pixel size of 6nm because each staple strand at each specific location has unique sequence.[73] This unprecedented addressability has drawn serious attention in multidisciplinary research.[74, 75] But there are reports where QDs and gold nanoparicles

have been organized with nanometer precision on the orgami scaffold which has helped to engineer the optical properties of QDs.[20] But the QDs that have been used are streptavidin coated QDs. Streptavidin coated QDs are large in size. On the top of CdSe/ZnS core shell structure, they have a shell of cross-linked polymer followed by large streptavidin proteins. Exact distance is a matter of speculation. More precise information should be obtained with DNA conjugated particles only.

To obtain the desired structure, a two steps process was followed. First, origami was annealed with M13, the normal staple strands, modified capture strands carrying the complimentary sequence that is displayed on the QD surface and the gold nanoparticle. The gold nanoparticle was 10nm in diameter and has one DNA on its surface. The DNA displayed on its surface, when annealed will be inserted into the structure as a part of the staples strands. In the AFM image represents the unpurified structure which shows one gold nanoparticle at one end of the origami (Figure 3.13). In the second step the DNA conjugated particles were annealed with the purified pre-engineered origami bearing the gold nanoparticle. Three different color QDs are placed at three different positions with varying distances. A zoom out AFM image shows the yield is above 50%. The zoom in AFM and TEM image clearly show the architecture with various distances. Corresponding AFM height profile also reveals information about the size of the particles. Unfortunately we were unable to develop any method to purify these constructs to get rid of excess QDs. So the effect of gold nanoparticles on the fluorescence intensity and lifetime of the QDs could not be studied in bulk. However, a single molecule measure is always an open option to investigate it which is our future plan.

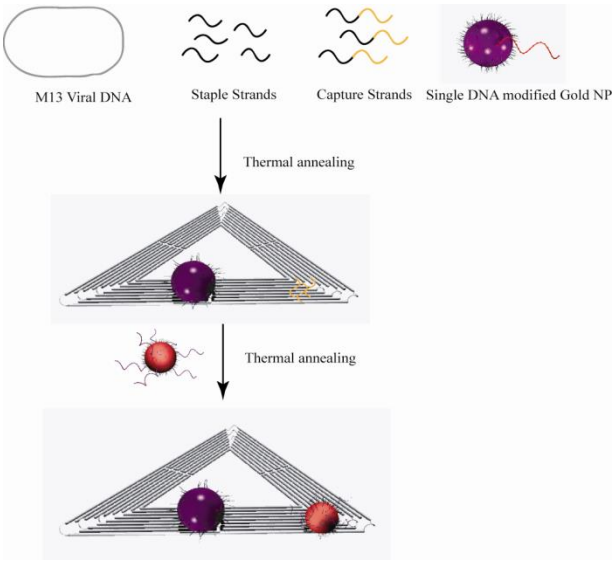

Figure 3.12. Schematic depicting the two step assembly of gold nano particles and QDs on the triangle origami.

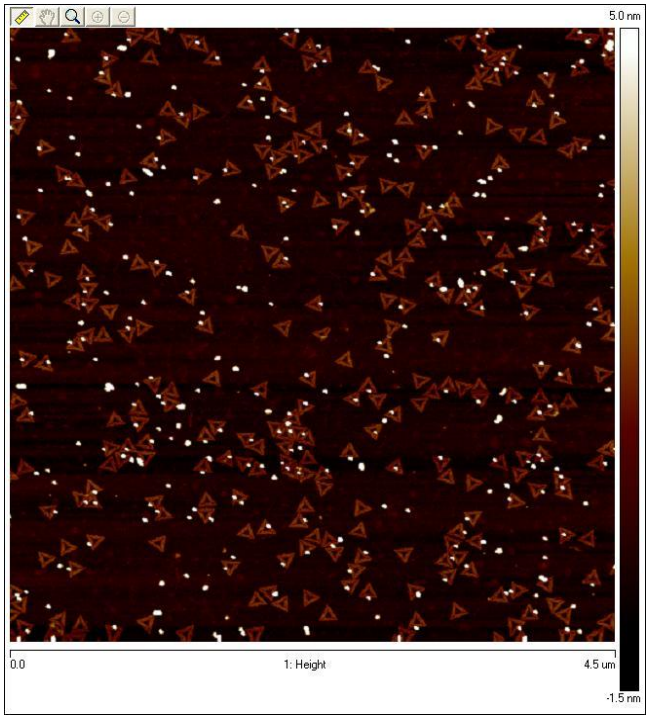

Figure 3.13. Zoom out AFM image of the unpurified triangle origami bearing a 10nm gold nanoparticle positioned at the center of one arm.

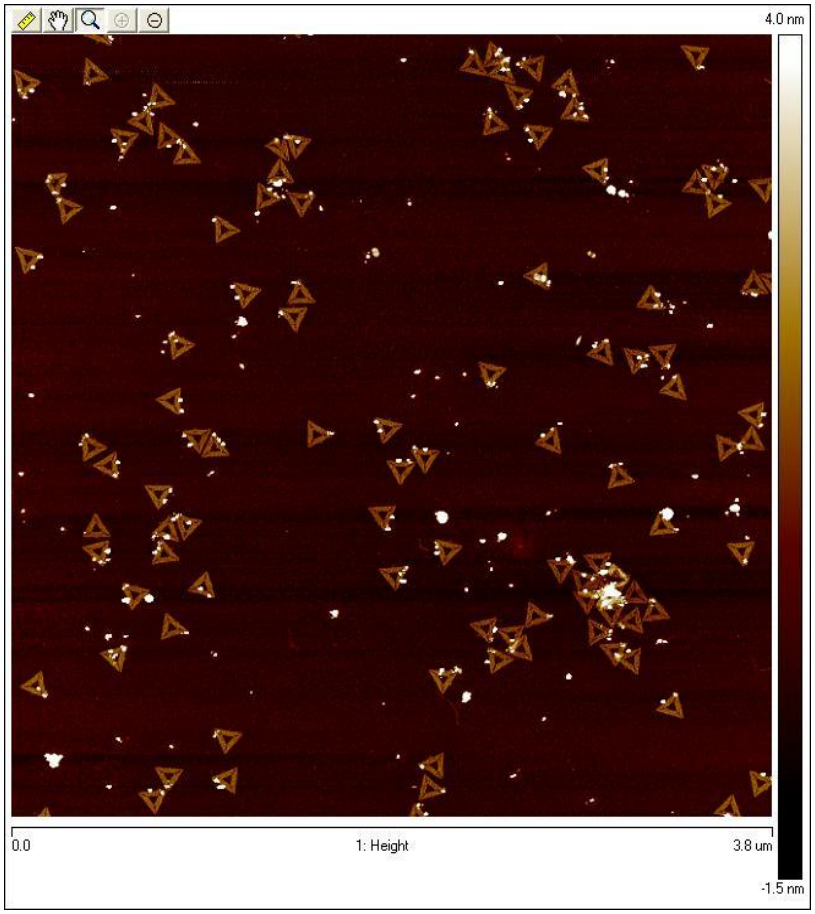

Figure 3.14. Zoom out AFM image of the unpurified triangle origami bearing 10nm gold nanoparticle and a QD.

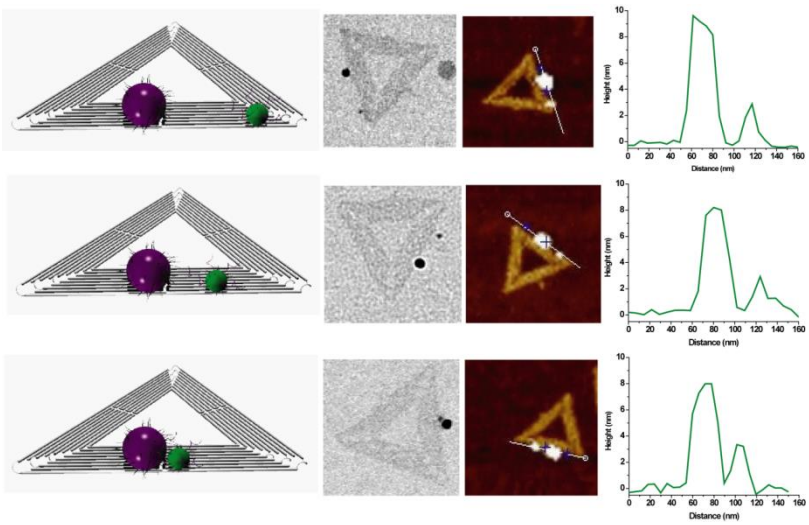

Figure 3.15. Zoom in TEM and AFM image of the triangle origami displaying one 10nm gold nanoparticle and QD emitting at 520nm positioned at three different distances. Corresponding height profile shows QD is around 2.5nm in diameter which matches well with the TEM image.

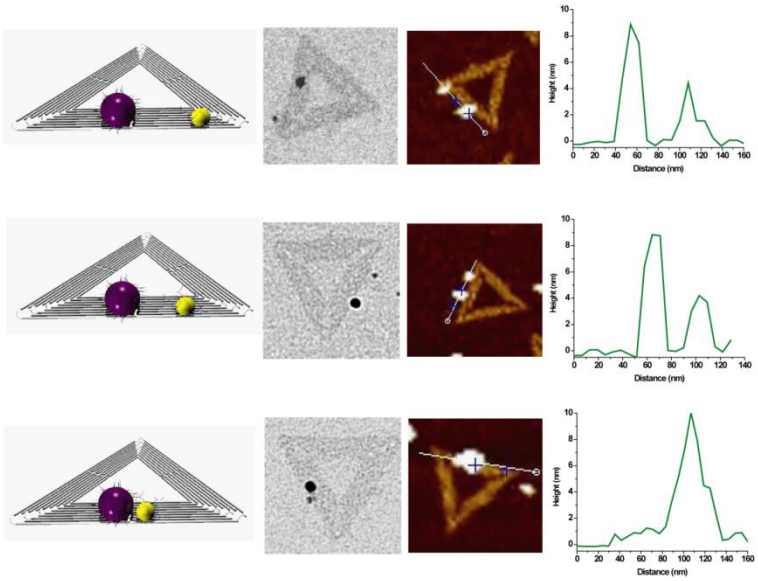

Figure 3.16. Zoom in TEM and AFM image of the triangle origami displaying one 10nm gold nanoparticle and QD emitting at 575nm positioned at three different distances.

Corresponding height profile shows QD is around 4nm in diameter which matches well with the TEM image

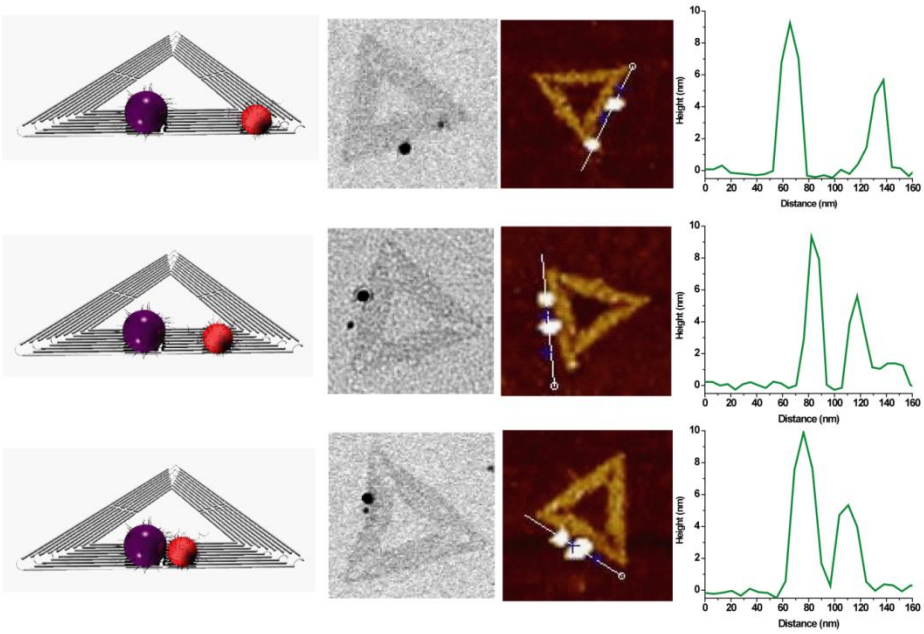

Figure 3.17. Zoom in TEM and AFM image of the triangle origami displaying one 10nm gold nanoparticle and QD emitting at 610nm positioned at three different distances. Corresponding height profile shows QD is around 5.5nm in diameter which matches well with the TEM image.

3.4.4. Infrared Emitting Quantum Dots: DNA Conjugation and DNA Origami Directed Self-Assembly

QDs that emit in the Infrared (IR) range are of special interest at the moment because of their potential as tissue imaging reagents. Due to autofluorescence from tissues, QDs that emit in the visible range fail to produce good signal to noise ratios. Here we report the production of $Cd_xPb_{1-x}Te$ tertiary-alloyed QDs that emit in the 1100-1300 nm wavelength range, capped with the hydrophilic ligands mercaptopropionic acid (MPA) or glutathione (GSH), together with DNA, as specific surface tags. We observed

an interesting dependence of the QD emission peaks on the species of capping ligand used. ICP-MS analysis confirmed that changing the identity of the surface ligand in the reaction mixture shifted the elemental composition of the particles and resulted in different Cd/Pb ratios. Further, DNA directed assembly of the particles onto DNA nanostructures ensures that the particle remains stable in high salt conditions, which is crucial to biological applications.

In the past decade, quantum dots (QDs) have emerged as an important subject of research due to their unique optical properties and their potential use in bio-imaging and bio-labeling applications. Tremendous developments have occurred in the synthesis and characterization of various types of QDs.[76-78] Visible light emitting QDs have been commercialized for various labeling purposes. However, the ultimate objective of using QDs for *in vivo* optical fluorescence imaging of human or animal tissues for disease diagnosis and early detection has yet to be realized. Absorption by hemoglobin, melanin, and various proteins, and the auto fluorescence from tissues themselves limit the depth of tissue penetration of any quantum emitter in the visible light range.[79] QDs that emit at near infrared (NIR) and mid-IR regions of the electromagnetic spectrum are superior, since the absorbance and auto fluorescence of biological samples are dramatically lower in this spectral window.[79]

In 2004, Kim et al. demonstrated the use of CdTe/CdSe core/shell QDs emitting in the near IR (850 nm) for real time surgical aids.[80] Water soluble Ag_2S QDs that emit in the near infrared zone has been reported that can be used for targeted imaging of different cell lines and in vivo imaging.[81-85] Alloyed and core-shell QDs that emit in the NIR region have been synthesized in both organic and aqueous media.[25, 86-88] However, in

order to achieve QDs that emit in the true IR range, materials with smaller band gaps must be used. Several strategies have been reported to synthesize IR emitting QDs from low band gap materials, including lead chalcogenides (PbS, PbSe), indium arsenide (InAs), mercuric telluride (HgTe), etc.[89-93] Most of these QDs are synthesized in organic media, which is a major drawback for biological applications, as it is necessary to perform a ligand exchange process that is generally detrimental to the photoluminescence quantum yield (PLQY) of the samples. Water-soluble QDs have been synthesized directly in aqueous buffer, and it is important to further develop these methods to obtain QDs with desirable IR emission, and to explore their bio-functionalization. [94-96]

Here we report the "one-pot synthesis" of IR emitting $Cd_xPb_{1-x}Te$ alloyed QDs functionalized with single stranded DNA (ssDNA). Additionally, we demonstrated DNA origami directed self-assembly of these QDs into discrete nanostructures. Surface modification with DNA has been shown to give the QDs excellent solubility in water and colloidal stability.[22, 97] DNA is a smart molecule with recognition behavior enabled by predictable Watson-Crick base pairing. Displaying specific sequences (such as DNA aptamers) from the nanoparticle allows it to specifically recognize proteins, small molecules or even cell surfaces.[24, 98] Our approach allows us to directly attach DNA oligomers, of any sequence, to the QDs during synthesis. We choose two different materials to make an alloy, one with a moderate band gap, CdTe (1.49 eV), and one with a small band gap, PbTe (0.29 eV). The crystal parameters for CdTe and PbTe are comparable (a_{CdTe} = 0.648 nm and a_{PbTe} = 0.646 nm), but they have different crystal forms: CdTe is zinc blende and PbTe is rock salt. In addition, the diameter of Cd^{2+} ion is

significantly smaller than that of Pb^{2+} ion. The formation of alloyed crystals of $Cd_xPb_{1-x}Te$ with $0.85 > x > 0.15$ has never been reported before.[99]

We employed a recently reported method to attach DNA to the surface of the alloyed QDs. This method involves the use of DNA with two unique domains, a binding domain that is attached to the surface of the particle, and a recognition domain that is designed to bind other biomolecules such as complementary ssDNA.[24] The DNA backbone of the binding domain is modified with phosphorothioate moieties to impart high affinity to the inorganic surface, while the backbone of the recognition domain remains the natural phosphate diester bonds. In a typical synthesis following Shih et al., we held the molar ratio between the surface ligands, the sum of the cations (Cd^{2+} and Pb^{2+}) and tellurium at 8:5:1[96], and the ratio between Cd^{2+} and Pb^{2+} at 3:1. Here, two different types of surface ligands, mercaptopropionic acid (MPA) or glutathione (GSH, a tripeptide) were used as the primary ligand, and phosphothioated DNA was used as the secondary ligand. A molar ratio of 40:1 between the primary capping ligands (MPA or GSH) and the secondary DNA ligands was maintained. One interesting observation was that for the same reaction DNA ligands was maintained. One interesting observation was that for the same reaction conditions in the absence of DNA, the emission maxima of the resulted QDs were significantly different when the two different primary capping ligands were used. For MPA capped QDs, the emission maximum was at 1310 nm, while for GSH capped QDs, the maximum was at 1110 nm (Figure 3.18 A-B). The peak position shifted ~ 200 nm, corresponding to a difference in band gap of ~ 170 meV.

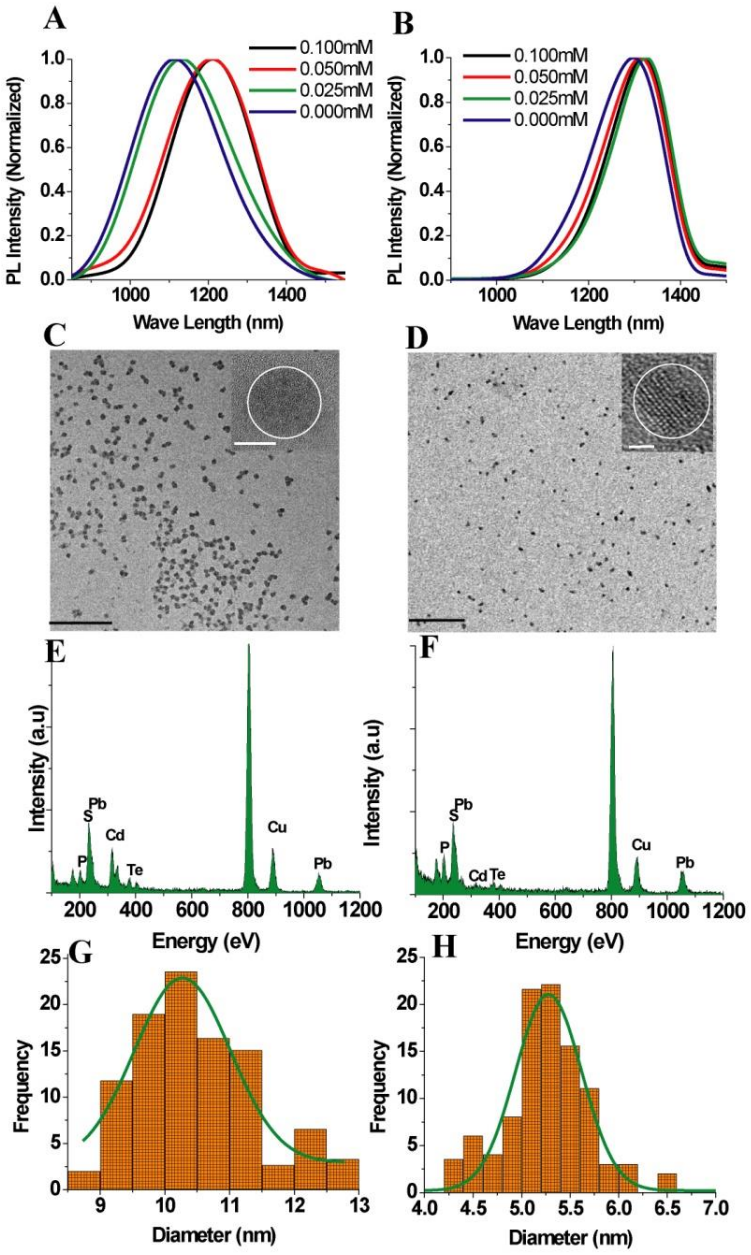

Figure 3.18. A-B) PL emission spectra of $Cd_xPb_{1-x}Te$ QDs capped with GSH (A) and MPA (B) with varying concentrations of DNA. C-D) TEM image of DNA functionalized $Cd_xPb_{1-x}Te$ QDs capped with GSH (C) and MPA (D). Scale Bars are 100 nm. (Insets in C and D) Respective high resolution TEM images. Scale bars are 5 nm (inset in C) and 2

nm (inset in D). E-F) EDS spectra of DNA conjugated CdPbTe QDs capped with GSH (E) and MPA (F). G-H) Size distribution histogram of the QD samples with average diameters of 10.5±1.1nm for the GSH capped particles in (G) and 5.4±0.6 nm for the MPA capped particles in (H).

We observed that as the concentration of phosphothioated DNA present in the reaction mixture increased from 0 to 100 μM, the emission maximum of the CdPbTe QDs exhibited a significant red shift from 1110 nm to 1215 nm, when the primary ligand was GSH (Figure 3.18 A). While for the same DNA concentration range, no significant (< 20 nm) emission shift of the QDs was observed when MPA was the primary capping ligand (Figure 3.18 B). The DNA conjugated QDs were characterized by transmission electron microscopy (TEM) (Figure 3.18 C-D), which showed the average diameter of the GSH capped QDs was ~10.5±1.1 nm, while the average diameter of the MPA capped QDs was ~5.4±0.6 nm (Figure 3.18 G-H). A careful examination of TEM images (Figure 3.18 C) of the GSH capped QDs revealed tiny (~1-2 nm) crystalline domains within the particles (more enlarged zoom in images shown in Fig. S5), indicating that the particles with an average diameter of ~ 10.5 nm were not single crystals, but rather poly-crystalline with crystal domains in the range of 1-2 nm. Energy-dispersive X-ray spectroscopy (EDS) also confirmed the presence of Cd, Pb, and Te from the QD particles and P from the DNA backbone (Figure 3.18 E-F). The small S peak originates from the thiol moieties in the primary capping ligands (MPA or GSH), and the phosphorothioated binding domain of the DNA backbone.

The measured sizes of the QDs from TEM images could not sufficiently explain the observed shift of the QD emission maxima, as the smaller MPA capped QDs showed

emission peaks at a longer wavelength, which is opposite to the prediction based on quantum confinement effects. One hypothesis is that the presence of unique capping ligands and different amounts of DNA actually cause variations in the composition of the alloyed QDs, even though the reaction mixtures contained the same ratio of the constituent elements (Cd:Pb = 3:1). To test this hypothesis, we determined the ratio of Cd and Pb in the QDs using inductively coupled plasma-mass spectrometry (ICP-MS). The synthesized nanoparticles were first washed and filtered 4 times through Amicon centrifugal devices with 30 kD molecular weight cut off (MWCO) membranes to remove the unreacted precursors, and then redispersed in nanopure water before the ICP-MS measurement. The ICP-MS data (Fig. S1) revealed the resulted QDs contained different ratios of Cd and Pb from what were initially injected into the reaction mixtures. In the absence of DNA, the empirical formula of the GSH and MPA capped particles are $Cd_{0.53}Pb_{0.47}Te$ and $Cd_{0.35}Pb_{0.65}Te$, respectively. The higher content of Pb in the MPA capped QDs is consistent with its longer wavelength emission peak. When the amount of DNA in the reaction mixture was increased, the GSH capped particles contained significantly more Pb, and the empirical formula changed from $Cd_{0.53}Pb_{0.47}Te$ to $Cd_{0.39}Pb_{0.61}Te$. In contrast, increasing the concentration of DNA in the MPA capped QD mixture did not have a striking effect. Here, the empirical formula changed only slightly, from $Cd_{0.35}Pb_{0.65}Te$ to $Cd_{0.33}Pb_{0.67}Te$. These changes in the chemical composition of the QDs are sufficient to explain the unique emission properties of the QDs obtained, i.e. higher Pb content in the QDs lead to longer emission wavelength.

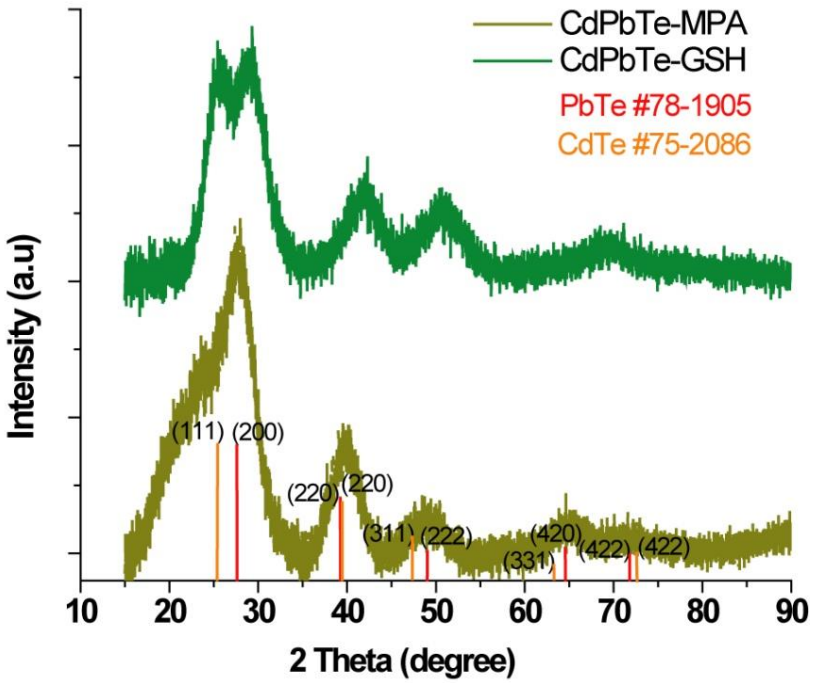

Figure 3.19. Powder X ray diffraction pattern of $Cd_xPb_{1-x}Te$ QDs encapsulated with GSH ($Cd_{0.52}Pb_{0.48}Te$) (green trace) or MPA ($Cd_{0.35}Pb_{0.65}Te$) (dark yellow trace). The bulk XRD data of CdTe (orange) and PbTe (red) are also shown as vertical lines for comparison.

Powder x-ray diffraction was used to study the obtained nanocrystals (Figure 3.19). The peaks were assigned according to the x-ray diffraction patterns of pure cubic phase crystals of PbTe (*JCPDS card* No. 78-1905) and CdTe (*JCPDS Card* No. 75-2086). The coexistence of the rock salt (200, 220, 222, 420) and the zinc blende type of diffraction (111, 220, 311) also supports the alloyed structure. There is a significant shift of all of the peaks between the two samples studied: a shift to smaller angles for the sample with MPA capped QDs ($Cd_{0.35}Pb_{0.65}Te$), compared to that of the GSH capped QDs ($Cd_{0.53}Pb_{0.47}Te$). It is known that the radius of the Pb^{2+} ion (133 pm) is larger than that of the Cd^{2+} ion (109 pm) by 22%. This direction of the peak shift is consistent with the Bragg's law ($\sin\theta = n\lambda/2d$) that the larger the *d*, the smaller the diffraction angle. Another observation is the change in the relative peak heights. The unique zinc blende peaks (111,

311) are more prominent in the GSH capped QDs than the MPA capped QDs, also consistent with the higher Cd content in the GSH capped QDs.

One question remained, why was the final elemental composition of the QDs affected by the identity of the capping ligand. We propose that this phenomenon is based on the unique structures of the particular capping ligands, which make them to have different affinities for the metal cations. MPA is a simple linear molecule with a thiol group that interacts with the QD surface, and a carboxylate group that projects into solution to make the QDs water-soluble. GSH differs from MPA that it has a branched molecular structure and is therefore relatively bulky. In addition, it contains one thiol, two amide bonds, and two carboxylate groups, therefore it may chelate the metal cations and interact with the QD surface through multiple functional groups. Our results seem to indicate that MPA has a stronger affinity for Pb^{2+} than for Cd^{2+}. This is supported by the fact that Pb-S bonds have a higher enthalpy (398 kJ/mol) than Cd-S bonds (208 kJ/mol).[100] Thus, MPA can selectively bring significantly more Pb^{2+} than Cd^{2+} into the QDs as they grow, even in the presence of excess Cd^{2+} in solution, resulting in QDs with longer emission wavelengths. On the other hand, GSH has comparable affinities to these two cations, with an overall affinity to both that is stronger than that of MPA due to the chelating effect. GSH has been successfully used as a capping ligand to synthesize various Cd-based QDs, demonstrating its strong affinity to Cd^{2+}.[86, 101] However, quantifying the affinity of GSH to Cd^{2+} and Pb^{2+} cations will require further study.

In both cases, in the presence of phosphothioated DNA, significant amounts of sulfur atoms are added to the reaction mixtures (with ~ 5 phosphothioate groups per DNA strand). Similar to MPA, these phosphothioate groups exhibit stronger affinity for Pb^{2+}

than for Cd^{2+}, and thus, do not significantly affect the size or composition of the QDs in the presence of MPA. A small red shift (< 20 nm) in emission was observed, which may be due to the slight increase of Pb content (~ 2%) in the nanocrystals. In the case of GSH capped QDs, the phosphorothioate groups in the DNA backbones have higher affinity for Pb^{2+} than Cd^{2+} (due to favorable Pb-S bond energy), which significantly shifts the composition of the alloy toward more Pb^{2+} that account for the 100 nm red shift in the emission. Due to stronger affinity of GSH to the metal ions, they may compete with the DNA binding domain on the surface of the QDs and cause less density of DNA on the QDs surfaces, compared to that of the MPA/DNA capped QDs.

The successful conjugation of DNA to the QD surface was demonstrated through site-specific organization of the resulting QDs on DNA nanostructures. DNA origami has proven to be an excellent platform for organizing various nanoparticles into versatile nano-architectures and can be used to fine-tune the distance between the nanoparticles.[97, 102, 103] In a typical assembly process, approximately 200 unique staple strands with rationally designed sequences are mixed with a single stranded genomic DNA scaffold (M13mp18) to create addressable DNA origami structures.[73] At selected addresses, some of the staple strands are extended with DNA sequences complimentary to the binding domain of the DNA displayed from the QDs, so that the QDs are captured at specific locations on the DNA origami. Here, clusters of capture strands (3 per cluster), were arranged 6 nm from one another, on one or all three arms of a triangular origami structure (Figure 3.20). An important requirement of the DNA directed assembly process is the stability of the nanoparticles in aqueous buffers that contain high salt concentrations. For Au or Ag nanoparticles, dense coverage of the surface with DNA is crucial for stability in

such conditions.[9] Recently, we reported the synthesis of DNA conjugated core-shell QDs with UV to NIR emission that are stable in high salt concentrations.[97] We did not observe any precipitation of the DNA capped $Cd_xPb_{1-x}Te$ QDs in 1×TAE-Mg^{2+} buffer containing 12.5 mM Mg^{2+} during the 24 hour DNA origami assembly process. This is likely due to the presence of a sufficient number of DNA molecules on the surface of the particles that render the QDs less prone to aggregation. In contrast, the $Cd_xPb_{1-x}Te$ QDs that contained only the primary capping ligands, GSH or MPA, aggregated overnight in the same buffer.

The assembly of the DNA origami and the QDs was performed in two steps (Figure 3.20A). First, the origami was assembled with the required staple strands, the capture strands (each extended with 20 adenine nucleotides at the 5' end), and the circular M13 genomic DNA (3 nM) in a molar ratio of 5:50:1, and annealed from 90°C to 4°C overnight. To remove the excess staple and capture strands, the annealed samples were washed three times and filtered using Amicon filter with 100kD MWCO. The high yield formation of the DNA origami was confirmed by atomic force microscopy (AFM). In the second step, the QDs, each functionalized with ssDNA (20 thymine nucleotides in the DNA recognition domain), was mixed with pre-assembled DNA origami structures and was annealed from 40°C to 4°C over 24 hours. Since the concentration of the QDs is very difficult to determine, we titrated the QD mixtures with a known concentration of the origami, and back calculated the approximate concentration of the particles from the yield of assembled structures. To reduce the probability of cross-hybridized structures, the QD-DNA origami samples were diluted to 0.5 nM with 1×TAE-Mg^{2+} buffer before the second annealing step. The self-assembled structures were characterized by AFM and TEM (Figure 3.20B).

For the GSH-DNA capped QDs, one particle was positioned site specifically on one side of the triangular origami. AFM analysis revealed ~50% yield of the origami-QD constructs (Figure 3.20Bi). AFM height profile measurements indicated QDs with a diameter of ~10.5 nm, in good agreement with the corresponding TEM data (Figure 3.20Bv). For MPA-DNA capped QDs, we organized a total of three QDs, one on each arm of the triangular origami. The assembly yield was approximately 70% (Fig. 3Bii), and the height profile measurements indicated ~5.5 nm diameter particles with a narrow size distribution (Figure 3.4.3iv). The lower assembly yield of the GSH-DNA capped QDs on the DNA origami could be explained by the larger size and lower surface DNA coverage of these QDs thus lower colloidal stability. For the MPA-DNA encapsulated QDs, incubation with 1×TAE-Mg^{2+} buffer (12.5mM $MgCl_2$) resulted in quenching of fluorescent intensity by 12% with no shift in the emission maxima. Incubating the same QDs with DNA origami in the same buffer cause a 18% decrease of the fluorescence associated with ~10 nm red shift in the emission maxima, compared to the original synthesized QDs. For the GSH-DNA encapsulated QDs, incubation with buffer alone and with DNA origami both causes quenching of fluorescence by 20% and 26%, respectively, and a red shift of ~22 nm in the emission maxima (Figure S6). The significant quenching of the fluorescence intensity and the red shift of the emission maximum could be explained by the slight aggregation of the QDs nanoparticles, which is consistent with the relatively lower assembly yield with DNA origami.

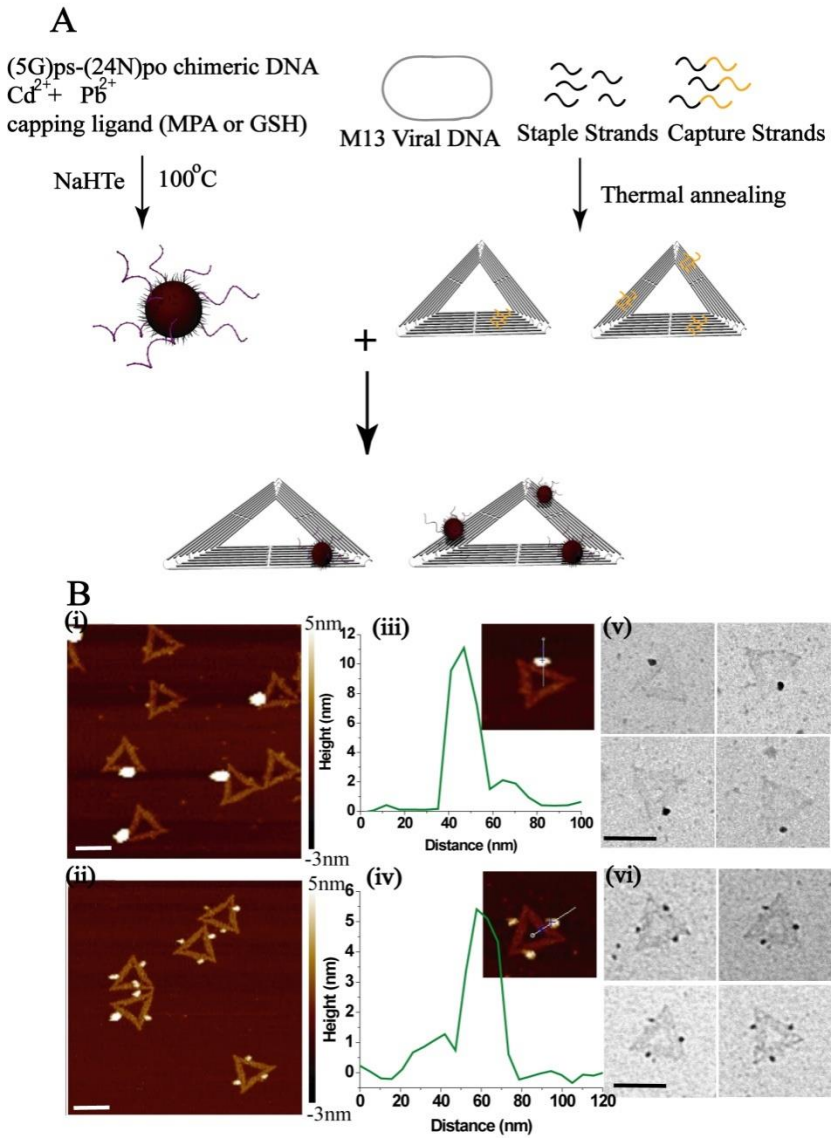

Figure 3.20. (A) Schematic depicting the synthesis of IR emitting DNA functionalized $Cd_xPb_{1-x}Te$ QDs, the DNA origami and the subsequent self-assembly. (B) i-ii) AFM images of the QDs self-assembled on triangular origami structures, (i) GSH capped (ii) MPA capped. iii-iv) Height profiles from the AFM images of a single QD on the triangular origami as shown in i and ii, respectively. v-vi) Zoom in TEM images of the self-assembled structures (v) GSH capped and (vi) MPA capped, after negative staining with 0.7% uranyl formate solution in water. The scale bar is 100 nm in all images.

3.5. Conclusion:

In summary, we developed a simple and efficient method to synthesize robust core/shell QD-DNA conjugates that can withstand the conditions necessary for DNA-directed assembly. In contrast to QD functionalization strategies in which the DNA ligands are simple 'adhered' to the QD surface, we achieved 'incorporation' of the DNA within the shell material themselves, thus providing a higher level of stabilization. We demonstrated that our strategy can be used with a wide variety of semiconductor materials that display fluorescent emission spanning from UV-Vis to NIR. We also demonstrated that discrete numbers of QD-DNA conjugates can be organized by DNA origami nanostructures, an essential component of hierarchical nanoparticle assembly efforts. This work will facilitate the construction of discrete, multicomponent semiconductor or semiconductor-metal hybrid nanostructures for energy, nanophotonics, and biosensing applications. We also demonstrated a simple yet reliable 'one pot synthetic strategy' to conjugate DNA to alloyed $Cd_xPb_{1-x}Te$ QDs that emit in the true IR range. The DNA conjugated particles are stable in aqueous solution with high salt concentration, and are potential candidates for future tissue imaging or labeling applications. Any toxicity due to leaching of cadmium or lead can be prevented by encapsulating the particles with a bio-friendly ZnS shell. Moreover, the successful assembly of the QD particles on DNA origami to produce discrete nano-architectures further facilitates future applications in biosensors and biophotonics.

3.6. References

1. Service, R. F., How far can we push chemical self-assembly. *Science* **2005**, 309, 95-95.

2. Srivastava, S.; Santos, A.; Critchley, K.; Kim, K.-S.; Podsiadlo, P.; Sun, K.; Lee, J.; Xu, C.; Lilly, G. D.; Glotzer, S. C.; Kotov, N. A., Light-Controlled Self-Assembly of Semiconductor Nanoparticles into Twisted Ribbons. *Science* **2010**, 327, 1355-1359.

3. Liu, Y., NANOMATERIALS DNA brings quantum dots to order. *Nat. Nanotechnol.* **2011**, 6, 463-464.

4. Seeman, N. C., DNA in a material world. *Nature* **2003**, 421, 427-431.

5. Pinheiro, A. V.; Han, D.; Shih, W. M.; Yan, H., Challenges and opportunities for structural DNA nanotechnology. *Nat. Nanotechnol.* **2011**, 6, 763-772.

6. Tan, S. J.; Campolongo, M. J.; Luo, D.; Cheng, W., Building plasmonic nanostructures with DNA. *Nat. Nanotechnol.* **2011**, 6, 268-276.

7. Mirkin, C. A.; Letsinger, R. L.; Mucic, R. C.; Storhoff, J. J., A DNA-based method for rationally assembling nanoparticles into macroscopic materials. *Nature* **1996**, 382, 607-609.

8. Alivisatos, A. P.; Johnsson, K. P.; Peng, X. G.; Wilson, T. E.; Loweth, C. J.; Bruchez, M. P.; Schultz, P. G., Organization of 'nanocrystal molecules' using DNA. *Nature* **1996**, 382, 609-611.

9. Hurst, S. J.; Lytton-Jean, A. K. R.; Mirkin, C. A., Maximizing DNA loading on a range of gold nanoparticle sizes. *Anal. Chem.* **2006**, 78, 8313-8318.

10. Cutler, J. I.; Auyeung, E.; Mirkin, C. A., Spherical Nucleic Acids. *J. Am. Chem. Soc.* **2012**, 134, 1376-1391.

11. Elghanian, R.; Storhoff, J. J.; Mucic, R. C.; Letsinger, R. L.; Mirkin, C. A., Selective colorimetric detection of polynucleotides based on the distance-dependent optical properties of gold nanoparticles. *Science* **1997**, 277, 1078-1081.

12. Zhang, J. P.; Liu, Y.; Ke, Y. G.; Yan, H., Periodic square-like gold nanoparticle arrays templated by self-assembled 2D DNA nanogrids on a surface. *Nano Lett.* **2006**, 6, 248-251.

13. Ding, B.; Deng, Z.; Yan, H.; Cabrini, S.; Zuckermann, R. N.; Bokor, J., Gold Nanoparticle Self-Similar Chain Structure Organized by DNA Origami. *J. Am. Chem. Soc.* **2010**, 132, 3248-3249.

14. Cheng, W.; Campolongo, M. J.; Cha, J. J.; Tan, S. J.; Umbach, C. C.; Muller, D. A.; Luo, D., Free-standing nanoparticle superlattice sheets controlled by DNA. *Nat. Mater.* **2009**, 8, 519-525.

15. Sharma, J.; Chhabra, R.; Cheng, A.; Brownell, J.; Liu, Y.; Yan, H., Control of Self-Assembly of DNA Tubules Through Integration of Gold Nanoparticles. *Science* **2009**, 323, 112-116.

16. Macfarlane, R. J.; Lee, B.; Jones, M. R.; Harris, N.; Schatz, G. C.; Mirkin, C. A., Nanoparticle Superlattice Engineering with DNA. *Science* **2011**, 334, 204-208.

17. Kuzyk, A.; Schreiber, R.; Fan, Z.; Pardatscher, G.; Roller, E.-M.; Hoegele, A.; Simmel, F. C.; Govorov, A. O.; Liedl, T., DNA-based self-assembly of chiral plasmonic nanostructures with tailored optical response. *Nature* **2012**, 483, 311-314.

18. Sharma, J.; Ke, Y. G.; Lin, C. X.; Chhabra, R.; Wang, Q. B.; Nangreave, J.; Liu, Y.; Yan, H., DNA-tile-directed self-assembly of quantum dots into two-dimensional nanopatterns. *Angew. Chem. Int. Ed.* **2008**, 47, 5157-5159.

19. Bui, H.; Onodera, C.; Kidwell, C.; Tan, Y.; Graugnard, E.; Kuang, W.; Lee, J.; Knowlton, W. B.; Yurke, B.; Hughes, W. L., Programmable Periodicity of Quantum Dot Arrays with DNA Origami Nanotubes. *Nano Lett.* **2010**, 10, 3367-3372.

20. Ko, S. H.; Du, K.; Liddle, J. A., Quantum-Dot Fluorescence Lifetime Engineering with DNA Origami Constructs. *Angew. Chem. Int. Ed.* **2013**, 52, 1193-1197.

21. Mitchell, G. P.; Mirkin, C. A.; Letsinger, R. L., Programmed assembly of DNA functionalized quantum dots. *J. Am. Chem. Soc.* **1999**, 121, 8122-8123.

22. Wang, Q. B.; Liu, Y.; Ke, Y. G.; Yan, H., Quantum dot bioconjugation during core-shell synthesis. *Angew. Chem. Int. Ed.* **2008**, 47, 316-319.

23. Tikhomirov, G.; Hoogland, S.; Lee, P. E.; Fischer, A.; Sargent, E. H.; Kelley, S. O., DNA-based programming of quantum dot valency, self-assembly and luminescence. *Nat. Nanotechnol.* **2011**, 6, 485-490.

24. Ma, N.; Sargent, E. H.; Kelley, S. O., One-step DNA-programmed growth of luminescent and biofunctionalized nanocrystals. *Nat. Nanotechnol.* **2009**, 4, 121-125.

25. Deng, Z. T.; Schulz, O.; Lin, S.; Ding, B. Q.; Liu, X. W.; Wei, X. X.; Ros, R.; Yan, H.; Liu, Y., Aqueous Synthesis of Zinc Blende CdTe/CdS Magic-Core/Thick-Shell Tetrahedral-Shaped Nanocrystals with Emission Tunable to Near-Infrared. *J. Am. Chem. Soc.* **2010**, 132, 5592-5593.

26. Chen, Y.; Vela, J.; Htoon, H.; Casson, J. L.; Werder, D. J.; Bussian, D. A.; Klimov, V. I.; Hollingsworth, J. A., "Giant" multishell CdSe nanocrystal quantum dots with suppressed blinking. *J. Am. Chem. Soc.* **2008**, 130, 5026-5027.

27. Mahler, B.; Spinicelli, P.; Buil, S.; Quelin, X.; Hermier, J.-P.; Dubertret, B., Towards non-blinking colloidal quantum dots. *Nat. Mater.* **2008**, 7, 659-664.

28. Deng, Z. T.; Cao, L.; Tang, F. Q.; Zou, B. S., A new route to zinc-blende CdSe nanocrystals: Mechanism and synthesis. *J. Phys. Chem. B* **2005**, 109, 16671-16675.

29. Smith, A. M.; Mohs, A. M.; Nie, S., Tuning the optical and electronic properties of colloidal nanocrystals by lattice strain. *Nat. Nanotechnol.* **2009**, 4, 56-63.

30. Deng, Z.; Lie, F. L.; Shen, S.; Ghosh, I.; Mansuripur, M.; Muscat, A. J., Water-Based Route to Ligand-Selective Synthesis of ZnSe and Cd-Doped ZnSe Quantum Dots with Tunable Ultraviolet A to Blue Photoluminescence. *Langmuir* **2009**, 25, 434-442.

31. Deng, Z.; Yan, H.; Liu, Y., Band Gap Engineering of Quaternary-Alloyed ZnCdSSe Quantum Dots via a Facile Phosphine-Free Colloidal Method. *J. Am. Chem. Soc.* **2009**, 131, 17744-17745.

32. Nirmal, M.; Dabbousi, B. O.; Bawendi, M. G.; Macklin, J. J.; Trautman, J. K.; Harris, T. D.; Brus, L. E., Fluorescence intermittency in single cadmium selenide nanocrystals. *Nature* **1996**, 383, 802-804.

33. Kuno, M.; Fromm, D. P.; Hamann, H. F.; Gallagher, A.; Nesbitt, D. J., Nonexponential "blinking" kinetics of single CdSe quantum dots: A universal power law behavior. *J. Chem. Phys.* **2000**, 112, 3117-3120.

34. Shimizu, K. T.; Neuhauser, R. G.; Leatherdale, C. A.; Empedocles, S. A.; Woo, W. K.; Bawendi, M. G., Blinking statistics in single semiconductor nanocrystal quantum dots. *Phys. Rev. B* **2001**, 63.

35. Maria Galvez, E.; Zimmermann, B.; Rombach-Riegraf, V.; Bienert, R.; Graeber, P., Fluorescence resonance energy transfer in single enzyme molecules with a quantum dot as donor. *Eur. Biophys. J. Biophy* **2008**, 37, 1367-1371.

36. Galvez, E.; Dueser, M.; Boersch, M.; Wrachtrup, J.; Graeber, P., Quantum dots for single-pair fluorescence resonance energy transfer in membrane-integrated EF0F1. *Biochem. Soc. Trans.* **2008**, 36, 1017-1021.

37. Hohng, S.; Ha, T., Single-molecule quantum-dot fluorescence resonance energy transfer. *Chem. Phys. Chem* **2005**, 6, 956-960.

38. Fisher, B. R.; Eisler, H. J.; Stott, N. E.; Bawendi, M. G., Emission intensity dependence and single-exponential behavior in single colloidal quantum dot fluorescence lifetimes. *J. Phys. Chem. B* **2004**, 108, 143-148.

39. Frantsuzov, P. A.; Volkan-Kacso, S.; Janko, B., Model of Fluorescence Intermittency of Single Colloidal Semiconductor Quantum Dots Using Multiple Recombination Centers. *Phys. Rev. Lett.* **2009**, 103.

40. Chung, I.; Witkoskie, J. B.; Cao, J. S.; Bawendi, M. G., Description of the fluorescence intensity time trace of collections of CdSe nanocrystal quantum dots based on single quantum dot fluorescence blinking statistics. *Phys. Rev. E* **2006**, 73.

41. Schlegel, G.; Bohnenberger, J.; Potapova, I.; Mews, A., Fluorescence decay time of single semiconductor nanocrystals. *Phys. Rev. Lett.* **2002**, 88.

42. Biju, V.; Makita, Y.; Nagase, T.; Yamaoka, Y.; Yokoyama, H.; Baba, Y.; Ishikawa, M., Subsecond luminescence intensity fluctuations of single CdSe quantum dots. *J. Phys. Chem.B* **2005**, 109, 14350-14355.

43. Brokmann, X.; Hermier, J. P.; Messin, G.; Desbiolles, P.; Bouchaud, J. P.; Dahan, M., Statistical aging and nonergodicity in the fluorescence of single nanocrystals. *Phys. Rev. Lett.* **2003**, 90.

44. Tang, J.; Marcus, R. A., Diffusion-controlled electron transfer processes and power-law statistics of fluorescence intermittency of nanoparticles. *Phys. Rev. Lett.* **2005**, 95.

45. Tang, J.; Marcus, R. A., Mechanisms of fluorescence blinking in semiconductor nanocrystal quantum dots. *J. Chem.Phys.***2005**, 123.

46. Ye, M.; Searson, P. C., Blinking in quantum dots: The origin of the grey state and power law statistics. *Phys. Rev. B* **2011**, 84.

47. Goushi, K.; Yamada, T.; Otomo, A., Excitation Intensity Dependence of Power-Law Blinking Statistics in Nanocrystal Quantum Dots. *J. Phys. Chem. C* **2009**, 113, 20161-20168.

48. Tang, J.; Lee, D.-H.; Yeh, Y.-C.; Yuan, C.-T., Short-time power-law blinking statistics of single quantum dots and a test of the diffusion-controlled electron transfer model. *J. Chem. Phys* .**2009**, 131.

49. Peterson, J. J.; Nesbitt, D. J., Modified Power Law Behavior in Quantum Dot Blinking: A Novel Role for Biexcitons and Auger Ionization. *Nano Lett.* **2009**, 9, 338-345.

50. Margolin, G.; Protasenko, V.; Kuno, M.; Barkai, E., Power-law blinking quantum dots: stochastic and physical models. Adv. Chem. Phys. **2006**; 133, 327-356.

51. Bianco, S.; Grigolini, P.; Paradisi, P., Fluorescence intermittency in blinking quantum dots: Renewal or slow modulation? *J. Chem. Phys.* **2005**, 123.

52. Verberk, R.; van Oijen, A. M.; Orrit, M., Simple model for the power-law blinking of single semiconductor nanocrystals. *Phys. Rev. B* **2002**, 66.

53. Frantsuzov, P. A.; Marcus, R. A., Explanation of quantum dot blinking without the long-lived trap hypothesis. *Phys. Rev. B* **2005**, 72.

54. Efros, A. L.; Rosen, M., Random telegraph signal in the photoluminescence intensity of a single quantum dot. *Phys. Rev. Lett.* **1997**, 78, 1110-1113.

55. Galland, C.; Ghosh, Y.; Steinbrueck, A.; Sykora, M.; Hollingsworth, J. A.; Klimov, V. I.; Htoon, H., Two types of luminescence blinking revealed by spectroelectrochemistry of single quantum dots. *Nature* **2011**, 479, 203-U75.

56. Wang, X.; Ren, X.; Kahen, K.; Hahn, M. A.; Rajeswaran, M.; Maccagnano-Zacher, S.; Silcox, J.; Cragg, G. E.; Efros, A. L.; Krauss, T. D., Non-blinking semiconductor nanocrystals. *Nature* **2009**, 459, 686-689.

57. Hammer, N. I.; Early, K. T.; Sill, K.; Odoi, M. Y.; Emrick, T.; Barnes, M. D., Coverage-mediated suppression of blinking in solid state quantum dot conjugated organic composite nanostructures. *J. Phys. Chem. B* **2006**, 110, 14167-14171.

58. Hamada, M.; Nakanishi, S.; Itoh, T.; Ishikawa, M.; Biju, V., Blinking Suppression in CdSe/ZnS Single Quantum Dots by TiO2 Nanoparticles. *Acs Nano* **2010**, 4, 4445-4454.

59. Antelman, J.; Ebenstein, Y.; Dertinger, T.; Michalet, X.; Weiss, S., Suppression of Quantum Dot Blinking in DTT-Doped Polymer Films. *J. Phys. Chem. C* **2009**, 113, 11541-11545.

60. Yuan, C. T.; Yu, P.; Ko, H. C.; Huang, J.; Tang, J., Antibunching Single-Photon Emission and Blinking Suppression of CdSe/ZnS Quantum Dots. *Acs Nano* **2009**, 3, 3051-3056.

61. Lin, C.; Liu, Y.; Yan, H., Designer DNA Nanoarchitectures. *Biochemistry* **2009**, 48, 1663-1674.

62. Sharma, J.; Chhabra, R.; Liu, Y.; Ke, Y. G.; Yan, H., DNA-templated self-assembly of two-dimensional and periodical gold nanoparticle arrays. *Angew. Chem. Int. Ed.* **2006**, 45, 730-735.

63. Chhabra, R.; Sharma, J.; Ke, Y.; Liu, Y.; Rinker, S.; Lindsay, S.; Yan, H., Spatially addressable multiprotein nanoarrays templated by aptamer-tagged DNA nanoarchitectures. *J. Am. Chem. Soc.* **2007**, 129, 10304-10304.

64. Lin, C.; Jungmann, R.; Leifer, A. M.; Li, C.; Levner, D.; Church, G. M.; Shih, W. M.; Yin, P., Submicrometre geometrically encoded fluorescent barcodes self-assembled from DNA. *Nat. Chem.* **2012**, 4, 832-839.

65. Kelly, K. L.; Coronado, E.; Zhao, L. L.; Schatz, G. C., The optical properties of metal nanoparticles: The influence of size, shape, and dielectric environment. *J. Phys. Chem. B* **2003**, 107, 668-677.

66. Jain, P. K.; Lee, K. S.; El-Sayed, I. H.; El-Sayed, M. A., Calculated absorption and scattering properties of gold nanoparticles of different size, shape, and composition: Applications in biological imaging and biomedicine. *J. Phys. Chem. B* **2006**, 110, 7238-7248.

67. Chen, J.; Jin, Y.; Fahruddin, N.; Zhao, J. X., Development of Gold Nanoparticle-Enhanced Fluorescent Nanocomposites. *Langmuir* **2013**, 29, 1584-1591.

68. Myroshnychenko, V.; Rodriguez-Fernandez, J.; Pastoriza-Santos, I.; Funston, A. M.; Novo, C.; Mulvaney, P.; Liz-Marzan, L. M.; Garcia de Abajo, F. J., Modelling the optical response of gold nanoparticles. *Chem. Soc. Rev.* 2008, 37, 1792-1805.

69. Wang, Y.; Yan, B.; Chen, L., SERS Tags: Novel Optical Nanoprobes for Bioanalysis. *Chem. Rev.* **2013**, 113, 1391-1428.

70. Acuna, G. P.; Moeller, F. M.; Holzmeister, P.; Beater, S.; Lalkens, B.; Tinnefeld, P., Fluorescence Enhancement at Docking Sites of DNA-Directed Self-Assembled Nanoantennas. *Science* 2012, 338, 506-510.

71. Eustis, S.; El-Sayed, M. A., Why gold nanoparticles are more precious than pretty gold: Noble metal surface plasmon resonance and its enhancement of the radiative and nonradiative properties of nanocrystals of different shapes. *Chem. Soc. Rev.* **2006**, 35, 209-217.

72. Chhabra, R.; Sharma, J.; Wang, H. N.; Zou, S. L.; Lin, S.; Yan, H.; Lindsay, S.; Liu, Y., Distance-dependent interactions between gold nanoparticles and fluorescent molecules with DNA as tunable spacers. *Nanotechnology* **2009**, 20.

73. Rothemund, P. W. K., Folding DNA to create nanoscale shapes and patterns. *Nature* **2006**, 440, 297-302.

74. Torring, T.; Voigt, N. V.; Nangreave, J.; Yan, H.; Gothelf, K. V., DNA origami: a quantum leap for self-assembly of complex structures. *Chem. Soc. Rev.* **2011**, 40, 5636-5646.

75. Nangreave, J.; Han, D. R.; Liu, Y.; Yan, H., DNA origami: a history and current perspective. *Curr. Opin. Chem. Biol.* **2010**, 14, 608-615.

76. Michalet, X.; Pinaud, F. F.; Bentolila, L. A.; Tsay, J. M.; Doose, S.; Li, J. J.; Sundaresan, G.; Wu, A. M.; Gambhir, S. S.; Weiss, S., Quantum dots for live cells, in vivo imaging, and diagnostics. *Science* **2005**, 307, 538-544.

77. Jaiswal, J. K.; Simon, S. M., Potentials and pitfalls of fluorescent quantum dots for biological imaging. *Trends in Cell Biology* **2004**, 14, 497-504.

78. Medintz, I. L.; Uyeda, H. T.; Goldman, E. R.; Mattoussi, H., Quantum dot bioconjugates for imaging, labelling and sensing. *Nat. Mater.* **2005**, 4, 435-446.

79. Pansare, V. J.; Hejazi, S.; Faenza, W. J.; Prud'homme, R. K., Review of Long-Wavelength Optical and NIR Imaging Materials: Contrast Agents, Fluorophores, and Multifunctional Nano Carriers. *Chem. Mater.* **2012**, 24, 812-827.

80. Kim, S.; Lim, Y. T.; Soltesz, E. G.; De Grand, A. M.; Lee, J.; Nakayama, A.; Parker, J. A.; Mihaljevic, T.; Laurence, R. G.; Dor, D. M.; Cohn, L. H.; Bawendi, M. G.; Frangioni, J. V., Near-infrared fluorescent type II quantum dots for sentinel lymph node mapping. *Nat. Biotechnol.* **2004,** 22, 93-97.

81. Zhang, Y.; Hong, G.; Zhang, Y.; Chen, G.; Li, F.; Dai, H.; Wang, Q., Ag2S Quantum Dot: A Bright and Biocompatible Fluorescent Nanoprobe in the Second Near-Infrared Window. *Acs Nano* **2012**, 6, 3695-3702.

82. Du, Y.; Xu, B.; Fu, T.; Cai, M.; Li, F.; Zhang, Y.; Wang, Q., Near-infrared Photoluminescent Ag2S Quantum Dots from a Single Source Precursor. *J. Am. Chem. Soc.* **2010**, 132, 1470-1471.

83. Shen, S.; Zhang, Y.; Peng, L.; Du, Y.; Wang, Q., Matchstick-Shaped Ag2S-ZnS Heteronanostructures Preserving both UV/Blue and Near-Infrared Photoluminescence. *Angew. Chem. Int. Ed.* **2011**, 50, 7115-7118.

84. Hong, G.; Robinson, J. T.; Zhang, Y.; Diao, S.; Antaris, A. L.; Wang, Q.; Dai, H., In Vivo Fluorescence Imaging with Ag2S Quantum Dots in the Second Near-Infrared Region. *Angew. Chem. Int. Ed.* **2012**, 51, 9818-9821.

85. Li, C.; Zhang, Y.; Wang, M.; Zhang, Y.; Chen, G.; Li, L.; Wu, D.; Wang, Q., In vivo real-time visualization of tissue blood flow and angiogenesis using Ag2S quantum dots in the NIR-II window. *Biomaterials* **2014**, 35, 393-400.

86. Samanta, A.; Deng, Z.; Liu, Y., Aqueous Synthesis of Glutathione-Capped CdTe/CdS/ZnS and CdTe/CdSe/ZnS Core/Shell/Shell Nanocrystal Heterostructures. *Langmuir* **2012**, 28, 8205-8215.

87. Liang, G.-X.; Gu, M.-M.; Zhang, J.-R.; Zhu, J.-J., Preparation and bioapplication of high-quality, water-soluble, biocompatible, and near-infrared-emitting CdSeTe alloyed quantum dots. *Nanotechnology* **2009**, 20.

88. Mao, W.; Guo, J.; Yang, W.; Wang, C.; He, J.; Chen, J., Synthesis of high-quality near-infrared-emitting CdTeS alloyed quantum dots via the hydrothermal method. *Nanotechnology* **2007**, 18.

89. Keuleyan, S.; Lhuillier, E.; Guyot-Sionnest, P., Synthesis of Colloidal HgTe Quantum Dots for Narrow Mid-IR Emission and Detection. *J. Am. Chem. Soc.* **2011**, 133, 16422-16424.

90. Harris, D. K.; Allen, P. M.; Han, H.-S.; Walker, B. J.; Lee, J.; Bawendi, M. G., Synthesis of Cadmium Arsenide Quantum Dots Luminescent in the Infrared. *J. Am. Chem. Soc.* **2011**, 133, 4676-4679.

91. Pietryga, J. M.; Schaller, R. D.; Werder, D.; Stewart, M. H.; Klimov, V. I.; Hollingsworth, J. A., Pushing the band gap envelope: Mid-infrared emitting colloidal PbSe quantum dots. *J. Am. Chem. Soc.* **2004**, 126, 11752-11753.

92. Hines, M. A.; Scholes, G. D., Colloidal PbS nanocrystals with size-tunable near-infrared emission: Observation of post-synthesis self-narrowing of the particle size distribution. *Adv. Mater.s* **2003**, 15, 1844-1849.

93. Zhao, X. S.; Gorelikov, I.; Musikhin, S.; Cauchi, S.; Sukhovatkin, V.; Sargent, E. H.; Kumacheva, E., Synthesis and optical properties of thiol-stabilized PbS nanocrystals. *Langmuir* **2005**, 21, 1086-1090.

94. Deng, D.; Zhang, W.; Chen, X.; Liu, F.; Zhang, J.; Gu, Y.; Hong, J., Facile Synthesis of High-Quality, Water-Soluble, Near-Infrared-Emitting PbS Quantum Dots. *Eur. J. Inorg. Chem.* **2009**, 3440-3446.

95. Levina, L.; Sukhovatkin, W.; Musikhin, S.; Cauchi, S.; Nisman, R.; Bazett-Jones, D. P.; Sargent, E. H., Efficient infrared-emitting PbS quantum dots grown on DNA and stable in aqueous solution and blood plasma. *Adv. Mater.* **2005**, 17, 1854-1855.

96. Au, G. H. T.; Shih, W. Y.; Tseng, S. J.; Shih, W.-H., Aqueous CdPbS quantum dots for near-infrared imaging. *Nanotechnology* **2012**, 23.

97. Deng, Z.; Samanta, A.; Nangreave, J.; Yan, H.; Liu, Y., Robust DNA-Functionalized Core/Shell Quantum Dots with Fluorescent Emission Spanning from UV-vis to Near-IR and Compatible with DNA-Directed Self-Assembly. *J. Am. Chem. Soc.* **2012**, 134, 17424-17427.

98. Lin, Y.-W.; Liu, C.-W.; Chang, H.-T., DNA functionalized gold nanoparticles for bioanalysis. *Anal. Methods* **2009**, 1, 14-24.

99. Nikolic, P. M., Solid solutions of CdSe and CdTe in PbTe and their optical properties. *Br. J. Appl. Phys.* **1966**, 17, 341-&.

100. Deng, Z.; Pal, S.; Samanta, A.; Yan, H.; Liu, Y., DNA functionalization of colloidal II-VI semiconductor nanowires for multiplex nanoheterostructures. *Chem.Sci.* **2013**, 4, 2234-2240.

101. Qian, H. F.; Dong, C. Q.; Weng, J. F.; Ren, J. C., Facile one-pot synthesis of luminescent, water-soluble, and biocompatible glutathione-coated CdTe nanocrystals. *Small* **2006**, 2, 747-751.

102. Ding, B. Q.; Deng, Z. T.; Yan, H.; Cabrini, S.; Zuckermann, R. N.; Bokor, J., Gold Nanoparticle Self-Similar Chain Structure Organized by DNA Origami. *J. Am. Chem. Soc.* **2010**, 132, 3248-3249.

103. Pal, S.; Deng, Z. T.; Ding, B. Q.; Yan, H.; Liu, Y., DNA-Origami-Directed Self-Assembly of Discrete Silver-Nanoparticle Architectures. *Angew. Chem. Int. Ed.* **2010**, 49, 2700-2704.

CHAPTER 4

CONTROLLED ENGINEERING OF PHOTOPHYSICAL PROPERTIES OF QDS BY PLASMONIC NANOPARTICLES.

4.1. Abstract

In this chapter we have created heteromer of metallic nanoparticles and quantum dots with varying distances. It has two parts. In the first part we have studied the quenching of fluorescence intensity of QDs emitting at 650nm in the presence of large gold nanoparticle with diameter 30nm. We have observed a profound dependence of intensity with distance between the two particles. Quenching was due to the increased rate of nonradiatve decay rate while the radiative decay rate almost remained constant. Unlike FRET this dependence is much relaxed and follows an inverse order of less than 3. This long range quenching could be really useful as longer spectroscopic ruler. Second part is an ongoing experiment currently. Here we are trying to create hotspot with gold/silver hybrid nanoparticles which will be utilized to enhance fluorescence of quantum dots. Our preliminary result in single molecule analysis shows that fluorescence count rate per unit time has increased almost 7-10times with a significant reduction in the PL life time of the QDs.

4.2. Introduction

Förster resonance energy transfer (FRET), due to its sensitivity to distance has become a well-accepted tool to measure distance at molecular level. It is an electrodynamic phenomenon where two nearby oscillating dipoles interact and energy is transferred from an excited state donor to the ground state of an acceptor in a nonradiative fashion. The rate of FRET is proportional to the inverse sixth power of

distance and the transfer efficiency is described as The distance between the interacting dipole is r. R_0 is Förster radius which is defined as the distance at which FRET efficiency is 50%. R_0 depends on various factors which include spectral overlap integral, quantum yield of the donor in absence of acceptor, dipole angular orientation etc. For commonly used organic fluorophore pairs, R_0 lies in the range of 2-6 nm. Energy transfer efficiency in FRET is extremely sensitive when the distance is close to the Förster radius. For example at $r = 0.8R_0$ and $r = 1.2R_0$ the energy transfer efficiency is ~80% and ~25%. In fact it is useless to look for a distance outside the range of $r = 0.5R_0$ and $2R_0$. This gives a very tight window in the 1-10 nm range. This is a favorable distance as long as interactions between proteins, nucleic acids or with cell membranes are concerned.[1-6] But many other biomolecular processes work on a longer distance range and become difficult to follow their dynamics and interactions using FRET. This motivate researchers to look for a longer "spectroscopic ruler".

In the last decade, Nanometal Surface Energy Transfer (NSET) has emerged as a longer spectroscopic ruler that can go up to 50 nm depending on the size of the metallic nanoparticle.[7-10] It is based on the phenomenon that lifetime of an oscillating dipole is damped when it is placed at a certain distance away from a metal surface. Experimentally it has been observed that presence of a proximal gold nanoparticle quenches the fluorescence of an organic dye, which follows an inverse fourth power of distance dependence (refs).[9, 11] The electrodynamic coupling in FRET is considered weak since it is the interaction between two point dipoles. In NSET, it is an array of dipoles that the fluorescent molecule is interacting with, which makes it to display a longer distance dependence than FRET. [12]

The underlying mechanism of NSET is still under debate (refs).[13-20] In the seminal work by CPS-Kuhn, the quenching effect was considered due to an absorption by the metal nanoparticle upon formation of an image dipole on the metal nanoparticle surface.[14] Although it can explain the experimental result of fluorescence quenching by a 2 nm AuNP, yet it failed to predict the quenching behavior when the size of the nanoparticle changes.[8] Other theories have evolved to predict and explain the experimental result of different sized AuNPs, for instance Gerstein-Nitzan model[19], but an adequate depiction of the real picture is yet to be unveiled. Recently an attempt has been made by Breshike *et el.* by introducing some empirical correction in the model in terms of the change in absorptivity and dielectric constant as size of the AuNP changes (ref).[8] The theoretical prediction made by them matches fairly well with experimental results with different sized AuNPs.

So far the experiments mainly involved the interaction of AuNPs with organic dyes. Another type of quantum emitters, semiconductor photoluminescent nanoparticles, also known as quantum dots, have largely been ignored.[21-23] QDs offer some special advantage over the organic dyes. Due to their broad absorption and narrow emission spectra, high quantum yield and excellent chemical and photo stability, they have emerged as new group of imaging and labeling agents. Although there are numerous reports available where QDs have been used as universal donor fluorophores for FRET-like energy transfer to organic dyes,[24-27] systematic studies on the distance dependent quenching of the QD emission by plasmonic nanoparticles is very scarce. Pons et al. investigated the nature of distance dependent quenching phenomenon of semiconductor QDs by 1.4 nm (diameter) gold nanoparticle and observed NSET type quenching

behavior.[21] But smaller than 2 nm gold nanoparticles do not have well developed surface and hence do not show a clear surface plasmon band. This indicates that the mechanism of quenching interaction could be different for a larger gold nanoparticle compared to the 1.4 nm particles.

In the work reported here, we motivate to investigate the nature of distance dependent quenching by larger AuNPs with prominent surface plasmon band and search for a potential optical ruler that can be used for measuring longer distances.

4.3. Materials and Methods

Chemicals: Cadmium nitrate tetrahydrate ($Cd(NO_3)_2 \cdot 4H_2O$, 99.8%), Tellurium (Te, powder, ≥99%, powder) Sodium borohydride ($NaBH_4$, ≥99%), 3-Mercaptopropionic acid ($HSCH_2CH_2CO_2H$, ≥99%), isopropyl alcohol (IPA, 99%), Rhodamine 6G (QY = 95% in ethanol), Tris-(carboxyethyl)phosphine hydrochloride (TCEP) and sodium chloride (NaCl) were purchased from Sigma-Aldrich and used without further purification. M13mp18 single stranded DNA was purchased from New England Biolabs and was also used without further treatment. All unmodified helper strands were purchased from Integrated DNA Technologies, Inc. (IDT, www.idtdna.com) in 96-well plate format, suspended in nanopure water (H_2O, with resistivity up to 18.2 MΩ·cm) and used without further purification. All modified helper strands were purchased from IDT and purified by denaturing PAGE gel electrophoresis. Phosphorothiolated backbone modified ps-po-chimeric ssDNA and 5' thiol modified strands were purchased from IDT and used without purification. 30nm gold nanoparticle was purchased from Tedpella, Inc. and was used without any further purification.

Buffers: The buffers used in this study are: 1xTAE/Mg^{2+}: 40 mM Tris acetate, 2 mM EDTA, and 12.5 mM magnesium acetate, pH 8.0. 1xTBE/Mg^{2+}: 50 mM Tris, 100 mM Borate, 10 mM EDTA, pH 8.2.

Characterization: Ultraviolet-Visible (UV-Vis) absorption spectra were recorded at room temperature with a JASCO-V670 spectrophotometer. Photoluminescence (PL) spectra were measured at room temperature using a NanoLog spectrometer manufactured by HORIBA Jobin Yvon equipped with a thermoelectric cooled PMT (R928 in the range 200 nm to 850 nm). Fluorescence decay kinetics were measured using the time-correlated single photon counting (TCSPC) technique. The excitation source was a fiber super continuum laser based on a passive mode locked fiber laser and a highnonlinearity photonic crystal fiber super continuum generator (Fianium SC450). The laser provides 6-ps pulses at a repetition rate variable between 0.1 – 40 MHz. The laser output was sent through an Acousto-Optical Tunable Filer (Fianium AOTF) to obtain excitation pulses at desired wavelength of 520 nm. Fluorescence emission was collected at 90° and detected using a double-grating monochromator (Jobin-Yvon, Gemini-180) and a microchannel plate photomultiplier tube (Hamamatsu R3809U-50). The polarization of the emission was 54.7° relative to that of the excitation. Data acquisition was done using a single photon counting card (Becker-Hickl, SPC-830). The IRF had a FWHM of 50 ps, measured from the scattering of sample at the excitation wavelength. The excitation repetition rate was 10 MHz. The data was fitted with a sum of exponential decay model globally or at a single wavelength using ASUFIT.

TEM samples were prepared by depositing 2 μL of the purified sample solution on a negative glow discharged (Emitech K100X) carbon-coated grid (400 mesh, Ted Pella).

After 2 mins, the sample drop was removed by absorbing into a filter paper. It was washed twice with water to remove any salt crystal. Next, the grid was treated with a drop of 0.7% uranyl formate solution for 5 seconds and the excess solution removed filter paper. The grid was then treated with a second drop of uranyl formate solution for 12 s, and the excess solution was removed by filter paper. Finally, the grid was kept at room temperature to allow drying. TEM studies were conducted using a Philips CM12 transmission electron microscope, operated at 80 kV in bright field mode.

Synthesis of 1.6 nm CdTe core QDs: CdTe core QDs with 1.6 nm diameter were synthesized according to our previous published procedure.[1] A freshly prepared NaHTe solution (the source of Te, 1.0 mol/L, 10 μL) was injected through a syringe into an N_2-saturated $Cd(NO_3)_2$ solution (the source of Cd, 0.005 mol/L, 50 mL) at room temperature (20 ^oC) in the presence of 3-mercaptopropionic acid (MPA, 37 μL) as a stabilizing agent. The pH was tuned to 12.2 by adding NaOH (1M). The molar ratio of Cd^{2+}/MPA/NaHTe in the mixture was fixed at 1:1.7:0.04. Special attention should be paid since the NaHTe is very easy to be oxidized by trace amount of oxygen in a short time. The solution was subsequently aged at 4 ^oC and magic-sized CdTe clusters with photoluminescence emission peak at 480 nm were formed overnight. The diameter of the resulting CdTe QDs was ~ 1.6 nm. These small QDs were purified by adding IPA (1:1 in volume ratio), followed by centrifugation at 15,000 rpm for 15 minutes and were subsequently re-dispersed in DI water. In some cases, the crude, unpurified CdTe QD solutions were also used directly as the stock solution for the next step shell growth. Both pure and impure solutions were used as the cores for synthesizing the oligonucleotides conjugated CdTe/CdS core/shell QDs.

Oligonucleotide functionalized CdTe/CdS core/shell QDs: The above precipitated 1.6 nm CdTe QDs (from 100 µL stock solution) were re-suspended in 100 µL of nano-pure water. The concentration of the core CdTe QDs and amount of additional shell precursor to obtain specific shell thicknesses were calculated following a reported method.[2-3] For a typical experiment to synthesize CdTe/4 CdS core/shell QDs with 1.6 nm CdTe core diameter (0.25 nM in 100 µL DI water), 4.5 µL Cd^{2+} stock solution (25 mM) and 9.0 µL MPA stock solution (25 mM) were combined with the core, vortexed and gently sonicated in a 1.5 mL plastic tube. Next, 50 µL of 5'-TTATTATTATTATTATTATTAG*G*G*G*G* G -3' oligonucleotide stock solution (100 nM) was also added and gently vortexed. The molar ratio of QD: oligonucleotide was approximately 1: 200. The pH was tuned to 12.2 by adding NaOH (1M). The reaction mixture was placed on a heating block at 90 ^{o}C for 40 minutes, and then cooled down by submerging the tube in a water bath at room temperature. The reacted solution was loaded into a 0.5 mL Amicon filter (MWCO 30KDa), 250 µL DI water was added to the filter, and the sample was subjected to centrifugation at 7000 rpm for 3 minutes. The washing (each washing was performed with 350 µL of DI water) and centrifugation steps were repeated four times. This ultrafiltration process removed the free DNA and unreacted precursor from the QDs. If buffer exchange with DI water is desired, 350 µL of 1XTA buffer, rather than DI water, could be added before and after the centrifugation. The final sample is highly fluorescent and stable in buffer or in DI water.

DNA Functionalization of AuNPs: The protected thiol-modified oligonucleotides as dithiol were reduced to monothiol using TCEP (1:200 molar ratio of DNA:TCEP, overnight) in water. The oligonucleotides were purified using G-25 size exclusion

columns (GE Healthcare) to remove the small molecules. The purified monothiol-modified oligonucleotides were incubated with purchased AuNPs in a 1000:1 ratio in 1 × TBE buffer (44 mM Tris, 44 mM boric acid, 1 mM EDTA, pH 8.0). The NaCl concentration was gradually increased to 400 mM over 36 h at room temperature to ensure full coverage of the AuNPs by the thiolated DNA. The AuNP−DNA conjugates were washed 3 times just by centrifugation to remove excess oligonucleotides and were finally resuspended the pellet in 0.5 × TAE-Mg2+ buffer. The concentration of these AuNP-DNA conjugates was estimated from the optical absorbance at ∼527 nm using the previously mentioned extinction coefficients.

Preparation of the origami: Triangular DNA Origami was synthesized following the typical procedure described by Rothemund in 2006 (Nature, 2006). The long single stranded M13 scaffold and each of the short staple strands without purification were mixed at molar ratio of 1:5. The binding sites on the origami for the QD and AuNP were generated by modifying 3 adjacent staple stands (arranged in a triangle) at selective positions on the origami by adding specific nucleotide sequence at the 5' ends, which act as the capturing strands. The ratio between the M13 DNA and the modified staple strands (purified) was 1:20 in the mixture. The assembly was done (3nM) in 1×TAE-Mg^{2+} buffer (Tris base 40 mM; Acetic Acid 20 mM; EDTA 2 mM; Magnesium Acetate 12.5 mM; pH 8) by cooling down slowly from 90°C to 4°C. In order to get rid of the excess staple strands and the capture strands, the assembled origami was washed 3 times with 1×TAE-Mg^{2+} buffer in a Amicon filter (100kD MWCO).

Conjugation of AuNPs and QDs to DNA Origami and Purification: The DNA-functionalized NP solution was added to a 3 nM DNA origami solution (purified) in 0.5 ×

TAE-Mg2+, with a molar ratio of 3:1 to ensure high yield of the desired structure. The mixture was simply left overnight at room temperature. The resulting mixture was subjected to 1% agarose gel electrophoresis for 1.5hour at a constant 10V/cm. The band containing the desired structure was excised from the gel, extracted using a Freeze 'N Squeeze column (Biorad) and concentrated by centrifugation at 7000 rpm for 7 minutes and finally redispersed in 0.5 × TAE-Mg^{2+} buffer. The AuNPs decorated origami was annealed with DNA functionalized QDs from 37°C to 4°C over the course of 24 hours. Finally the sample was centrifuged to get a pellet. The top solution containing unbound QDs is discarded. The pellet was re-suspended in 0.5 × TAE-Mg^{2+} buffer and the process was repeated for three more times.

4.4. Results and discussions

4.4.1 Fluorescence quenching by 30nm gold nanoparticles

We employed a bottom up approach to build up the AuNP-QD hetero-dimer with the help of DNA nanotechnology. In recent years DNA nanostructures have emerged as novel scaffolds for spatially organizing nanoparticles or biomolecules with nanometer precision (refs).[28-32] Among other DNA nanostructures, DNA origami is suitable for fine tuning the distance between the nanoparticles. DNA functionalized gold and silver nanoparticles of different shapes and sizes have been organized in various fashions on DNA origami (refs).[33, 34] DNA origami has also served as the scaffold for organization of DNA conjugated and streptavidin coated QDs (refs).[35] Moreover DNA origami offers special advantage of attaching multifunctional components. Attachment of a different number of gold nanoparticles and QDs on the origami platform has been demonstrated by multiple groups recently.[36, 37] But the quantum dots used in both reports were streptavidin

coated QDs, which are much larger in size due to the cross linked polymer and the streptavidin proteins on the surface and it has been proved that they perform poorly in distance dependent energy transfer studies than the purely DNA functionalized QDs. [38]

We have recently developed the method for synthesis of stable DNA conjugated water-soluble core/shell quantum dots of various elemental compositions and realized their site-specific attachments to DNA origami (refs). [31] Here we choose to use a triangle shaped DNA origami and selectively attached one 30 nm gold nanoparticle and one red emitting QD (CdTe/CdS) at 5 different controlled inter-particle distances, ranging from 10 nm to 70 nm. Both static fluorescence spectroscopy and lifetime measurement were used to study the distance dependence of the fluorescence of the quantum dot.

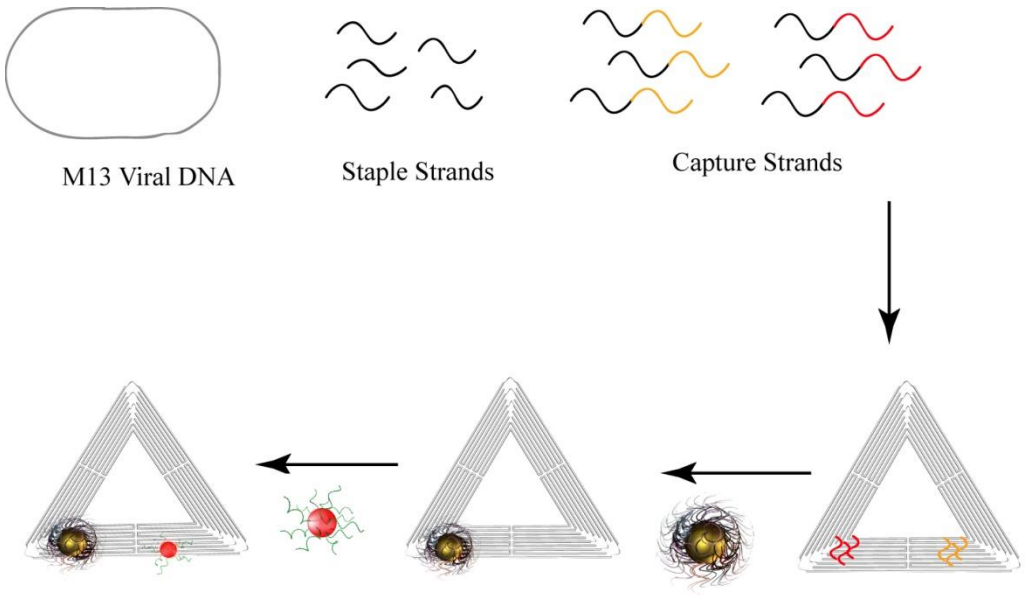

Figure 4.1. Schematic depicting stepwise assembly of 30 nm gold nanoparticle (gold) and CdTe/CdS Core/shell QD (red) on DNA origami (grey). The hybridization domains of the capture strands for the gold NP and the QDs are displayed in red and the orange, respectively. 1) The scaffold (M13 viral DNA) and staple strands (including the capture

strands, three for each particle) were mixed together in 1:5:10 molar ratio in 1x TAE-Mg buffer and annealed (by increase the temperature to 90 °C and cool down slowly over 12 hours. The excess staple strands were removed by using an Amicon centrifugal filter device (MWCO 100 kD). 2) DNA coated gold nanoparticle (diameter 30 nm) were mixed with the DNA origami (in 1:5 ratio) and incubated for overnight to ensure the nanoparticle capturing. Purification was done by native agarose gel electrophoresis to remove the free excess gold NPs and higher order structures. 3) DNA coated QDs (emission peak at 645 nm) were mixed with the purified DNA origami carrying one 30 nm gold NP, incubated to ensuring QD capturing, then purified by gentle centrifugation to remove the free excess QDs.

In a typical assembly process approximately 200 unique short staple strands were mixed with a long single stranded DNA (M13mp18) to obtain a triangle shaped nanostructure with each arm nearly 115 nm in length. Binding site for DNA conjugated AuNP and QD were created at specific location by extending staple strands with DNA sequence complimentary to the binding domain of the DNA displayed on AuNPs and QDs. To reduce the flexibility of the bound NPs, each binding site was designed to have three capture strands located at ~6 nm away from one another. The resulting nanostructures were purified by washing with 1X TAE-Mg^{2+} buffer in 100KD molecular weight cut off (MWCO) Amicon filter to get rid of the excess staple and capture strands. High yield and integrity of the purified origami was confirmed by Atomic Force Microscopy (AFM).

We made total five different designs where the position of the AuNP was fixed while the position of the QD was varied. Commercially available citrate stabilized

spherical gold nanoparticle of 30±1 nm diameter was used as the quencher and homemade DNA conjugated CdTe/CdS core shell QDs were used as the quantum emitter with emission maxima at ~645 nm. The reason behind choosing 30 nm AuNP is because it has high extinction cross-section yet minimal scattering. Besides significant scattering, the extinction spectrum of AuNP larger than 30 nm is dominated by quadrupole and octapole resonances, which can make the system more complicated to explain theoretically.

The assembly of these hetero elements was achieved in four steps (Figure 4.1). Firstly the DNA conjugated 30nm AuNPs were incubated with DNA origami for overnight at room temperature. Mg^{2+} ion concentration was reduced from normal 12.5 mM to 6.25 mM due to the intrinsic instability of the large AuNPs in high salt concentration. Since we had to incubate the pre-engineered origami with excess AuNPs to ensure maximum yield, the second step was the purification of the AuNP decorated DNA origami by gel electrophoresis to remove the excess unbound AuNPs and some higher order structures formed during annealing. High yield of the desired structure was confirmed by transmission electron microscopy (TEM) before proceeding to the next step. Thirdly, the DNA functionalized QDs were incubated with the purified structure containing one gold nanoparticle on each origami. Finally the extra unbound QDs were removed by simple gentle centrifugation (rcf 4000, for 5 min). Due to conjugation with the heavy 30 nm AuNP, the DNA origami tends to form a pellet when centrifuged. The upper solution containing the free unbound QDs was discarded. The pellet was re-suspended in 0.5X TAE-Mg^{2+} buffer solution by gentle agitation. This process does not

cause any severe damage to the final structure, although some loss of our final product, the origami bearing two distinct nanoparticles, was inevitable.

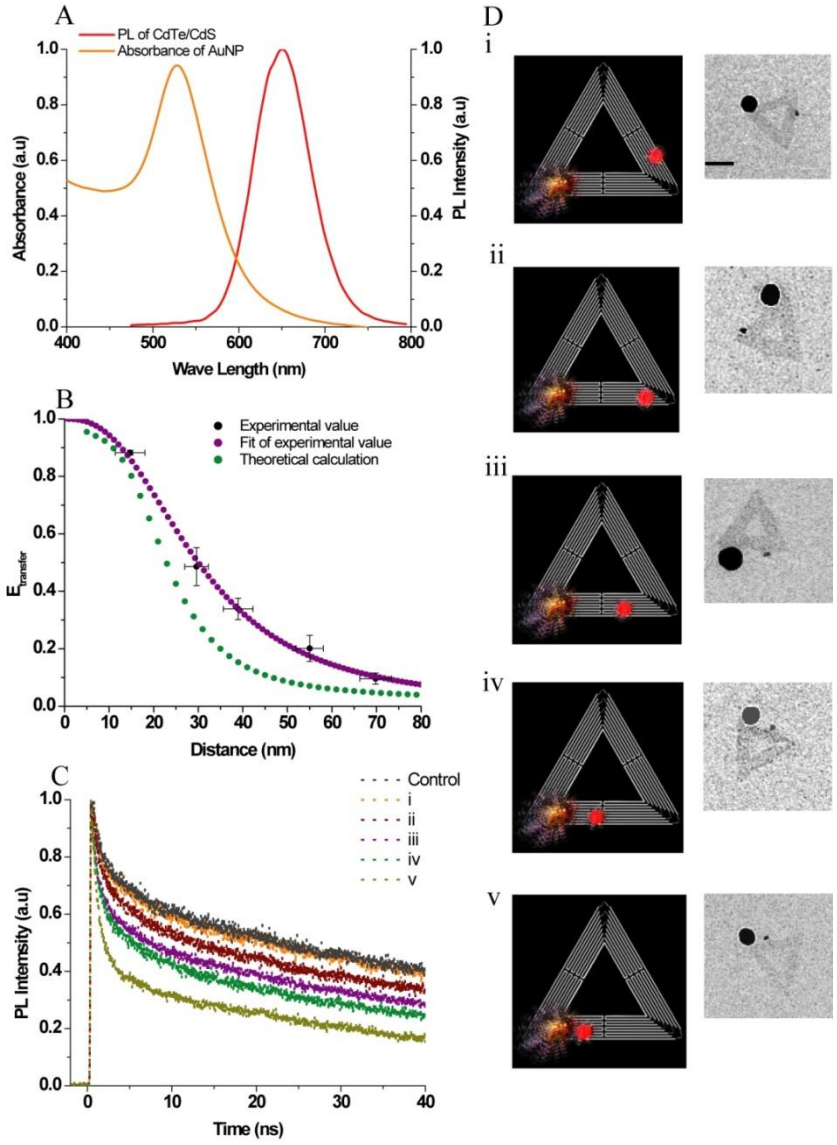

Figure 4.2. (A) Absorption spectra of 30 nm AuNP and PL emission spectra of QD with emission maxiam at 645nm. (B) Quenching efficiency (defined as 1- (PL sample/PL control)) is plotted against distance between the two particles. Green trace is theoretical

prediction. (C) Life time decay of different constructs. (D) Design of the five constructs and their corresponding TEM images. Scale bar 100 nm.

Normalized photoluminescence intensity obtained from steady state fluorescence measurement was plotted against the distance of the QD from AuNP surface (Figure 4.2). The energy transfer efficiency was defined as $E_T = 1-(PL_{sample}/PL_{control})$. Here the control should be the PL of QDs in the absence of AuNPs. We followed a rather simple but elegant strategy employed by Pal et al (ref) recently to prepare the control sample. The origami containing the particles was just heated above its melting temperature for 5 minutes followed by quick immersion into ice. Doing so the origami structure is melted and all DNA strands dissociate from each other so that the particles are released to be free in the solution. Quick immersion into ice makes sure that the melted origami have no chance to refold and the nanoparticles also have no chance to assemble together. Considering the sub-nanomolar concentration of the particles, we can safely conclude that in the solution they are far apart spatially (with ~ um average distance) to exert any effect on each other. The inter-particle distance on the same origami was measured and calculated from the TEM images. Since TEM is 2D projection of 3D object, appropriate correction was introduced into the calculation to take the height difference of the two nanoparticles into consideration.

From Figure 4.2 it is evident that proximal gold nanoparticle reduces the fluorescent intensity of QDs and that depends strongly on the distance between them. Theoretical calculation data (green trace) using electrodynamic dipole model is plotted together with the experimental data (black balls). An overestimation of fluorescence

quenching compared to the calculated data was observed. The green trace is a fit to the equation bellow where D_0 and n are the fitting parameters,

$$Y = 1 - \frac{1}{1 - \left(\frac{d}{D_0}\right)^n}$$

which yielded n = 2.72 and D_0 = 27.8 nm. In case of semi infinite surface model pioneered by Person, the value of n was 4. We also fitted the data predicted by electrodynamic calculation with the aforementioned equation and that gives n = 3.05 and D_0 = 22.9 nm.

Table 4.1: Average life time of QDs emission in the 5 different constructs

	Free QDs	Construct (i)	Construct (ii)	Construct (iii)	Construct (iv)	Construct (v)
Experimental (ns)	23.90	23.28	19.76	17.16	14.07	8.11
Theoretical (ns)		23.63	23.1	21.27	18.64	4.78

We further investigated the photoluminescence lifetimes of the QDs in these constructs using the time correlated single photon counting (TCSPC) method. If the PL intensity quenching was mainly caused by rate increase of the nonradiative pathways, the lifetime decrease should also be correlated with the distance between the two particles. The data were analyzed with a home-built software package ASUFIT and was fitted with sum of multi-exponential decay model. (URL http://www.public.asu.edu/~laserweb/asufit/asufit.html)

$$F(t) = \sum A_i e^{-t/\tau_i}$$

Where F(*t)* is the obtained kinetic decay curve, A_i is the amplitude of the i^{th} decay channel and τ_i is the corresponding life time. Since three exponentials were required to fit the decay data, the average lifetime was calculated using

$$<\tau> = \sum_{i=1}^{3} A_i \ \tau_i \ / \sum_{i=1}^{3} A_i$$

where A_i is the amplitude of the i^{th} component. The experimentally obtained average lifetime and the theoretically predicted values are listed in the Table 1.

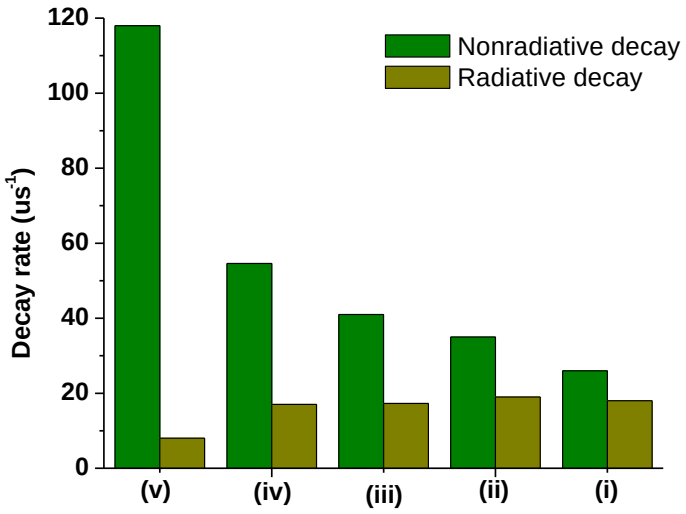

Figure 4.3. The average radiative and nonradiative decay rate of the QD photoluminescence from the 5 different constructs.

From the steady state fluorescence measurement and the average lifetime, the average radiative and nonradiative decay rate can be calculated. Quantum efficiency is expressed as QE = $\frac{k_r}{k_r+k_{nr}}$ and the average life time τ_{av} = $\frac{1}{k_r+k_{nr}}$. In the presence of a metallic nanoparticle additional pathways are introduced in the relaxation mechanism of the excited states. The modified expressions of QE and average lifetime are QE_m =

$\frac{k_r+k_{rm}}{k_r+k_{rm}+k_{nr}+k_{nrm}}$ and $\tau_{av} = \frac{1}{k_r+k_{rm}+k_{nr}+k_{nrm}}$. From the steady state fluorescence measurement we can calculate the modified quantum yield of individual construct considering the quantum yield of free QDs is 45%. The effective rate constant of radiate (k_{rf}) and nonradiative (k_{nrf}) pathways now are ($k_r + k_{rm}$) and ($k_{nr} + k_{nrm}$), respectively. The result shows that the nonradiative decay rate constant enhanced greatly (by more than 10 folds) with decreasing distance between the two particles (Figure 4.3). On the other hand, the radiative decay rate constant remained almost constant except when the QD is very close to the AuNP (< 15 nm) when a slight drop in the radiative decay rate constant was also observed.

4.4.2. Fluorescence enhancement by Au/Ag core/shell particles

Today it is a well known fact that presence of a nearby conducting metallic nanoparticle influences the fluorescence of a radiating dipole in many different ways.[39-43] Although the underlying mechanism is still debated, yet three mechanisms are generally proposed.[39, 44] One is damping of dipole oscillation which results in quenching of fluorescence intensity and that depends on the third or fourth power of distance between the metal surface and the dipole. Second mechanism is the enhancement of local electric field around the metal particle which can increase emission intensity by raising the rate of excitation. Third mechanism is the increase of radiative decay rate of the fluorophore. This can be better understood mathematically using Jablonski diagram. When a fluorophore absorbs a photon it goes to the excited state. After spending sometime there, it comes back to the ground state following either radiative (k_r) or nonradiative (k_{nr}) pathways. In case of quenching additional nonradiative channels are opened which do not significantly alter the radiative decay rate. In the presence of metallic nanoparticles rate

constant of additional nonradiative decay is k_{nmr}. So the Quantum Yield (QY) is expressed as

$$QY = \frac{k_r}{k_r + k_{nr} + k_{nmr}}$$

When a fluorophore is placed at a very close distance to the surface of the metallic nanoparticle intrinsic transition probability by radiating a photon is increased. Then the QY is modified as

$$QY_m = \frac{k_r + k_{mr}}{k_r + k_{mr} + k_{nr} + k_{nmr}}$$

Increased radiative decay rates means excited state will come back to ground state faster and will be ready to be excited again. This will increase the number cycles of excitation and de-excitation in unit time which will make the fluorophore look brighter. Moreover since the fluorophore will spend shorter time in the excited state photodegradation will be minimized.[45] For fluorophore like QDs, blinking could be suppressed for the same reason.[46] It is predicted that local electric field can be enhanced to 140 fold by careful composition of shape and size of the metallic nanoparticles.[47] Since the intensity is proportional to square of the field strength, theoretically nearly 20,000 fold enhancement of fluorescence intensity is possible. Additionally radiative decay rate can be increased up to 1000times which makes the total enhancement factor in the order of 10^7.[39] The detail theory behind these three pathways has been described in a simplified manner in a recent paper.[48]

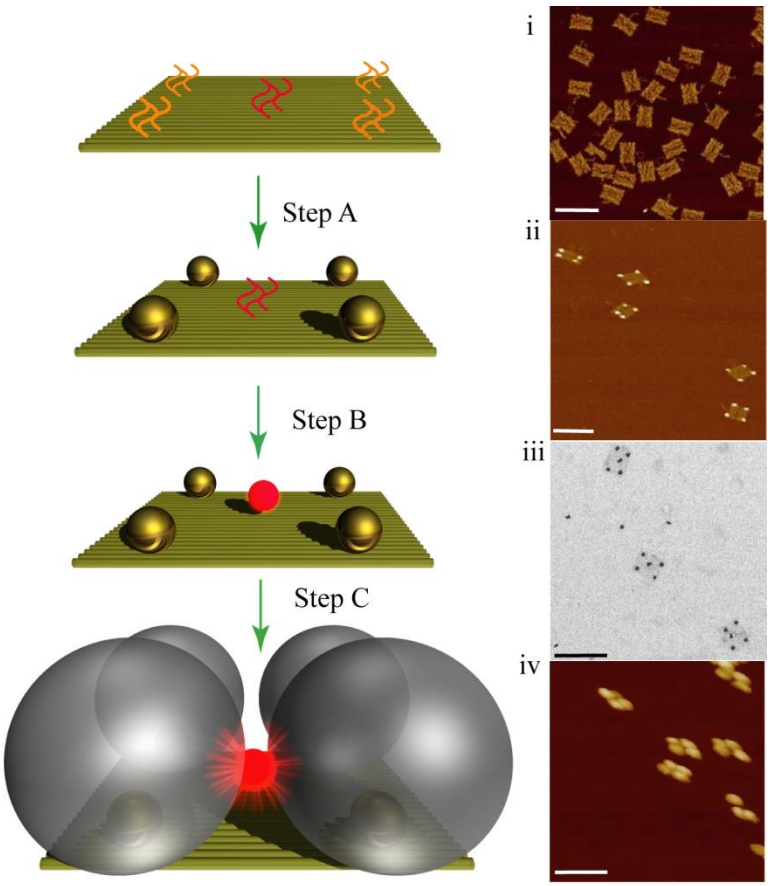

Figure 4.4. (Left) Schematic depicting preparation of the sample. Step A is the conjugation of 10nm AuNPs at the designated places of the rectangular origami marked by yellow capture strands. Purified structure was incubated with QDs in step B which binds at the center of the origami. Step C portrays the grown particles represented as grey balls. (Right) Corresponding AFM images of the constructs except from the third one from the top with four gold nanoparticles and one QD which is a TEM image. Scale bar 200nm.

Because of its tremendous potential to be used in analytical spectroscopy or as biosensors[49] it has attracted significant research interest in recent time.[50] Several groups

have reported enhancement of photoluminescence from 2 to 100 times.[51-56] Unfortunately most of them have been achieved by gold or silver nanostructures that are produced by electron beam lithography or by using nanoparticles in an uncontrolled fashion. They might have some application in other area but for biotechnological purpose that cannot be very useful. Here the basic idea is to bring the fluorophore either very close to the metal nanostructure or put in a sandwich fashion between them. Metal nanoparticles are really useful to serve this purpose. Slightly bigger size Au/Ag NPs that have significant scattering cross section that is useful for this purpose.[57] They can be decorated with biomolecules that can be further utilized for detecting other biomolecules or binding another particle. Biomolecules like DNA can be attached to the NPs surface which has been recently utilized to organize them on DNA based soft nanostructure.[30, 33, 58] Bringing two or more gold nanoparticle (or silver nanoparticles) close can create a hotspot at their contact point. Hot spot acts like antenna to concentrate the incident electromagnetic field. When a fluorophore is placed in right orientation at the hotspot it can serve as a better enhancing factor than single gold or silver nanoparticle. Recently some attempt has been made to enhance the fluorescence intensity of organic dye using DNA scaffold to bring the gold nanoparticles together creating a hotspot.[56, 58] However in both cases gold nanoparticles of various sizes have been used. Well controlled organization of silver nanoparticles, which is known for stronger plasmonic effect, on bio-friendly platform to create hotspot is still missing.

In this ongoing work we have tried create a hotspot with a hybrid Au (core)/Ag (shell) nanoparticle on DNA origami scaffold. We have used Quantum Dots as our fluorphore which are in many ways better than organic fluorophore dyes. Their broad

absorption and narrow emission spectra make them a wonderful candidate for multiplex imaging using a single excitation wavelength. Enhancing the fluorescence intensity of QDs can be a leap forward to their already existing application for *in vivo* imaging to increase signal to noise ratio. As we said earlier bringing the fluorophore close enough to the metallic nanoparticle is very crucial so that it can sense the condensed electric field. But QDs are not like organic dyes; they have finite size, some surface ligands to protect them and overall a much larger hydrodynamic radii which prevent the two particles to come to contact distance. Also the assembly yield of the hybrid sandwich type structure was low. To combat this problem we chose a rather new strategy to build that.

First a rectangular origami was prepared with four designated area at the four corners for capturing four gold nanoparticles of average diameter 10nm. Three staple strands at each position were extended with a sequence of nucleotides that are complimentary to the DNA displayed on the AuNPs. At the center of the origami equidistant from the four gold nanoparticle four staples strands were replaced with four strands of same sequence but bearing a biotin tag. Four biotin tag were approximately 6nm from each other will capture a streptavidin coated quantum dot. The origami was prepared and purified following standard procedure already described in the previous chapter. The purified origami was then mixed with 8 times more DNA functionalized AuNPs and the resulting mixture was annealed from 40°C to 4°C over the course of 15 hours. The product was purified in agarose gel electrophoresis and was confirmed with Transmission Electron Microscopy that most of the origami has four gold nanoparticles on it, except some has three. The purified structure was then mixed with QDs and left at room temperature in dark for several hours. Again the product was confirmed with TEM

which proved our desired structure bearing four gold nanoparticles at the four corners and a QD at the center. But 10nm gold nanoparticles at such long distance can only quench the fluorescence. So we grew the particles with a coating of Ag which can improve the plasmonic effect as well as reduce the distance between two particles. A recently reported method was followed to grow the particles. Figure 4.5 shows the growth kinetics of this process. After 5 minutes of incubation the particle diameter increased from 10nm to 25nm and after 7.5 minutes they grow as large as 35nm.

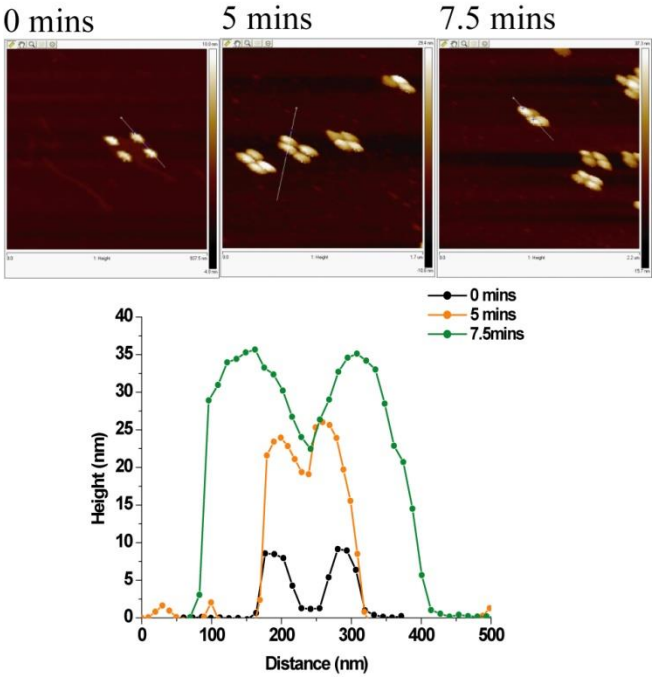

Figure 4.5: Ag mediated growth of the gold nanoparticles. On the top AFM images of the samples collected at different time after incubation. At the bottom the corresponding height profile has been plotted.

The measurement of the sample was done in an instrument with combined atomic force microscopy and single molecule sensitive confocal fluorescence microscopy. AFM will provide the structural information while confocal will give the information about the fluorescence labels. We immobilized our sample to the mica which was mounted on the glass using glue. In our experiment we see increased count rate from the sample containing QDs and Au/Ag hybrid nanoparticles. Life time of the QDs was also significantly reduced in the presence of metallic nanoparticles. Comparing the photon count rate we speculate the enhancement factor is in the order of 7 to 10. However this is an ongoing experiment which needs more time to make any conclusive remark.

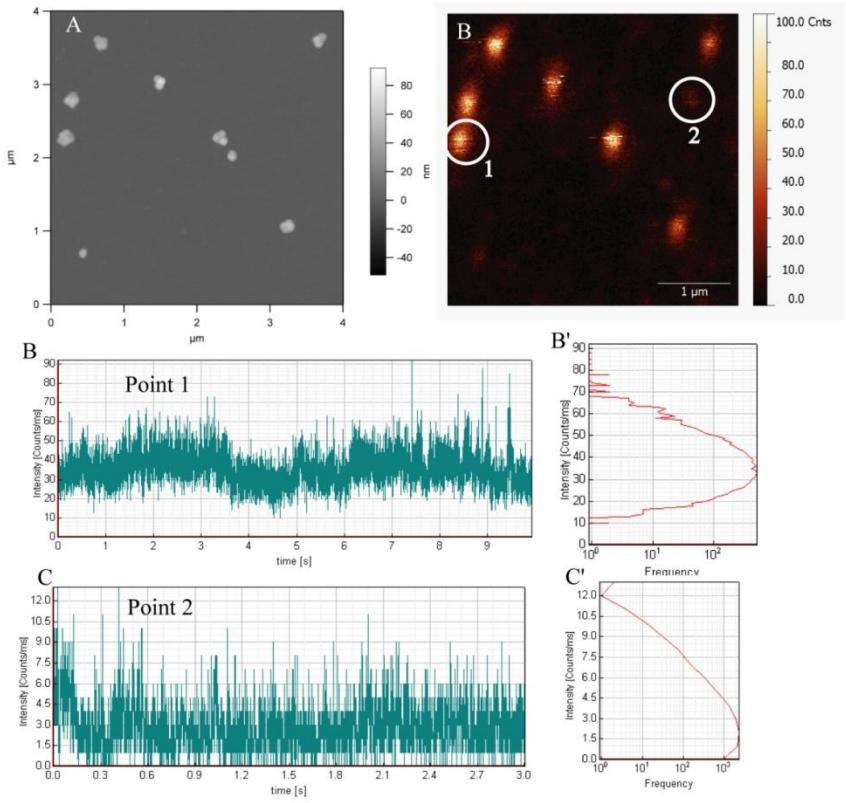

Figure 4.6. Simultaneous tapping mode AFM and confocal laser scanning microscope image of the sample. (A) AFM topography (B) confocal fluorescence intensity image (B

and B') Point scan of point 1 and its statistics (C and C') Point scan of point 2 and its statistics.

4.5. Conclusion

In summary, we have developed a reliable method for bringing metallic and semiconducting nanoparticles together using DNA directed self-assembly. This gives unprecedented control over the stoichiometry and the distance between two particles and allowed us to do bulk measurements to better our understanding of the plasmonic interactions between a gold nanoparticle and a photoluminescent semiconductor nanoparticle. A long range quenching of the photoluminescence of quantum dots driven by the large gold nanoparticles attached to the same DNA origami were observed. The quenching effect goes several folds beyond the traditional dye-dye or QD-dye FRET range or NSET between a gold nanopartciel with an organic dye. The quenching was mainly due to the increased nonradiatve decay channels in the presence of proximal AuNP, without affecting much the radiative decay rate. The measured quenching efficiency is always higher than the predicted values. This might be due to the slight bending in the 2D origami structure due to presence of heavy nanoparticles or some electrostatic interaction. Further studies are required with more rigid system and with new insight into the theoretical input. The long range effect within this bio-friendly system can be really useful in future for sensing studies both *in vitro* and *in vivo*. In case of enhancement of QD fluorescence though the preliminary result shows some enhancement, yet more control experiment is needed to draw a sold conclusion.

4.6. References

1. Stryer, L., Fluorescence energy-transfer as a spectroscopic ruler. *Annu. Rev. of Bioche.* **1978**, 47, 819-846.

2. Sekar, R. B.; Periasamy, A., Fluorescence resonance energy transfer (FRET) microscopy imaging of live cell protein localizations. *J. Cell Biol.* **2003**, 160, 629-633.

3. Dosremedios, C. G.; Moens, P. D. J., Fluorescence resonance energy-transfer spectroscopy is a reliable ruler for measuring structural-changes in proteins - dispelling the problem of the unknown orientation factor. *J. Struct. Biol.* **1995**, 115, 175-185.

4. Lilley, D. M. J.; Wilson, T. J., Fluorescence resonance energy transfer as a structural tool for nucleic acids. *Curr. Opin. Chem. Biol.* **2000**, 4, 507-517.

5. Selvin, P. R., The renaissance of fluorescence resonance energy transfer. *Nat. Struct. Mol. Biol.* **2000**, 7, 730-734.

6. Parkhurst, L. J.; Parkhurst, K. M.; Powell, R.; Wu, J.; Williams, S., Time-resolved fluorescence resonance energy transfer studies of DNA bending in double-stranded oligonucleotides and in DNA-protein complexes. *Biopolymers* **2001**, 61, 180-200.

7. Yun, C. S.; Javier, A.; Jennings, T.; Fisher, M.; Hira, S.; Peterson, S.; Hopkins, B.; Reich, N. O.; Strouse, G. F., Nanometal surface energy transfer in optical rulers, breaking the FRET barrier. *J. Am. Chem. Soc.* **2005**, 127, 3115-3119.

8. Breshike, C. J.; Riskowski, R. A.; Strouse, G. F., Leaving Forster Resonance Energy Transfer Behind: Nanometal Surface Energy Transfer Predicts the Size-Enhanced Energy Coupling between a Metal Nanoparticle and an Emitting Dipole. *J. Phys. Chem. C* **2013**, 117, 23942-23949.

9. Jennings, T. L.; Singh, M. P.; Strouse, G. F., Fluorescent lifetime quenching near d=1.5 nm gold nanoparticles: Probing NSET validity. *J. Am. Chem. Soc.* **2006**, 128, 5462-5467.

10. Chowdhury, S.; Wu, Z.; Jaquins-Gerstl, A.; Liu, S.; Dembska, A.; Armitage, B. A.; Jin, R.; Peteanu, L. A., Wavelength Dependence of the Fluorescence Quenching Efficiency of Nearby Dyes by Gold Nanoclusters and Nanoparticles: The Roles of Spectral Overlap and Particle Size. *J. Phys. Chem. C* **2011**, 115, 20105-20112.

11. Griffin, J.; Singh, A. K.; Senapati, D.; Rhodes, P.; Mitchell, K.; Robinson, B.; Yu, E.; Ray, P. C., Size- and Distance-Dependent Nanoparticle Surface-Energy Transfer (NSET) Method for Selective Sensing of Hepatitis C Virus RNA. *Chem. Eur. J.* **2009**, 15, 342-351.

12. Chance, R. R.; Prock, A.; Silbey, R., Comments on classical theory of energy-transfer. *J. Chem. Phys.* **1975**, 62, 2245-2253.

13. Persson, B. N. J.; Lang, N. D., Electron-hole-pair quenching of excited-states near a metal. *Phys. Rev. B* **1982**, 26, 5409-5415.

14. Kuhn, H., Classical aspects of energy transfer in molecular systems. *J. Chem. Phys.* **1970**, 53, 101-&.

15. Singh, M. P.; Strouse, G. F., Involvement of the LSPR Spectral Overlap for Energy Transfer between a Dye and Au Nanoparticle. *J. Am. Chem. Soc.* **2010**, 132, 9383-9391.

16. Pustovit, V. N.; Shahbazyan, T. V., Fluorescence quenching near small metal nanoparticles. *J. Chem. Phys.* **2012**, 136.

17. Carminati, R.; Greffet, J. J.; Henkel, C.; Vigoureux, J. M., Radiative and non-radiative decay of a single molecule close to a metallic nanoparticle. *Opt. Commun.* **2006**, 261, 368-375.

18. Ruppin, R., Decay of an excited molecule near a small metal sphere. *J. Chem. Phys.* **1982**, 76, 1681-1684.

19. Gersten, J.; Nitzan, A., Spectroscopic properties of molecules interacting with small dielectric particles. *J. Chem. Phys.* **1981**, 75, 1139-1152.

20. Saini, S.; Srinivas, G.; Bagchi, B., Distance and Orientation Dependence of Excitation Energy Transfer: From Molecular Systems to Metal Nanoparticles. *J.Phys. Chem. B* **2009**, 113, 1817-1832.

21. Pons, T.; Medintz, I. L.; Sapsford, K. E.; Higashiya, S.; Grimes, A. F.; English, D. S.; Mattoussi, H., On the quenching of semiconductor quantum dot photoluminescence by proximal gold nanoparticles. *Nano Lett.* **2007**, 7, 3157-3164.

22. Li, X.; Qian, J.; Jiang, L.; He, S., Fluorescence quenching of quantum dots by gold nanorods and its application to DNA detection. *Appl.Phys. Lett.* **2009**, 94.

23. Gueroui, Z.; Libchaber, A., Single-molecule measurements of gold-quenched quantum dots. *Phys. Rev. Lett.* **2004**, 93.

24. Medintz, I. L.; Uyeda, H. T.; Goldman, E. R.; Mattoussi, H., Quantum dot bioconjugates for imaging, labelling and sensing. *Nat. Mater.* **2005**, 4, 435-446.

25. Medintz, I. L.; Clapp, A. R.; Mattoussi, H.; Goldman, E. R.; Fisher, B.; Mauro, J. M., Self-assembled nanoscale biosensors based on quantum dot FRET donors. *Nat. Mater.* **2003**, 2, 630-638.

26. Boeneman, K.; Prasuhn, D. E.; Blanco-Canosa, J. B.; Dawson, P. E.; Melinger, J. S.; Ancona, M.; Stewart, M. H.; Susumu, K.; Huston, A.; Medintz, I. L., Self-Assembled Quantum Dot-Sensitized Multivalent DNA Photonic Wires. *J. Am. Chem. Soc.* **2010**, 132, 18177-18190.

27. Clapp, A. R.; Medintz, I. L.; Mattoussi, H., Forster resonance energy transfer investigations using quantum-dot fluorophores. *Chem. Phys. Chem.* **2006**, 7, 47-57.

28. Sharma, J.; Chhabra, R.; Liu, Y.; Ke, Y. G.; Yan, H., DNA-templated self-assembly of two-dimensional and periodical gold nanoparticle arrays. *Angew. Chem. Int. Ed.* **2006**, 45, 730-735.

29. Sharma, J.; Chhabra, R.; Andersen, C. S.; Gothelf, K. V.; Yan, H.; Liu, Y., Toward reliable gold nanoparticle patterning on self-assembled DNA nanoscaffold. *J. Am. Chem. Soc.* **2008**, 130, 7820-7821.

30. Ding, B. Q.; Deng, Z. T.; Yan, H.; Cabrini, S.; Zuckermann, R. N.; Bokor, J., Gold Nanoparticle Self-Similar Chain Structure Organized by DNA Origami. *J. Am. Chem. Soc.* **2010**, 132, 3248-3249.

31. Deng, Z.; Samanta, A.; Nangreave, J.; Yan, H.; Liu, Y., Robust DNA-Functionalized Core/Shell Quantum Dots with Fluorescent Emission Spanning from UV-vis to Near-IR and Compatible with DNA-Directed Self-Assembly. *J. Am. Chem. Soc.* **2012**, 134, 17424-17427.

32. Lin, C.; Liu, Y.; Yan, H., Designer DNA Nanoarchitectures. *Biochemistry* **2009**, 48, 1663-1674.

33. Pal, S.; Deng, Z. T.; Ding, B. Q.; Yan, H.; Liu, Y., DNA-Origami-Directed Self-Assembly of Discrete Silver-Nanoparticle Architectures. *Angew. Chem. Int. Ed.* **2010**, 49, 2700-2704.

34. Ding, B.; Deng, Z.; Yan, H.; Cabrini, S.; Zuckermann, R. N.; Bokor, J., Gold Nanoparticle Self-Similar Chain Structure Organized by DNA Origami. *J. Am. Chem. Soc.* **2010**, 132, 3248-3249.

35. Bui, H.; Onodera, C.; Kidwell, C.; Tan, Y.; Graugnard, E.; Kuang, W.; Lee, J.; Knowlton, W. B.; Yurke, B.; Hughes, W. L., Programmable Periodicity of Quantum Dot Arrays with DNA Origami Nanotubes. *Nano Lett.* **2010**, 10, 3367-3372.

36. Ko, S. H.; Du, K.; Liddle, J. A., Quantum-Dot Fluorescence Lifetime Engineering with DNA Origami Constructs. *Angew. Chem. Int. Ed.* **2013**, 52, 1193-1197.

37. Wang, R.; Nuckolls, C.; Wind, S. J., Assembly of Heterogeneous Functional Nanomaterials on DNA Origami Scaffolds. *Angew. Chem. Int. Ed.* **2012**, 51, 11325-11327.

38. Boeneman, K.; Deschamps, J. R.; Buckhout-White, S.; Prasuhn, D. E.; Blanco-Canosa, J. B.; Dawson, P. E.; Stewart, M. H.; Susumu, K.; Goldman, E. R.; Ancona, M.; Medintz, I. L., Quantum Dot DNA Bioconjugates: Attachment Chemistry Strongly Influences the Resulting Composite Architecture. *Acs Nano* **2010**, 4, 7253-7266.

39. Geddes, C. D.; Lakowicz, J. R., Metal-enhanced fluorescence. *J. Fluoresc.* **2002**, 12, 121-129.

40. Dragan, A. I.; Bishop, E. S.; Casas-Finet, J. R.; Strouse, R. J.; McGivney, J.; Schenerman, M. A.; Geddes, C. D., Distance Dependence of Metal-Enhanced Fluorescence. *Plasmonics* **2012**, 7, 739-744.

41. Kang, K. A.; Wang, J.; Jasinski, J. B.; Achilefu, S., Fluorescence Manipulation by Gold Nanoparticles: From Complete Quenching to Extensive Enhancement. *J. Nanobiotechnology* **2011**, 9.

42. Raikar, U. S.; Tangod, V. B.; Mastiholi, B. M.; Fulari, V. J., Fluorescence quenching using plasmonic gold nanoparticles. *Opt. Commun.* **2011**, 284, 4761-4765.

43. Lakowicz, J. R.; Shen, Y. B.; D'Auria, S.; Malicka, J.; Fang, J. Y.; Gryczynski, Z.; Gryczynski, I., Radiative decay engineering 2. Effects of silver island films on fluorescence intensity, lifetimes, and resonance energy transfer. *Anal. Biochem.* **2002**, 301, 261-277.

44. Lakowicz, J. R., Radiative decay engineering 5: metal-enhanced fluorescence and plasmon emission. *Anal. Biochem.* **2005**, 337, 171-194.

45. Anker, J. N.; Hall, W. P.; Lyandres, O.; Shah, N. C.; Zhao, J.; Van Duyne, R. P., Biosensing with plasmonic nanosensors. *Nat. Mater.* **2008**, 7, 442-453.

46. Fu, Y.; Zhang, J.; Lakowicz, J. R., Reduced blinking and long-lasting fluorescence of single fluorophores coupling to silver nanoparticles. *Langmuir* **2008**, 24, 3429-3433.

47. Kummerlen, J.; Leitner, A.; Brunner, H.; Aussenegg, F. R.; Wokaun, A., Enhanced dye fluorescence over silver island films - analysis of the distance dependence. *Mol. Phys.* **1993**, 80, 1031-1046.

48. Guzatov, D. V.; Vaschenko, S. V.; Stankevich, V. V.; Lunevich, A. Y.; Glukhov, Y. F.; Gaponenko, S. V., Plasmonic Enhancement of Molecular Fluorescence near Silver Nanoparticles: Theory, Modeling, and Experiment. *J. Phys. Chem. C* **2012**, 116, 10723-10733.

49. Lakowicz, J. R., Radiative decay engineering: Biophysical and biomedical applications. *Anal. Biochem.* **2001**, 298, 1-24.

50. Deng, W.; Xie, F.; Baltar, H. T. M. C. M.; Goldys, E. M., Metal-enhanced fluorescence in the life sciences: here, now and beyond. *Phys. Chem. Chem. Phys.* **2013**, 15, 15695-15708.

51. Corrigan, T. D.; Guo, S.; Phaneuf, R. J.; Szmacinski, H., Enhanced fluorescence from periodic arrays of silver nanoparticles. *J. Fluoresc.* **2005**, 15, 777-784.

52. Szmacinski, H.; Lakowicz, J. R.; Catchmark, J. M.; Eid, K.; Anderson, J. P.; Middendorf, L., Correlation between scattering properties of silver particle arrays and fluorescence enhancement. *Appl. Spectrosc.* **2008**, 62, 733-738.

53. Cade, N. I.; Ritman-Meer, T.; Kwakwa, K. A.; Richards, D., The plasmonic engineering of metal nanoparticles for enhanced fluorescence and Raman scattering. *Nanotechnology* **2009**, 20.

54. Anderson, J. P.; Griffiths, M.; Boveia, V. R., Near-infrared fluorescence enhancement using silver island films. *Plasmonics* **2006**, 1, 103-110.

55. McDonagh, C.; Stranik, O.; Nooney, R.; MacCraith, B. D., Nanoparticle strategies for enhancing the sensitivity of fluorescence-based biochips. *Nanomedicine* **2009**, 4, 645-656.

56. Acuna, G. P.; Moeller, F. M.; Holzmeister, P.; Beater, S.; Lalkens, B.; Tinnefeld, P., Fluorescence Enhancement at Docking Sites of DNA-Directed Self-Assembled Nanoantennas. *Science* **2012**, 338, 506-510.

57. Lee, K.-S.; El-Sayed, M. A., Gold and silver nanoparticles in sensing and imaging: Sensitivity of plasmon response to size, shape, and metal composition. *J. Phys. Chem. B* **2006**, 110, 19220-19225.

58. Pal, S.; Dutta, P.; Wang, H.; Deng, Z.; Zou, S.; Yan, H.; Liu, Y., Quantum Efficiency Modification of Organic Fluorophores Using Gold Nanoparticles on DNA Origami Scaffolds. *J. Phys. Chem. C* **2013**, 117, 12735-12744.

CHAPTER 5

SUMMARY AND OUTLOOK

5.1. Conclusion:

In this thesis I have demonstrated the power of DNA directed bottom up self assembly to bring up nano material in the same platform and showed a new direction to solve some real world problems. I began with synthesis of nano particles which was later modified with DNA to control their self assembly and finally their optical properties were manipulated with proximal metallic nanoparticles. In the chapter one I reported the development of water soluble multi-shell QDs encapsulated with biofriendly inorganic material (ZnS) and ligands (Glutathione). These QDs are exceedingly stable when stored at 4°C in ambient atmosphere in the presence of light. In the related paper I have stated there was no visible aggregation after few months of their synthesis with slight drop in the photoluminescence quantum yield. In reality, after 2 years of the synthesis, they are still very bright without any sign of aggregation, while the same kind of particle (built up of same material) capped with mercaptopropionic acid gets aggregated after few weeks. This indicates the role of glutathione is crucial. I speculate due to the branched structure of glutathione and presence of multiple charged sites they are more stable than those with relatively simple looking MPA. The same shell synthesis strategy was later employed for the DNA functionalized core-shell QDs. We have developed a robust, simple yet reliable strategy to functionalize QDs during shell synthesis. A library of QDs of varieties of material composition with emission spanning from blue to near infrared was produced. Those QDs were organized in different style on DNA origami proving the stability as well as high addressability of the particles. QDs emitting different colors were patterned

in a specific style which can serve as potential optical marker. Beyond the traditional visible range, we have produced QDs that can emit in real IR range and are DNA functionalized. IR emitting QDs are really useful for imaging tissues because the low background due to autofluorescence in that range. We have addressed another major issue about QDs namely blinking. We have produced thick shell of CdS around the CdSe core which showed dramatic reduction of fluorescence intermittency. In chapter 4 we have we have developed a reliable method for bringing metallic and semiconducting nanoparticles together using DNA directed self-assembly. This gives unprecedented control over the stoichiometry and the distance between two particles and allowed us to do bulk measurements to better our understanding of the plasmonic interactions between a gold nanoparticle and a photo luminescent semiconductor nanoparticle. A long range quenching of the photoluminescence of quantum dots driven by the large gold nanoparticles attached to the same DNA origami were observed. The quenching effect goes several folds beyond the traditional dye-dye or QD-dye FRET range or NSET between a gold nanopartciel with an organic dye. The quenching was mainly due to the increased nonradiatve decay channels in the presence of proximal AuNP, without affecting much the radiative decay rate. And currently we have engineered a system consisting a QD surrounded by proximal gold/silver nanoparticle to enhance the photoluminescence of the QD.

5.2. Future Direction

Great progress has been made toward achieving water-soluble DNA-functionalized QDs that have emission wavelengths spanning from the UV to NIR, high photoluminescence quantum efficiency, strong DNA–QD surface linkages, high stability

in high salt concentrations, resistance to various oxidizing and reducing agents as in real cellular environments, and robust enough performance to be assembled with other nanomaterials. However, there are several challenges that still need to be addressed.

A great challenge that must be addressed if QDs are to be used for diagnostic imaging is the nonspecific binding of QDs to cells, and their subsequent internalization which reduces the signal to noise ratio and affects the detection sensitivity. Several factors contribute to the mechanism of nonspecific binding, including surface charge, particle size, functional surface groups, and the molecular weight of the surface ligands, among which surface charge has a profound effect on nonspecific internalization. PEG modifications on the surface of QDs were shown to be effective in reducing the nonspecific adsorption to cells, mainly due to the near zero zeta potential of PEG-coated QDs. It is proposed that by using thiolated PEG along with phosphothiolated DNA in the shell formation step, both PEG and DNA functionality can be simultaneously introduced on the QD surface. Other analogs of DNA, like PNA and GNA with neutral backbones, can also be used if the backbone charge of DNA cannot be mediated.

The higher order organization of QDs using DNA recognition is a very active research direction. DNA conjugated AuNPs have been investigated intensively and organized into 2D and 3D arrays or into chiral arrangements that display novel optical properties. The few reports that exist of 3D crystallization of DNA-conjugated QDs, are solely based on spherical QDs. The synthesis of anisotropic QDs, needle or branched shaped structures, for example, or even metallic–semiconductor hybrid nanostructures, has only been performed in organic media. Linking them to DNA and other biomolecules still requires attention.

We also need to pay attention to DNA directed self assembly of nanoparticles. Two major challenges here are to scale up the product and to meet the top down lithographic surface patterning so that it can be sued for solid state device. Another challenge is to develop proper purification methodology. In general gel electrophoresis is used to get rid of the unwanted side products, aggregated or higher order structure and the unbound particles. Sometime it appears gel is a harsh method for some delicate construct which causes damage at the end. Biomolecule coated beads can be used to handle that problem. But more research is needed in that area.

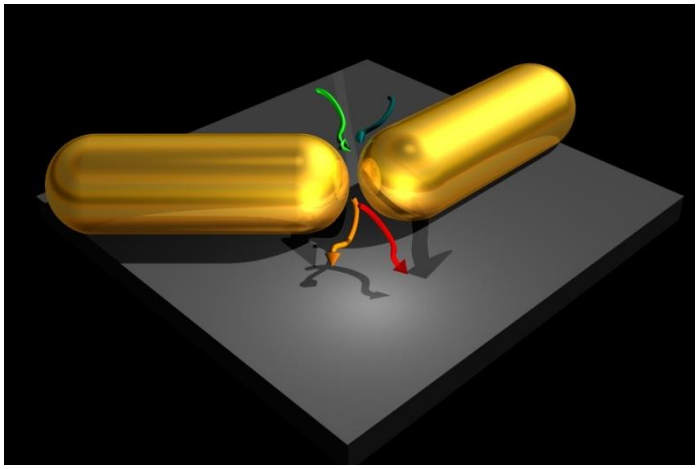

Figure 5.1: Plasmonic hot spot can be created by DNA based assembly of gold nanorod that can harvest light and induce photocatalytic organic reaction.

Assembly of spherical gold nanoparticle has been widely reported but the DNA directed self assembly of anisotropic gold nanoparticle is scarce. They can be used to create hot spot which can be very useful for fluorescence intensity enhancement of QDs that emit in the IR range and has very low photoluminescence quantum yield. Metal nanoparticles are not only famous for the plasmonics but they have a huge application

side as catalytic agent. Other anisotropic plasmonic nanoparticles such as gold triangles or prisms are capable of producing stronger plasmonic field enhancement but reliable DNA conjugation and proper control over the orientation has to be achieved. With the help of DNA directed self assembly we can create plasmonic hot spot than can induce photocatalytic reaction by concentrating and channeling low intensity visible light. This can be done with gold nanorod which has been assembled with controlled angles. This kind of discreet structure in large number can be further integrated as cheap and can be industrially used for catalytic purpose.

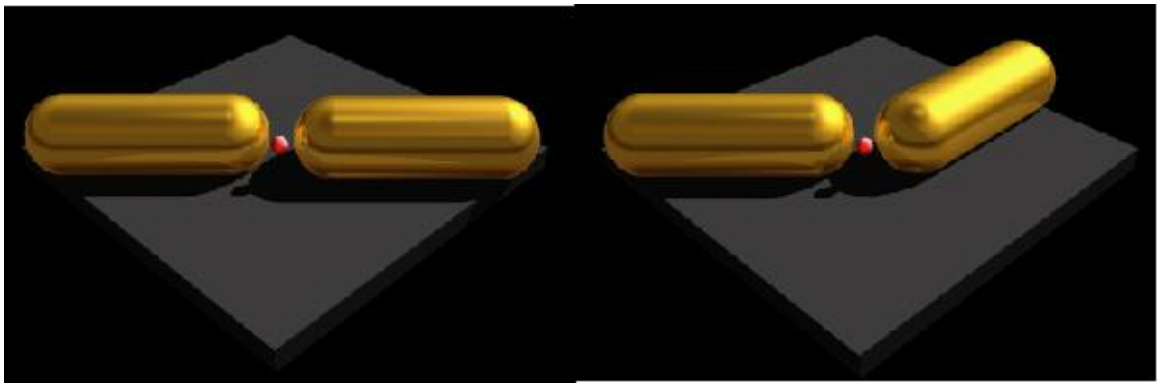

Figure 5.2: Engineering the electric field enhancement by monitoring the angle and distance between the nanorod that will be reflected into the fluorescence intensity of the fluorophore sitting in the middle of the two rod.

We can dream of more sophisticated DNA based robotic system carrying nanoparticles that will give proper signal in the presence of some target DNA. A possible design is given bellow. The three arm DNA based structure can rotate in the presence of a target DNA that will trigger some strand displacement. When the gold nanoparticle will

be close to any three QDs, its fluorescence will be quenched. In this way we can make a three color sensor.

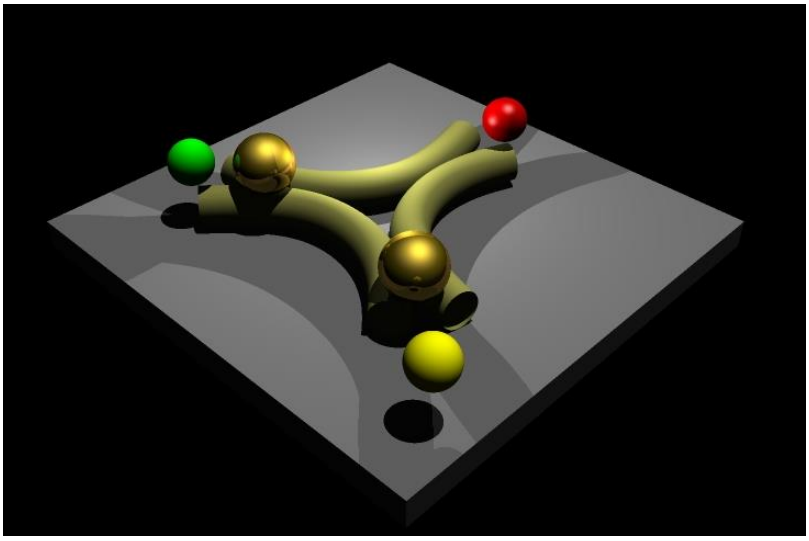

Figure 5.3: Schematic design of a proposed DNA based motor that can rotate if triggered by specific DNA. The position of the gold nanoparticles will dictate the output signal.

Today we are well poised to continue exploring this field and to discover novel optoelectronic properties that may lead to the future bio-optics.

REFERENCES

Chapter 1 References

1. Murray, C. B.; Norris, D. J.; Bawendi, M. G., Synthesis and characterization of nearly monodisperse CdE (E = S, Se, Te) semiconductor nanocrystallites. *J. Am. Chem. Soc.* **1993**, 115, 8706-8715.

2. Colvin, V. L.; Schlamp, M. C.; Alivisatos, A. P., Light-emitting-diodes made from cadmium selenide nanocrystals and a semiconducting polymer. *Nature* **1994**, 370, 354-357.

3. Schlamp, M. C.; Peng, X. G.; Alivisatos, A. P., Improved efficiencies in light emitting diodes made with CdSe(CdS) core/shell type nanocrystals and a semiconducting polymer. *J. Appl. Phys.***1997**, 82, 5837-5842.

4. Schaller, R. D.; Klimov, V. I., High efficiency carrier multiplication in PbSe nanocrystals: Implications for solar energy conversion. *Phys. Rev. Lett.* **2004**, 92.

5. Brichkin, S. B.; Chernykh, E. V., Hydrophilic semiconductor quantum dots. *High Energ. Chem.* **2011**, 45, 1-12.

6. Chan, W. C. W.; Nie, S. M., Quantum dot bioconjugates for ultrasensitive nonisotopic detection. *Science* **1998**, 281, 2016-2018.

7. Pradhan, N.; Battaglia, D. M.; Liu, Y.; Peng, X., Efficient, stable, small, and water-soluble doped ZnSe nanocrystal emitters as non-cadmium biomedical labels. *Nano Lett.* **2007**, 7, 312-317.

8. Wuister, S. F.; Swart, I.; van Driel, F.; Hickey, S. G.; Donega, C. D., Highly luminescent water-soluble CdTe quantum dots. *Nano Lett.s* **2003**, 3, 503-507.

9. Liu, W.; Choi, H. S.; Zimmer, J. P.; Tanaka, E.; Frangioni, J. V.; Bawendi, M., Compact cysteine-coated CdSe(ZnCdS) quantum dots for in vivo applications. *J. Am. Chem. Soc.* **2007**, 129, 14530-14531.

10. Algar, W. R.; Krull, U. J., Multidentate surface ligand exchange for the immobilization of CdSe/ZnS quantum dots and surface quantum dot-oligonucleotide conjugates. *Langmuir* **2008**, 24, 5514-5520.

11. Kim, S.; Bawendi, M. G., Oligomeric Ligands for luminescent and stable nanocrystal quantum dots. *J. Am. Chem. Soc.* **2003**, 125, 14652-14653.

12. Wang, Y. A.; Li, J. J.; Chen, H. Y.; Peng, X. G., Stabilization of inorganic nanocrystals by organic dendrons. *J. Am. Chem. Soc.* **2002**, 124, 2293-2298.

13. Pinaud, F.; King, D.; Moore, H. P.; Weiss, S., Bioactivation and cell targeting of semiconductor CdSe/ZnS nanocrystals with phytochelatin-related peptides. *J. Am. Chem. Soc.* **2004**, 126, 6115-6123.

14. Wu, X. Y.; Liu, H. J.; Liu, J. Q.; Haley, K. N.; Treadway, J. A.; Larson, J. P.; Ge, N. F.; Peale, F.; Bruchez, M. P., Immunofluorescent labeling of cancer marker Her2 and other cellular targets with semiconductor quantum dots. *Nat. Biotechnol.* **2003**, 21, 41-46.

15. Dubertret, B.; Skourides, P.; Norris, D. J.; Noireaux, V.; Brivanlou, A. H.; Libchaber, A., In vivo imaging of quantum dots encapsulated in phospholipid micelles. *Science* **2002**, 298, 1759-1762.

16. Gerion, D.; Pinaud, F.; Williams, S. C.; Parak, W. J.; Zanchet, D.; Weiss, S.; Alivisatos, A. P., Synthesis and properties of biocompatible water-soluble silica-coated CdSe/ZnS semiconductor quantum dots. *J. Phys. Chem. B* **2001**, 105, 8861-8871.

17. Selvan, S. T.; Tan, T. T.; Ying, J. Y., Robust, non-cytotoxic, silica-coated CdSe quantum dots with efficient photoluminescence. *Adv. Mater.* **2005**, 17, 1620-1625.

18. Rogach, A. L.; Franzl, T.; Klar, T. A.; Feldmann, J.; Gaponik, N.; Lesnyak, V.; Shavel, A.; Eychmueller, A.; Rakovich, Y. P.; Donegan, J. F., Aqueous synthesis of thiol-capped CdTe nanocrystals: State-of-the-art. *J. Phys. Chem. C* **2007**, 111, 14628-14637.

19. Bao, H. F.; Wang, E. K.; Dong, S. J., One-pot synthesis of CdTe nanocrystals and shape control of luminescent CdTe-cystine nanocomposites. *Small* **2006**, 2, 476-480.

20. Qian, H. F.; Dong, C. Q.; Weng, J. F.; Ren, J. C., Facile one-pot synthesis of luminescent, water-soluble, and biocompatible glutathione-coated CdTe nanocrystals. *Small* **2006**, 2, 747-751.

21. Zhang, Z. H.; Chin, W. S.; Vittal, J. J., Water-soluble CdS quantum dots prepared from a refluxing single precursor in aqueous solution. *J. Phys. Chem. B* **2004**, 108, 18569-18574.

22. Kho, R.; Torres-Martinez, C. L.; Mehra, R. K., A simple colloidal synthesis for gram-quantity production of water-soluble ZnS nanocrystal powders. *J. Colloid. Interface Sci.* **2000**, 227, 561-566.

23. Rogach, A.; Kershaw, S.; Burt, M.; Harrison, M.; Kornowski, A.; Eychmuller, A.; Weller, H., Colloidally prepared HgTe nanocrystals with strong room-temperature infrared luminescence. *Adv. Mater.* **1999**, 11, 552-555.

24. He, Y.; Lu, H.-T.; Sai, L.-M.; Su, Y.-Y.; Hu, M.; Fan, C.-H.; Huang, W.; Wang, L.-H., Microwave synthesis of water-dispersed CdTe/CdS/ZnS core-shell-shell quantum dots with excellent photostability and biocompatibility. *Adv. Mater.* **2008**, 20, 3416-3421.

25. Samanta, A.; Deng, Z.; Liu, Y., Aqueous Synthesis of Glutathione-Capped CdTe/CdS/ZnS and CdTe/CdSe/ZnS Core/Shell/Shell Nanocrystal Heterostructures. *Langmuir* **2012**, 28, 8205-8215.

26. Murphy, C. J.; Gole, A. M.; Stone, J. W.; Sisco, P. N.; Alkilany, A. M.; Goldsmith, E. C.; Baxter, S. C., Gold Nanoparticles in Biology: Beyond Toxicity to Cellular Imaging. *Acc. Chem. Res.* **2008**, 41, 1721-1730.

27. Pankhurst, Q. A.; Connolly, J.; Jones, S. K.; Dobson, J., Applications of magnetic nanoparticles in biomedicine. *J. Phys. D: Appl. Phys.* **2003**, 36, R167-R181.

28. Resch-Genger, U.; Grabolle, M.; Cavaliere-Jaricot, S.; Nitschke, R.; Nann, T., Quantum dots versus organic dyes as fluorescent labels. *Nat. Methods* **2008**, 5, 763-775.

29. Medintz, I. L.; Uyeda, H. T.; Goldman, E. R.; Mattoussi, H., Quantum dot bioconjugates for imaging, labelling and sensing. *Nat. Mater.* **2005**, 4, 435-446.

30. Michalet, X.; Pinaud, F. F.; Bentolila, L. A.; Tsay, J. M.; Doose, S.; Li, J. J.; Sundaresan, G.; Wu, A. M.; Gambhir, S. S.; Weiss, S., Quantum dots for live cells, in vivo imaging, and diagnostics. *Science* **2005**, 307, 538-544.

31. Xing, Y.; Chaudry, Q.; Shen, C.; Kong, K. Y.; Zhau, H. E.; Wchung, L.; Petros, J. A.; O'Regan, R. M.; Yezhelyev, M. V.; Simons, J. W.; Wang, M. D.; Nie, S., Bioconjugated quantum dots for multiplexed and quantitative immunohistochemistry. *Nat. Protoc.* **2007**, 2, 1152-1165.

32. Pinheiro, A. V.; Han, D.; Shih, W. M.; Yan, H., Challenges and opportunities for structural DNA nanotechnology. *Nat.e Nanotechnol.* **2011**, 6, 763-772.

33. Alivisatos, A. P.; Johnsson, K. P.; Peng, X. G.; Wilson, T. E.; Loweth, C. J.; Bruchez, M. P.; Schultz, P. G., Organization of 'nanocrystal molecules' using DNA. *Nature* **1996**, 382, 609-611.

34. Mirkin, C. A.; Letsinger, R. L.; Mucic, R. C.; Storhoff, J. J., A DNA-based method for rationally assembling nanoparticles into macroscopic materials. *Nature* **1996**, 382, 607-609.

35. Tan, S. J.; Campolongo, M. J.; Luo, D.; Cheng, W., Building plasmonic nanostructures with DNA. *Nat. Nanotechnol.* **2011**, 6, 268-276.

36. Torimoto, T.; Yamashita, M.; Kuwabata, S.; Sakata, T.; Mori, H.; Yoneyama, H., Fabrication of CdS nanoparticle chains along DNA double strands. *J. Phys. Chem. B* **1999**, 103, 8799-8803.

37. Levina, L.; Sukhovatkin, W.; Musikhin, S.; Cauchi, S.; Nisman, R.; Bazett-Jones, D. P.; Sargent, E. H., Efficient infrared-emitting PbS quantum dots grown on DNA and stable in aqueous solution and blood plasma. *Adv. Mater.* **2005**, 17, 1854-1857.

38. Coffer, J. L.; Bigham, S. R.; Li, X.; Pinizzotto, R. F.; Rho, Y. G.; Pirtle, R. M.; Pirtle, I. L., Dictation of the shape of mesoscale semiconductor nanoparticle assemblies by plasmid DNA. *Appl. Phys. Lett.* **1996**, 69, 3851-3853.

39. Mitchell, G. P.; Mirkin, C. A.; Letsinger, R. L., Programmed assembly of DNA functionalized quantum dots. *J. Am. Chem. Soc.* **1999**, 121, 8122-8123.

40. Boeneman, K.; Prasuhn, D. E.; Blanco-Canosa, J. B.; Dawson, P. E.; Melinger, J. S.; Ancona, M.; Stewart, M. H.; Susumu, K.; Huston, A.; Medintz, I. L., Self-Assembled Quantum Dot-Sensitized Multivalent DNA Photonic Wires. *J. Am. Chem. Soc.* **2010**, 132, 18177-18190.

41. Dyadyusha, L.; Yin, H.; Jaiswal, S.; Brown, T.; Baumberg, J. J.; Booy, F. P.; Melvin, T., Quenching of CdSe quantum dot emission, a new approach for biosensing. *Chem. Commun.* **2005**, 3201-3203.

42. Algar, W. R.; Krull, U. J., Adsorption and hybridization of oligonucleotides on mercaptoacetic acid-capped CdSe/ZnS quantum dots and quantum dot-oligonucleotide conjugates. *Langmuir* **2006**, 22, 11346-11352.

43. He, S.; Huang, B.-H.; Tan, J.; Luo, Q.-Y.; Lin, Y.; Li, J.; Hu, Y.; Zhang, L.; Yan, S.; Zhang, Q.; Pang, D.-W.; Li, L., One-to-one quantum dot-labeled single long DNA probes. *Biomaterials* **2011**, 32, 5471-5477.

44. Zhou, D.; Ying, L.; Hong, X.; Hall, E. A.; Abell, C.; Klenerman, D., A compact functional quantum dot-DNA conjugate: Preparation, hybridization, and specific label-free DNA detection. *Langmuir* **2008**, 24, 1659-1664.

45. Pathak, S.; Choi, S. K.; Arnheim, N.; Thompson, M. E., Hydroxylated quantum dots as luminescent probes for in situ hybridization. *J. Am. Chem. Soc.* **2001**, 123, 4103-4104.

46. Zhang, C.; Macfarlane, R. J.; Young, K. L.; Choi, C. H. J.; Hao, L.; Auyeung, E.; Liu, G.; Zhou, X.; Mirkin, C. A., A General Approach to DNa-programmable atom equivalents. *Nat.e Mater.* **2013**, 12, 741-746.

47. Parak, W. J.; Gerion, D.; Zanchet, D.; Woerz, A. S.; Pellegrino, T.; Micheel, C.; Williams, S. C.; Seitz, M.; Bruehl, R. E.; Bryant, Z.; Bustamante, C.; Bertozzi, C.

R.; Alivisatos, A. P., Conjugation of DNA to silanized colloidal semiconductor nanocrystalline quantum dots. *Chem. .Mater*. **2002**, 14, 2113-2119.

48. Tikhomirov, G.; Hoogland, S.; Lee, P. E.; Fischer, A.; Sargent, E. H.; Kelley, S. O., DNA-based programming of quantum dot valency, self-assembly and luminescence. *Nat.e Nanotechnol.* **2011**, 6, 485-490.

49. Lin, C.; Liu, Y.; Yan, H., Designer DNA Nanoarchitectures. *Biochemistry* **2009**, 48, 1663-1674.

50. He, Y.; Chen, Y.; Liu, H. P.; Ribbe, A. E.; Mao, C. D., Self-assembly of hexagonal DNA two-dimensional (2D) arrays. *J. Am. Chem. Soc.* **2005**, 127, 12202-12203.

51. Zheng, J.; Birktoft, J. J.; Chen, Y.; Wang, T.; Sha, R.; Constantinou, P. E.; Ginell, S. L.; Mao, C.; Seeman, N. C., From molecular to macroscopic via the rational design of a self-assembled 3D DNA crystal. *Nature* **2009**, 461, 74-77.

52. He, Y.; Ye, T.; Su, M.; Zhang, C.; Ribbe, A. E.; Jiang, W.; Mao, C., Hierarchical self-assembly of DNA into symmetric supramolecular polyhedra. *Nature* **2008**, 452, 198-201.

53. Rothemund, P. W. K., Folding DNA to create nanoscale shapes and patterns. *Nature* **2006**, 440, 297-302.

54. Han, D. R.; Pal, S.; Nangreave, J.; Deng, Z. T.; Liu, Y.; Yan, H., DNA Origami with Complex Curvatures in Three-Dimensional Space. *Science* **2011**, 332, 342-346.

55. Le, J. D.; Pinto, Y.; Seeman, N. C.; Musier-Forsyth, K.; Taton, T. A.; Kiehl, R. A., DNA-templated self-assembly of metallic nanocomponent arrays on a surface. *Nano Lett.* **2004**, 4, 2343-2347.

56. Zhang, J. P.; Liu, Y.; Ke, Y. G.; Yan, H., Periodic square-like gold nanoparticle arrays templated by self-assembled 2D DNA nanogrids on a surface. *Nano Lett.s* **2006**, 6, 248-251.

57. Sharma, J.; Chhabra, R.; Liu, Y.; Ke, Y. G.; Yan, H., DNA-templated self-assembly of two-dimensional and periodical gold nanoparticle arrays. *Angew. Chem. Int. Ed.* **2006**, 45, 730-735.

58. Zheng, J.; Constantinou, P. E.; Micheel, C.; Alivisatos, A. P.; Kiehl, R. A.; Seeman, N. C., Two-dimensional nanoparticle arrays show the organizational power of robust DNA motifs. *Nano Lett.* **2006**, 6, 1502-1504.

59. Sharma, J.; Ke, Y. G.; Lin, C. X.; Chhabra, R.; Wang, Q. B.; Nangreave, J.; Liu, Y.; Yan, H., DNA-tile-directed self-assembly of quantum dots into two-dimensional nanopatterns. *Angew. Chem. Int. Ed.* **2008**, 47, 5157-5159.

60. Park, S. H.; Yin, P.; Liu, Y.; Reif, J. H.; LaBean, T. H.; Yan, H., Programmable DNA self-assemblies for nanoscale organization of ligands and proteins. *Nano Lett.* **2005**, 5, 729-733.

61. Liu, Y.; Lin, C. X.; Li, H. Y.; Yan, H., Protein nanoarrays - Aptamer-directed self-assembly of protein arrays on a DNA nanostructure. *Angew. Chem. Int. Ed.* **2005**, 44, 4333-4338.

62. Chhabra, R.; Sharma, J.; Ke, Y.; Liu, Y.; Rinker, S.; Lindsay, S.; Yan, H., Spatially addressable multiprotein nanoarrays templated by aptamer-tagged DNA nanoarchitectures. *J. Am. Chem. Soc.* **2007**, 129, 10304-10305.

63. Ding, B. Q.; Deng, Z. T.; Yan, H.; Cabrini, S.; Zuckermann, R. N.; Bokor, J., Gold Nanoparticle Self-Similar Chain Structure Organized by DNA Origami. *J. Am. Chem. Soc.* **2010**, 132, 3248-3249.

64. Pal, S.; Deng, Z. T.; Ding, B. Q.; Yan, H.; Liu, Y., DNA-Origami-Directed Self-Assembly of Discrete Silver-Nanoparticle Architectures. *Angew. Chem. Int. Ed.* **2010**, 49, 2700-2704.

65. Bui, H.; Onodera, C.; Kidwell, C.; Tan, Y.; Graugnard, E.; Kuang, W.; Lee, J.; Knowlton, W. B.; Yurke, B.; Hughes, W. L., Programmable Periodicity of Quantum Dot Arrays with DNA Origami Nanotubes. *Nano Lett.* **2010**, 10, 3367-3372.

66. Maune, H. T.; Han, S.-p.; Barish, R. D.; Bockrath, M.; Goddard, W. A., III; Rothemund, P. W. K.; Winfree, E., Self-assembly of carbon nanotubes into two-dimensional geometries using DNA origami templates. *Nat. Nanotechnol.* **2010**, 5, 61-66.

67. Stephanopoulos, N.; Liu, M.; Tong, G. J.; Li, Z.; Liu, Y.; Yan, H.; Francis, M. B., Immobilization and One-Dimensional Arrangement of Virus Capsids with Nanoscale Precision Using DNA Origami. *Nano Lett.* **2010**, 10, 2714-2720.

68. Kuzyk, A.; Laitinen, K. T.; Torma, P., DNA origami as a nanoscale template for protein assembly. *Nanotechnology* **2009**, 20.

69. Shen, X.; Song, C.; Wang, J.; Shi, D.; Wang, Z.; Liu, N.; Ding, B., Rolling Up Gold Nanoparticle-Dressed DNA Origami into Three-Dimensional Plasmonic Chiral Nanostructures. *J. Am. Chem. Soc.* **2012**, 134, 146-149.

70. Shen, X.; Asenjo-Garcia, A.; Liu, Q.; Jiang, Q.; Favier Garcia de Abajo, F.; Liu, N.; Ding, B., Three-Dimensional Plasmonic Chiral Tetramers Assembled by DNA Origami. *Nano Lett.* **2013**, 13, 2128-2133.

71. Maye, M. M.; Kumara, M. T.; Nykypanchuk, D.; Sherman, W. B.; Gang, O., Switching binary states of nanoparticle superlattices and dimer clusters by DNA strands. *Nat. Nanotechnol.* **2010**, 5, 116-120.

72. Macfarlane, R. J.; Lee, B.; Jones, M. R.; Harris, N.; Schatz, G. C.; Mirkin, C. A., Nanoparticle Superlattice Engineering with DNA. *Science* **2011**, 334, 204-208.

73. Fu, A. H.; Micheel, C. M.; Cha, J.; Chang, H.; Yang, H.; Alivisatos, A. P., Discrete nanostructures of quantum dots/Au with DNA. *J. Am. Chem. Soc.* **2004**, 126, 10832-10833.

74. Wang, Q.; Wang, H.; Lin, C.; Sharma, J.; Zou, S.; Liu, Y., Photonic interaction between quantum dots and gold nanoparticles in discrete nanostructures through DNA directed self-assembly. *Chem. Commun.* **2010**, 46, 240-242.

Chapter 2 References

1. Michalet, X.; Pinaud, F. F.; Bentolila, L. A.; Tsay, J. M.; Doose, S.; Li, J. J.; Sundaresan, G.; Wu, A. M.; Gambhir, S. S.; Weiss, S., Quantum dots for live cells, in vivo imaging, and diagnostics. *Science* **2005**, *307*, 538-544.

2. Medintz, I. L.; Uyeda, H. T.; Goldman, E. R.; Mattoussi, H., Quantum dot bioconjugates for imaging, labelling and sensing. *Nature Mater.* **2005**, *4*, 435-446.

3. Dabbousi, B. O.; RodriguezViejo, J.; Mikulec, F. V.; Heine, J. R.; Mattoussi, H.; Ober, R.; Jensen, K. F.; Bawendi, M. G., (CdSe)ZnS core-shell quantum dots: Synthesis and characterization of a size series of highly luminescent nanocrystallites. *J. Phys. Chem. B* **1997**, *101*, 9463-9475.

4. Peng, X. G.; Schlamp, M. C.; Kadavanich, A. V.; Alivisatos, A. P., Epitaxial growth of highly luminescent CdSe/CdS core/shell nanocrystals with photostability and electronic accessibility. *J. Am. Chem. Soc.* **1997**, *119*, 7019-7029.

5. Piryatinski, A.; Ivanov, S. A.; Tretiak, S.; Klimov, V. I., Effect of quantum and dielectric confinement on the exciton-exciton interaction energy in type II core/shell semiconductor nanocrystals. *Nano Lett.* **2007**, *7*, 108-115.

6. Chen, C. Y.; Cheng, C. T.; Lai, C. W.; Hu, Y. H.; Chou, P. T.; Chou, Y. H.; Chiu, H. T., Type-II CdSe/CdTe/ZnTe (core-shell-shell) quantum dots with cascade

band edges: The separation of electron (at CdSe) and hole (at ZnTe) by the CdTe layer. *Small* **2005**, *1*, 1215-1220.

7. Hatami, F.; Grundmann, M.; Ledentsov, N. N.; Heinrichsdorff, F.; Heitz, R.; Bohrer, J.; Bimberg, D.; Ruvimov, S. S.; Werner, P.; Ustinov, V. M.; Kop'ev, P. S.; Alferov, Z. I., Carrier dynamics in type-II GaSb/GaAs quantum dots. *Phys. Rev. B* **1998**, *57*, 4635-4641.

8. Yoffe, A. D., Semiconductor quantum dots and related systems: electronic, optical, luminescence and related properties of low dimensional systems. *Adv. Phys.* **2001**, *50*, 1-208.

9. Deng, Z. T.; Schulz, O.; Lin, S.; Ding, B. Q.; Liu, X. W.; Wei, X. X.; Ros, R.; Yan, H.; Liu, Y., Aqueous Synthesis of Zinc Blende CdTe/CdS Magic-Core/Thick-Shell Tetrahedral-Shaped Nanocrystals with Emission Tunable to Near-Infrared. *J. Am. Chem. Soc.* **2010**, *132*, 5592-5593.

10. Kim, S.; Fisher, B.; Eisler, H. J.; Bawendi, M., Type-II quantum dots: CdTe/CdSe(core/shell) and CdSe/ZinTe(core/shell) heterostructures. *J. Am. Chem. Soc.* **2003**, *125*, 11466-11467.

11. Yu, K.; Zaman, B.; Romanova, S.; Wang, D. S.; Ripmeester, J. A., Sequential synthesis of type II colloidal CdTe/CdSe core-shell nanocrystals. *Small* **2005**, *1*, 332-338.

12. Wang, C. H.; Chen, T. T.; Tan, K. W.; Chen, Y. F.; Cheng, C. T.; Chou, P. T., Photoluminescence properties of CdTe/CdSe core-shell type-II quantumdots. *J. Appl. Phys.* **2006**, *99*, 123521.

13. Chang, J. Y.; Wang, S. R.; Yang, C. H., Synthesis and characterization of CdTe/CdS and CdTe/CdSe core/shell type-II quantum dots in a noncoordinating solvent. *Nanotechnology* **2007**, *18*, 345602.

14. Blackman, B.; Battaglia, D. M.; Mishima, T. D.; Johnson, M. B.; Peng, X. G., Control of the morphology of complex semiconductor nanocrystals with a type II heterojunction, dots vs peanuts, by thermal cycling. *Chem. Mater.* **2007**, *19*, 3815-3821.

15. Blackman, B.; Battaglia, D.; Peng, X. G., Bright and water-soluble near IR-Emitting CdSe/CdTe/ZnSe Type-II/Type-I nanocrystals, tuning the efficiency and stability by growth. *Chem. Mater.* **2008**, *20*, 4847-4853.

16. Dooley, C. J.; Dimitrov, S. D.; Fiebig, T., Ultrafast electron transfer dynamics in CdSe/CdTe donor-acceptor nanorods. *J. Phys. Chem. C* **2008**, *112*, 12074-12076.

17. Mattoussi, H.; Mauro, J. M.; Goldman, E. R.; Anderson, G. P.; Sundar, V. C.; Mikulec, F. V.; Bawendi, M. G., Self-assembly of CdSe-ZnS quantum dot bioconjugates using an engineered recombinant protein. *J. Am. Chem. Soc.* **2000**, *122*, 12142-12150.

18. Talapin, D. V.; Rogach, A. L.; Kornowski, A.; Haase, M.; Weller, H., Highly luminescent monodisperse CdSe and CdSe/ZnS nanocrystals synthesized in a hexadecylamine-trioctylphosphine oxide-trioctylphospine mixture. *Nano Lett.* **2001**, *1*, 207-211.

19. Talapin, D. V.; Mekis, I.; Gotzinger, S.; Kornowski, A.; Benson, O.; Weller, H., CdSe/CdS/ZnS and CdSe/ZnSe/ZnS core-shell-shell nanocrystals. *J. Phys. Chem. B* **2004**, *108*, 18826-18831.

20. Zhang, W. J.; Chen, G. J.; Wang, J.; Ye, B. C.; Zhong, X. H., Design and Synthesis of Highly Luminescent Near-Infrared-Emitting Water-Soluble CdTe/CdSe/ZnS Core/Shell/Shell Quantum Dots. *Inorg. Chem.* **2009**, *48*, 9723-9731.

21. Gao, M. Y.; Kirstein, S.; Mohwald, H.; Rogach, A. L.; Kornowski, A.; Eychmuller, A.; Weller, H., Strongly photoluminescent CdTe nanocrystals by proper surface modification. *J. Phys. Chem. B* **1998**, *102*, 8360-8363.

22. He, Y.; Lu, H. T.; Sai, L. M.; Lai, W. Y.; Fan, Q. L.; Wang, L. H.; Huang, W., Microwave-assisted growth and characterization of water-dispersed CdTe/CdS core-shell nanocrystals with high photoluminescence. *J. Phys. Chem. B* **2006**, *110*, 13370-13374.

23. Wang, C. L.; Zhang, H.; Zhang, J. H.; Li, M. J.; Sun, H. Z.; Yang, B., Application of ultrasonic irradiation in aqueous synthesis of highly fluorescent CdTe/CdS core-shell nanocrystals. *J. Phys. Chem. C* **2007**, *111*, 2465-2469.

24. Zhang, W. H.; Yu, J. S., Synthesis and Characterization of High Fluorescence, Type-II Core/Shell CdTe/CdSe Quantum Dots in Aqueous Medium. *Chin. J. Inorg. Chem.* **2010**, *26*, 775-780.

25. Taniguchi, S.; Green, M.; Rizvi, S. B.; Seifalian, A., The one-pot synthesis of core/shell/shell CdTe/CdSe/ZnSe quantum dots in aqueous media for in vivo deep tissue imaging. *J. Mater. Chem.* **2011**, *21*, 2877-2882.

26. Green, M.; Williamson, P.; Samalova, M.; Davis, J.; Brovelli, S.; Dobson, P.; Cacialli, F., Synthesis of type II/type I CdTe/CdS/ZnS quantum dots and their use in cellular imaging. *J. Mater. Chem.* **2009**, *19*, 8341-8346.

27. Yan, C.; Tang, F.; Li, L.; Li, H.; Huang, X.; Chen, D.; Meng, X.; Ren, J., Synthesis of Aqueous CdTe/CdS/ZnS Core/shell/shell Quantum Dots by a Chemical Aerosol Flow Method. *Nanoscale Res. Lett.* **2010**, *5*, 189-194.

28. He, Y.; Lu, H.-T.; Sai, L.-M.; Su, Y.-Y.; Hu, M.; Fan, C.-H.; Huang, W.; Wang, L.-H., Microwave synthesis of water-dispersed CdTe/CdS/ZnS core-shell-shell quantum dots with excellent photostability and biocompatibility. *Adv. Mater.* **2008**, *20*, 3416-3419.

29. Hoshino, A.; Fujioka, K.; Oku, T.; Suga, M.; Sasaki, Y. F.; Ohta, T.; Yasuhara, M.; Suzuki, K.; Yamamoto, K., Physicochemical properties and cellular toxicity of nanocrystal quantum dots depend on their surface modification. *Nano Lett.* **2004**, *4*, 2163-2169.

30. Jamieson, T.; Bakhshi, R.; Petrova, D.; Pocock, R.; Imani, M.; Seifalian, A. M., Biological applications of quantum dots. *Biomaterials* **2007**, *28*, 4717-4732.

31. Kirchner, C.; Liedl, T.; Kudera, S.; Pellegrino, T.; Javier, A. M.; Gaub, H. E.; Stolzle, S.; Fertig, N.; Parak, W. J., Cytotoxicity of colloidal CdSe and CdSe/ZnS nanoparticles. *Nano Lett.* **2005**, *5*, 331-338.

32. Wei, S. H.; Zhang, S. B.; Zunger, A., First-principles calculation of band offsets, optical bowings, and defects in CdS, CdSe, CdTe, and their alloys. *J. Appl. Phys.* **2000**, *87*, 1304-1311.

33. Deng, Z. T.; Zhang, Y.; Yue, J. C.; Tang, F. Q.; Wei, Q., Green and orange CdTe quantum dots as effective pH-sensitive fluorescent probes for dual simultaneous and independent detection of viruses. *J. Phys. Chem. B* **2007**, *111*, 12024-12031.

34. Yu, W. W.; Qu, L. H.; Guo, W. Z.; Peng, X. G., Experimental determination of the extinction coefficient of CdTe, CdSe, and CdS nanocrystals. *Chem. Mater.* **2003**, *15*, 2854-2860.

35. Deng, Z. T.; Yan, H.; Liu, Y., Band Gap Engineering of Quaternary-Alloyed ZnCdSSe Quantum Dots via a Facile Phosphine-Free Colloidal Method. *J. Am. Chem. Soc.* **2009**, *131*, 17744-17745.

36. Zeng, Q. H.; Kong, X. G.; Sun, Y. J.; Zhang, Y. L.; Tu, L. P.; Zhao, J. L.; Zhang, H., Synthesis and optical properties of type IICdTe/CdS core/shell quantum dots in aqueous solution via successive ion layer adsorption and reaction. *J. Phys. Chem. C* **2008**, *112*, 8587-8593.

37. Smith, A. M.; Mohs, A. M.; Nie, S., Tuning the optical and electronic properties of colloidal nanocrystals by lattice strain. *Nature Nanotech.* **2009**, *4*, 56-63.

38. Gurusinghe, N. P.; Hewa-Kasakarage, N. N.; Zamkov, M., Composition-tunable properties of CdSxTe1-x alloy nanocrystals. *J. Phys. Chem. C* **2008**, *112*, 12795-12800.

39. Panda, S. K.; Hickey, S. G.; Waurisch, C.; Eychmuller, A., Gradated alloyed CdZnSe nanocrystals with high luminescence quantum yields and stability for optoelectronic and biological applications. *J. Mater. Chem.* **2011**, *21*, 11550-11555.

40. Smith, A. M.; Nie, S. M., Semiconductor Nanocrystals: Structure, Properties, and Band Gap Engineering. *Acc. Chem. Res.* **2010**, *43*, 190-200.

Chapter 3 References

1. Service, R. F., How far can we push chemical self-assembly. *Science* **2005**, 309, 95-95.

2. Srivastava, S.; Santos, A.; Critchley, K.; Kim, K.-S.; Podsiadlo, P.; Sun, K.; Lee, J.; Xu, C.; Lilly, G. D.; Glotzer, S. C.; Kotov, N. A., Light-Controlled Self-Assembly of Semiconductor Nanoparticles into Twisted Ribbons. *Science* **2010**, 327, 1355-1359.

3. Liu, Y., NANOMATERIALS DNA brings quantum dots to order. *Nat. Nanotechnol.* **2011**, 6, 463-464.

4. Seeman, N. C., DNA in a material world. *Nature* **2003**, 421, 427-431.

5. Pinheiro, A. V.; Han, D.; Shih, W. M.; Yan, H., Challenges and opportunities for structural DNA nanotechnology. *Nat. Nanotechnol.* **2011**, 6, 763-772.

6. Tan, S. J.; Campolongo, M. J.; Luo, D.; Cheng, W., Building plasmonic nanostructures with DNA. *Nat. Nanotechnol.* **2011**, 6, 268-276.

7. Mirkin, C. A.; Letsinger, R. L.; Mucic, R. C.; Storhoff, J. J., A DNA-based method for rationally assembling nanoparticles into macroscopic materials. *Nature* **1996**, 382, 607-609.

8. Alivisatos, A. P.; Johnsson, K. P.; Peng, X. G.; Wilson, T. E.; Loweth, C. J.; Bruchez, M. P.; Schultz, P. G., Organization of 'nanocrystal molecules' using DNA. *Nature* **1996**, 382, 609-611.

9. Hurst, S. J.; Lytton-Jean, A. K. R.; Mirkin, C. A., Maximizing DNA loading on a range of gold nanoparticle sizes. *Anal. Chem.* **2006**, 78, 8313-8318.

10. Cutler, J. I.; Auyeung, E.; Mirkin, C. A., Spherical Nucleic Acids. *J. Am. Chem. Soc.* **2012**, 134, 1376-1391.

11. Elghanian, R.; Storhoff, J. J.; Mucic, R. C.; Letsinger, R. L.; Mirkin, C. A., Selective colorimetric detection of polynucleotides based on the distance-dependent optical properties of gold nanoparticles. *Science* **1997**, 277, 1078-1081.

12. Zhang, J. P.; Liu, Y.; Ke, Y. G.; Yan, H., Periodic square-like gold nanoparticle arrays templated by self-assembled 2D DNA nanogrids on a surface. *Nano Lett.* **2006**, 6, 248-251.

13. Ding, B.; Deng, Z.; Yan, H.; Cabrini, S.; Zuckermann, R. N.; Bokor, J., Gold Nanoparticle Self-Similar Chain Structure Organized by DNA Origami. *J. Am. Chem. Soc.* **2010**, 132, 3248-3249.

14. Cheng, W.; Campolongo, M. J.; Cha, J. J.; Tan, S. J.; Umbach, C. C.; Muller, D. A.; Luo, D., Free-standing nanoparticle superlattice sheets controlled by DNA. *Nat. Mater.* **2009**, 8, 519-525.

15. Sharma, J.; Chhabra, R.; Cheng, A.; Brownell, J.; Liu, Y.; Yan, H., Control of Self-Assembly of DNA Tubules Through Integration of Gold Nanoparticles. *Science* **2009**, 323, 112-116.

16. Macfarlane, R. J.; Lee, B.; Jones, M. R.; Harris, N.; Schatz, G. C.; Mirkin, C. A., Nanoparticle Superlattice Engineering with DNA. *Science* **2011**, 334, 204-208.

17. Kuzyk, A.; Schreiber, R.; Fan, Z.; Pardatscher, G.; Roller, E.-M.; Hoegele, A.; Simmel, F. C.; Govorov, A. O.; Liedl, T., DNA-based self-assembly of chiral plasmonic nanostructures with tailored optical response. *Nature* **2012**, 483, 311-314.

18. Sharma, J.; Ke, Y. G.; Lin, C. X.; Chhabra, R.; Wang, Q. B.; Nangreave, J.; Liu, Y.; Yan, H., DNA-tile-directed self-assembly of quantum dots into two-dimensional nanopatterns. *Angew. Chem. Int. Ed.* **2008**, 47, 5157-5159.

19. Bui, H.; Onodera, C.; Kidwell, C.; Tan, Y.; Graugnard, E.; Kuang, W.; Lee, J.; Knowlton, W. B.; Yurke, B.; Hughes, W. L., Programmable Periodicity of Quantum Dot Arrays with DNA Origami Nanotubes. *Nano Lett.* **2010**, 10, 3367-3372.

20. Ko, S. H.; Du, K.; Liddle, J. A., Quantum-Dot Fluorescence Lifetime Engineering with DNA Origami Constructs. *Angew. Chem. Int. Ed.* **2013**, 52, 1193-1197.

21. Mitchell, G. P.; Mirkin, C. A.; Letsinger, R. L., Programmed assembly of DNA functionalized quantum dots. *J. Am. Chem. Soc.* **1999**, 121, 8122-8123.

22. Wang, Q. B.; Liu, Y.; Ke, Y. G.; Yan, H., Quantum dot bioconjugation during core-shell synthesis. *Angew. Chem. Int. Ed.* **2008**, 47, 316-319.

23. Tikhomirov, G.; Hoogland, S.; Lee, P. E.; Fischer, A.; Sargent, E. H.; Kelley, S. O., DNA-based programming of quantum dot valency, self-assembly and luminescence. *Nat. Nanotechnol.* **2011**, 6, 485-490.

24. Ma, N.; Sargent, E. H.; Kelley, S. O., One-step DNA-programmed growth of luminescent and biofunctionalized nanocrystals. *Nat. Nanotechnol.* **2009**, 4, 121-125.

25. Deng, Z. T.; Schulz, O.; Lin, S.; Ding, B. Q.; Liu, X. W.; Wei, X. X.; Ros, R.; Yan, H.; Liu, Y., Aqueous Synthesis of Zinc Blende CdTe/CdS Magic-Core/Thick-Shell Tetrahedral-Shaped Nanocrystals with Emission Tunable to Near-Infrared. *J. Am. Chem. Soc.* **2010**, 132, 5592-5593.

26. Chen, Y.; Vela, J.; Htoon, H.; Casson, J. L.; Werder, D. J.; Bussian, D. A.; Klimov, V. I.; Hollingsworth, J. A., "Giant" multishell CdSe nanocrystal quantum dots with suppressed blinking. *J. Am. Chem. Soc.* **2008**, 130, 5026-5027.

27. Mahler, B.; Spinicelli, P.; Buil, S.; Quelin, X.; Hermier, J.-P.; Dubertret, B., Towards non-blinking colloidal quantum dots. *Nat. Mater.* **2008**, 7, 659-664.

28. Deng, Z. T.; Cao, L.; Tang, F. Q.; Zou, B. S., A new route to zinc-blende CdSe nanocrystals: Mechanism and synthesis. *J. Phys. Chem. B* **2005**, 109, 16671-16675.

29. Smith, A. M.; Mohs, A. M.; Nie, S., Tuning the optical and electronic properties of colloidal nanocrystals by lattice strain. *Nat. Nanotechnol.* **2009**, 4, 56-63.

30. Deng, Z.; Lie, F. L.; Shen, S.; Ghosh, I.; Mansuripur, M.; Muscat, A. J., Water-Based Route to Ligand-Selective Synthesis of ZnSe and Cd-Doped ZnSe Quantum Dots with Tunable Ultraviolet A to Blue Photoluminescence. *Langmuir* **2009**, 25, 434-442.

31. Deng, Z.; Yan, H.; Liu, Y., Band Gap Engineering of Quaternary-Alloyed ZnCdSSe Quantum Dots via a Facile Phosphine-Free Colloidal Method. *J. Am. Chem. Soc.* **2009**, 131, 17744-17745.

32. Nirmal, M.; Dabbousi, B. O.; Bawendi, M. G.; Macklin, J. J.; Trautman, J. K.; Harris, T. D.; Brus, L. E., Fluorescence intermittency in single cadmium selenide nanocrystals. *Nature* **1996**, 383, 802-804.

33. Kuno, M.; Fromm, D. P.; Hamann, H. F.; Gallagher, A.; Nesbitt, D. J., Nonexponential "blinking" kinetics of single CdSe quantum dots: A universal power law behavior. *J. Chem. Phys.* **2000**, 112, 3117-3120.

34. Shimizu, K. T.; Neuhauser, R. G.; Leatherdale, C. A.; Empedocles, S. A.; Woo, W. K.; Bawendi, M. G., Blinking statistics in single semiconductor nanocrystal quantum dots. *Phys. Rev. B* **2001**, 63.

35. Maria Galvez, E.; Zimmermann, B.; Rombach-Riegraf, V.; Bienert, R.; Graeber, P., Fluorescence resonance energy transfer in single enzyme molecules with a quantum dot as donor. *Eur. Biophys. J. Biophy* **2008**, 37, 1367-1371.

36. Galvez, E.; Dueser, M.; Boersch, M.; Wrachtrup, J.; Graeber, P., Quantum dots for single-pair fluorescence resonance energy transfer in membrane-integrated EF0F1. *Biochem. Soc. Trans.* **2008**, 36, 1017-1021.

37. Hohng, S.; Ha, T., Single-molecule quantum-dot fluorescence resonance energy transfer. *Chem. Phys. Chem* **2005**, 6, 956-960.

38. Fisher, B. R.; Eisler, H. J.; Stott, N. E.; Bawendi, M. G., Emission intensity dependence and single-exponential behavior in single colloidal quantum dot fluorescence lifetimes. *J. Phys. Chem. B* **2004**, 108, 143-148.

39. Frantsuzov, P. A.; Volkan-Kacso, S.; Janko, B., Model of Fluorescence Intermittency of Single Colloidal Semiconductor Quantum Dots Using Multiple Recombination Centers. *Phys. Rev. Lett.* **2009**, 103.

40. Chung, I.; Witkoskie, J. B.; Cao, J. S.; Bawendi, M. G., Description of the fluorescence intensity time trace of collections of CdSe nanocrystal quantum dots based on single quantum dot fluorescence blinking statistics. *Phys. Rev. E* **2006**, 73.

41. Schlegel, G.; Bohnenberger, J.; Potapova, I.; Mews, A., Fluorescence decay time of single semiconductor nanocrystals. *Phys. Rev. Lett.* **2002**, 88.

42. Biju, V.; Makita, Y.; Nagase, T.; Yamaoka, Y.; Yokoyama, H.; Baba, Y.; Ishikawa, M., Subsecond luminescence intensity fluctuations of single CdSe quantum dots. *J. Phys. Chem.B* **2005**, 109, 14350-14355.

43. Brokmann, X.; Hermier, J. P.; Messin, G.; Desbiolles, P.; Bouchaud, J. P.; Dahan, M., Statistical aging and nonergodicity in the fluorescence of single nanocrystals. *Phys. Rev. Lett.* **2003**, 90.

44. Tang, J.; Marcus, R. A., Diffusion-controlled electron transfer processes and power-law statistics of fluorescence intermittency of nanoparticles. *Phys. Rev. Lett.* **2005**, 95.

45. Tang, J.; Marcus, R. A., Mechanisms of fluorescence blinking in semiconductor nanocrystal quantum dots. *J. Chem.Phys.***2005**, 123.

46. Ye, M.; Searson, P. C., Blinking in quantum dots: The origin of the grey state and power law statistics. *Phys. Rev. B* **2011**, 84.

47. Goushi, K.; Yamada, T.; Otomo, A., Excitation Intensity Dependence of Power-Law Blinking Statistics in Nanocrystal Quantum Dots. *J. Phys. Chem. C* **2009**, 113, 20161-20168.

48. Tang, J.; Lee, D.-H.; Yeh, Y.-C.; Yuan, C.-T., Short-time power-law blinking statistics of single quantum dots and a test of the diffusion-controlled electron transfer model. *J. Chem. Phys* .**2009**, 131.

49. Peterson, J. J.; Nesbitt, D. J., Modified Power Law Behavior in Quantum Dot Blinking: A Novel Role for Biexcitons and Auger Ionization. *Nano Lett.* **2009**, 9, 338-345.

50. Margolin, G.; Protasenko, V.; Kuno, M.; Barkai, E., Power-law blinking quantum dots: stochastic and physical models. Adv. Chem. Phys. **2006**; 133, 327-356.

51. Bianco, S.; Grigolini, P.; Paradisi, P., Fluorescence intermittency in blinking quantum dots: Renewal or slow modulation? *J. Chem. Phys.* **2005**, 123.

52. Verberk, R.; van Oijen, A. M.; Orrit, M., Simple model for the power-law blinking of single semiconductor nanocrystals. *Phys. Rev. B* **2002**, 66.

53. Frantsuzov, P. A.; Marcus, R. A., Explanation of quantum dot blinking without the long-lived trap hypothesis. *Phys. Rev. B* **2005**, 72.

54. Efros, A. L.; Rosen, M., Random telegraph signal in the photoluminescence intensity of a single quantum dot. *Phys. Rev. Lett.* **1997**, 78, 1110-1113.

55. Galland, C.; Ghosh, Y.; Steinbrueck, A.; Sykora, M.; Hollingsworth, J. A.; Klimov, V. I.; Htoon, H., Two types of luminescence blinking revealed by spectroelectrochemistry of single quantum dots. *Nature* **2011**, 479, 203-U75.

56. Wang, X.; Ren, X.; Kahen, K.; Hahn, M. A.; Rajeswaran, M.; Maccagnano-Zacher, S.; Silcox, J.; Cragg, G. E.; Efros, A. L.; Krauss, T. D., Non-blinking semiconductor nanocrystals. *Nature* **2009**, 459, 686-689.

57. Hammer, N. I.; Early, K. T.; Sill, K.; Odoi, M. Y.; Emrick, T.; Barnes, M. D., Coverage-mediated suppression of blinking in solid state quantum dot conjugated organic composite nanostructures. *J. Phys. Chem. B* **2006**, 110, 14167-14171.

58. Hamada, M.; Nakanishi, S.; Itoh, T.; Ishikawa, M.; Biju, V., Blinking Suppression in CdSe/ZnS Single Quantum Dots by TiO2 Nanoparticles. *Acs Nano* **2010**, 4, 4445-4454.

59. Antelman, J.; Ebenstein, Y.; Dertinger, T.; Michalet, X.; Weiss, S., Suppression of Quantum Dot Blinking in DTT-Doped Polymer Films. *J. Phys. Chem. C* **2009**, 113, 11541-11545.

60. Yuan, C. T.; Yu, P.; Ko, H. C.; Huang, J.; Tang, J., Antibunching Single-Photon Emission and Blinking Suppression of CdSe/ZnS Quantum Dots. *Acs Nano* **2009**, 3, 3051-3056.

61. Lin, C.; Liu, Y.; Yan, H., Designer DNA Nanoarchitectures. *Biochemistry* **2009**, 48, 1663-1674.

62. Sharma, J.; Chhabra, R.; Liu, Y.; Ke, Y. G.; Yan, H., DNA-templated self-assembly of two-dimensional and periodical gold nanoparticle arrays. *Angew. Chem. Int. Ed.* **2006**, 45, 730-735.

63. Chhabra, R.; Sharma, J.; Ke, Y.; Liu, Y.; Rinker, S.; Lindsay, S.; Yan, H., Spatially addressable multiprotein nanoarrays templated by aptamer-tagged DNA nanoarchitectures. *J. Am. Chem. Soc.* **2007**, 129, 10304-10304.

64. Lin, C.; Jungmann, R.; Leifer, A. M.; Li, C.; Levner, D.; Church, G. M.; Shih, W. M.; Yin, P., Submicrometre geometrically encoded fluorescent barcodes self-assembled from DNA. *Nat. Chem.* **2012**, 4, 832-839.

65. Kelly, K. L.; Coronado, E.; Zhao, L. L.; Schatz, G. C., The optical properties of metal nanoparticles: The influence of size, shape, and dielectric environment. *J. Phys. Chem. B* **2003**, 107, 668-677.

66. Jain, P. K.; Lee, K. S.; El-Sayed, I. H.; El-Sayed, M. A., Calculated absorption and scattering properties of gold nanoparticles of different size, shape, and composition: Applications in biological imaging and biomedicine. *J. Phys. Chem. B* **2006**, 110, 7238-7248.

67. Chen, J.; Jin, Y.; Fahruddin, N.; Zhao, J. X., Development of Gold Nanoparticle-Enhanced Fluorescent Nanocomposites. *Langmuir* **2013**, 29, 1584-1591.

68. Myroshnychenko, V.; Rodriguez-Fernandez, J.; Pastoriza-Santos, I.; Funston, A. M.; Novo, C.; Mulvaney, P.; Liz-Marzan, L. M.; Garcia de Abajo, F. J., Modelling the optical response of gold nanoparticles. *Chem. Soc. Rev.* 2008, 37, 1792-1805.

69. Wang, Y.; Yan, B.; Chen, L., SERS Tags: Novel Optical Nanoprobes for Bioanalysis. *Chem. Rev.* **2013**, 113, 1391-1428.

70. Acuna, G. P.; Moeller, F. M.; Holzmeister, P.; Beater, S.; Lalkens, B.; Tinnefeld, P., Fluorescence Enhancement at Docking Sites of DNA-Directed Self-Assembled Nanoantennas. *Science* 2012, 338, 506-510.

71. Eustis, S.; El-Sayed, M. A., Why gold nanoparticles are more precious than pretty gold: Noble metal surface plasmon resonance and its enhancement of the radiative and nonradiative properties of nanocrystals of different shapes. *Chem. Soc. Rev.* **2006**, 35, 209-217.

72. Chhabra, R.; Sharma, J.; Wang, H. N.; Zou, S. L.; Lin, S.; Yan, H.; Lindsay, S.; Liu, Y., Distance-dependent interactions between gold nanoparticles and fluorescent molecules with DNA as tunable spacers. *Nanotechnology* **2009**, 20.

73. Rothemund, P. W. K., Folding DNA to create nanoscale shapes and patterns. *Nature* **2006**, 440, 297-302.

74. Torring, T.; Voigt, N. V.; Nangreave, J.; Yan, H.; Gothelf, K. V., DNA origami: a quantum leap for self-assembly of complex structures. *Chem. Soc. Rev.* **2011**, 40, 5636-5646.

75. Nangreave, J.; Han, D. R.; Liu, Y.; Yan, H., DNA origami: a history and current perspective. *Curr. Opin. Chem. Biol.* **2010**, 14, 608-615.

76. Michalet, X.; Pinaud, F. F.; Bentolila, L. A.; Tsay, J. M.; Doose, S.; Li, J. J.; Sundaresan, G.; Wu, A. M.; Gambhir, S. S.; Weiss, S., Quantum dots for live cells, in vivo imaging, and diagnostics. *Science* **2005**, 307, 538-544.

77. Jaiswal, J. K.; Simon, S. M., Potentials and pitfalls of fluorescent quantum dots for biological imaging. *Trends in Cell Biology* **2004**, 14, 497-504.

78. Medintz, I. L.; Uyeda, H. T.; Goldman, E. R.; Mattoussi, H., Quantum dot bioconjugates for imaging, labelling and sensing. *Nat. Mater.* **2005**, 4, 435-446.

79. Pansare, V. J.; Hejazi, S.; Faenza, W. J.; Prud'homme, R. K., Review of Long-Wavelength Optical and NIR Imaging Materials: Contrast Agents, Fluorophores, and Multifunctional Nano Carriers. *Chem. Mater.* **2012**, 24, 812-827.

80. Kim, S.; Lim, Y. T.; Soltesz, E. G.; De Grand, A. M.; Lee, J.; Nakayama, A.; Parker, J. A.; Mihaljevic, T.; Laurence, R. G.; Dor, D. M.; Cohn, L. H.; Bawendi, M. G.; Frangioni, J. V., Near-infrared fluorescent type II quantum dots for sentinel lymph node mapping. *Nat. Biotechnol.* **2004,** 22, 93-97.

81. Zhang, Y.; Hong, G.; Zhang, Y.; Chen, G.; Li, F.; Dai, H.; Wang, Q., Ag2S Quantum Dot: A Bright and Biocompatible Fluorescent Nanoprobe in the Second Near-Infrared Window. *Acs Nano* **2012**, 6, 3695-3702.

82. Du, Y.; Xu, B.; Fu, T.; Cai, M.; Li, F.; Zhang, Y.; Wang, Q., Near-infrared Photoluminescent Ag2S Quantum Dots from a Single Source Precursor. *J. Am. Chem. Soc.* **2010**, 132, 1470-1471.

83. Shen, S.; Zhang, Y.; Peng, L.; Du, Y.; Wang, Q., Matchstick-Shaped Ag2S-ZnS Heteronanostructures Preserving both UV/Blue and Near-Infrared Photoluminescence. *Angew. Chem. Int. Ed.* **2011**, 50, 7115-7118.

84. Hong, G.; Robinson, J. T.; Zhang, Y.; Diao, S.; Antaris, A. L.; Wang, Q.; Dai, H., In Vivo Fluorescence Imaging with Ag2S Quantum Dots in the Second Near-Infrared Region. *Angew. Chem. Int. Ed.* **2012**, 51, 9818-9821.

85. Li, C.; Zhang, Y.; Wang, M.; Zhang, Y.; Chen, G.; Li, L.; Wu, D.; Wang, Q., In vivo real-time visualization of tissue blood flow and angiogenesis using Ag2S quantum dots in the NIR-II window. *Biomaterials* **2014**, 35, 393-400.

86. Samanta, A.; Deng, Z.; Liu, Y., Aqueous Synthesis of Glutathione-Capped CdTe/CdS/ZnS and CdTe/CdSe/ZnS Core/Shell/Shell Nanocrystal Heterostructures. *Langmuir* **2012**, 28, 8205-8215.

87. Liang, G.-X.; Gu, M.-M.; Zhang, J.-R.; Zhu, J.-J., Preparation and bioapplication of high-quality, water-soluble, biocompatible, and near-infrared-emitting CdSeTe alloyed quantum dots. *Nanotechnology* **2009**, 20.

88. Mao, W.; Guo, J.; Yang, W.; Wang, C.; He, J.; Chen, J., Synthesis of high-quality near-infrared-emitting CdTeS alloyed quantum dots via the hydrothermal method. *Nanotechnology* **2007**, 18.

89. Keuleyan, S.; Lhuillier, E.; Guyot-Sionnest, P., Synthesis of Colloidal HgTe Quantum Dots for Narrow Mid-IR Emission and Detection. *J. Am. Chem. Soc.* **2011**, 133, 16422-16424.

90. Harris, D. K.; Allen, P. M.; Han, H.-S.; Walker, B. J.; Lee, J.; Bawendi, M. G., Synthesis of Cadmium Arsenide Quantum Dots Luminescent in the Infrared. *J. Am. Chem. Soc.* **2011**, 133, 4676-4679.

91. Pietryga, J. M.; Schaller, R. D.; Werder, D.; Stewart, M. H.; Klimov, V. I.; Hollingsworth, J. A., Pushing the band gap envelope: Mid-infrared emitting colloidal PbSe quantum dots. *J. Am. Chem. Soc.* **2004**, 126, 11752-11753.

92. Hines, M. A.; Scholes, G. D., Colloidal PbS nanocrystals with size-tunable near-infrared emission: Observation of post-synthesis self-narrowing of the particle size distribution. *Adv. Mater.s* **2003**, 15, 1844-1849.

93. Zhao, X. S.; Gorelikov, I.; Musikhin, S.; Cauchi, S.; Sukhovatkin, V.; Sargent, E. H.; Kumacheva, E., Synthesis and optical properties of thiol-stabilized PbS nanocrystals. *Langmuir* **2005**, 21, 1086-1090.

94. Deng, D.; Zhang, W.; Chen, X.; Liu, F.; Zhang, J.; Gu, Y.; Hong, J., Facile Synthesis of High-Quality, Water-Soluble, Near-Infrared-Emitting PbS Quantum Dots. *Eur. J. Inorg. Chem.* **2009**, 3440-3446.

95. Levina, L.; Sukhovatkin, W.; Musikhin, S.; Cauchi, S.; Nisman, R.; Bazett-Jones, D. P.; Sargent, E. H., Efficient infrared-emitting PbS quantum dots grown on DNA and stable in aqueous solution and blood plasma. *Adv. Mater.* **2005**, 17, 1854-1855.

96. Au, G. H. T.; Shih, W. Y.; Tseng, S. J.; Shih, W.-H., Aqueous CdPbS quantum dots for near-infrared imaging. *Nanotechnology* **2012**, 23.

97. Deng, Z.; Samanta, A.; Nangreave, J.; Yan, H.; Liu, Y., Robust DNA-Functionalized Core/Shell Quantum Dots with Fluorescent Emission Spanning from UV-vis to Near-IR and Compatible with DNA-Directed Self-Assembly. *J. Am. Chem. Soc.* **2012**, 134, 17424-17427.

98. Lin, Y.-W.; Liu, C.-W.; Chang, H.-T., DNA functionalized gold nanoparticles for bioanalysis. *Anal. Methods* **2009**, 1, 14-24.

99. Nikolic, P. M., SOLID SOLUTIONS OF CDSE AND CDTE IN PBTE AND THEIR OPTICAL PROPERTIES. *Br. J. Appl. Phys.* **1966**, 17, 341-&.

100. Deng, Z.; Pal, S.; Samanta, A.; Yan, H.; Liu, Y., DNA functionalization of colloidal II-VI semiconductor nanowires for multiplex nanoheterostructures. *Chem.Sci.* **2013**, 4, 2234-2240.

101. Qian, H. F.; Dong, C. Q.; Weng, J. F.; Ren, J. C., Facile one-pot synthesis of luminescent, water-soluble, and biocompatible glutathione-coated CdTe nanocrystals. *Small* **2006**, 2, 747-751.

102. Ding, B. Q.; Deng, Z. T.; Yan, H.; Cabrini, S.; Zuckermann, R. N.; Bokor, J., Gold Nanoparticle Self-Similar Chain Structure Organized by DNA Origami. *J. Am. Chem. Soc.* **2010**, 132, 3248-3249.

103. Pal, S.; Deng, Z. T.; Ding, B. Q.; Yan, H.; Liu, Y., DNA-Origami-Directed Self-Assembly of Discrete Silver-Nanoparticle Architectures. *Angew. Chem. Int. Ed.* **2010**, 49, 2700-2704.

Chapter 4 References

1. Stryer, L., Fluorescence energy-transfer as a spectroscopic ruler. *Annu. Rev. of Bioche.* **1978**, 47, 819-846.

2. Sekar, R. B.; Periasamy, A., Fluorescence resonance energy transfer (FRET) microscopy imaging of live cell protein localizations. *J. Cell Biol.* **2003**, 160, 629-633.

3. Dosremedios, C. G.; Moens, P. D. J., Fluorescence resonance energy-transfer spectroscopy is a reliable ruler for measuring structural-changes in proteins - dispelling the problem of the unknown orientation factor. *J. Struct. Biol.* **1995**, 115, 175-185.

4. Lilley, D. M. J.; Wilson, T. J., Fluorescence resonance energy transfer as a structural tool for nucleic acids. *Curr. Opin. Chem. Biol.* **2000**, 4, 507-517.

5. Selvin, P. R., The renaissance of fluorescence resonance energy transfer. *Nat. Struct. Mol. Biol.* **2000**, 7, 730-734.

6. Parkhurst, L. J.; Parkhurst, K. M.; Powell, R.; Wu, J.; Williams, S., Time-resolved fluorescence resonance energy transfer studies of DNA bending in double-stranded oligonucleotides and in DNA-protein complexes. *Biopolymers* **2001**, 61, 180-200.

7. Yun, C. S.; Javier, A.; Jennings, T.; Fisher, M.; Hira, S.; Peterson, S.; Hopkins, B.; Reich, N. O.; Strouse, G. F., Nanometal surface energy transfer in optical rulers, breaking the FRET barrier. *J. Am. Chem. Soc.* **2005**, 127, 3115-3119.

8. Breshike, C. J.; Riskowski, R. A.; Strouse, G. F., Leaving Forster Resonance Energy Transfer Behind: Nanometal Surface Energy Transfer Predicts the Size-Enhanced Energy Coupling between a Metal Nanoparticle and an Emitting Dipole. *J. Phys. Chem. C* **2013**, 117, 23942-23949.

9. Jennings, T. L.; Singh, M. P.; Strouse, G. F., Fluorescent lifetime quenching near d=1.5 nm gold nanoparticles: Probing NSET validity. *J. Am. Chem. Soc.* **2006**, 128, 5462-5467.

10. Chowdhury, S.; Wu, Z.; Jaquins-Gerstl, A.; Liu, S.; Dembska, A.; Armitage, B. A.; Jin, R.; Peteanu, L. A., Wavelength Dependence of the Fluorescence Quenching Efficiency of Nearby Dyes by Gold Nanoclusters and Nanoparticles: The Roles of Spectral Overlap and Particle Size. *J. Phys. Chem. C* **2011**, 115, 20105-20112.

11. Griffin, J.; Singh, A. K.; Senapati, D.; Rhodes, P.; Mitchell, K.; Robinson, B.; Yu, E.; Ray, P. C., Size- and Distance-Dependent Nanoparticle Surface-Energy Transfer (NSET) Method for Selective Sensing of Hepatitis C Virus RNA. *Chem. Eur. J.* **2009**, 15, 342-351.

12. Chance, R. R.; Prock, A.; Silbey, R., Comments on classical theory of energy-transfer. *J. Chem. Phys.* **1975**, 62, 2245-2253.

13. Persson, B. N. J.; Lang, N. D., Electron-hole-pair quenching of excited-states near a metal. *Phys. Rev. B* **1982**, 26, 5409-5415.

14. Kuhn, H., Classical aspects of energy transfer in molecular systems. *J. Chem. Phys.* **1970**, 53, 101-&.

15. Singh, M. P.; Strouse, G. F., Involvement of the LSPR Spectral Overlap for Energy Transfer between a Dye and Au Nanoparticle. *J. Am. Chem. Soc.* **2010**, 132, 9383-9391.

16. Pustovit, V. N.; Shahbazyan, T. V., Fluorescence quenching near small metal nanoparticles. *J. Chem. Phys.* **2012**, 136.

17. Carminati, R.; Greffet, J. J.; Henkel, C.; Vigoureux, J. M., Radiative and non-radiative decay of a single molecule close to a metallic nanoparticle. *Opt. Commun.* **2006**, 261, 368-375.

18. Ruppin, R., Decay of an excited molecule near a small metal sphere. *J. Chem. Phys.* **1982**, 76, 1681-1684.

19. Gersten, J.; Nitzan, A., Spectroscopic properties of molecules interacting with small dielectric particles. *J. Chem. Phys.* **1981**, 75, 1139-1152.

20. Saini, S.; Srinivas, G.; Bagchi, B., Distance and Orientation Dependence of Excitation Energy Transfer: From Molecular Systems to Metal Nanoparticles. *J.Phys. Chem. B* **2009**, 113, 1817-1832.

21. Pons, T.; Medintz, I. L.; Sapsford, K. E.; Higashiya, S.; Grimes, A. F.; English, D. S.; Mattoussi, H., On the quenching of semiconductor quantum dot photoluminescence by proximal gold nanoparticles. *Nano Lett.* **2007**, 7, 3157-3164.

22. Li, X.; Qian, J.; Jiang, L.; He, S., Fluorescence quenching of quantum dots by gold nanorods and its application to DNA detection. *Appl.Phys. Lett.* **2009**, 94.

23. Gueroui, Z.; Libchaber, A., Single-molecule measurements of gold-quenched quantum dots. *Phys. Rev. Lett.* **2004**, 93.

24. Medintz, I. L.; Uyeda, H. T.; Goldman, E. R.; Mattoussi, H., Quantum dot bioconjugates for imaging, labelling and sensing. *Nat. Mater.* **2005**, 4, 435-446.

25. Medintz, I. L.; Clapp, A. R.; Mattoussi, H.; Goldman, E. R.; Fisher, B.; Mauro, J. M., Self-assembled nanoscale biosensors based on quantum dot FRET donors. *Nat. Mater.* **2003**, 2, 630-638.

26. Boeneman, K.; Prasuhn, D. E.; Blanco-Canosa, J. B.; Dawson, P. E.; Melinger, J. S.; Ancona, M.; Stewart, M. H.; Susumu, K.; Huston, A.; Medintz, I. L., Self-Assembled Quantum Dot-Sensitized Multivalent DNA Photonic Wires. *J. Am. Chem. Soc.* **2010**, 132, 18177-18190.

27. Clapp, A. R.; Medintz, I. L.; Mattoussi, H., Forster resonance energy transfer investigations using quantum-dot fluorophores. *Chem. Phys. Chem.* **2006**, 7, 47-57.

28. Sharma, J.; Chhabra, R.; Liu, Y.; Ke, Y. G.; Yan, H., DNA-templated self-assembly of two-dimensional and periodical gold nanoparticle arrays. *Angew. Chem. Int. Ed.* **2006**, 45, 730-735.

29. Sharma, J.; Chhabra, R.; Andersen, C. S.; Gothelf, K. V.; Yan, H.; Liu, Y., Toward reliable gold nanoparticle patterning on self-assembled DNA nanoscaffold. *J. Am. Chem. Soc.* **2008**, 130, 7820-7821.

30. Ding, B. Q.; Deng, Z. T.; Yan, H.; Cabrini, S.; Zuckermann, R. N.; Bokor, J., Gold Nanoparticle Self-Similar Chain Structure Organized by DNA Origami. *J. Am. Chem. Soc.* **2010**, 132, 3248-3249.

31. Deng, Z.; Samanta, A.; Nangreave, J.; Yan, H.; Liu, Y., Robust DNA-Functionalized Core/Shell Quantum Dots with Fluorescent Emission Spanning from UV-vis to Near-IR and Compatible with DNA-Directed Self-Assembly. *J. Am. Chem. Soc.* **2012**, 134, 17424-17427.

32. Lin, C.; Liu, Y.; Yan, H., Designer DNA Nanoarchitectures. *Biochemistry* **2009**, 48, 1663-1674.

33. Pal, S.; Deng, Z. T.; Ding, B. Q.; Yan, H.; Liu, Y., DNA-Origami-Directed Self-Assembly of Discrete Silver-Nanoparticle Architectures. *Angew. Chem. Int. Ed.* **2010**, 49, 2700-2704.

34. Ding, B.; Deng, Z.; Yan, H.; Cabrini, S.; Zuckermann, R. N.; Bokor, J., Gold Nanoparticle Self-Similar Chain Structure Organized by DNA Origami. *J. Am. Chem. Soc.* **2010**, 132, 3248-3249.

35. Bui, H.; Onodera, C.; Kidwell, C.; Tan, Y.; Graugnard, E.; Kuang, W.; Lee, J.; Knowlton, W. B.; Yurke, B.; Hughes, W. L., Programmable Periodicity of Quantum Dot Arrays with DNA Origami Nanotubes. *Nano Lett.* **2010**, 10, 3367-3372.

36. Ko, S. H.; Du, K.; Liddle, J. A., Quantum-Dot Fluorescence Lifetime Engineering with DNA Origami Constructs. *Angew. Chem. Int. Ed.* **2013**, 52, 1193-1197.

37. Wang, R.; Nuckolls, C.; Wind, S. J., Assembly of Heterogeneous Functional Nanomaterials on DNA Origami Scaffolds. *Angew. Chem. Int. Ed.* **2012**, 51, 11325-11327.

38. Boeneman, K.; Deschamps, J. R.; Buckhout-White, S.; Prasuhn, D. E.; Blanco-Canosa, J. B.; Dawson, P. E.; Stewart, M. H.; Susumu, K.; Goldman, E. R.; Ancona, M.; Medintz, I. L., Quantum Dot DNA Bioconjugates: Attachment Chemistry Strongly Influences the Resulting Composite Architecture. *Acs Nano* **2010**, 4, 7253-7266.

39. Geddes, C. D.; Lakowicz, J. R., Metal-enhanced fluorescence. *J. Fluoresc.* **2002**, 12, 121-129.

40. Dragan, A. I.; Bishop, E. S.; Casas-Finet, J. R.; Strouse, R. J.; McGivney, J.; Schenerman, M. A.; Geddes, C. D., Distance Dependence of Metal-Enhanced Fluorescence. *Plasmonics* **2012**, 7, 739-744.

41. Kang, K. A.; Wang, J.; Jasinski, J. B.; Achilefu, S., Fluorescence Manipulation by Gold Nanoparticles: From Complete Quenching to Extensive Enhancement. *J. Nanobiotechnology* **2011**, 9.

42. Raikar, U. S.; Tangod, V. B.; Mastiholi, B. M.; Fulari, V. J., Fluorescence quenching using plasmonic gold nanoparticles. *Opt. Commun.* **2011**, 284, 4761-4765.

43. Lakowicz, J. R.; Shen, Y. B.; D'Auria, S.; Malicka, J.; Fang, J. Y.; Gryczynski, Z.; Gryczynski, I., Radiative decay engineering 2. Effects of silver island films on

fluorescence intensity, lifetimes, and resonance energy transfer. *Anal. Biochem.* **2002**, 301, 261-277.

44. Lakowicz, J. R., Radiative decay engineering 5: metal-enhanced fluorescence and plasmon emission. *Anal. Biochem.* **2005**, 337, 171-194.

45. Anker, J. N.; Hall, W. P.; Lyandres, O.; Shah, N. C.; Zhao, J.; Van Duyne, R. P., Biosensing with plasmonic nanosensors. *Nat. Mater.* **2008**, 7, 442-453.

46. Fu, Y.; Zhang, J.; Lakowicz, J. R., Reduced blinking and long-lasting fluorescence of single fluorophores coupling to silver nanoparticles. *Langmuir* **2008**, 24, 3429-3433.

47. Kummerlen, J.; Leitner, A.; Brunner, H.; Aussenegg, F. R.; Wokaun, A., Enhanced dye fluorescence over silver island films - analysis of the distance dependence. *Mol. Phys.* **1993**, 80, 1031-1046.

48. Guzatov, D. V.; Vaschenko, S. V.; Stankevich, V. V.; Lunevich, A. Y.; Glukhov, Y. F.; Gaponenko, S. V., Plasmonic Enhancement of Molecular Fluorescence near Silver Nanoparticles: Theory, Modeling, and Experiment. *J. Phys. Chem. C* **2012**, 116, 10723-10733.

49. Lakowicz, J. R., Radiative decay engineering: Biophysical and biomedical applications. *Anal. Biochem.* **2001**, 298, 1-24.

50. Deng, W.; Xie, F.; Baltar, H. T. M. C. M.; Goldys, E. M., Metal-enhanced fluorescence in the life sciences: here, now and beyond. *Phys. Chem. Chem. Phys.* **2013**, 15, 15695-15708.

51. Corrigan, T. D.; Guo, S.; Phaneuf, R. J.; Szmacinski, H., Enhanced fluorescence from periodic arrays of silver nanoparticles. *J. Fluoresc.* **2005**, 15, 777-784.

52. Szmacinski, H.; Lakowicz, J. R.; Catchmark, J. M.; Eid, K.; Anderson, J. P.; Middendorf, L., Correlation between scattering properties of silver particle arrays and fluorescence enhancement. *Appl. Spectrosc.* **2008**, 62, 733-738.

53. Cade, N. I.; Ritman-Meer, T.; Kwakwa, K. A.; Richards, D., The plasmonic engineering of metal nanoparticles for enhanced fluorescence and Raman scattering. *Nanotechnology* **2009**, 20.

54. Anderson, J. P.; Griffiths, M.; Boveia, V. R., Near-infrared fluorescence enhancement using silver island films. *Plasmonics* **2006**, 1, 103-110.

55. McDonagh, C.; Stranik, O.; Nooney, R.; MacCraith, B. D., Nanoparticle strategies for enhancing the sensitivity of fluorescence-based biochips. *Nanomedicine* **2009**, 4, 645-656.

56. Acuna, G. P.; Moeller, F. M.; Holzmeister, P.; Beater, S.; Lalkens, B.; Tinnefeld, P., Fluorescence Enhancement at Docking Sites of DNA-Directed Self-Assembled Nanoantennas. *Science* **2012**, 338, 506-510.

57. Lee, K.-S.; El-Sayed, M. A., Gold and silver nanoparticles in sensing and imaging: Sensitivity of plasmon response to size, shape, and metal composition. *J. Phys. Chem. B* **2006**, 110, 19220-19225.

58. Pal, S.; Dutta, P.; Wang, H.; Deng, Z.; Zou, S.; Yan, H.; Liu, Y., Quantum Efficiency Modification of Organic Fluorophores Using Gold Nanoparticles on DNA Origami Scaffolds. *J. Phys. Chem. C* **2013**, 117, 12735-12744.

APPENDIX A

SUPPLEMENTAL INFORMATION FOR CHAPTER 2

Supplemental information for

Aqueous Synthesis of Glutathione-Capped CdTe/CdS/ZnS and CdTe/CdSe/ZnS Core/Shell/Shell Nanocrystal Heterostructures

*Anirban Samanta, Zhengtao Deng, Yan Liu**

The Biodesign Institute and Department of Chemistry and Biochemistry, Arizona State University, Tempe, Arizona 85287

Experimental methods and materials:

Chemicals*:* Se powder, Te powder (99.8%), L-Glutathione (reduced) (99%), sodium borohydride $NaBH_4$ (99%), Thiourea (99%), and Rhodamine 6G (λ_{em}=547 nm) were purchased from Sigma Aldrich. $Cd(NO_3)_2 \cdot 4H_2O$ (99%) was purchased from Fluka. All chemicals were used without further purification. All solutions were prepared with nano-pure water as the solvent. 250 mL, three-neck round-bottom flasks were used for the synthesis of all nanocrystals.

Synthesis of CdTe core nanocrystals: In a typical synthesis of CdTe core nanocrystals, firstly, a NaHTe solution was prepared by dissolving Te powder (1 mmol) with $NaBH_4$ (4 mmol) in 2 mL of degassed nano-pure water in a thick walled glass tube. A needle was inserted into the capped tube to release the pressure, and the solution was stirred for a few hours at 4 °C. The Cd^{2+} precursor solution was prepared by dissolving GSH (0.625 mmol) and $Cd(NO_3)_2$ (0.25mmol) in 100 mL of nano-pure water. The pH was adjusted to 8.5 by adding 1 M NaOH. The NaHTe solution (125 µL) was injected into N_2 saturated Cd^{2+} solution, with a molar ratio of 4:1:10 for Cd^{2+}:NaHTe:GSH. After injection, the color of the solution immediately changed from colorless to yellow. The reaction mixture

was heated at 100°C, and aliquots of the reaction mixture (0.5mL) were collected every 10 minutes, after which the reaction was quenched by quickly cooling down to 0°C in an ice-bath.

Synthesis of CdTe/CdS core/shell nanocrystals: Core CdTe nanocrystals were synthesized following a protocol in literature[30] (details are described in Supporting Information). Next, the core nanocrystals were precipitated by adding 2-propanol (1:1 volume ratio), followed by centrifugation at 15,000 rpm for 45 minutes. The precipitate was re-suspended in 2 mL of nano-pure water for characterization, or alternatively, used in the next step of synthesis. The size and concentration of the purified CdTe QDs were calculated using the extinction coefficient of CdTe nanocrystals following a reported method.[31] For CdS shell synthesis, a Cd^{2+} precursor solution was prepared by dissolving GSH (0.2 mmol) and $Cd(NO_3)_2$ (0.1 mmol) in 25 mL of nano-pure water, with the pH of the solution adjusted to 7 by drop-wise addition of 1 M NaOH. Next, the purifed CdTe QDs (0.025 μmol/L) and thiourea (0.1 mmol) were added to the Cd^{2+} precursor solution, and the pH was adjusted to 11. The molar ratio of Cd^{2+}:thiourea:GSH in the reaction mixture was 1:1:2. The reaction mixture was held at 90°C and aliquots (0.5 mL) were collected at a series of different times. Each reaction was quenched by cooling down to 0°C using an ice-bath. The core/shell nanocrystals were precipitated by adding 2-Propanol (1:1 volume ratio), followed by centrifugation at 15,000 rpm for 30 minutes. The precipitate was re-suspended in 2 mL nanopure water for characterization, or alternatively, used in the next step synthesis.

Synthesis of CdTe/CdS/ZnS core/shell/shell nanocrystals*:* The core/shell/shell nanocrystals were prepared in a similar way as the core/shell nanocrystals. First, a Zn^{2+} precursor solution was prepared by dissolving GSH (0.2 mmol) and $Zn(NO_3)_2$ (0.1 mmol) in 25 mL of nano-pure water, with subsequent adjustment of the pH of the solution to 7. Next, 0.025 μmol/L of purified CdTe/CdS QDs and thiourea (0.1 mmol) were added and the pH was adjusted to 11. The molar ratio of Zn^{2+}:thiourea:GSH in the reaction mixture was 1:1:2. The reaction mixture was held at 90°C, and aliquots of the mixture (0.5 mL) were collected at various times and subsequently cooled in an ice-bath to quench the reaction. The resulting nanocrystals were purified by precipitation using 2-Propanol and centrifugation. Finally they were resuspended in nano-pure water (2 mL) for characterization.

Synthesis of CdTe/CdSe core/shell and CdTe/CdSe/ZnS core/shell/shell nanocrystals*:* For the preparation of CdTe/CdSe core/shell nanocrystals, the successive ion layer adsorption and reaction technique (SILAR) was used. This is because that Se is first reduced to NaHSe, which is highly reactive, the direct addition of the entire Se precursor solution to the pre-formed CdTe core solution will result in the formation of CdSe core nanocrystals, rather than the growth of a CdSe shell around the core. First, the Se precursor solution, NaHSe, was prepared by dissolving 20 mg of Se powder (0.25 mmol) in 10 mL of $NaBH_4$ solution (1 mmol) under N_2. Next, the purified 0.050 μmol CdTe core nanocrystals were suspended in 25 mL of degassed water and the pH was adjusted to 10.5. Meanwhile, the Cd^{2+} solution was prepared by dissolving $Cd(NO_{3)2}4H_2O$ (0.3 mmol) and GSH (0.75 mmol) in 10 mL of degassed water and adjusting the pH of the solution to 10.5. An excess of Cd^{2+} (30 mM) compared to NaHSe (25 mM) was

maintained throughout the reaction to minimize the undesired oxidation of NaHSe to Se during the reaction, which would contaminate the desired QD products. The formation of each CdSe monolayer corresponds to the addition of a 0.35 nm thick shell around the core. To generate the monolayer shells, deliberate amounts of Cd^{2+} and NaHSe solutions were added to the CdTe core in discrete steps. For example, to a solution containing 0.05 μmoles of green emitting CdTe nanocrystals (diameter ~1.5 nm), 79.8 μL of the Cd^{2+} and NaHSe solutions were first added to form the first monolayer. Next, 102.6 μL of each were added to form the second monolayer, and so on. At each step, the temperature was held at 90°C for 20 minutes to facilitate monolayer growth, and samples were subsequently collected for purification and characterization. The final ZnS shell was formed using the same procedure as for the CdTe/CdS/ZnS nanocrystals.

Synthesis of CdTe/CdS nanocrystals starting from different sized cores*:* First, green emitting CdTe core nanocrystals (0.053 μmol) were purified and resuspended in 25 mL of degassed water, and the pH of the solution was adjusted to 10.5. The Cd^{2+} precursor solution contained 30 mM $Cd(NO_3)_2$, 75 mM GSH and 25 mM thiourea. Assuming that each CdS monolayer adds 0.35 nm to the radius of the ~1.5 nm (diameter) core, 84.6 μL of the Cd^{2+} and thiourea solutions were injected to form the first monolayer, and 108.7 μL were added for the second monolayer. The layer by layer growth of the CdS shell for the yellow ($\lambda_{ab,max}$= 520 nm, $\lambda_{em,max}$= 565 nm) and red emitting CdTe cores ($\lambda_{ab,max}$= 550 nm, $\lambda_{em,max}$= 590 nm) was performed in a similar manner, with the diameters of the cores assumed to be ~ 2.5 nm and 3.0 nm, respectively.[26] The temperature of each reaction mixture was held at 90°C for 60 min before samples were collected for subsequent purification and characterization.

***Structural and optical characterization**:* High-resolution transmission electron microscopy (HRTEM), high angle annular dark field scanning transmission electron microscopy (HAADF-STEM), and energy dispersive X-ray spectroscopy (EDS) were performed on a JEOL JEM 2010F electron microscope operating at 200 kV. Samples were deposited on carbon coated copper grids (400 mesh, Ted Pella) and air-dried before imaging. Powder X-ray diffraction (XRD) measurements employed a PANalytical X'Pert Pro Materials Research X-ray Diffractometer with Cu Kα radiation (λ=1.5418 Å). To prepare a powder XRD sample, a highly concentrated QD solution was deposited on a glass substrate and dried in air. UV-Vis absorption spectra were obtained with a Shimadzu UV-2401PC spectral photometer using a 1 cm path length quartz cuvette. Fluorescence spectra were collected by a Horiba Nanolog spectrophotometer (Horiba Jobin Yvon) equipped with 450W Xenon lamp and thermal electrically cooled R928 PMT detector. All spectra were collected at room temperature under ambient conditions.

***Quantum Yield Measurements**:* The quantum yield (QY) of the nanocrystals was measured relative to standard Rhodamine 6G (QY = 95% in ethanol) with excitation at 400 nm. Solutions of nanocrystals in nanopure water and the dye in ethanol were optically matched at the excitation wavelength. fluorescence spectra of the nanocrystals and dye were measured multiple times under identical spectrometer onditions and averaged. The optical density was kept below 0.1 at the excitation wavelength, and the integrated intensities of the emission spectra, corrected for differences in the index of refraction and concentration, were used to calculate the quantum yields using the method reported in the literature.[32]

Lifetime measurements: Fluorescence decay kinetics were measured using the time-correlated single photon counting (TCSPC) technique. The excitation source was a titanium sapphire (Ti:S) laser (Spectra-Physics, Tsunami), which provides 130-fs pulses at 80 MHz. The laser output was sent through a frequency doubler and pulse selector (Spectra Physics, Model 3980) to obtain excitations tunable between 360 – 460 nm at 0.8 MHz. Fluorescence emission was collected at 90° relative to the excitation source and detected using a double-grating monochromator (Jobin-Yvon, Gemini-180) and a microchannel plate photomultiplier tube (Hamamatsu R3809U-50). Data acquisition was performed using a single photon counting card (Becker-Hickl, SPC-830). The instrument response function (IRF) was 35-45 ps at FWHM. Data analysis was carried out using locally written software ASUFIT (URL: www.public.asu.edu/~laserweb/asufit/asufit.html). Data was fit by a sum of exponential decay model.

Calculation of amount of CdS and CdSe precursors used to encapsulate the CdTe core

1. CdTe/CdS core/shell nanocrystals

A typical CdTe core solution (25 mL), where the first excitonic absorbance peak appears at 505nm and an absorbance value of 0.0793 (at 505 nm).

The diameter of the CdTe Core nanocrystal could be calculated according to reference 33:

$D = (9.8127\times10^{-7})\times \lambda^3 - (1.7147 \times 10^{-3})\times \lambda^2 + (1.0064)\times \lambda - 194.84$

$= (9.8127\times 10^{-7})\times (505)^3 - (1.7147\times 10^{-3})\times (505)^2 + (1.0064)\times (505) - 194.84 = 2.47$ nm,

And the extinction coefficient $\varepsilon = 10043\times (2.47)^{2.12} = 68294\ M^{-1}\ cm^{-1}$.

Using $A = \varepsilon\ c\ l$, the concentration of the CdTe core is 1.16 µM.

Total volume of solution = 25 ml, thus, there are 0.029 µmoles of CdTe nanocrystals .

The average thickness of monolayer of CdS is 0.335 nm, after one monolayer of CdS growth, the diameter is increased by 0.67 nm.

The volume of the 1st shell is: $\frac{\pi}{6}(3.14^3-2.47^3)\ nm^3 = 8.32\ nm^3$.

The volume of the second shell is: $\frac{\pi}{6}(3.81^3-3.14^3)\ nm^3 = 12.75\ nm^3$.

The density of CdS is $4.825 g/cm^3 = 4.825\times 10^{-21}\ g/nm^3$.

The mass of CdS that corresponds to one monolayer CdS per CdTe nanocrystal is $4.825\times 10^{-21}\ g/nm^3 \times 8.32\ nm^3 = 4.014\times 10^{-20}$ g.

For 0.029 µmole of CdTe core, the amount of CdS to be added is $4.236\times 10^{-20}\times 0.029\times 10^{-6}\times 6.023\times 10^{23} g = 7.01\times 10^{-4}$ g, or 7.4×10^{-4} g/ 144.48 g mol^{-1} = 4.85 µmole.

The concentration of Cd and S precursor was 25 mM.

Thus, the amount of Cd and S precursors added for the first monolayer growth is 194 µl,

And the amount of Cd and S precursors added for the second monolayer growth is 297 µl.

2. CdTe/CdSe core/shell nanocrystals

A typical CdTe core solution (25 mL) where the first excitonic absorbance peak appears at 520 nm and an absorbance value of 0.1136 (at 520 nm).

The diameter of the CdTe Core nanocrystal could be calculated according to reference 33:

$D = (9.8127\times 10^{-7})\times \lambda^3 - (1.7147 \times 10^{-3})\times \lambda^2 + (1.0064)\times \lambda - 194.84$

$= (9.8127\times 10^{-7})\times (520)^3 - (1.7147 \times 10^{-3})\times (520)^2 + (1.0064)\times (520) - 194.84 = 2.8$ nm

and the extinction coefficient $\varepsilon = 10043\times (2.8)^{2.12} = 89092\ M^{-1}\ cm^{-1}$.

Using $A= \varepsilon\ c\ l$, the concentration of CdTe core is calculated to be 1.27 µM.

Total volume of solution = 25 ml, thus there are 0.03175 µmole of CdTe nanocrystal.

The average thickness of monolayer of CdSe is 0.35 nm, after one monolayer CdTe diameter is increased by 0.70 nm.

The volume of the 1st shell is: $\frac{\pi}{6}(3.5^3-2.8^3)\ nm^3 = 10.949\ nm^3$.

The volume of the second shell is: $\frac{\pi}{6}(4.2^3-2.8^3)\ nm^3 = 16.33\ nm^3$.

The density of CdSe is $5.816 g/cm^3 = 5.816\times 10^{-21}\ g/nm^3$.

The mass of CdSe that corresponds to one monolayer per nanocrystal is $5.816\times 10^{-21}\times 10.949\ nm^3 = 6.368 \times 10^{-20}$ g.

For 0.03175 µmol amount of CdSe to be added is $6.368 \times 10^{-20}\times 0.03175 \times 10^{-6}\times 6.023 \times 10^{23} = 1.218 \times 10^{-3} / 191.37 gmol^{-1} = 6.36$ µmole.

The concentration of Se was 25 mM.

Thus, the amount of Cd and Se precursors added for the first monolayer growth is 254 µl,

And the amount of Cd and Se precursors added for the second monolayer growth is 379 µl.

Summary of the full width at half maximum of each photoluminescence spectra of the samples

1. CdTe Core nanocrystals

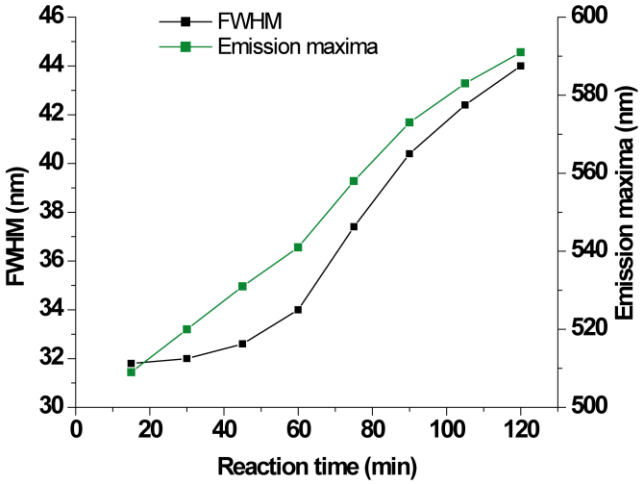

Reaction time (min)	FWHM (nm)	Emission maxima (nm)
15	31.8	509
30	32	520
45	32.5	531
60	34	541
75	37.4	558
90	40.4	573
105	42.4	583
120	44	591

1. CdTe/CdS core/shell nanocrystals

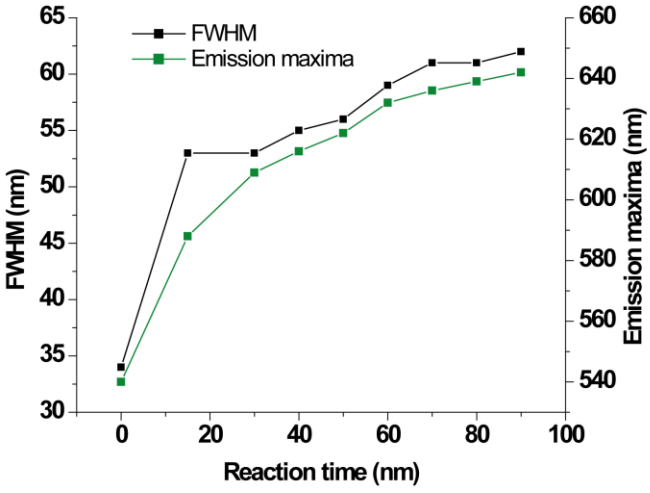

Reaction time (min)	FWHM (nm)	Emission maxima (nm)
0	34.2	540
15	53	588
30	53	609
40	55.3	616
50	56	622
60	59.1	632
70	61	636
80	61.2	639
90	62	642

2. CdTe/CdSe core/shell nanocrystals

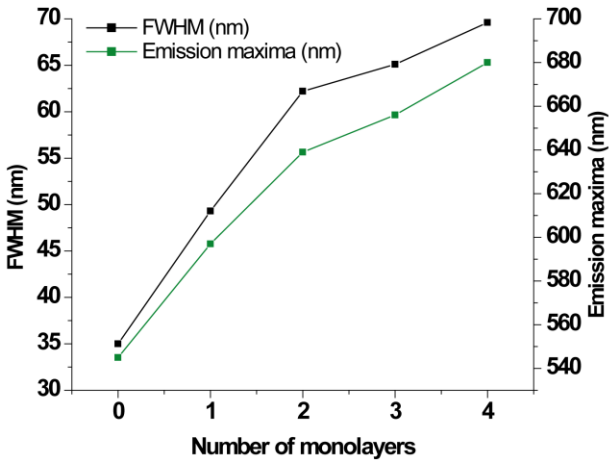

Number of CdSe monolayer	FWHM (nm)	Emission maxima (nm)
0	35	545
1	49.3	597
2	62.2	639
3	65.1	656
4	69.6	680

3. CdTe/CdS/ZnS core/shell/shell nanocrystals

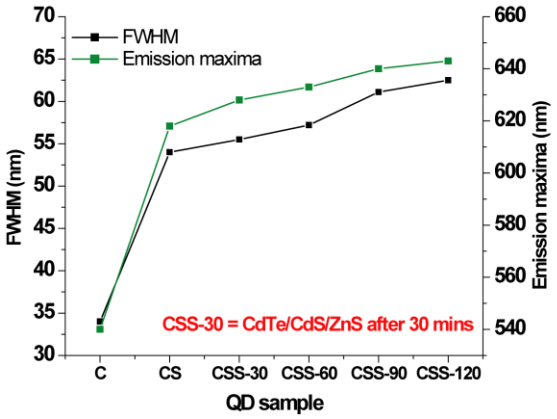

QD sample	FWHM (nm)	Emission maxima (nm)
C (CdTe)	34	540
CS(CdTe-CdS)	54	618
CSS-30	55.5	628
CSS-60	57.2	633
CSS-90	61	640
CSS-120	62.5	643

4. CdTe/CdSe/ZnS core/shell/shell nanocrystals

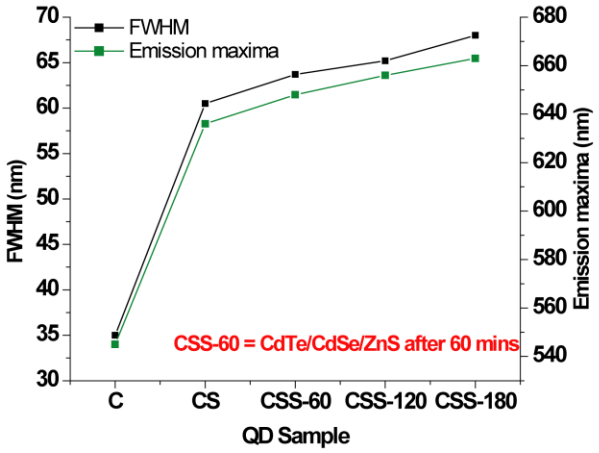

QD sample	FWHM (nm)	Emission maxima (nm)
C (CdTe)	35	545
CS(CdTe-CdSe)	60.5	636
CS-60	63.7	648
CS-120	65.2	656
CS-180	68	663

Decay curve for CdTe/CdS core/shell QDs as successive layers of shell were deposited on the CdTe core:

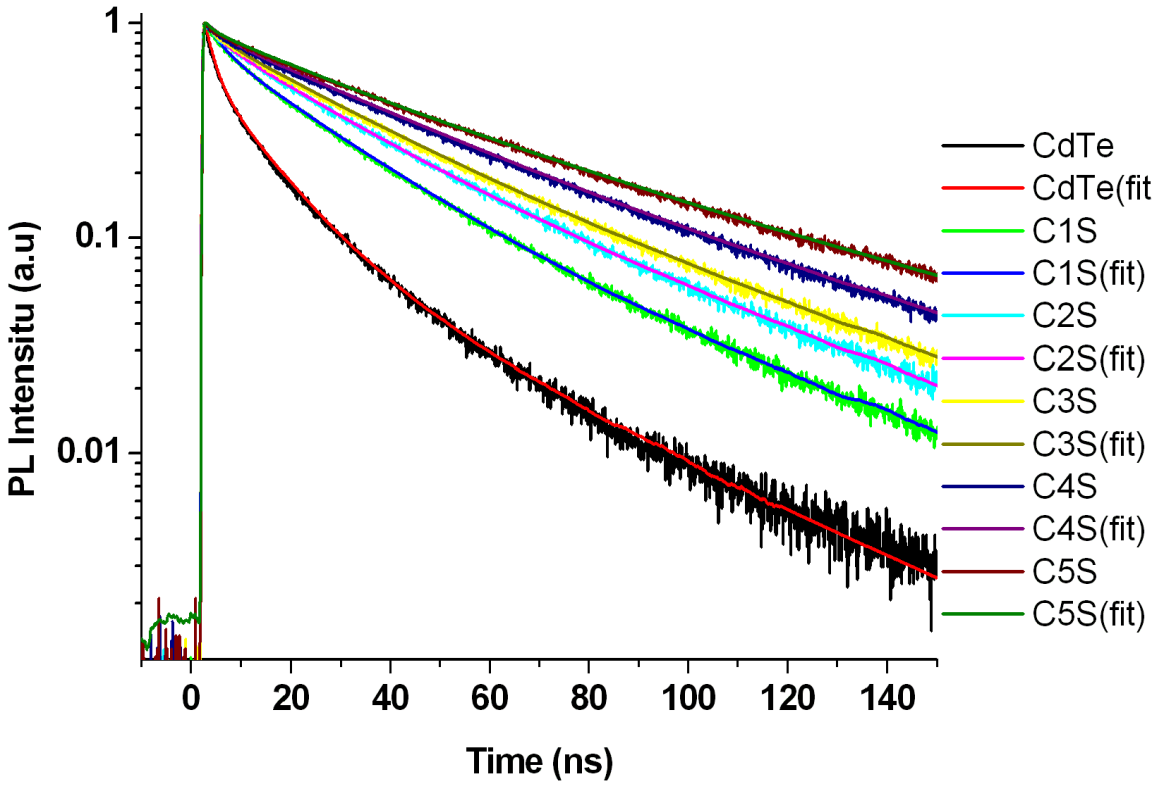

Figure S1. Emission decay was measured for CdTe and CdTe/CdS samples with different numbers of monolayers of CdS. The decay lifetime was measured using time-correlated single photon counting with excitation wavelength 400 nm and the emission wavelength at the maximum of each sample. CnS represents the CdTe/CdS core/shell with n monolayers of CdS. A three-exponential function was required to sufficiently fit the emission decay curves, and the average lifetimes are calculated by $\langle\tau\rangle = \sum_{i=1}^{3} A_i$,

where A_i is the normalized amplitude of each component. The chi square values are all between 1.2-1.4.

Decay curve for CdTe/CdSe core/shell QDs as successive layers of shell were deposited on the CdTe core:

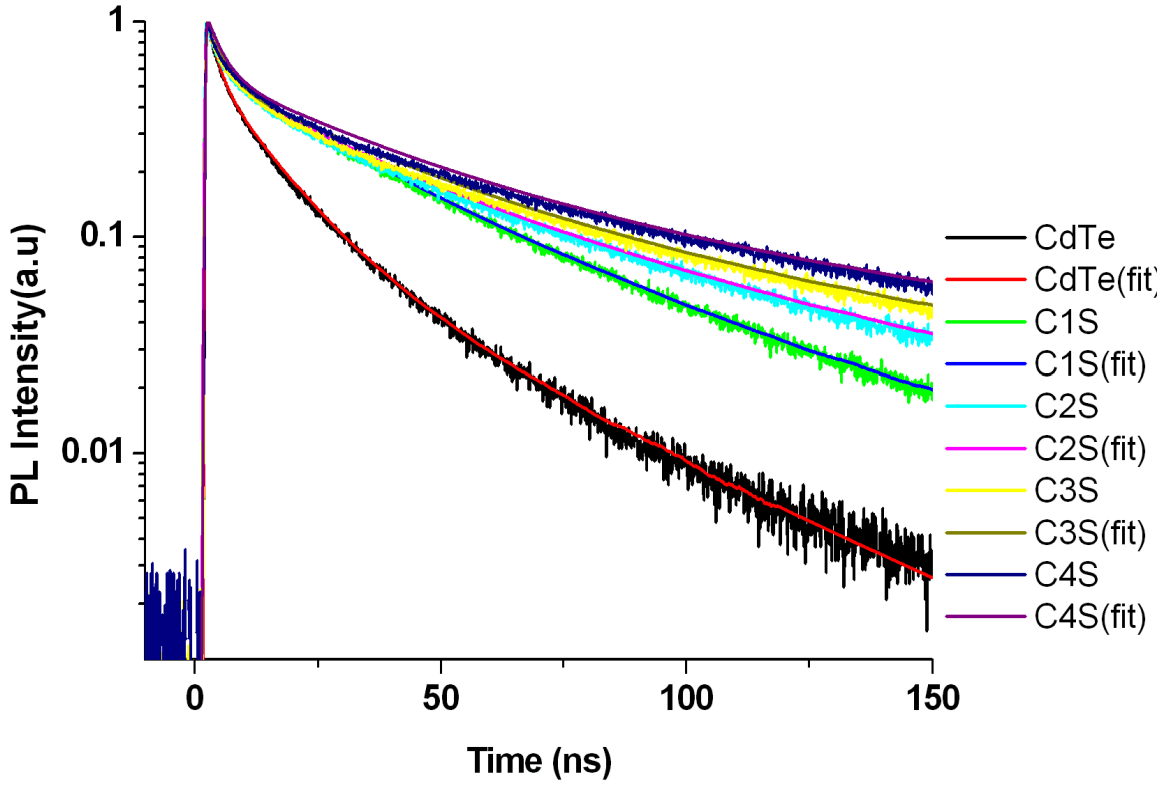

Figure S2. Emission decay was measured for CdTe, CdTe/CdSe samples with different numbers of monolayers of CdSe. The decay lifetime was measured using time-correlated single photon counting with excitation wavelength 400 nm and the emission wavelength at the maximum of each sample. Here, CnS represents the CdTe/CdSe core/shell with n monolayers of CdSe. A three-exponential function was required to sufficiently fit the emission decay curves, and the average lifetimes are calculated by $\langle\tau\rangle = \sum_{i=1}^{3} A_i$, where

A_i is the normalized amplitude of each component. The chi square values are all in between 1.3-1.5.

Table S1. The QY and average lifetime of the CdTe/CdS core/shell QDs with different numbers of CdS monolayers. The radiative and nonradiative rate constants (k_r and k_{nr}) were calculated using $QY=k_r/(k_r+k_{nr})$ and average life time $\tau= 1/(k_r+k_{nr})$.

QD	Average Life time (ns)	QY(%)	k_r (μs^{-1})	k_{nr} (μs^{-1})
CdTe	7.9	8.5	10.8	116
CdTe-1CdS	23.5	39.1	16.6	25.9
CdTe-2CdS	29.16	41.8	14.3	20.0
CdTe-3CdS	33.3	33.3	10.0	20.0
CdTe-4CdS	41.08	29.1	7.08	17.3
CdTe-5CdS	45.7	22.2	4.86	17.0
CdTe-2CdS-ZnS	36.8	43.7	11.9	15.3

Table S2. The QY and average lifetime of the CdTe/CdSe core/shell QDs with different numbers of CdSe monolayers.

QD	Average life time(ns)	QY (%)	k_r (μs^{-1})	k_{nr} (μs^{-1})
CdTe	7.9	8.5	10.8	116
CdTe-1CdSe	23.49	28.3	12.1	30.5
CdTe-2CdSe	26.47	33.5	12.7	25.1
CdTe-3CdSe	30.75	31.2	10.2	22.4
CdTe-4CdSe	35.77	25.4	7.11	20.8
CdTe-2CdSe-ZnS	37.75	35.1	9.30	17.2

Table S3. The PL quantum yield of fresh and aged nanocrystal samples. Aged nanocrystals were exposed to air and kept in the dark at 4°C for 4 and 5.5 months. The excitation wavelengths for the QY measurements were 400 nm, 450 nm or 500 nm. The absorption values of the sample to be measured and the reference dye at the excitation wavelengths were carefully matched.

Nanocrystal samples	Fresh sample (400nm)	4 months (400nm)	5.5 months (400nm)	5.5 months (450nm)	5.5 months (500nm)
CdTe-2CdS	41.8	35.9	32.1	36.5	34.2
CdTe-3CdS	33.8	31.4	27.6	30.5	28.8
CdTe-2CdS-ZnS	43.7	34.5	31.2	35.3	32.9
CdTe-2CdSe	33.5	33.3	30.8	36.7	31.6
CdTe-3CdSe	31.2	21.4	17.2	21.4	18.5
CdTe-2CdSe-ZnS	35.1	28.6	23.1	26.2	23.9

From the table, the QY of the 4 and 5.5 months old samples are slightly lower than that of the freshly prepared samples, indicating the highly stable of these nanocrystal samples.

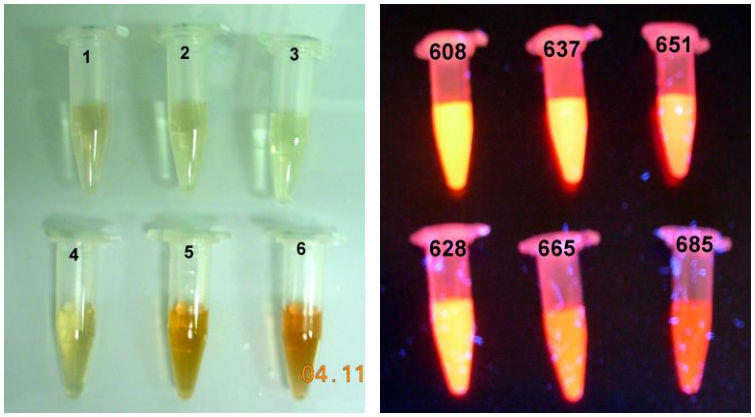

Figure S3. Picture of six nanocrystal samples under room light (Left) and 365 nm UV light (Right) after 6 months storage: 1. CdTe-2CdS (emission max at 608 nm), 2. CdTe-3CdS (emission max at 637 nm), 3. CdTe-2CdS-ZnS (emission max at 651 nm), 4. CdTe-

2CdSe (emission max at 628 nm), 5. CdTe-3CdSe (emission max at 665 nm), 6. CdTe-2CdSe-ZnS (emission max at 685 nm). No visible precipitation is observed.

APPENDIX B

SUPPLEMENTAL INFORMATION FOR CHAPTER 3

Supporting information

Robust DNA Functionalized Core/Shell Quantum Dots with Fluorescent Emission Spanning from UV-Vis to Near IR and Compatible with DNA Directed Self-Assembly

Zhengtao Deng, Anirban Samanta, Jeanette Nangreave, Hao Yan and Yan Liu

The Biodesign Institute, Department of Chemistry and Biochemistry, Arizona State University, Tempe, Arizona, 85287

Table of content

Part 1. Chemicals, buffers and characterization details

Chemicals: Cadmium nitrate tetrahydrate ($Cd(NO_3)_2{\cdot}4H_2O$, 99.8%), Zinc nitrate tetrahydrate ($Zn(NO_3)_2{\cdot}4H_2O$, 99.8%), Zinc oxide (ZnO, 99.9%, powder < 5 micron), Cadmium oxide (CdO, 99.99+%, powder), Tellurium (Te, powder, -200 mesh, ≥99%, powder), Selenium (Se, powder, <100 mesh, 99.99%), Sulfur (S, 99.998% powder), paraffin liquid (C_nH_{2n+2}, n = 16−22), oleic acid (OLA, $CH_3(CH_2)_7CH{=}CH(CH_2)_7COOH$, 90%), 2-ethylhexanoic acid (EHA, $CH_3(CH_2)_3CH(C_2H_5)COOH$, 99+%), Thiourea ($NH_2CSNH_2$, ≥99.0%), Sodium borohydride ($NaBH_4$, powder, ≥99%), 3-Mercaptopropionic acid ($HSCH_2CH_2CO_2H$, ≥99%), isopropyl alcohol (IPA, 99%), hexane (≥95%), methanol (≥99.5%), Rhodamine 6G (QY = 95% in ethanol), and Rhodamine 101 (λem=589 nm, QY = 100% in ethanol + 0.01 HCl), were purchased from Sigma-Aldrich and used without further purification. M13mp18 single stranded DNA was purchased from New England Biolabs and was also used without further treatment. All unmodified helper strands were purchased from Integrated DNA Technologies, Inc. (IDT, www.idtdna.com) in 96-well plate format, suspended in nanopure water (H_2O, with resistivity up to 18.2 MΩ·cm) and used without further purification. All modified helper strands were purchased from IDT and purified by denaturing PAGE gel electrophoresis. Phosphorothiolated backbone modified ps-po-chimeric ssDNA strands were purchased from IDT and used without purification.

Buffers: the buffers used in this study are:

1xPBS: 150 mM NaCl, 0.1 mM EDTA, 20 mM sodium phosphate, pH 4.0, 7.0, 10.0

1xTAE/Mg^{2+}: 40 mM Tris acetate, 2 mM EDTA, and 12.5 mM magnesium acetate, pH 8.0.

1xTBE/Mg^{2+}: 50 mM Tris, 100 mM Borate, 10 mM EDTA, pH 8.2.

Characterization: Ultraviolet-Visible (UV-Vis) absorption spectra were recorded at room temperature with a JASCO-V670 spectrophotometer. Photoluminescence (PL) spectra were measured at room temperature using a NanoLog spectrometer manufactured by HORIBA Jobin Yvon equipped with a thermoelectric cooled PMT (R928 in the range 200 nm to 850 nm). Atomic force microscopy (AFM) was performed using a Veeco 8 AFM in tapping in air mode. High-resolution transmission electron microscopy (HRTEM), high angle annular dark field scanning transmission electron microscopy (HAADF-STEM), and energy dispersive X-ray spectroscopy (EDS) were performed on a JEOL JEM 2010F electron microscope operating at 200 kV.

Part 2. Oligonucleotide functionalized CdTe/CdS QDs

2.1 Synthesis of 1.6 nm CdTe core QDs: CdTe core QDs with 1.6 nm diameter were synthesized according to our previous published procedure.[1] A freshly prepared NaHTe solution (the source of Te, 1.0 mol/L, 10 μL) was injected through a syringe into an N_2-saturated $Cd(NO_3)_2$ solution (the source of Cd, 0.005 mol/L, 50 mL) at room temperature (20 ^oC) in the presence of 3-mercaptopropionic acid (MPA, 37 μL) as a stabilizing agent. The pH was tuned to 12.2 by adding NaOH (1M). The molar ratio of Cd^{2+}/MPA/NaHTe in the mixture was fixed at 1:1.7:0.04. Special attention should be paid since the NaHTe is very easy to be oxidized by trace amount of oxygen in a short time. The solution was subsequently aged at 4 ^oC and magic-sized CdTe clusters with photoluminescence emission peak at 480 nm were formed overnight. The diameter of the resulting CdTe QDs was ~ 1.6 nm. These small QDs were purified by adding IPA (1:1 in volume ratio),

followed by centrifugation at 15,000 rpm for 15 minutes and were subsequently re-dispersed in DI water. In some cases, the crude, unpurified CdTe QD solutions were also used directly as the stock solution for the next step shell growth. Both pure and impure solutions were used as the cores for synthesizing the oligonucleotides conjugated CdTe/CdS core/shell QDs.

2.2 Oligonucleotide functionalized CdTe/CdS core/shell QDs: The above precipitated 1.6 nm CdTe QDs (from 100 µL stock solution) were re-suspended in 100 µL of nano-pure water. The concentration of the core CdTe QDs and amount of additional shell precursor to obtain specific shell thicknesses were calculated following a reported method.[2-3] For a typical experiment to synthesize CdTe/4 CdS core/shell QDs with 1.6 nm CdTe core diameter (0.25 nM in 100 µL DI water), 4.5 µL Cd^{2+} stock solution (25 mM) and 9.0 µL MPA stock solution (25 mM) were combined with the core, vortexed and gently sonicated in a 1.5 mL plastic tube. Next, 50 µL of 5'-TTTTTTTTTTTTTTTTTTTTTTTTTTTTG*G*G*G*G* G -3' oligonucleotide stock solution (100 nM) was also added and gently vortexed. The molar ratio of QD: oligonucleotide was approximately 1: 200. The pH was tuned to 12.2 by adding NaOH (1M). The reaction mixture was placed on a heating block at 90 ^{o}C for 40 minutes, and then cooled down by submerging the tube in a water bath at room temperature. The reacted solution was loaded into a 0.5 mL Amicon filter (MWCO 30KDa), 250 µL DI water was added to the filter, and the sample was subjected to centrifugation at 7000 rpm for 3 minutes. The washing (each washing was performed with 350 µL of DI water) and centrifugation steps were repeated four times. This ultrafiltration process removed the free DNA and unreacted precursor from the QDs. If buffer exchange with DI water is

desired, 350 µL of 1XTA buffer, rather than DI water, could be added before and after the centrifugation. The final sample is highly fluorescent and stable in buffer or in DI water.

We found that the un-purified crude CdTe QD cores could also be used for synthesis of oligonucleotide functionalized CdTe/CdS core/shell QDs. For a typical synthesis, 100 µL of crude 1.6 nm CdTe core stock solution (0.25 nM) was added to a 1.5 mL plastic tube. Then 2.5 µL of Cd^{2+} stock solution (25 mM) and 5.6 µL of MPA stock solution (25 mM) was added to the core, vortexed and gently sonicated. Next, 50 µL of 5'-TTTTTTTTTTTTTTTTTTTTTTT TTTTG*G*G*G*G*G -3' oligonucleotide stock solution (100 nM) was added and gently vortexed. The molar ratio of QD:oligonucleotide was about 1:200. The pH was tuned to 12.2 by adding NaOH (1M). Finally, the reacted solution was heated and purified as before.

Photoluminescence quantum yield measurements

We used a cross-calibrated method to measure the quantum yield of the as-synthesized quantum dots.[4] For orange and red emission QDs, their PL quantum yields were obtained by comparison to a standard Rhodamine 101 reference dye (QY = 100% in ethanol + 0.01 HCl). The standard dye was cross-calibrated by referencing to Rhodamine 6G (QY = 95% in ethanol). The PL quantum yield was calculated using the following equation:

$$\varphi = \varphi'\left(\frac{I}{I'}\right)\left(\frac{A'}{A}\right)\left(\frac{n}{n'}\right)^2$$

where φ and φ' are the PL QY for the sample and standard, respectively; I (sample) and I' (standard) are the integrated emission peak areas at a given wavelength; A (sample) and

A' (standard) are the absorption intensities at the same wavelength used for PL excitation; n (sample) and n' (standard) are the refractive indices of the solvents.

Figure S1. Quantum yield measurement of oligonucleotide functionalized CdTe/7 CdS core/shell QDs using purified CdTe core. (a) UV-Vis absorption and (b) photoluminescence emission spectra of QDs and the standard Rhodamine 101.

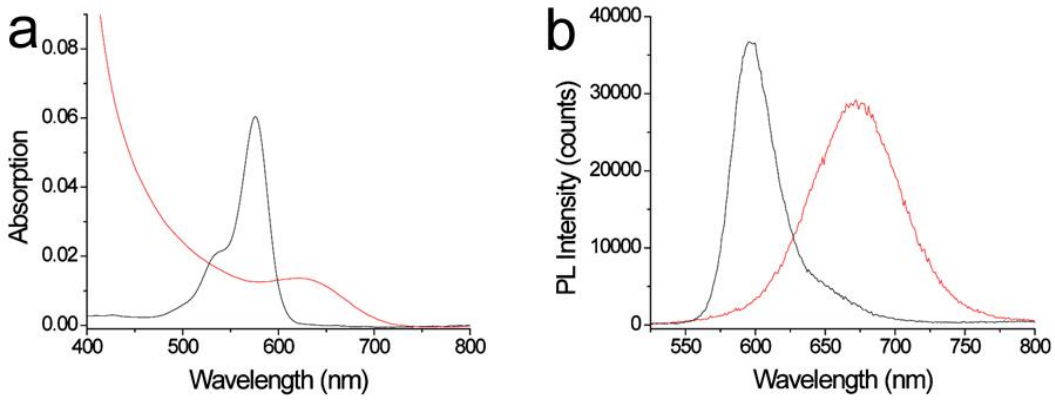

Area	Peak at	Width	Height
1.71753E6	595	37	36740
2.43762E6	672	75	29210

At 515 nm Abs(R110)=0.0101; Abs (QDs)=0.0204

QY=70.3%

Figure S2. Quantum yield measurement of oligonucleotide functionalized CdTe/7 CdS core/shell QDs using unpurified CdTe core. (a) UV-Vis absorption and (b) photoluminescence emission spectra of QDs and the standard Rhodamine 101.

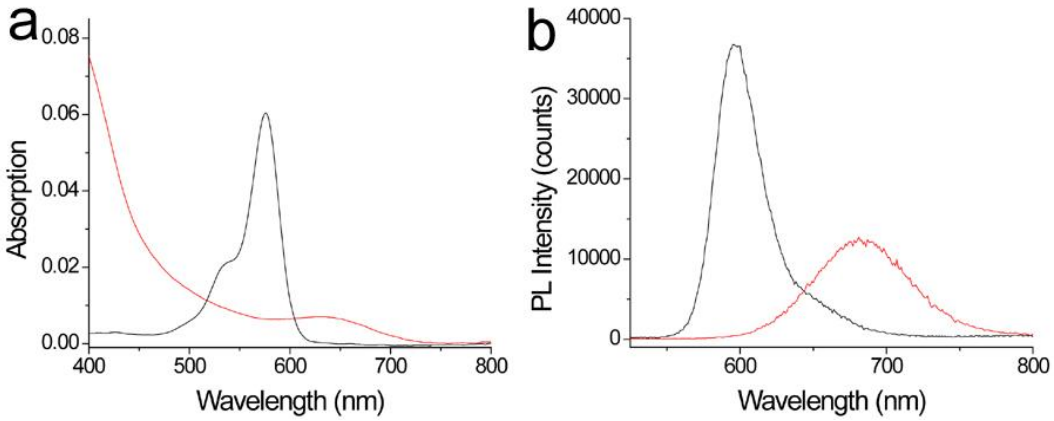

Area	Peak at	Width	Height
1.71753E6	595	37	36740
1.05615E6	681	77	12695

Abs(R110)=0.0101; Abs (QDs)=0.0107

QY=58.0%

Figure S3. (a) TEM and (b) HRTEM images of the oligonucleotide functionalized CdTe/7CdS core/shell QDs with emission at 672 nm using purified CdTe core.

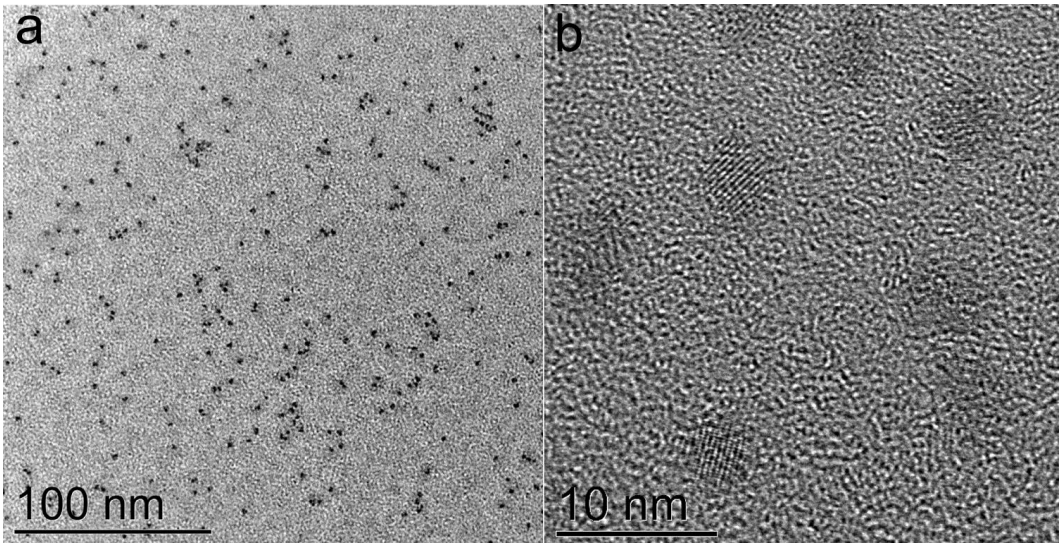

Figure S4. TEM and HRTEM images of the oligonucleotide functionalized CdTe/13CdS core/shell QDs with emission at 800 nm using purified CdTe core.

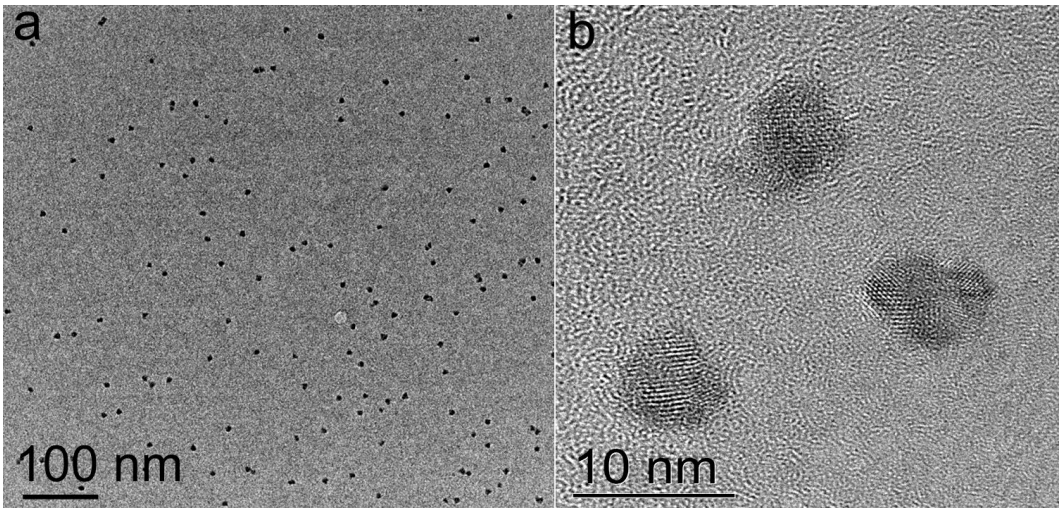

Figure S5. Additional STEM image of the self-assembled QDs on DNA origami and EDS pattern of the oligonucleotide functionalized CdTe/7CdS QDs measured from the sample shown in the STEM image. Note that the phosphorus signal is derived from the DNA, and the uranium is derived from the negative stain.

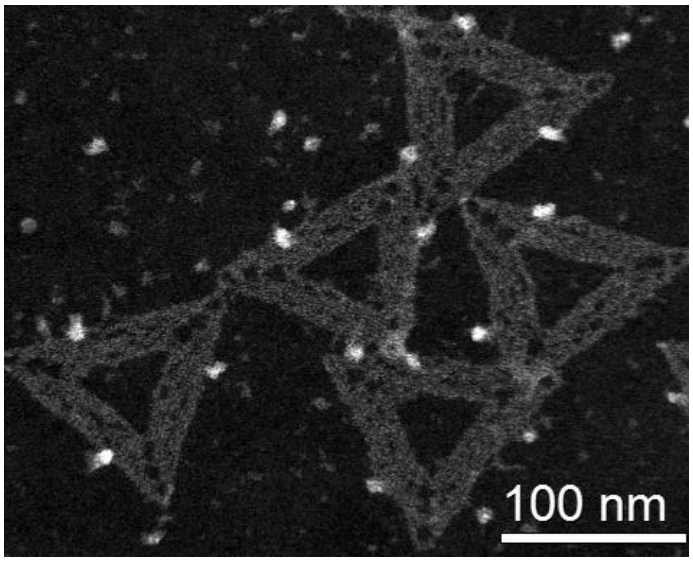

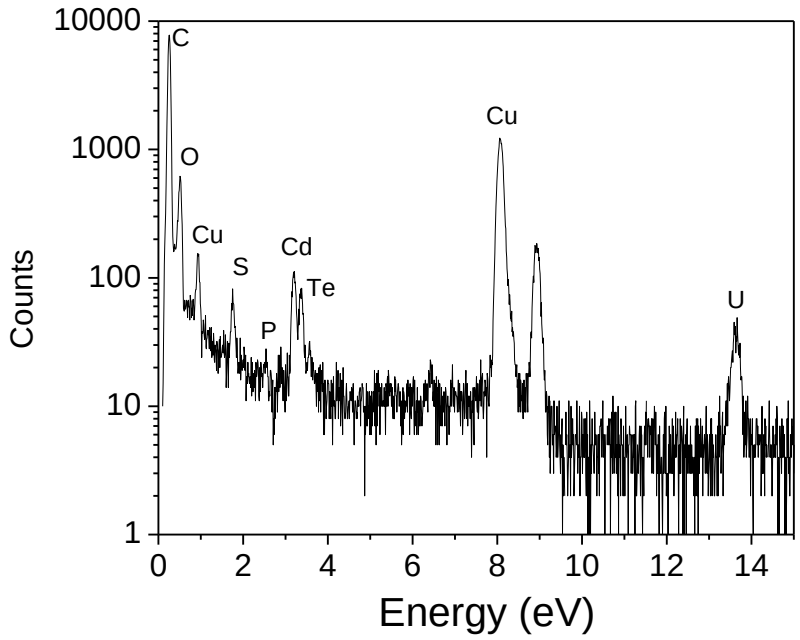

Figure S6. Additional AFM images of the oligonucleotide functionalized CdTe/2CdS core/shell QDs (emission at 575 nm) organized by DNA origami. Nearly 100% yield of QD assembly on the origami was obtained.

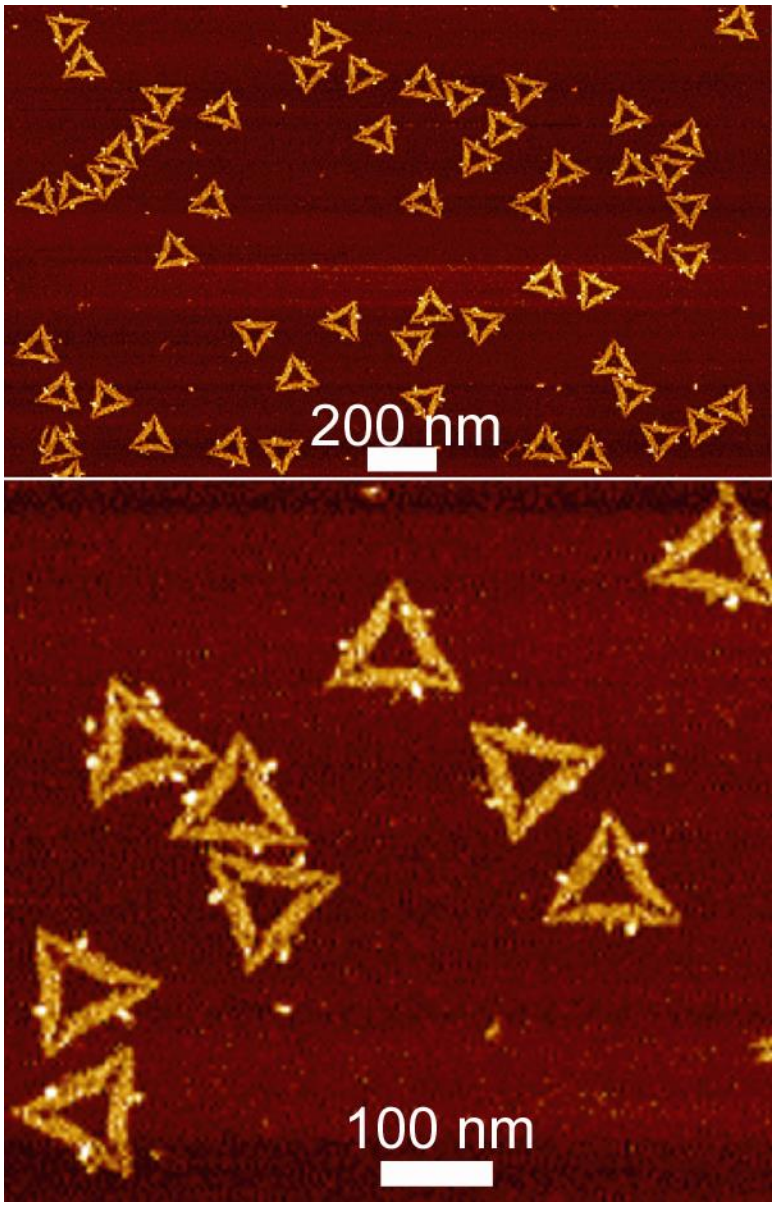

Figure S7. Additional AFM images of the oligonucleotide functionalized CdTe/7CdS core/shell QDs self-assembled on DNA origami. Nearly 100% yield of QD assembly on the origami was obtained.

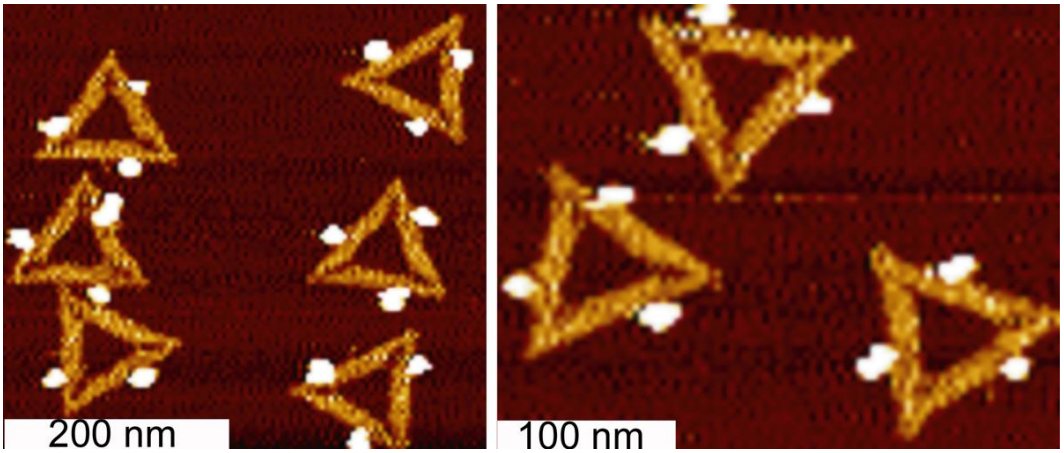

Figure S8. Evidence of the DNA being 'embedded' within the QD shell. The PL spectra of the oligonucleotide functionalized CdTe/5CdS core/shell QDs before and after etching using citrate buffer (pH=3, 5 minute exposure). The PL emission is shifted from 625 nm to 585 nm as shown in (a), indicating etching of the surface layer. Next, the sample was purified by a 0.5 mL Amicon filter (MWCO 30KDa). The purified QDs were attached to DNA origami with a yield of 60% as shown in (b-c), indicating that the oligonucleotides were actually 'nailed' into the CdS shell.

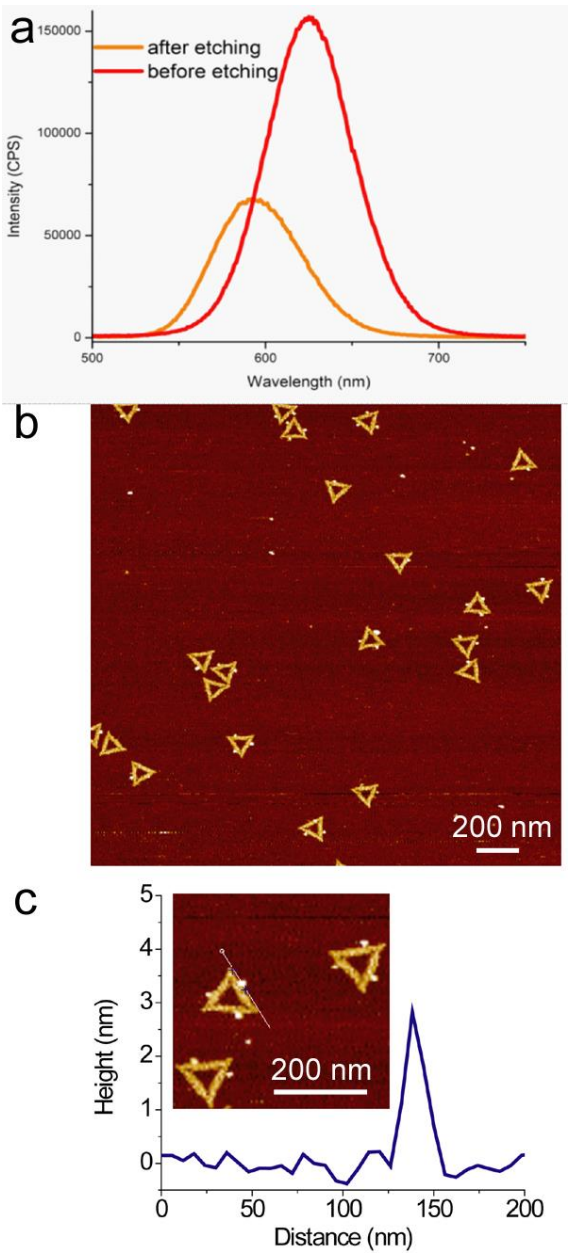

Figure S9. Estimation of numbers of ssDNA on each QD. As an example, we use a random ssDNA sequence (5'- G*G*G* G*G*T TTA GGA GGA TAG TTC GGT GGC TGT TCA GGG TCT CCT CCT -3') to attach to a magic-core QDs during the shell growth process. After the synthesis, the samples were purified 4 times using Amicon filter (MWCO 30KDa) to get rid of free un-attached ssDNA.

According to the UV-Vis spectra showing in Figure 9a, we have

$$\varepsilon(DNA260) \times c(DNA) + \varepsilon(QD260) \times c(QD) = A(260)$$

$$\varepsilon(DNA630) \times c(DNA) + \varepsilon(QD630) \times c(QD) = A(630)$$

We suppose: $\varepsilon(DNA630) = 0$

Thus:

$$\frac{c(DNA)}{c(QDs)} = \left(\frac{A260}{A630} \times \frac{\varepsilon\,(QD630)}{\varepsilon(DNA260)} - \frac{\varepsilon(QD260)}{\varepsilon(DNA260)}\right)$$

According to the known Ext. Coefficients for QDs and ssDNA

$\varepsilon(DNA260)$ = 424,200 L/(mole·cm)

$\varepsilon(QD630)$ = 650,000 L/(mole·cm)

$\varepsilon(QD260)$=64× 650,000 L/(mole·cm)

$A(260)$=1.4240

$A(630)$=0.02036

$c(DNA)/c(QD)$=9.1

Finally, we calculate the numbers of DNA per QD is around 9.

Part 3. Oligonucleotide functionalized CdSe/20 CdS QDs

Synthesis of oleic acid (OLA) capped CdSe QDs[5]: Cd^{2+}-OLA complex precursor solution was prepared by adding 7.5 mmol CdO into a 100 mL flask containing 10 mL paraffin liquid and 15 mL oleic acid. The mixture was heated to 100 ^{o}C, degassed under 100 mtorr pressure for 30 minutes, filled with N2, and further heated to 200 ^{o}C to form a clear Cd^{2+} precursor solution. Then, Se precursor solution was prepared in a separate flask, where 0.30 mmol of Se powder was mixed with 15 mL paraffin liquid, degassed for 30 minutes, filled with N_2, and heated to 250 or 320 ^{o}C. Next, 1 mL Cd^{2+}-OLA complex precursor solution was quickly injected to the flask containing the above mixture. The molar ratio of Cd:Se in the reaction mixture was ~1:1. The mixture was maintained at 250 ^{o}C for 10 minutes (for 3 nm CdSe QDs) or at 320 ^{o}C for 10 minutes (for 6 nm CdSe QDs) with continuous stirring. A number of aliquots were collected in test tubes containing cold hexane to further quench QD growth at different intervals. The samples were purified by centrifugation (13,000 rpm for 30 minutes) several times after being precipitated with IPA and methanol. The final products were dispersed in hexane.

Oligonucleotide functionalized thick-shell CdSe/CdS QDs:

First, ligand exchange with MPA was performed to make the CdSe core QDs water soluble: The oleic acid capped CdSe QDs, with emission at 650 nm, were purified as described above and dissolved in hexane (200 µL). Formamide (100 µL) mixed with 5 µL of 25 mM MPA solution was added. The mixture was vortexed and sonicated for 15 minutes to allow for ligand exchange in which MPA displaces OLA on the QD surface to form Cd-S bonds (rather than Cd-O bonds). After the ligand exchange, the MPA-capped

QDs are soluble in the polar solvent, thus, can transfer from the non-polar hexane phase into the polar formamide phase. After settling, the upper hexane layer was removed, and the formamide layer was mixed with 1:1 IPA and centrifuged at 15K rpm for 10 minutes. The purified QDs were re-dissolved in DI water. The concentration of the QDs was determined according reported methods.

Next, 9 CdS shell monolayers were deposited on the 6 nm CdSe core. For a typical experiment, the water-soluble CdSe QD solution (with absorption of 0.0031 at 625 nm) was prepared in 100 µL of DI-water. Then, 11 µL of Cd^{2+} stock solution (25 mM) and 22 µL of MPA stock solution (25 mM) were added, vortexed and gently sonicated in a 1.5 mL plastic tube. The pH was tuned to 12.2 by adding NaOH (1M). The mixture was heated on a heating block at 90 ^{o}C for 90 minutes. The product was cooled down by submerging the tube in a water bath at room temperature. The sample was loaded into a 0.5 mL Amicon filter (MWCO 100KDa), and filtered in the same way as the CdTe/CdS QDs to remove the unreacted precursor.

Finally, 11 CdS shell monolayers were deposited on the 6 nm CdSe core. For a typical experiment, the water soluble CdSe QD solution (with absorption value of 0.0031 at 625 nm) was prepared in 100 µL of DI-water by gentle sonication. Then, 40 µL of Cd^{2+} stock solution (25 mM) and 80 µLof MPA stock solution (25 mM) were added, vortexed and gently sonicated in a 1.5 mL plastic tube. Then 100 µL 5'-TTTTTTTTTTTTTTTTTTTTTTTTTTTTG*G*G*G*G* G*G*G*G*G*G-3' oligonucleotide stock solution (100 nM) was added and gently vortexed. The molar ratio of QD:oligonucleotide was approximately 1: 8.3. The pH was tuned to 12.2 by adding NaOH (1M). The mixture was heated on the heating block at 90°C for 110 minutes.

Then, the product was cooled down by submerging the tube in a water bath at room temperature. The sample was loaded into a 0.5 mL Amicon filter (MWCO 100KDa), and filtered in the same way as for the CdTe/CdS QDs to remove the unreacted precursor from the QDs. If buffer exchange with DI water is desired, 350 µL of 1XTA buffer, rather than DI water could be added before and after the centrifugation. The final sample is fluorescent and stable in buffer or in DI water.

Figure S10. Photograph of the CdSe QDs (with emission at 650 nm) before (left) and after ligand exchange (right). The upper solvent is hexane, while the bottom layer solvent is formamide.

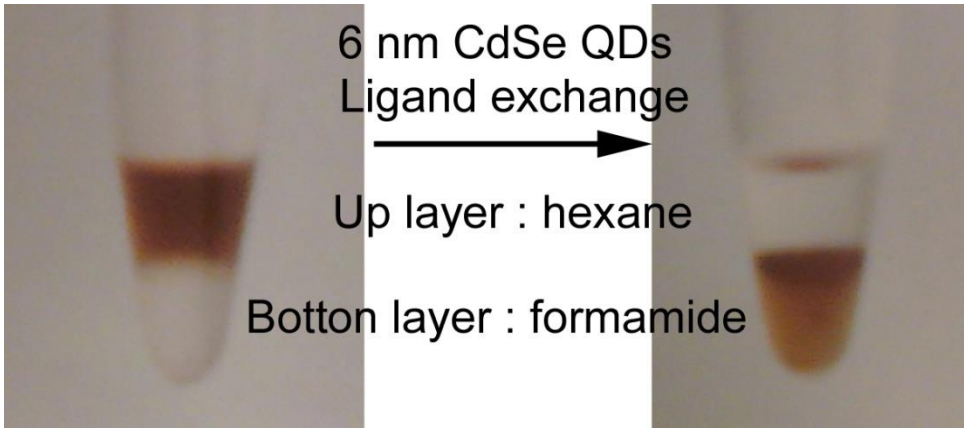

Figure S10. UV-Vis and PL spectra of the 3.0 nm CdSe core QDs (565 nm emission, green trace) and the CdSe/9 CdS core/shell QDs conjugated to DNA (635 nm emission, red trace). Note that the PL shift to a red wavelength is due to the formation of the thick-shell.

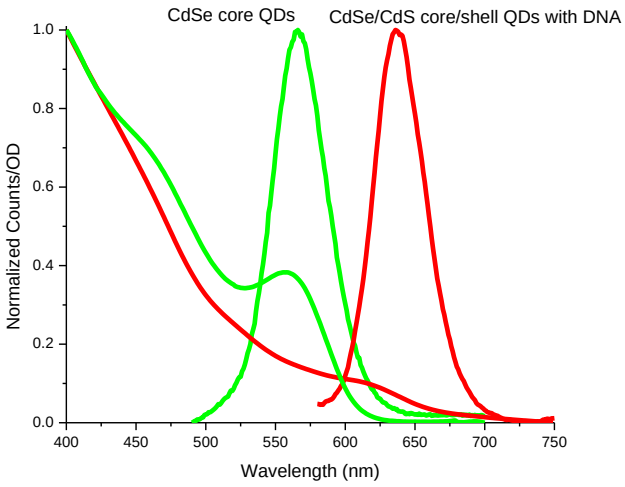

Figure S11. UV-Vis absorption and PL spectra of the 6.0 nm core CdSe QDs (black), CdSe/9CdS (red), and the CdSe/20CdS QDs (maroon). Note that the PL shift about ~13 nm after coating by the thick-shell.

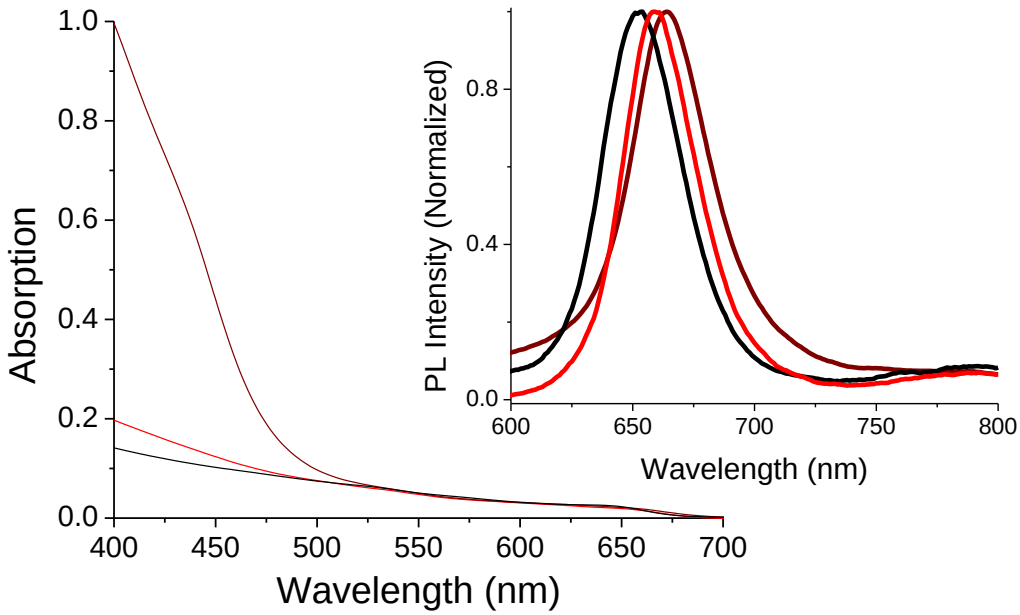

Figure S12. (a) TEM, (b) STEM and (c-d) HRTEM images of the 6.0 nm CdSe core QDs with emission at 650 nm.

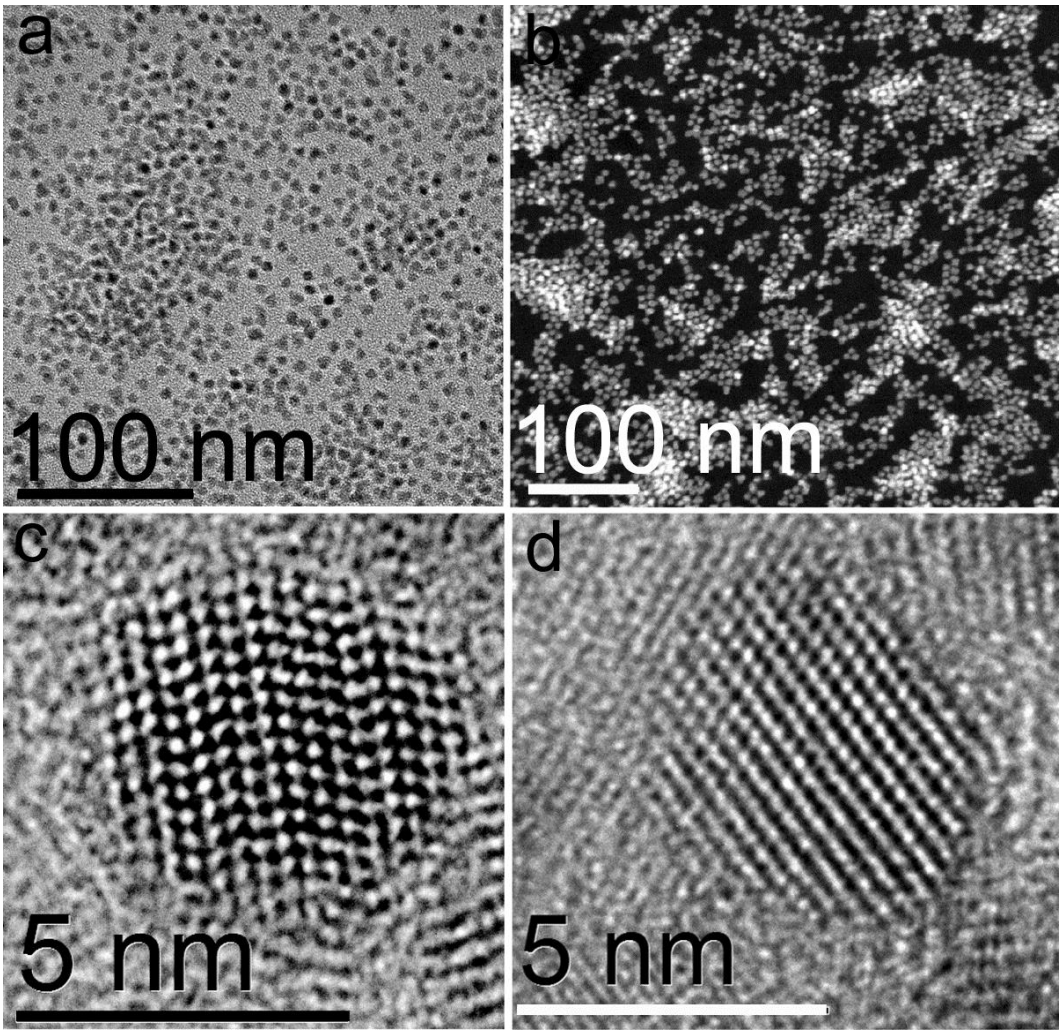

FigureS13. TEM (a, c, e) and STEM (b, d, f) images of the CdSe/9CdS core/shell QDs with 6.0 nm CdSe core.

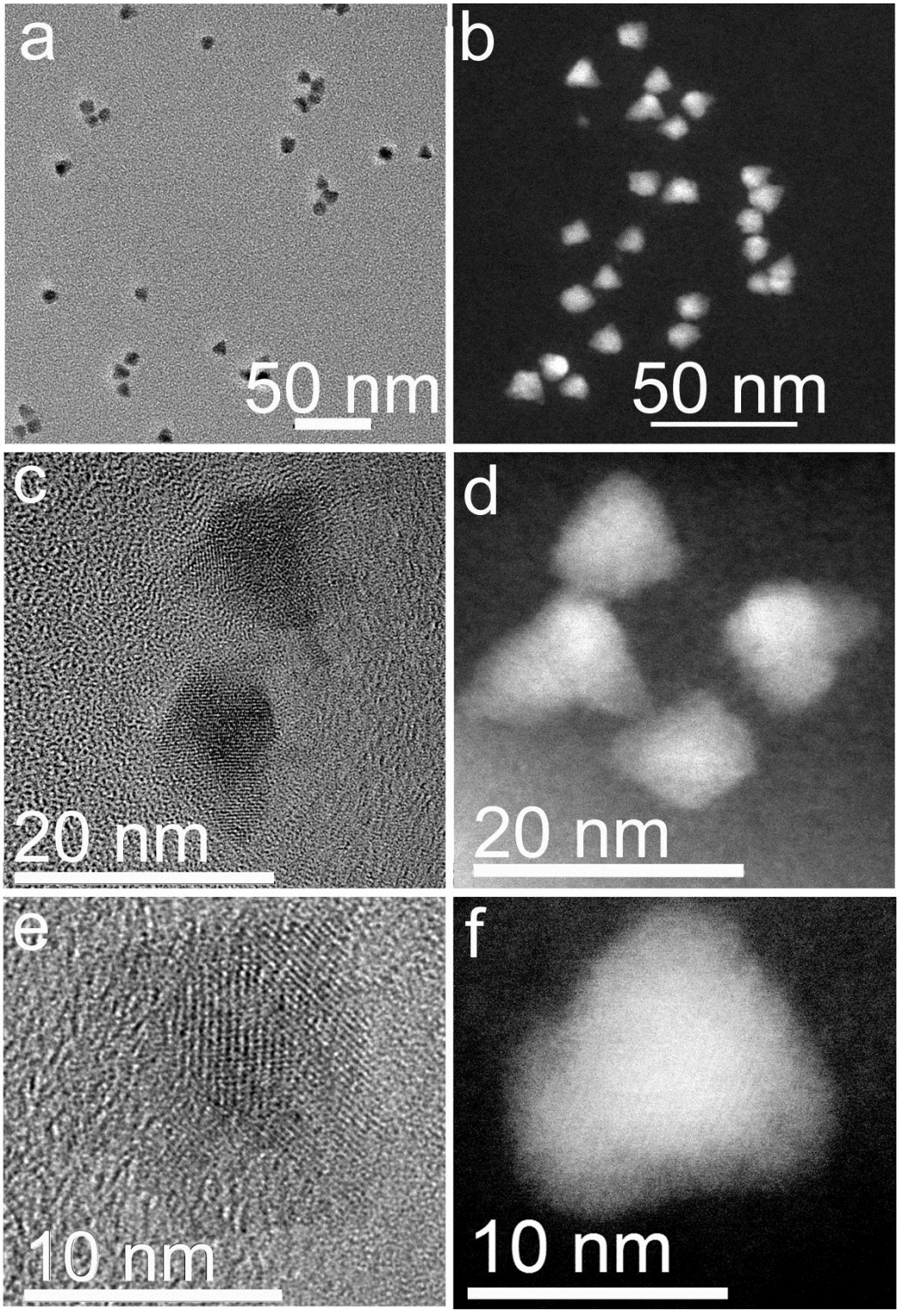

Figure S14. Additional TEM images of the oligonucleotides functionalized thick-shell CdTe/20 CdS QDs with 6.0 nm CdSe core.

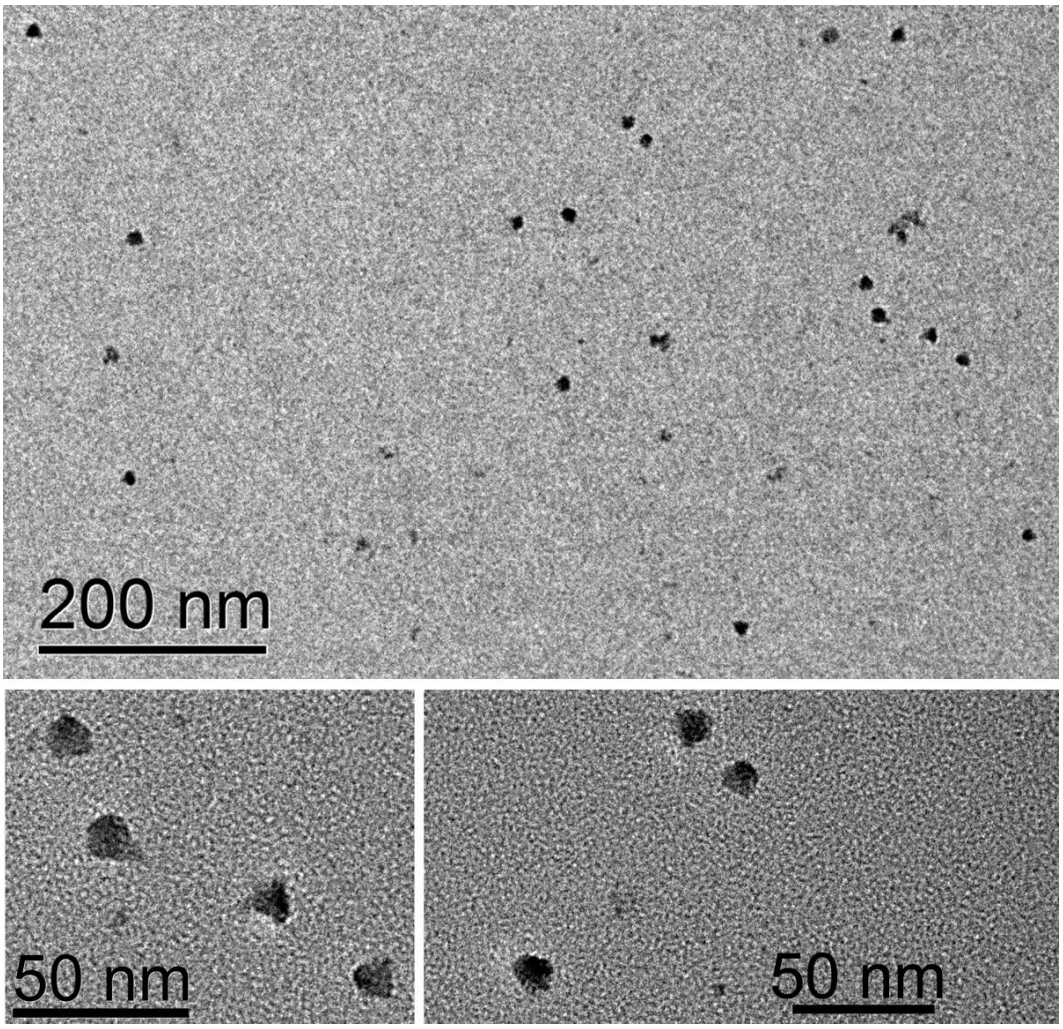

FigureS15. Enlarged HRTEM image of the oligonucleotide functionalized thick-shell CdTe/20 CdS QDs with 6.0 nm CdSe core. Note that the thick-shell QDs are well-crystallized. The blue box indicates the edges of a single nanoparticle.

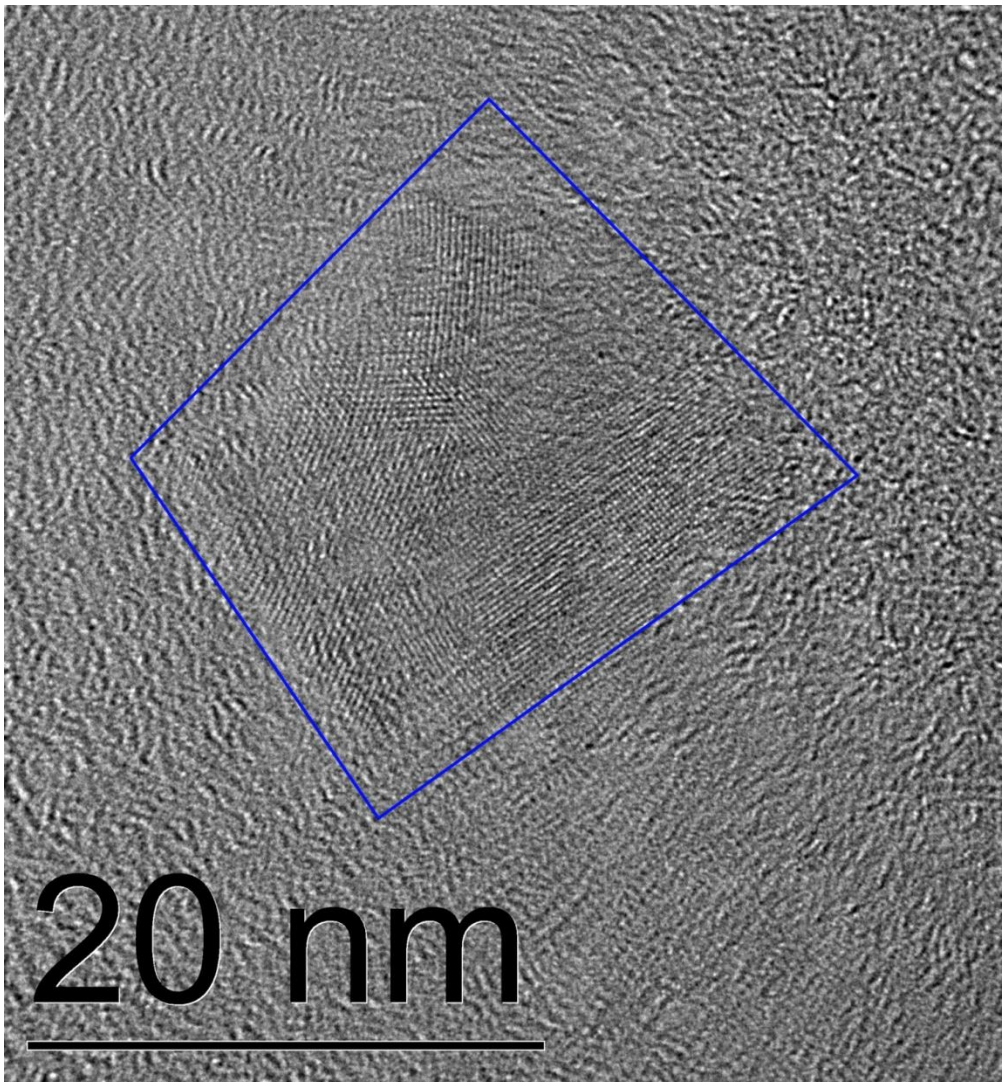

Figure S16. Enlarged STEM image of the oligonucleotide functionalized thick-shell CdTe/20 CdS QDs with 6.0 nm CdSe core.

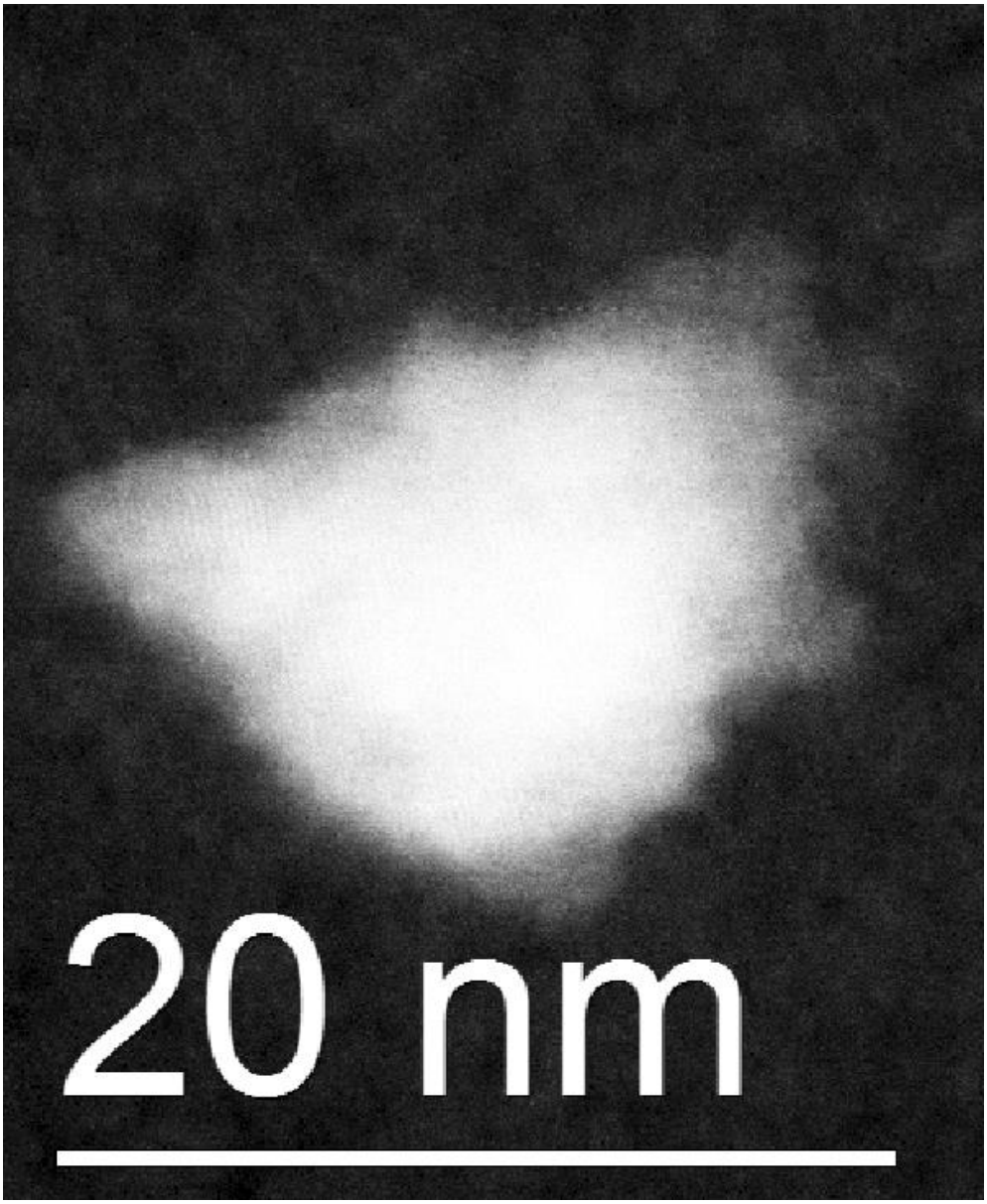

Figure S17. Additional STEM image of the QDs assembled on DNA origami and EDS pattern of the oligonucleotide functionalized CdSe/20CdS QDs with 6.0 nm CdSe core measured from the sample shown in the STEM image. Note that the phosphorus signal is derived from the DNA, and the uranium signal is derived from the negative stain.

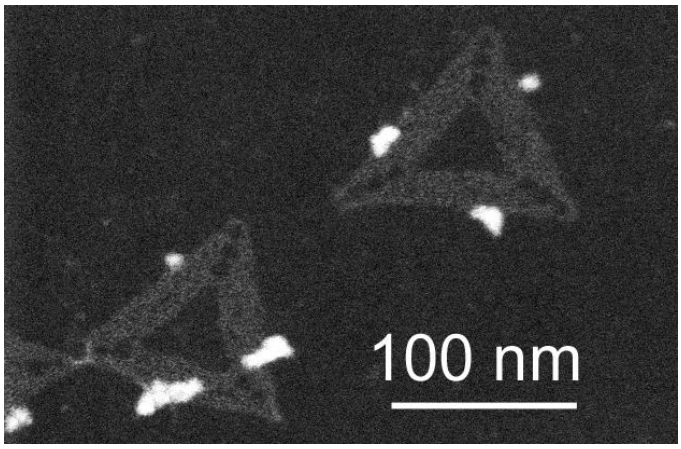

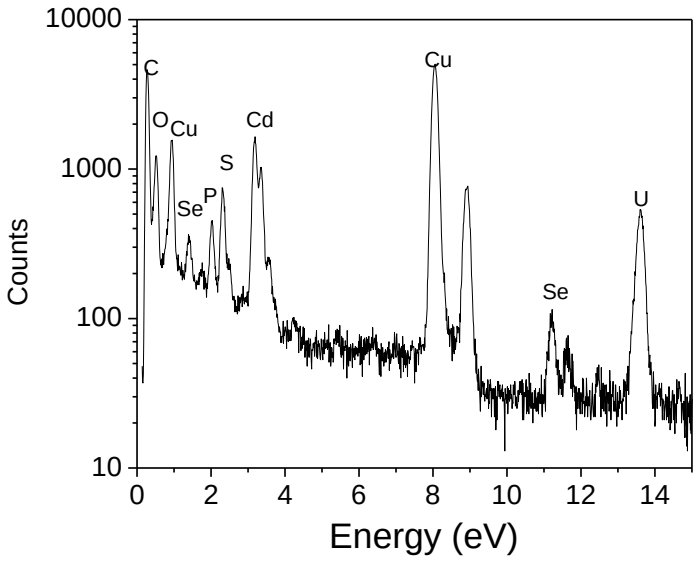

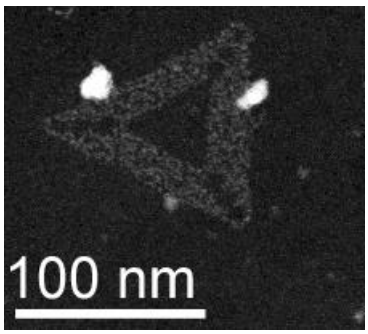

Part 4. Oligonucleotide functionalization of other core/shell QDs

4. 1. Oligonucleotide functionalization of CdTe/ZnS QDs

The precipitated 1.6 nm core CdTe QDs (from 100 µL stock solution) were re-suspended in 100 µL of nano-pure water as described in Part 2 above. For oligonucleotide functionalized CdTe/4 ZnS core/shell QDs synthesis, 4.5 µL of Zn^{2+} stock solution (25 mM) and 9.0 µL of MPA stock solution (25 mM) were added to the 1.6 nm CdTe core (0.25 nM in 100 µL DI water) solution in a 1.5 mL plastic tube, vortexed and gently sonicated. Then, 50 µL of 5'-TTTTTT TTTTTTTTTTTTTTTTTTTTTG*G*G*G*G*G -3' oligonucleotide stock solution (100 nM) was added and gently vortexed. The molar ratio of QD:oligonucleotide was approximately 1: 200. The pH was tuned to 12.2 by adding NaOH (1M). The reaction mixture was placed on the heating block at 90 ^{o}C for 40 minutes, and then cooled down at room temperature. The 0.5 mL Amicon filter (MWCO 30KDa) washing step is the same as for the CdTe/CdS QDs described above. The final samples are highly fluorescent and stable in buffer or in DI water.

Figure S18. Additional AFM image, typical HRTEM, and STEM image of the oligonucleotide functionalized CdTe/4ZnS QDs on DNA origami. Note that the red arrows are other DNA impurities.

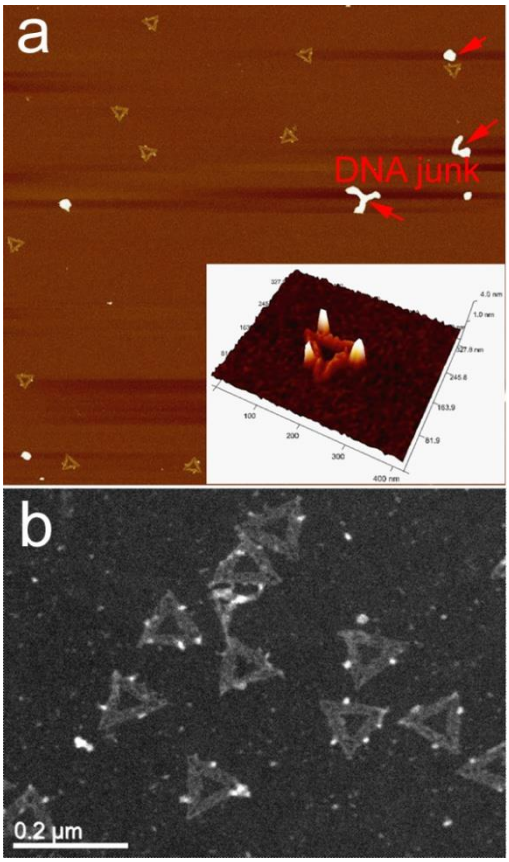

4.2 Oligonucleotids functionalization of ZnSe/ZnS QDs

Synthesis of MPA-capped ZnSe QD core in aqueous solution[6] proceeded as follows: a freshly prepared NaHSe solution (the source of Se, 1.0 mol/L, 10 μL) was injected through a syringe to N_2-saturated $Zn(NO_3)_2$ solution in water (the source of Zn, 0.005 mol/L, 50 mL) at room temperature (20 ^oC) in the presence of 3-mercaptopropionic acid (MPA, 37 μL) as a stabilizing agent. The pH was tuned to 11.5 by adding NaOH (1M). The molar ratio of Zn^{2+}/MPA/NaHSe in the mixture was fixed at 1:1.7:0.1. Then the

solution was aged at 4 ^{o}C and magic-sized ZnSe clusters with absorption peak at 290 nm (no detectable emission) were formed overnight. These ZnSe core QDs were purified by adding IPA and centrifugation at 15,000 rpm for 15 minutes and used as cores for the synthesis of ZnSe/ZnS core/shell QDs.

Oligonucleotide functionalization of ZnSe/4ZnS QDs: The synthesis is similar to that of the CdTe/ZnS core/shell nanocrystals. For a typical synthesis, 4.5 µL of Zn^{2+} stock solution (25 mM) and 9.0 µL of MPA stock solution (25 mM), were added to the ZnSe core (0.25 nM) QDs in 100 µL of DI water, vortexed and gently sonicated. Then, 50 µL of 5'-TTTTTTTTTTTTTTT TTTTTTTTTTTTTG*G*G*G*G*G -3' oligonucleotide stock solution (100 nM) was added and gently vortexed. The molar ratio of QD:oligonucleotide was approximately 1: 200. The pH was tuned to 12.2 by adding NaOH (1M). The reaction mixture was placed on a heating block at 90 ^{o}C for 40 minutes, and then cooled down at room temperature. The 0.5 mL Amicon filter (MWCO 30KDa) washing step is the same as for the CdTe/CdS QDs described above. The final sample is highly fluorescent and stable in buffer or in DI water.

Figure S19. (a) Additional AFM image, (b) STEM image and (c) EDS pattern of the oligonucleotide functionalized ZnSe/4ZnS QDs on DNA origami. Note that in the EDS spectra, the phosphorus signal is derived from the DNA, and the uranium signal is derived from the negative stain.

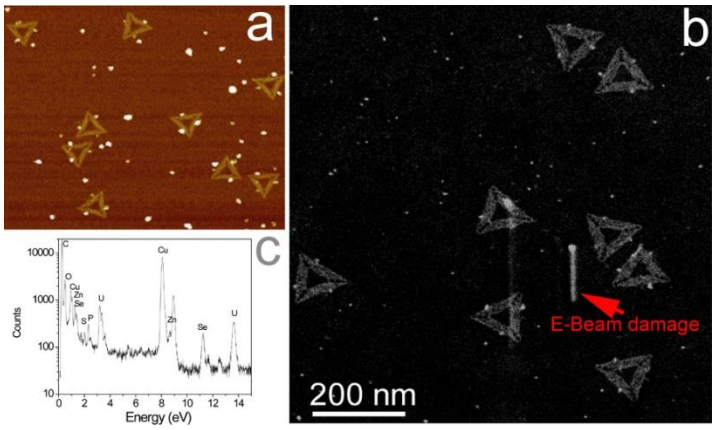

4.3 Oligonucleotide functionalization of CdS/ZnS QDs

Synthesis of Oleic acid capped CdS QDs[7]: Cd^{2+} -complex precursor solution was prepared by adding 7.5 mmol CdO to a 100 mL flask containing 10 mL of paraffin liquid and 15 mL of oleic acid. The mixture was heated to 100 ^{o}C, degassed under 100 mtorr pressure for 30 minutes, filled with N_2, and further heated to 200 ^{o}C to form a clear solution of Cd^{2+}precursor. Then, S precursor solution was prepared in a separate flask, where 0.3 mmol of S powder was mixed with 15 mL of paraffin liquid, degassed for 30 minutes, filled with N_2, and heated to 220^{o}C. At this temperature, 1 mL of Cd^{2+}precursor solution was quickly injected to the flask containing the above mixture. The molar ratio of Cd:S in the reaction mixture was 1:1. The mixture was then maintained at 220^{o}C with continuous stirring. A typical sample with emission at 410 nm was collected in a test tube containing 2 mL of cold hexane to further quench QD growth (10 minutes). The samples were purified by centrifugation (13,000 rpm for 30 minutes) several times after being precipitated with IPA and methanol.

First, ligand exchange with MPA was performed to render the CdS core QDs water soluble: The oleic acid capped CdS QDs with emission at 410 nm were purified as described above and dissolved in hexane (200 µL). Formamide (100 µL) mixed with 5

µL of 25 mM MPA solution was added to the solution. The mixture was vortexed and sonicated for 15 minutes to allow for ligand exchange. After the ligand exchange, the MPA-capped QDs were soluble in the polar solvent, thus, transferred from the non-polar hexane phase into the polar formamide phase. After settling, the upper hexane layer was removed, and the formamide layer was mixed with 1:1 IPA, and centrifuged at 15K rpm for 10 minutes. The purified QDs were re-dissolved in DI water.

Next, we further deposited 4 ZnS shell monolayers on the CdS core. For a typical experiment, the water soluble CdS QD solution (0.5 nM) was prepared in 100 µL DI-water by gentle sonication. Then, 4.5 µL of Zn^{2+} stock solution (25 mM) and 9 µL of MPA stock solution (25 mM) were added, vortexed and gently sonicated in a 1.5 mL plastic tube. Then 100 µL of 5'-TTT TTTTTTTTTTTTTTTTTTTTTTTTG*G*G*G*G* G-3' oligonucleotide stock solution (100 nM) was added and gently vortexed. The molar ratio of QD:oligonucleotide was approximately 1:200. The pH was tuned to 12.2 by adding NaOH (1M). The mixture was heated at on a heating block at 90 ^{o}C for 40 minutes. Then, the product was cooled down by submerging the tube in a water bath at room temperature. The 0.5 mL Amicon filter (MWCO 30KDa) washing step is the same as for the CdTe/CdS QDs described above. The final sample is fluorescent and stable in buffer or in DI water.

Figure S20. (a) Additional AFM image and (b) STEM image of the oligonucleotide functionalized CdS/4ZnS QDs on DNA origami.

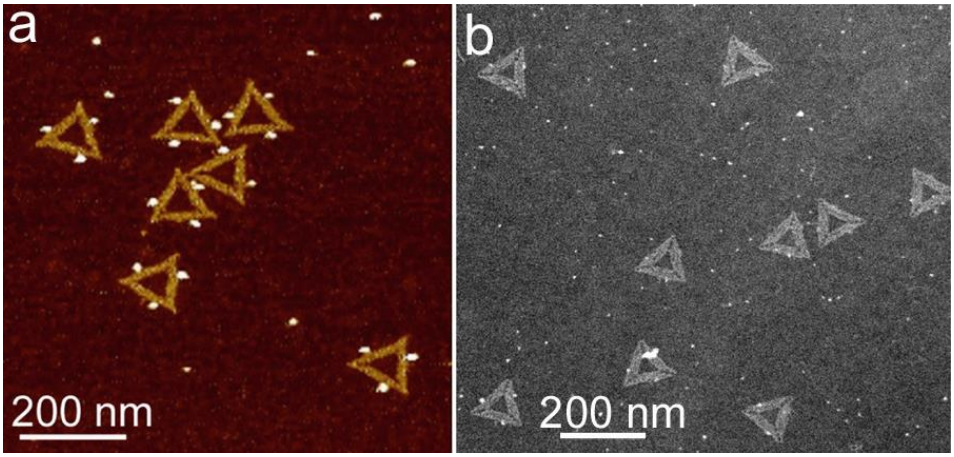

4.4 Oligonucleotide functionalization of ZnCdSSe/ZnS QDs

Oleic acid capped quaternary alloyed ZnCdSeS QDs[7]: In a typical reaction for $Zn_{0.60}Cd_{0.40}S_{0.33}Se_{0.66}$ QDs, Zn/Cd-complex precursor solution was prepared by adding 4.5 mmol of ZnO and 3.0 mmol of CdO (molar ratio of Zn:Cd is 3:2) into a 100 mL flask containing 10 mL of paraffin liquid, 10 mL of oleic acid, and 5 mL of 2-ethylhexanoic acid. The mixture was heated to 100 ^{o}C, degassed under 100 mtorr pressure for 30 minutes, filled with N_2, and further heated to 200 ^{o}C to form a clear solution of Zn/Cd precursor. Then, S/Se precursor solution was prepared in a separate flask, where 0.10 mmol of S and 0.20 mmol of Se (molar ratio of S:Se is 1:2) were mixed with 15 mL paraffin liquid, degassed for 30 minutes, filled with N_2, and heated to 280 ^{o}C. At this temperature, 1 mL of the Cd/Zn precursor solution was quickly injected to the flask containing the above mixture (the molar ratio of (Zn+Cd)/(S+Se)=1:1. The new mixture was then maintained at 280 ^{o}C with continuous stirring for 10 minutes. The samples were

purified by centrifugation (13,000 rpm for 30 minutes) several times after being precipitated with IPA and methanol. The final products were dispersed in hexane.

Next, ligand exchange with MPA rendered the $Zn_{0.6}Cd_{0.4}S_{0.33}Se_{0.66}$ core QDs water soluble in a similar manner as for the CdS QDs described above. Finally, 4 ZnS shell monolayers were deposited on the water soluble $Zn_{0.6}Cd_{0.4}S_{0.33}Se_{0.66}$ core. For a typical experiment, a diluted QD solution (1 nM) was prepared in 100 µL DI-water by gentle sonication. Then, 4.5 µL of Cd^{2+} stock solution (25 mM) and 9 µL of MPA stock solution (25 mM) were added, vortexed and gently sonicated in a 1.5 mL plastic tube. Then, 100 µL of 5'- TTTTTTTTTTTTTTTTTTTT TTTTTTTG*G*G*G*G*G-3' oligonucleotide stock solution (100 nM) was added and gently vortexed. The molar ratio of QD: oligonucleotide was approximately 1: 100. The pH was tuned to 12.2 by adding NaOH (1M). The mixture was heated on a heating block at 90 ^{o}C for 40 minutes. Then, the product was cooled down by submerging the tube in a water bath at room temperature. The 0.5 mL Amicon filter (MWCO 30KDa) washing step is the same as for the CdTe/CdS QDs described before. The final sample is fluorescent and stable in buffer or in DI water.

Figure 21. UV-Vis and PL spectra of the $Zn_{0.60}Cd_{0.40}S_{0.33}Se_{0.66}$ core QDs and oligonucleotide functionalized $Zn_{0.60}Cd_{0.40}S_{0.33}Se_{0.66}$/4 ZnS core/shell QDs.

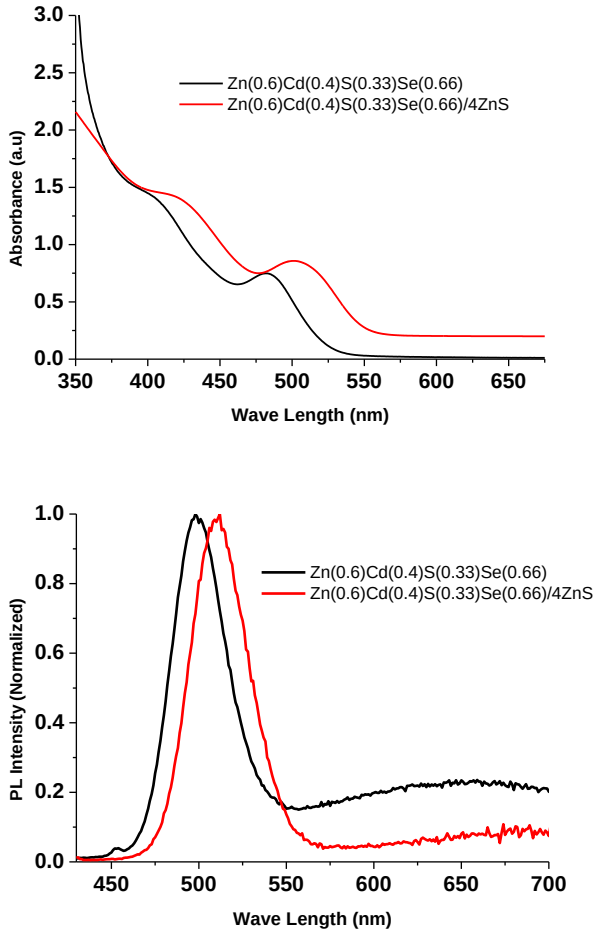

Figure S22. AFM image, STEM image and EDS spectrum of the oligonucleotide functionalized $Zn_{0.60}Cd_{0.40}S_{0.33}Se_{0.66}$/4 ZnS QDs on DNA origami. Note that the phosphorus signal is derived from the DNA, and the uranium signal is derived from the negative stain.

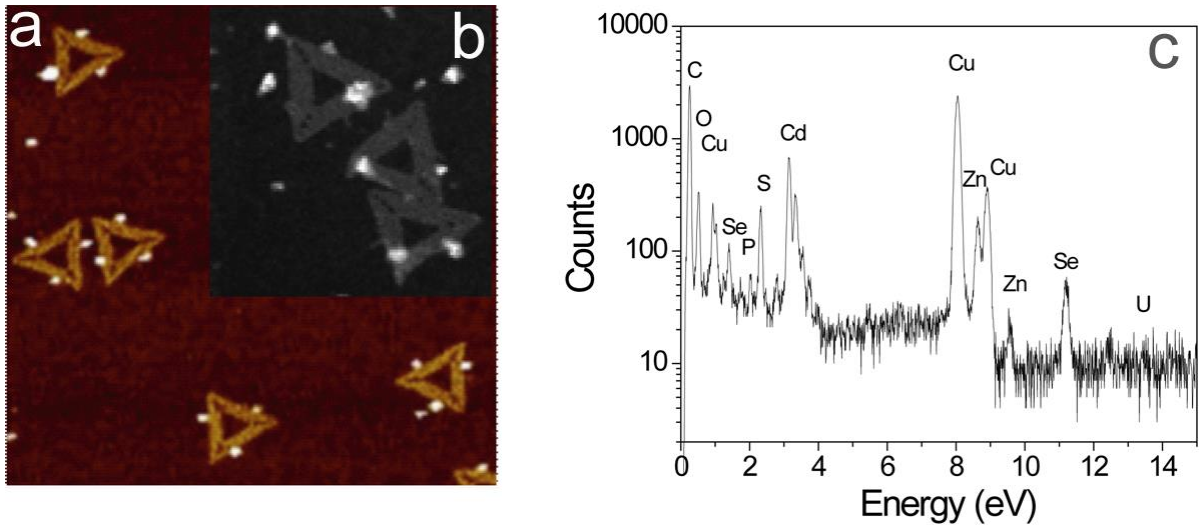

Part 5. Synthesis of DNA origami and organization of QDs.

Triangle and rectangular shaped DNA origami structures were formed following Rothemund's protocol[8]. 3nM single stranded M13mp18 DNA was mixed with staple strands in a 1:5 ratio. To organize the QDs at specific positions on the origami platform, selected staple strands were modified with a poly A extension to serve as capture probes. 10 equivalents of the capture strands (rather than 5) were added to ensure they were incorporated into the origami structure. The origami was assembled in 1XTA-Mg buffer (40mM Tris, 20mM Acetic acid, and 12.5 mM Mg-acetate, pH 8.0) by cooling down slowly from 90°C to 4°C. 100KDa MWCO Amicon filters were used to removed excess staple and capture strands from the sample.

For directed assembly of QDs on the DNA origami, first, the triangular or rectangular shaped DNA origami were assembled with the required number of staple strands and either 6 or 9 equivalents of the capture strands (each contained a 28 nucleotide single stranded overhang); here we used a 28 nucleotide Poly A sequence as the capture probe,

extending from the origami surface, and a 28 nucleotide Poly T sequence within the po domain of the chimeric DNA functionalized on the core/shell QDs. This choice of sequence ensures a greater degree of freedom for strand hybridization, allowing sliding of the strands against one another and enough flexibility for all three capture strands in one cluster to simultaneously bind to a single QD.

Next, pre-formed DNA origami (various molar ratios) was added to the DNA-functionalized CdTe QDs in 1xTAE, Mg^{2+} buffer to form the desired structures. Additional 1xTAE-Mg buffer was added to the sample to ensure that the solution was sufficiently dilute to reduce undesired crosslinking among the structures. Typically, 0.5 nM of triangle or rectangular origami was mixed with freshly prepared and purified QD-DNA conjugates in 1X TA-Mg buffer. The molar ratio of origami to QDs was 1:3 for triangular DNA origami and 1:2 for rectangular DNA origami. A typical total volume was 15 µL. The mixture was then annealed from 45 ^{o}C to 33 ^{o}C and recycled 20 times to complete the assembly process. The total self-assembly time is approximately 24 hours. High fidelity hybridization between capture strands and DNA strands on the core/shell QDs was verified by AFM and TEM of negatively stained samples. The position of the QDs reflect the design with nanometer precision.

Part 6. Design of triangular DNA origami

This design reflects our intent to place three QDs of the same color, one on each of the three arms, on the triangle origami. A total of nine strands were modified at the 5’ end with a 28 nucleotide extension from the surface of the origami, with a complimentary DNA sequence on the surface of the QDs. In the schematic below, a purple bar is drawn on the 5’ end of the selected capture probes. The green circles are drawn to represent a

diameter of 5 nm, illustrating how the probes are arranged into three clusters, each containing three probes that are intended to bind with the DNA strands on a single QD particle.

Figure S23. Design of the triangular DNA origami.

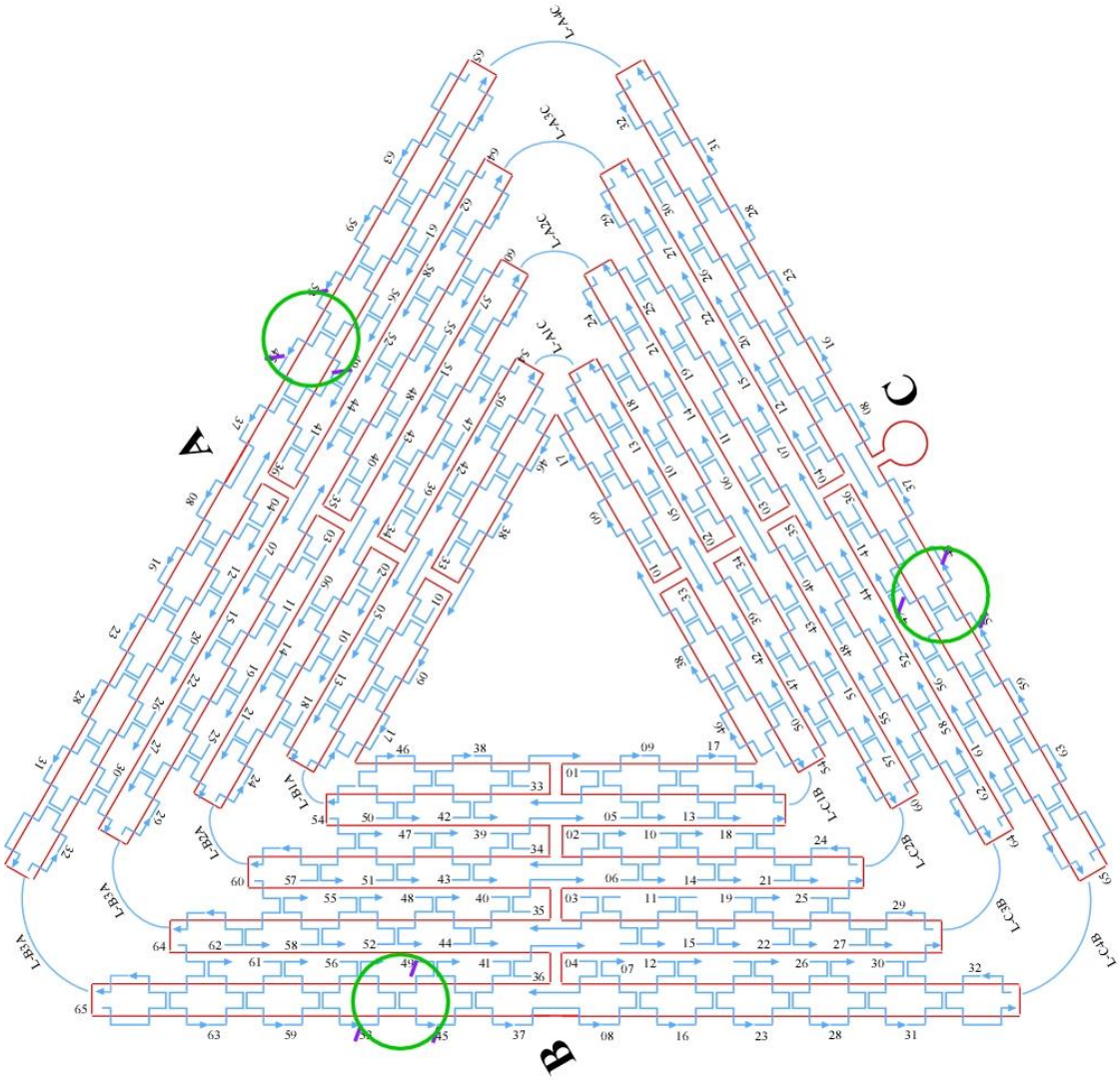

Design:

B49-capture:

AAAAAAAAAAAAAAAAAAAATTTTTATCATCGTTGAAAGAGGACAGATGGA

AGAAAAATCTACG

B45-capture:

AAAAAAAAAAAAAAAAAAAATTTTTTAATAAAACGAACTAACCGAACTGAC

CAACTCCTGATAA

B53-capture:

AAAAAAAAAAAAAAAAAAAATTTTACCAGTCAGGACGTTGGAACGGTGTAC

AGACCGAAACAAA

A49-capture:

AAAAAAAAAAAAAAAAAAAATTTTAGCATGTATTTCATCGTAGGAATCAAAC

GATTTTTTGTTT

A45-capture:

AAAAAAAAAAAAAAAAAAAATTTTAACGTCAAAAATGAAAAGCAAGCCGTT

TTTATGAAACCAA

A53-capture:

AAAAAAAAAAAAAAAAAAAATTTTTCCCAATCCAAATAAGATTACCGCGCCC

AATAAATAATAT

C49-capture:

AAAAAAAAAAAAAAAAAAAATTTTGTTTGCGTCACGCTGGTTTGCCCCAAGG

GAGCCCCCGATT

C45-capture:

AAAAAAAAAAAAAAAAAAAATTTTTAGAGCTTGACGGGGAGTTGCAGCAAG

CGGTCATTGGGCG

C53-capture:

AAAAAAAAAAAAAAAAAAAATTTTCTAAATCGGAACCCTAAGCAGGCGAAA

ATCCTTCGGCCAA

A01, CGGGGTTTCCTCAAGAGAAGGATTTTGAATTA,

A02, AGCGTCATGTCTCTGAATTTACCGACTACCTT,

A03, TTCATAATCCCCTTATTAGCGTTTTTCTTACC,

A04, ATGGTTTATGTCACAATCAATAGATATTAAAC,

A05, TTTGATGATTAAGAGGCTGAGACTTGCTCAGTACCAGGCG,

A06, CCGGAACCCAGAATGGAAAGCGCAACATGGCT,

A07, AAAGACAACATTTTCGGTCATAGCCAAAATCA,

A08, GACGGGAGAATTAACTCGGAATAAGTTTATTTCCAGCGCC,

A09, GATAAGTGCCGTCGAGCTGAAACATGAAAGTATACAGGAG,

A10, TGTACTGGAAATCCTCATTAAAGCAGAGCCAC,

A11, CACCGGAAAGCGCGTTTTCATCGGAAGGGCGA,

A12, CATTCAACAAACGCAAAGACACCAGAACACCCTGAACAAA,

A13, TTTAACGGTTCGGAACCTATTATTAGGGTTGATATAAGTA,

A14, CTCAGAGCATATTCACAAACAAATTAATAAGT,

A15, GGAGGGAATTTAGCGTCAGACTGTCCGCCTCC,

A16, GTCAGAGGGTAATTGATGGCAACATATAAAAGCGATTGAG,

A17, TAGCCCGGAATAGGTGAATGCCCCCTGCCTATGGTCAGTG,

A18, CCTTGAGTCAGACGATTGGCCTTGCGCCACCC,

A19, TCAGAACCCAGAATCAAGTTTGCCGGTAAATA,

A20, TTGACGGAAATACATACATAAAGGGCGCTAATATCAGAGA,

A21, CAGAGCCAGGAGGTTGAGGCAGGTAACAGTGCCCG,

A22, ATTAAAGGCCGTAATCAGTAGCGAGCCACCCT,

A23, GATAACCCACAAGAATGTTAGCAAACGTAGAAAATTATTC,

A24, GCCGCCAGCATTGACACCACCCTC,

A25, AGAGCCGCACCATCGATAGCAGCATGAATTAT,

A26, CACCGTCACCTTATTACGCAGTATTGAGTTAAGCCCAATA,

A27, AGCCATTTAAACGTCACCAATGAACACCAGAACCA,

A28, ATAAGAGCAAGAAACATGGCATGATTAAGACTCCGACTTG,

A29, CCATTAGCAAGGCCGGGGGAATTA,

A30, GAGCCAGCGAATACCCAAAAGAACATGAAATAGCAATAGC,

A31, TATCTTACCGAAGCCCAAACGCAATAATAACGAAAATCACCAG,

A32, CAGAAGGAAACCGAGGTTTTTAAGAAAAGTAAGCAGATAGCCG,

A33, CCTTTTTTCATTTAACAATTTCATAGGATTAG,

A34, TTTAACCTATCATAGGTCTGAGAGTTCCAGTA,

A35, AGTATAAAATATGCGTTATACAAAGCCATCTT,

A36, CAAGTACCTCATTCCAAGAACGGGAAATTCAT,

A37, AGAGAATAACATAAAAACAGGGAAGCGCATTA,

A38, AAAACAAAATTAATTAAATGGAAACAGTACATTAGTGAAT,

A39, TTATCAAACCGGCTTAGGTTGGGTAAGCCTGT,

A40, TTAGTATCGCCAACGCTCAACAGTCGGCTGTC,

A41, TTTCCTTAGCACTCATCGAGAACAATAGCAGCCTTTACAG,

A42, AGAGTCAAAAATCAATATATGTGATGAAACAAACATCAAG,

A43, ACTAGAAATATATAACTATATGTACGCTGAGA,

A44, TCAATAATAGGGCTTAATTGAGAATCATAATT,

A45, AACGTCAAAAATGAAAAGCAAGCCGTTTTTATGAAACCAA,

A46, GAGCAAAAGAAGATGAGTGAATAACCTTGCTTATAGCTTA,

A47, GATTAAGAAATGCTGATGCAAATCAGAATAAA,

A48, CACCGGAATCGCCATATTTAACAAAATTTACG,

A49, AGCATGTATTTCATCGTAGGAATCAAACGATTTTTTGTTT,

A50, ACATAGCGCTGTAAATCGTCGCTATTCATTTCAATTACCT,

A51, GTTAAATACAATCGCAAGACAAAGCCTTGAAA,

A52, CCCATCCTCGCCAACATGTAATTTAATAAGGC,

A53, TCCCAATCCAAATAAGATTACCGCGCCCAATAAATAATAT,

A54, TCCCTTAGAATAACGCGAGAAAACTTTTACCGACC,

A55, GTGTGATAAGGCAGAGGCATTTTCAGTCCTGA,

A56, ACAAGAAAGCAAGCAAATCAGATAACAGCCATATTATTTA,

A57, GTTTGAAATTCAAATATATTTTAG,

A58, AATAGATAGAGCCAGTAATAAGAGATTTAATG,

A59, GCCAGTTACAAAATAATAGAAGGCTTATCCGGTTATCAAC,

A60, TTCTGACCTAAAATATAAAGTACCGACTGCAGAAC,

A61, GCGCCTGTTATTCTAAGAACGCGATTCCAGAGCCTAATTT,

A62, TCAGCTAAAAAAGGTAAAGTAATT,

A63, ACGCTAACGAGCGTCTGGCGTTTTAGCGAACCCAACATGT,

A64, ACGACAATAAATCCCGACTTGCGGGAGATCCTGAATCTTACCA,

A65, TGCTATTTTGCACCCAGCTACAATTTTGTTTTGAAGCCTTAAA,

B01, TCATATGTGTAATCGTAAAACTAGTCATTTTC,

B02, GTGAGAAAATGTGTAGGTAAAGATACAACTTT,

B03, GGCATCAAATTTGGGGCGCGAGCTAGTTAAAG,

B04, TTCGAGCTAAGACTTCAAATATCGGGAACGAG,

B05, ACAGTCAAAGAGAATCGATGAACGACCCCGGTTGATAATC,

B06, ATAGTAGTATGCAATGCCTGAGTAGGCCGGAG,

B07, AACCAGACGTTTAGCTATATTTTCTTCTACTA,

B08, GAATACCACATTCAACTTAAGAGGAAGCCCGATCAAAGCG,

B09, AGAAAAGCCCCAAAAAGAGTCTGGAGCAAACAATCACCAT,

B10, CAATATGACCCTCATATATTTTAAAGCATTAA,

B11, CATCCAATAAATGGTCAATAACCTCGGAAGCA,

B12, AACTCCAAGATTGCATCAAAAAGATAATGCAGATACATAA,

B13, CGTTCTAGTCAGGTCATTGCCTGACAGGAAGATTGTATAA,

B14, CAGGCAAGATAAAAATTTTTAGAATATTCAAC,

B15, GATTAGAGATTAGATACATTTCGCAAATCATA,

B16, CGCCAAAAGGAATTACAGTCAGAAGCAAAGCGCAGGTCAG,

B17, GCAAATATTTAAATTGAGATCTACAAAGGCTACTGATAAA,

B18, TTAATGCCTTATTTCAACGCAAGGGCAAAGAA,

B19, TTAGCAAATAGATTTAGTTTGACCAGTACCTT,

B20, TAATTGCTTTACCCTGACTATTATGAGGCATAGTAAGAGC,

B21, ATAAAGCCTTTGCGGGAGAAGCCTGGAGAGGGTAG,

B22, TAAGAGGTCAATTCTGCGAACGAGATTAAGCA,

B23, AACACTATCATAACCCATCAAAAATCAGGTCTCCTTTTGA,

B24, ATGACCCTGTAATACTTCAGAGCA,

B25, TAAAGCTATATAACAGTTGATTCCCATTTTTG,

B26, CGGATGGCACGAGAATGACCATAATCGTTTACCAGACGAC,

B27, TAATTGCTTGGAAGTTTCATTCCAAATCGGTTGTA,

B28, GATAAAAACCAAAATATTAAACAGTTCAGAAATTAGAGCT,

B29, ACTAAAGTACGGTGTCGAATATAA,

B30, TGCTGTAGATCCCCCTCAAATGCTGCGAGAGGCTTTTGCA,

B31, AAAGAAGTTTTGCCAGCATAAATATTCATTGACTCAACATGTT,

B32, AATACTGCGGAATCGTAGGGGGTAATAGTAAAATGTTTAGACT,

B33, AGGGATAGCTCAGAGCCACCACCCCATGTCAA,

B34, CAACAGTTTATGGGATTTTGCTAATCAAAAGG,

B35, GCCGCTTTGCTGAGGCTTGCAGGGGAAAAGGT,

B36, GCGCAGACTCCATGTTACTTAGCCCGTTTTAA,

B37, ACAGGTAGAAAGATTCATCAGTTGAGATTTAG,

B38, CCTCAGAACCGCCACCCAAGCCCAATAGGAACGTAAATGA,

B39, ATTTTCTGTCAGCGGAGTGAGAATACCGATAT,

B40, ATTCGGTCTGCGGGATCGTCACCCGAAATCCG,

B41, CGACCTGCGGTCAATCATAAGGGAACGGAACAACATTATT,

B42, AGACGTTACCATGTACCGTAACACCCCTCAGAACCGCCAC,

B43, CACGCATAAGAAAGGAACAACTAAGTCTTTCC,

B44, ATTGTGTCTCAGCAGCGAAAGACACCATCGCC,

B45, TTAATAAAACGAACTAACCGAACTGACCAACTCCTGATAA,

B46, AGGTTTAGTACCGCCATGAGTTTCGTCACCAGGATCTAAA,

B47, GTTTTGTCAGGAATTGCGAATAATCCGACAAT,

B48, GACAACAAGCATCGGAACGAGGGTGAGATTTG,

B49, TATCATCGTTGAAAGAGGACAGATGGAAGAAAAATCTACG,

B50, AGCGTAACTACAAACTACAACGCCTATCACCGTACTCAGG,

B51, TAGTTGCGAATTTTTTCACGTTGATCATAGTT,

B52, GTACAACGAGCAACGGCTACAGAGGATACCGA,

B53, ACCAGTCAGGACGTTGGAACGGTGTACAGACCGAAACAAA,

B54, ACAGACAGCCCAAATCTCCAAAAAAAAATTTCTTA,

B55, AACAGCTTGCTTTGAGGACTAAAGCGATTATA,

B56, CCAAGCGCAGGCGCATAGGCTGGCAGAACTGGCTCATTAT,

B57, CGAGGTGAGGCTCCAAAAGGAGCC,

B58, ACCCCCAGACTTTTTCATGAGGAACTTGCTTT,

B59, ACCTTATGCGATTTTATGACCTTCATCAAGAGCATCTTTG,

B60, CGGTTTATCAGGTTTCCATTAAACGGGAATACACT,

B61, AAAACACTTAATCTTGACAAGAACTTAATCATTGTGAATT,

B62, GGCAAAAGTAAAATACGTAATGCC,

B63, TGGTTTAATTTCAACTCGGATATTCATTACCCACGAAAGA,

B64, ACCAACCTAAAAAATCAACGTAACAAATAAATTGGGCTTGAGA,

B65, CCTGACGAGAAACACCAGAACGAGTAGGCTGCTCATTCAGTGA,

C01, TCGGGAGATATACAGTAACAGTACAAATAATT,

C02, CCTGATTAAAGGAGCGGAATTATCTCGGCCTC,

C03, GCAAATCACCTCAATCAATATCTGCAGGTCGA,

C04, CGACCAGTACATTGGCAGATTCACCTGATTGC,

C05, TGGCAATTTTTAACGTCAGATGAAAACAATAACGGATTCG,

C06, AAGGAATTACAAAGAAACCACCAGTCAGATGA,

C07, GGACATTCACCTCAAATATCAAACACAGTTGA,

C08, TTGACGAGCACGTATACTGAAATGGATTATTTAATAAAAG,

C09, CCTGATTGCTTTGAATTGCGTAGATTTTCAGGCATCAATA,

C10, TAATCCTGATTATCATTTTGCGGAGAGGAAGG,

C11, TTATCTAAAGCATCACCTTGCTGATGGCCAAC,

C12, AGAGATAGTTTGACGCTCAATCGTACGTGCTTTCCTCGTT,

C13, GATTATACACAGAAATAAAGAAATACCAAGTTACAAAATC,

C14, TAGGAGCATAAAAGTTTGAGTAACATTGTTTG,

C15, TGACCTGACAAATGAAAAATCTAAAATATCTT,

C16, AGAATCAGAGCGGGAGATGGAAATACCTACATAACCCTTC,

C17, GCGCAGAGGCGAATTAATTATTTGCACGTAAATTCTGAAT,

C18, AATGGAAGCGAACGTTATTAATTTCTAACAAC,

C19, TAATAGATCGCTGAGAGCCAGCAGAAGCGTAA,

C20, GAATACGTAACAGGAAAAACGCTCCTAAACAGGAGGCCGA,

C21, TCAATAGATATTAAATCCTTTGCCGGTTAGAACCT,

C22, CAATATTTGCCTGCAACAGTGCCATAGAGCCG,

C23, TTAAAGGGATTTTAGATACCGCCAGCCATTGCGGCACAGA,

C24, ACAATTCGACAACTCGTAATACAT,

C25, TTGAGGATGGTCAGTATTAACACCTTGAATGG,

C26, CTATTAGTATATCCAGAACAATATCAGGAACGGTACGCCA,

C27, CGCGAACTAAAACAGAGGTGAGGCTTAGAAGTATT,

C28, GAATCCTGAGAAGTGTATCGGCCTTGCTGGTACTTTAATG,

C29, ACCACCAGCAGAAGATGATAGCCC,

C30, TAAAACATTAGAAGAACTCAAACTTTTTATAATCAGTGAG,

C31, GCCACCGAGTAAAAGAACATCACTTGCCTGAGCGCCATTAAAA,

C32, TCTTTGATTAGTAATAGTCTGTCCATCACGCAAATTAACCGTT,

C33, CGCGTCTGATAGGAACGCCATCAACTTTTACA,

C34, AGGAAGATGGGGACGACGACAGTAATCATATT,

C35, CTCTAGAGCAAGCTTGCATGCCTGGTCAGTTG,

C36, CCTTCACCGTGAGACGGGCAACAGCAGTCACA,

C37, CGAGAAAGGAAGGGAAGCGTACTATGGTTGCT,

C38, GCTCATTTTTTAACCAGCCTTCCTGTAGCCAGGCATCTGC,

C39, CAGTTTGACGCACTCCAGCCAGCTAAACGACG,

C40, GCCAGTGCGATCCCCGGGTACCGAGTTTTTCT,

C41, TTTCACCAGCCTGGCCCTGAGAGAAAGCCGGCGAACGTGG,

C42, GTAACCGTCTTTCATCAACATTAAAATTTTTGTTAAATCA,

C43, ACGTTGTATTCCGGCACCGCTTCTGGCGCATC,

C44, CCAGGGTGGCTCGAATTCGTAATCCAGTCACG,

C45, TAGAGCTTGACGGGGAGTTGCAGCAAGCGGTCATTGGGCG,

C46, GTTAAAATTCGCATTAATGTGAGCGAGTAACACACGTTGG,

C47, TGTAGATGGGTGCCGGAAACCAGGAACGCCAG,

C48, GGTTTTCCATGGTCATAGCTGTTTGAGAGGCG,

C49, GTTTGCGTCACGCTGGTTTGCCCCAAGGGAGCCCCCGATT,

C50, GGATAGGTACCCGTCGGATTCTCCTAAACGTTAATATTTT,

C51, AGTTGGGTCAAAGCGCCATTCGCCCCGTAATG,

C52, CGCGCGGGCCTGTGTGAAATTGTTGGCGATTA,

C53, CTAAATCGGAACCCTAAGCAGGCGAAAATCCTTCGGCCAA,

C54, CGGCGGATTGAATTCAGGCTGCGCAACGGGGGATG,

C55, TGCTGCAAATCCGCTCACAATTCCCAGCTGCA,

C56, TTAATGAAGTTTGATGGTGGTTCCGAGGTGCCGTAAAGCA,

C57, TGGCGAAATGTTGGGAAGGGCGAT,

C58, TGTCGTGCACACAACATACGAGCCACGCCAGC,

C59, CAAGTTTTTTGGGGTCGAAATCGGCAAAATCCGGGAAACC,

C60, TCTTCGCTATTGGAAGCATAAAGTGTATGCCCGCT,

C61, TTCCAGTCCTTATAAATCAAAAGAGAACCATCACCCAAAT,

C62, GCGCTCACAAGCCTGGGGTGCCTA,

C63, CGATGGCCCACTACGTATAGCCCGAGATAGGGATTGCGTT,

C64, AACTCACATTATTGAGTGTTGTTCCAGAAACCGTCTATCAGGG,

C65, ACGTGGACTCCAACGTCAAAGGGCGAATTTGGAACAAGAGTCC,

Link-A1C, TTAATTAATTTTTTACCATATCAAA,

Link-A2C, TTAATTTCATCTTAGACTTTACAA,

Link-A3C, CTGTCCAGACGTATACCGAACGA,

Link-A4C, TCAAGATTAGTGTAGCAATACT,

Link-B1A, TGTAGCATTCCTTTTATAAACAGTT,

Link-B2A, TTTAATTGTATTTCCACCAGAGCC,

Link-B3A, ACTACGAAGGCTTAGCACCATTA,

Link-B4A, ATAAGGCTTGCAACAAAGTTAC,

Link-C1B, GTGGGAACAAATTTCTATTTTTGAG,

Link-C2B, CGGTGCGGGCCTTCCAAAAACATT,

Link-C3B, ATGAGTGAGCTTTTAAATATGCA,

Link-C4B, ACTATTAAAGAGGATAGCGTCC,

Loop, GCGCTTAATGCGCCGCTACAGGGC,

Part 7. Design of rectangular DNA origami

This design reflects our intent to place two QDs of the same color in opposite corners of the asymmetric rectangle. A total of six strands were modified at the 5' end with a 28 nucleotide extension from the surface of the origami, with a complimentary DNA sequence on the surface of the QDs. In the schematic below, a green bar is drawn on the 5' end of the selected capture probes. The red circles are drawn to represent a diameter of 5 nm, illustrating how the probes are arranged into two clusters, each containing three probes that are intended to bind with the DNA strands on a single QD particle.

Figure S24. Design of the rectangular DNA origami.

Rec-159

AAAAAAAAAAAAAAAAAAA

TTTTGCGCAGAGATATCAAAATTATTTGACATTATC

Rec-135

AAAAAAAAAAAAAAAAAAA

TTTTCCTGATTGAAAGAAATTGCGTAGACCCGAACG

Rec-158

AAAAAAAAAAAAAAAAAAA

TTTTATTTTGCGTCTTTAGGAGCACTAAGCAACAGT

Rec-47

AAAAAAAAAAAAAAAAAAA

TTTTAATAATAAGGTCGCTGAGGCTTGCAAAGACTT

Rec-23

AAAAAAAAAAAAAAAAAAA

TTTTGAGAATAGCTTTTGCGGGATCGTCGGGTAGCA

Rec-46

AAAAAAAAAAAAAAAAAAA

TTTTTTTCATGAAAATTGTGTCGAAATCTGTACAGA

13	TGGTTTTTAACGTCAAAGGGCGAAGAACCATC
14	CTTGCATGCATTAATGAATCGGCCCGCCAGGG
15	TAGATGGGGGGTAACGCCAGGGTTGTGCCAAG
16	CATGTCAAGATTCTCCGTGGGAACCGTTGGTG
17	CTGTAATATTGCCTGAGAGTCTGGAAAACTAG
18	TGCAACTAAGCAATAAAGCCTCAGTTATGACC
19	AAACAGTTGATGGCTTAGAGCTTATTTAAATA
20	ACGAACTAGCGTCCAATACTGCGGAATGCTTT
21	CTTTGAAAAGAACTGGCTCATTATTTAATAAA

22 ACGGCTACTTACTTAGCCGGAACGCTGACCAA

23 GAGAATAGCTTTTGCGGGATCGTCGGGTAGCA

24 ACGTTAGTAAATGAATTTTCTGTAAGCGGAGT

25 ACCCAAATCAAGTTTTTTGGGGTCAAAGAACG

26 TGGACTCCCTTTTCACCAGTGAGACCTGTCGT

27 GCCAGCTGCCTGCAGGTCGACTCTGCAAGGCG

28 ATTAAGTTCGCATCGTAACCGTGCGAGTAACA

29 ACCCGTCGTCATATGTACCCCGGTAAAGGCTA

30 TCAGGTCACTTTTGCGGGAGAAGCAGAATTAG

31 CAAAATTAAAGTACGGTGTCTGGAAGAGGTCA

32 TTTTTGCGCAGAAAACGAGAATGAATGTTTAG

33 ACTGGATAACGGAACAACATTATTACCTTATG

34 CGATTTTAGAGGACAGATGAACGGCGCGACCT

35 GCTCCATGAGAGGCTTTGAGGACTAGGGAGTT

36 AAAGGCCGAAAGGAACAACTAAAGCTTTCCAG

37 AGCTGATTACAAGAGTCCACTATTGAGGTGCC

38 CCCGGGTACTTTCCAGTCGGGAAACGGGCAAC

39 GTTTGAGGGAAAGGGGGATGTGCTAGAGGATC

40 AGAAAAGCAACATTAAATGTGAGCATCTGCCA

41 CAACGCAATTTTTGAGAGATCTACTGATAATC

42 TCCATATACATACAGGCAAGGCAACTTTATTT

43 CAAAAATCATTGCTCCTTTTGATAAGTTTCAT

44	AAAGATTCAGGGGGTAATAGTAAACCATAAAT
45	CCAGGCGCTTAATCATTGTGAATTACAGGTAG
46	TTTCATGAAAATTGTGTCGAAATCTGTACAGA
47	AATAATAAGGTCGCTGAGGCTTGCAAAGACTT
48	CGTAACGATCTAAAGTTTTGTCGTGAATTGCG
49	GTAAAGCACTAAATCGGAACCCTAGTTGTTCC
50	AGTTTGGAGCCCTTCACCGCCTGGTTGCGCTC
51	ACTGCCCGCCGAGCTCGAATTCGTTATTACGC
52	CAGCTGGCGGACGACGACAGTATCGTAGCCAG
53	CTTTCATCCCCAAAAACAGGAAGACCGGAGAG
54	GGTAGCTAGGATAAAAATTTTTAGTTAACATC
55	CAATAAATACAGTTGATTCCCAATTTAGAGAG
56	TACCTTTAAGGTCTTTACCCTGACAAAGAAGT
57	TTTGCCAGATCAGTTGAGATTTAGTGGTTTAA
58	TTTCAACTATAGGCTGGCTGACCTTGTATCAT
59	CGCCTGATGGAAGTTTCCATTAAACATAACCG
60	ATATATTCTTTTTTCACGTTGAAAATAGTTAG
61	GAGTTGCACGAGATAGGGTTGAGTAAGGGAGC
62	TCATAGCTACTCACATTAATTGCGCCCTGAGA
63	GAAGATCGGTGCGGGCCTCTTCGCAATCATGG
64	GCAAATATCGCGTCTGGCCTTCCTGGCCTCAG
65	TATATTTTAGCTGATAAATTAATGTTGTATAA

66 CGAGTAGAACTAATAGTAGTAGCAAACCCTCA

67 TCAGAAGCCTCCAACAGGTCAGGATCTGCGAA

68 CATTCAACGCGAGAGGCTTTTGCATATTATAG

69 AGTAATCTTAAATTGGGCTTGAGAGAATACCA

70 ATACGTAAAAGTACAACGGAGATTTCATCAAG

71 AAAAAAGGACAACCATCGCCCACGCGGGTAAA

72 TGTAGCATTCCACAGACAGCCCTCATCTCCAA

73 CCCCGATTTAGAGCTTGACGGGGAAATCAAAA

74 GAATAGCCGCAAGCGGTCCACGCTCCTAATGA

75 GTGAGCTAGTTTCCTGTGTGAAATTTGGGAAG

76 GGCGATCGCACTCCAGCCAGCTTTGCCATCAA

77 AAATAATTTTAAATTGTAAACGTTGATATTCA

78 ACCGTTCTAAATGCAATGCCTGAGAGGTGGCA

79 TCAATTCTTTTAGTTTGACCATTACCAGACCG

80 GAAGCAAAAAAGCGGATTGCATCAGATAAAAA

81 CCAAAATATAATGCAGATACATAAACACCAGA

82 ACGAGTAGTGACAAGAACCGGATATACCAAGC

83 GCGAAACATGCCACTACGAAGGCATGCGCCGA

84 CAATGACACTCCAAAAGGAGCCTTACAACGCC

85 CCAGCAGGGGCAAAATCCCTTATAAAGCCGGC

86 GCTCACAATGTAAAGCCTGGGGTGGGTTTGCC

87 GCTTCTGGTCAGGCTGCGCAACTGTGTTATCC

88	GTTAAAATTTTAACCAATAGGAACCCGGCACC
89	AGGTAAAGAAATCACCATCAATATAATATTTT
90	TCGCAAATGGGGCGCGAGCTGAAATAATGTGT
91	AAGAGGAACGAGCTTCAAAGCGAAGATACATT
92	GGAATTACTCGTTTACCAGACGACAAAAGATT
93	CCAAATCACTTGCCCTGACGAGAACGCCAAAA
94	AAACGAAATGACCCCCAGCGATTATTCATTAC
95	TCGGTTTAGCTTGATACCGATAGTCCAACCTA
96	TGAGTTTCGTCACCAGTACAAACTTAATTGTA
97	GAACGTGGCGAGAAAGGAAGGGAACAAACTAT
98	CCGAAATCCGAAAATCCTGTTTGAAGCCGGAA
99	GCATAAAGTTCCACACAACATACGAAGCGCCA
100	TTCGCCATTGCCGGAAACCAGGCATTAAATCA
101	GCTCATTTTCGCATTAAATTTTTGAGCTTAGA
102	AGACAGTCATTCAAAAGGGTGAGAAGCTATAT
103	TTTCATTTGGTCAATAACCTGTTTATATCGCG
104	TTTTAATTGCCCGAAAGACTTCAAAACACTAT
105	CATAACCCGAGGCATAGTAAGAGCTTTTTAAG
106	GAATAAGGACGTAACAAAGCTGCTCTAAAACA
107	CTCATCTTGAGGCAAAAGAATACAGTGAATTT
108	CTTAAACATCAGCTTGCTTTCGAGCGTAACAC
109	ACGAACCAAAACATCGCCATTAAATGGTGGTT

110 CGACAACTAAGTATTAGACTTTACAATACCGA

111 CTTTTACACAGATGAATATACAGTAAACAATT

112 TTAAGACGTTGAAAACATAGCGATAACAGTAC

113 GCGTTATAGAAAAAGCCTGTTTAGAAGGCCGG

114 ATCGGCTGCGAGCATGTAGAAACCTATCATAT

115 CCTAATTTACGCTAACGAGCGTCTAATCAATA

116 AAAAGTAATATCTTACCGAAGCCCTTCCAGAG

117 TTATTCATAGGGAAGGTAAATATTCATTCAGT

118 GAGCCGCCCCACCACCGGAACCGCGACGGAAA

119 AATGCCCCGTAACAGTGCCCGTATCTCCCTCA

120 CAAGCCCAATAGGAACCCATGTACAAACAGTT

121 CGGCCTTGCTGGTAATATCCAGAACGAACTGA

122 TAGCCCTACCAGCAGAAGATAAAAACATTTGA

123 GGATTTAGCGTATTAAATCCTTTGTTTTCAGG

124 TTTAACGTTCGGGAGAAACAATAATTTTCCCT

125 TAGAATCCCTGAGAAGAGTCAATAGGAATCAT

126 AATTACTACAAATTCTTACCAGTAATCCCATC

127 CTAATTTATCTTTCCTTATCATTCATCCTGAA

128 TCTTACCAGCCAGTTACAAAATAAATGAAATA

129 GCAATAGCGCAGATAGCCGAACAATTCAACCG

130 ATTGAGGGTAAAGGTGAATTATCAATCACCGG

131 AACCAGAGACCCTCAGAACCGCCAGGGGTCAG

132	TGCCTTGACTGCCTATTTCGGAACAGGGATAG
133	AGGCGGTCATTAGTCTTTAATGCGCAATATTA
134	TTATTAATGCCGTCAATAGATAATCAGAGGTG
135	CCTGATTGAAAGAAATTGCGTAGACCCGAACG
136	ATCAAAATCGTCGCTATTAATTAACGGATTCG
137	ACGCTCAAAATAAGAATAAACACCGTGAATTT
138	GGTATTAAGAACAAGAAAAATAATTAAAGCCA
139	ATTATTTAACCCAGCTACAATTTTCAAGAACG
140	GAAGGAAAATAAGAGCAAGAAACAACAGCCAT
141	GACTTGAGAGACAAAAGGGCGACAAGTTACCA
142	GCCACCACTCTTTTCATAATCAAACCGTCACC
143	CTGAAACAGGTAATAAGTTTTAACCCCTCAGA
144	CTCAGAGCCACCACCCTCATTTTCCTATTATT
145	CCGCCAGCCATTGCAACAGGAAAAATATTTTT
146	GAATGGCTAGTATTAACACCGCCTCAACTAAT
147	AGATTAGATTTAAAAGTTTGAGTACACGTAAA
148	ACAGAAATCTTTGAATACCAAGTTCCTTGCTT
149	CTGTAAATCATAGGTCTGAGAGACGATAAATA
150	AGGCGTTACAGTAGGGCTTAATTGACAATAGA
151	TAAGTCCTACCAAGTACCGCACTCTTAGTTGC
152	TATTTTGCTCCCAATCCAAATAAGTGAGTTAA
153	GCCCAATACCGAGGAAACGCAATAGGTTTACC

154 AGCGCCAACCATTTGGGAATTAGATTATTAGC

155 GTTTGCCACCTCAGAGCCGCCACCGATACAGG

156 AGTGTACTTGAAAGTATTAAGAGGCCGCCACC

157 GCCACGCTATACGTGGCACAGACAACGCTCAT

158 ATTTTGCGTCTTTAGGAGCACTAAGCAACAGT

159 GCGCAGAGATATCAAAATTATTTGACATTATC

160 TAACCTCCATATGTGAGTGAATAAACAAAATC

161 CATATTTAGAAATACCGACCGTGTTACCTTTT

162 CAAGCAAGACGCGCCTGTTTATCAAGAATCGC

163 TTTTGTTTAAGCCTTAAATCAAGAATCGAGAA

164 ATACCCAAGATAACCCACAAGAATAAACGATT

165 AATCACCAAATAGAAAATTCATATATAACGGA

166 CACCAGAGTTCGGTCATAGCCCCCGCCAGCAA

167 CCTCAAGAATACATGGCTTTTGATAGAACCAC

168 CCCTCAGAACCGCCACCCTCAGAACTGAGACT

169 GGAAATACCTACATTTTGACGCTCACCTGAAA

170 GCGTAAGAGAGAGCCAGCAGCAAAAAGGTTAT

171 CTAAAATAGAACAAAGAAACCACCAGGGTTAG

172 AACCTACCGCGAATTATTCATTTCCAGTACAT

173 AAATCAATGGCTTAGGTTGGGTTACTAAATTT

174 AATGGTTTACAACGCCAACATGTAGTTCAGCT

175 AATGCAGACCGTTTTTATTTTCATCTTGCGGG

176 AGGTTTTGAACGTCAA AAATGAAAGCGCTAAT

177 ATCAGAGAAAGAACTG GCATGATTTTATTTTG

178 TCACAATCGTAGCACCATTACCATCGTTTTCA

179 TCGGCATTCCGCCGCCAGCATTGACGTTCCAG

180 TAAGCGTCGAAGGATT AGGATTAGTACCGCCA

181 CTAAAGCAAGATAGAA CCCTTCTGAATCGTCT

182 CGGAATTATTGAAAGGAATTGAGGTGAAAAAT

183 GAGCAAAAACTTCTGAATAATGGAAGAAGGAG

184 TATGTAAACCTTTTTTAATGGAAAAATTACCT

185 AGAGGCATAATTTCATCTTCTGACTATAACTA

186 TCATTACCCGACAATAAACAACATATTTAGGC

187 CTTTACAGTTAGCGAACCTCCCGACGTAGGAA

188 TTATTACGGTCAGAGG GTAATTGAATAGCAGC
CCGGAAACACACCACG

189 GAATAAGTAAGACTCC

190 TGAGGCAGGCGTCAGACTGTAGCGTAGCAAGG

191 TGCTCAGTCAGTCTCTGAATTTACCAGGAGGT

192 TATCACCGTACTCAGGAGGTTTAGCGGGGTTT

193 GAAATGGATTATTTACATTGGCAGACATTCTG

194 GCCAACAGTCACCTTGCTGAACCTGTTGGCAA

195 ATCAACAGTCATCATATTCCTGATTGATTGTT

196 TGGATTATGAAGATGA TGAAACAAAATTTCAT

197	TTGAATTATGCTGATG CAAATCCACAAATATA
198	TTTTAGTTTTTCGAGCCAGTAATAAATTCTGT
199	CCAGACGAGCGCCCAATAGCAAGCAAGAACGC
200	GAGGCGTTAGAGAATAACATAAAAGAACACCC
201	TGAACAAACAGTATGTTAGCAAACTAAAAGAA
202	ACGCAAAGGTCACCAATGAAACCAATCAAGTT
203	TGCCTTTAGTCAGACGATTGGCCTGCCAGAAT
204	GGAAAGCGACCAGGCGGATAAGTGAATAGGTG
205	AACATCACTTGCCTGAGTAGAAGAACT
206	TGTAGCAATACTTCTTTGATTAGTAAT
207	AGTCTGTCCATCACGCAAATTAACCGT
208	ATAATCAGTGAGGCCACCGAGTAAAAG
209	ACGCCAGAATCCTGAGAAGTGTTTTT
210	TTAAAGGGATTTTAGACAGGAACGGT
211	AGAGCGGGAGCTAAACAGGAGGCCGA
212	TATAACGTGCTTTCCTCGTTAGAATC
213	GTACTATGGTTGCTTTGACGAGCACG
214	GCGCTTAATGCGCCGCTACAGGGCGC

Supporting information for

IR Emitting Quantum Dots: DNA conjugation and DNA origami directed Self-assembly

Anirban Samanta, Zhengtao Deng, Yan Liu

Department of Chemistry and Biochemistry

& Biodesign Institute, Arizona State University

Tempe, AZ 85287

Yan_liu@asu.edu

Experimental Methods

Chemicals:

Cadmium nitrate tetrahydrate ($Cd(NO_3)_2 \cdot 4H_2O$, 99.8%), Lead nitrate ($Pb(NO_3)_2$, ≥99%) Tellurium (Te, powder, -200 mesh, ≥99%, powder), Sodium borohydride ($NaBH_4$, powder, ≥99%), 3-Mercaptopropionic acid (MPA, $HSCH_2CH_2CO_2H$, ≥99%), Glutathione (GSH, ≥99%), were purchased from Sigma-Aldrich and used without further purification. M13mp18 single stranded DNA was purchased from New England Biolabs and was used without further treatment. All unmodified helper strands were purchased from Integrated DNA Technologies, Inc. (IDT, www.idtdna.com) in 96-well plate format, suspended in nanopure water (H_2O, with resistivity up to 18.2 MΩ·cm) and used without further purification. All modified helper strands as QD capturing strands were purchased from IDT and purified by denaturing PAGE gel electrophoresis. Phosphorothioate backbone modified ps-po-chimeric ssDNA strands for capping QDs were purchased from IDT and used after denaturing PAGE purification.

DNA conjugation during the synthesis of the CdPbTe alloyed QDs:

First, a NaHTe solution was freshly prepared by dissolving Te powder (1 mmol) with $NaBH_4$ (4 mmol) in 2 mL degassed water in a thick walled glass tube. A needle was inserted into the capped tube to release the pressure of the evolved gas, and the solution was stirred for a few hours at 4 °C. Meanwhile the precursor solution was prepared by mixing $Cd(NO_3)_2 \cdot 4H_2O$ (1.75 mM), $Pb(NO_3)_2$ (0.75 mM) and GSH or MPA (4 mM). Solid DNA (G*G*G*G*G*T_{20}, * represents the phosphothioate linkage) was added to this mixture to get a final concentration of the DNA 0.1 mM. The pH was adjusted to 9 by adding 1 M NaOH drop-wises. Calculated amount of freshly prepared NaHTe solution was micro injected into N_2 saturated precursor solution so that the concentration of NaHTe in the reaction mixture was 0.5 mM. The color of the solution immediately changed from colorless to brownish after the injection. The reaction mixture was incubated at 90°C for 30 minutes and followed by quenching the reaction through quickly cooling down to 0°C in an ice-bath. The resulted QDs particles were purified to remove the excess DNA and the unreacted small ions and molecules by washing with nanopure water 3 times using an Amicon centrifugal filter (30kD MWCO).

Preparation of Triangular DNA Origami:

Triangular DNA Origami was synthesized following the typical procedure described by Rothemund in 2006 (Nature, 2006). The long single stranded M13 scaffold and each of the short staple strands without purification were mixed at molar ratio of 1:5. The binding sites on the origami for each of the QD were generated by modifying 3 adjacent staple stands (arranged in a triangle) at selective positions on the origami by adding 20A nucleotide at the 5' ends, which act as the capturing strands. The ratio between the M13 DNA and the modified staple strands (purified) was 1:20 in the mixture. The assembly was done in 1×TAE-Mg^{2+} buffer (Tris base 40 mM; Acetic Acid 20 mM; EDTA 2 mM; Magnesium Acetate 12.5 mM; pH 8) by cooling down

slowly from 90°C to 4°C. In order to get rid of the excess staple strands and the capture strands, the assembled origami was washed 3 times with 1×TAE-Mg^{2+} buffer in an Amicon filter (100kD MWCO). The purified origami was then mixed with the purified QDs and the mixture was cooled down from 37°C to room temperature over 24 hours.

Structure and Optical Characterization of the QDs:

Steady state fluorescence spectra were collected with a Horiba Nanolog spectrophotometer (Horiba Jovin Yvon) equipped with 450W Xenon lamp and Liquid N_2 cooled DSS-IGA020L InGaAs detector. High-resolution electron microscopy (HRTEM) and energy dispersive X-ray spectroscopy (EDS) were done in a JEOL JEM 2010F electron microscope operating at 200 kV. Carbon coated copper grid (400 mesh, Ted Pella) was used to deposit the sample, which was then washed, stained and air dried before imaging. Powder X-ray diffraction measurements were performed in a PANalytical X'pert Pro Materials research X-ray diffractometer with Cu Kα radiation (λ= 1.5418 Å). Atomic force microscopy (AFM) was performed using a Veeco 8 AFM in tapping in air mode. ICP-MS was performed on a Thermo X-series with Q-ICP-MS with CCT (Collision Cell Technology) instrument.

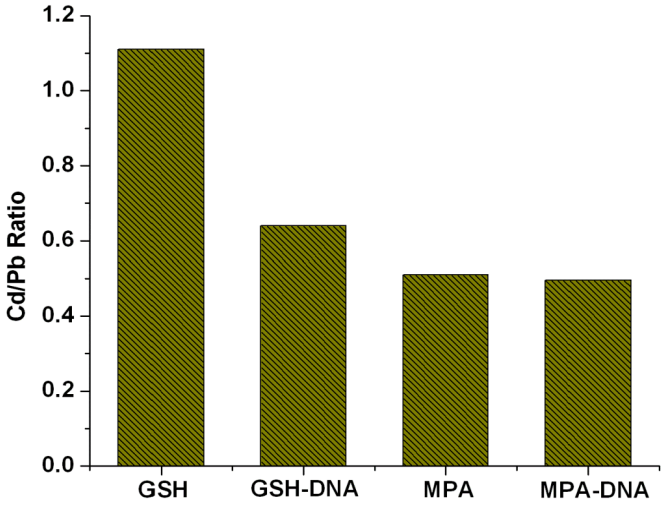

Figure S1. The atomic ratio of Cd/Pb in the QDs synthesized using different capping ligands measured by ICP-MS.

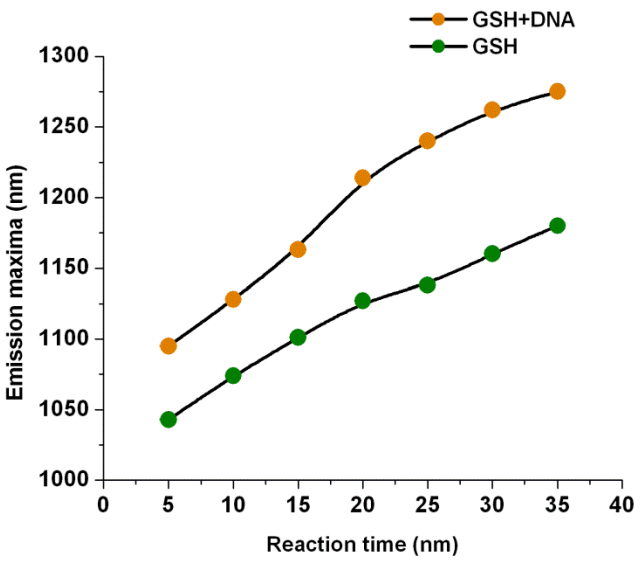

Figure S2. Comparison of the red shift of the QD photoluminescence peak positions monitored during the formation process of the GSH capped QDs in the presence (orange) and absence of DNA (green). The continuous red shift of the QDs obtained may reflect the growing of the size of the nanocrystals. In the presence of both GSH and DNA, the

QDs formed at short time already showed a red shift compared to that in the presence of GSH alone. This may reflect a higher incorporation of Pb ions in the nanocrystals.

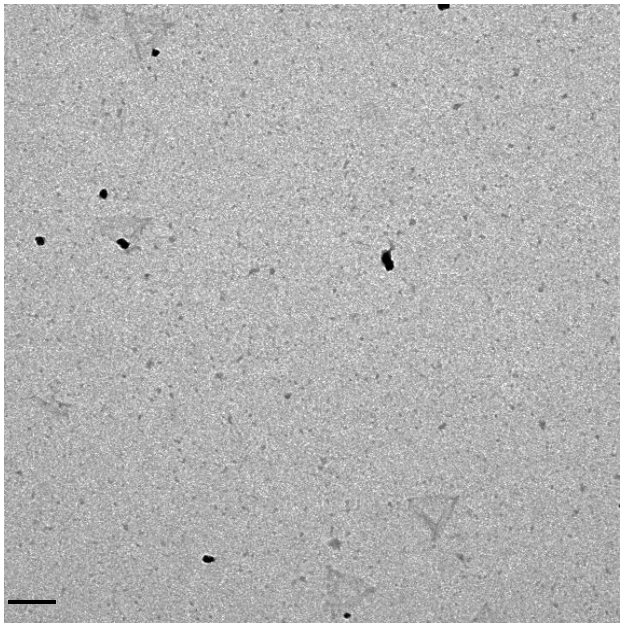

Figure S3. Additional zoom out TEM images of CdPbTe capped with GSH/DNA on DNA origami. (Scale bar 100nm) The DNA origami was quite diluted in this sample.

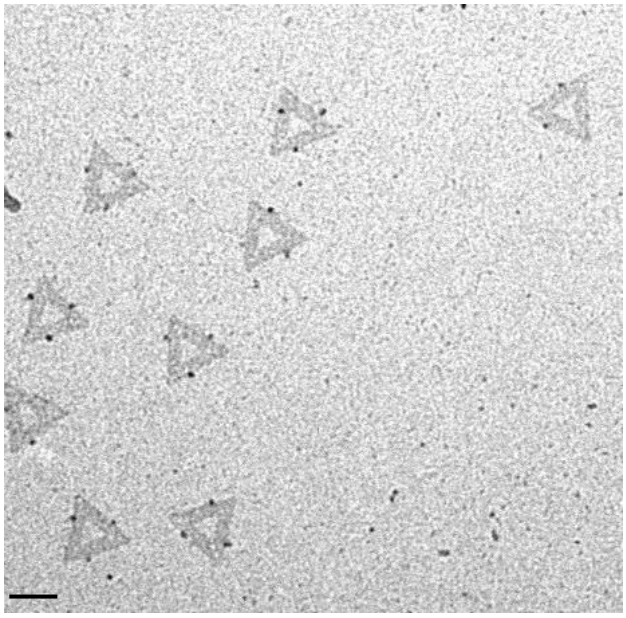

Figure S 4: Additional zoom out TEM images of CdPbTe capped with MPA/DNA on DNA origami. (Scale bar 100nm)

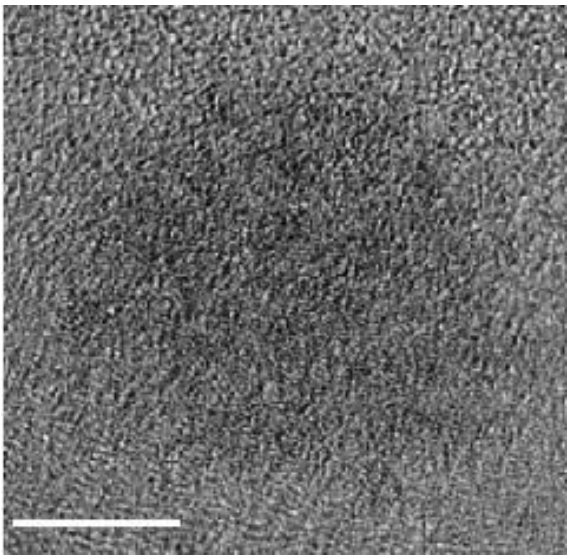

Figure S 5: Zoom in TEM image of $Cd_xPb_{1-x}Te$ QDs encapsulated with GSH and ps-DNA. Scale bar 5 nm. Multiple 1-2 nm crystal domains can be identified inside the ~ 10 nm diameter particle.

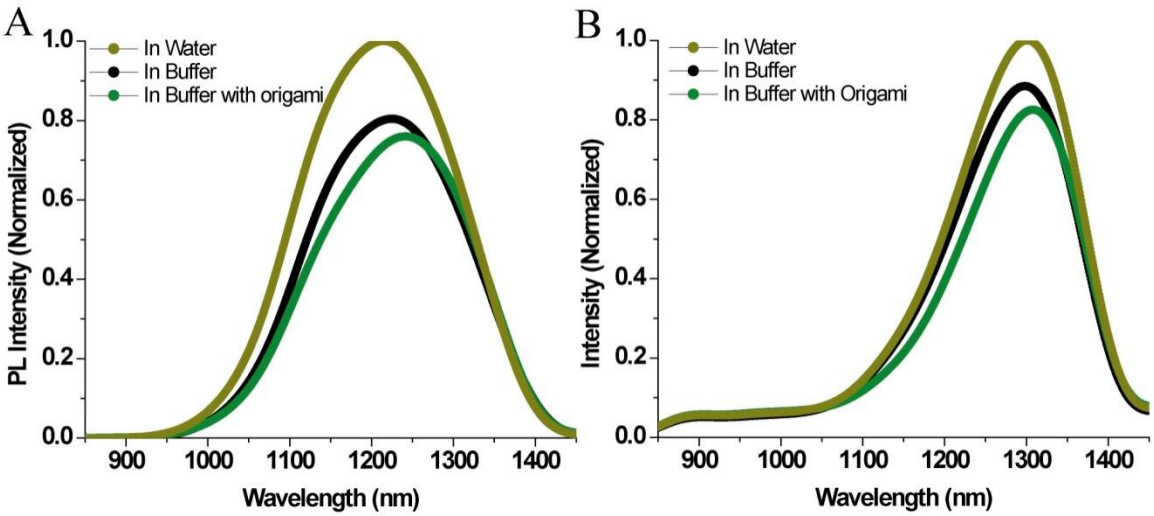

Figure S 6: PL emission spectra of $Cd_xPb_{1-x}Te$ QDs capped with GSH (A) and MPA (B) incubated in 1×TAE-Mg^{2+} buffer (12.5mM $MgCl_2$). In both cases quenching of fluorescence is observed along with slight red shift in the emaission maxima.

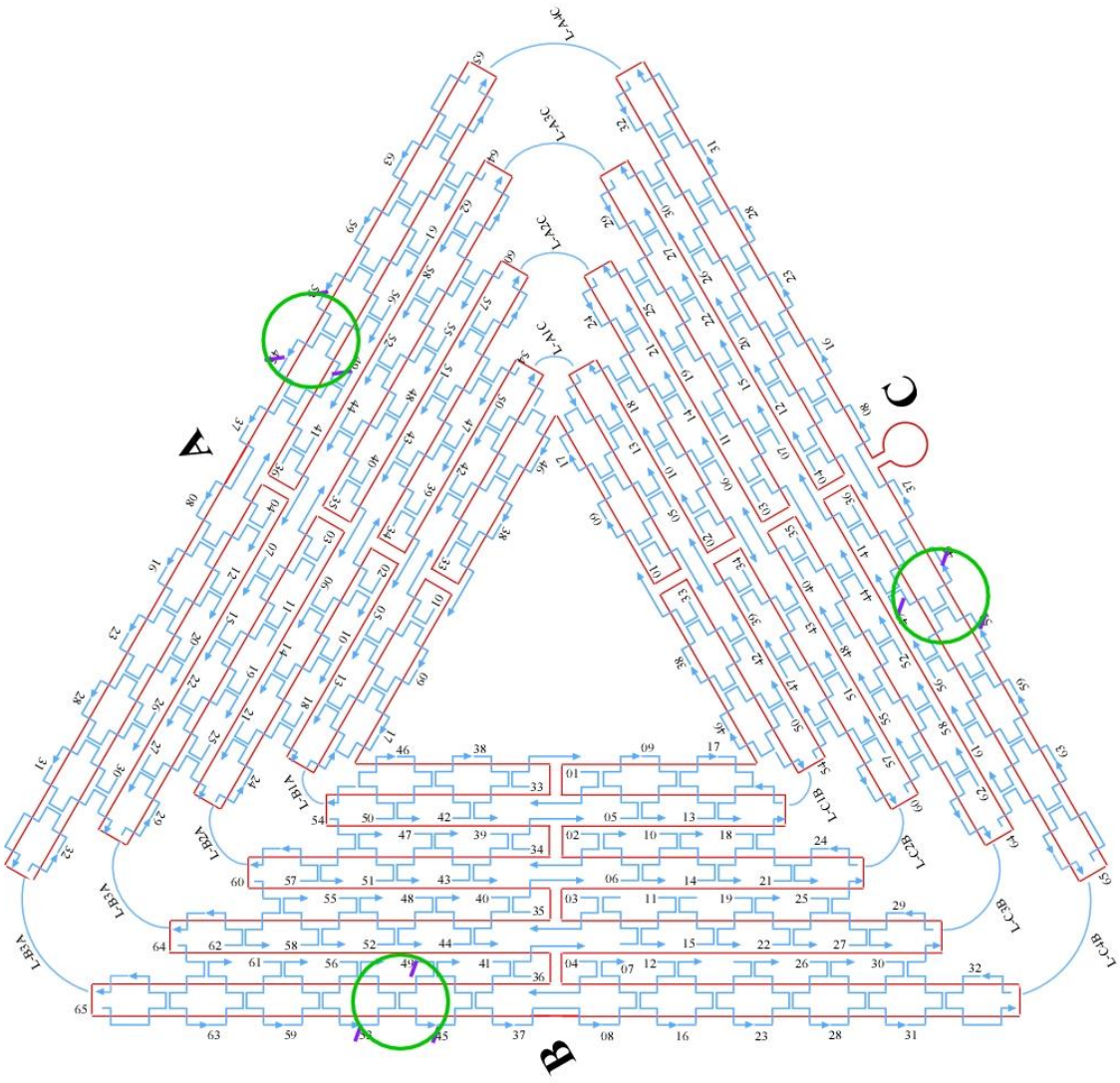

Figure S 7: Schematic design of the triangular DNA origami. The green circles represent the binding sites for the QDs. The short purple lines mark the extension of the A20.

Sequences of the capture strands:

B49-capture:

AAAAAAAAAAAAAAAAAAAATTTTTATCATCGTTGAAAGAGGACAGATGGAAGAAAAATCTACG

B45-capture:

AAAAAAAAAAAAAAAAAAAATTTTTTAATAAAACGAACTAACCGAACTGACCAACTCCTGATAA

B53-capture:

AAAAAAAAAAAAAAAAAAAATTTTACCAGTCAGGACGTTGGAACGGTGTACAGACCGAAACAAA

A49-capture:

AAAAAAAAAAAAAAAAAAAATTTTAGCATGTATTTCATCGTAGGAATCAAACGATTTTTTGTTT

A45-capture:

AAAAAAAAAAAAAAAAAAAATTTTAACGTCAAAAATGAAAAGCAAGCCGTTTTTATGAAACCAA

A53-capture:

AAAAAAAAAAAAAAAAAAAATTTTTCCCAATCCAAATAAGATTACCGCGCCCAATAAATAATAT

C49-capture:

AAAAAAAAAAAAAAAAAAAATTTTGTTTGCGTCACGCTGGTTTGCCCCAAGGGAGCCCCCGATT

C45-capture:

AAAAAAAAAAAAAAAAAAAATTTTTAGAGCTTGACGGGGAGTTGCAGCAAGCGGTCATTGGGCG

C53-capture:

AAAAAAAAAAAAAAAAAAAATTTTCTAAATCGGAACCCTAAGCAGGCGAAAATCCTTCGGCCAA

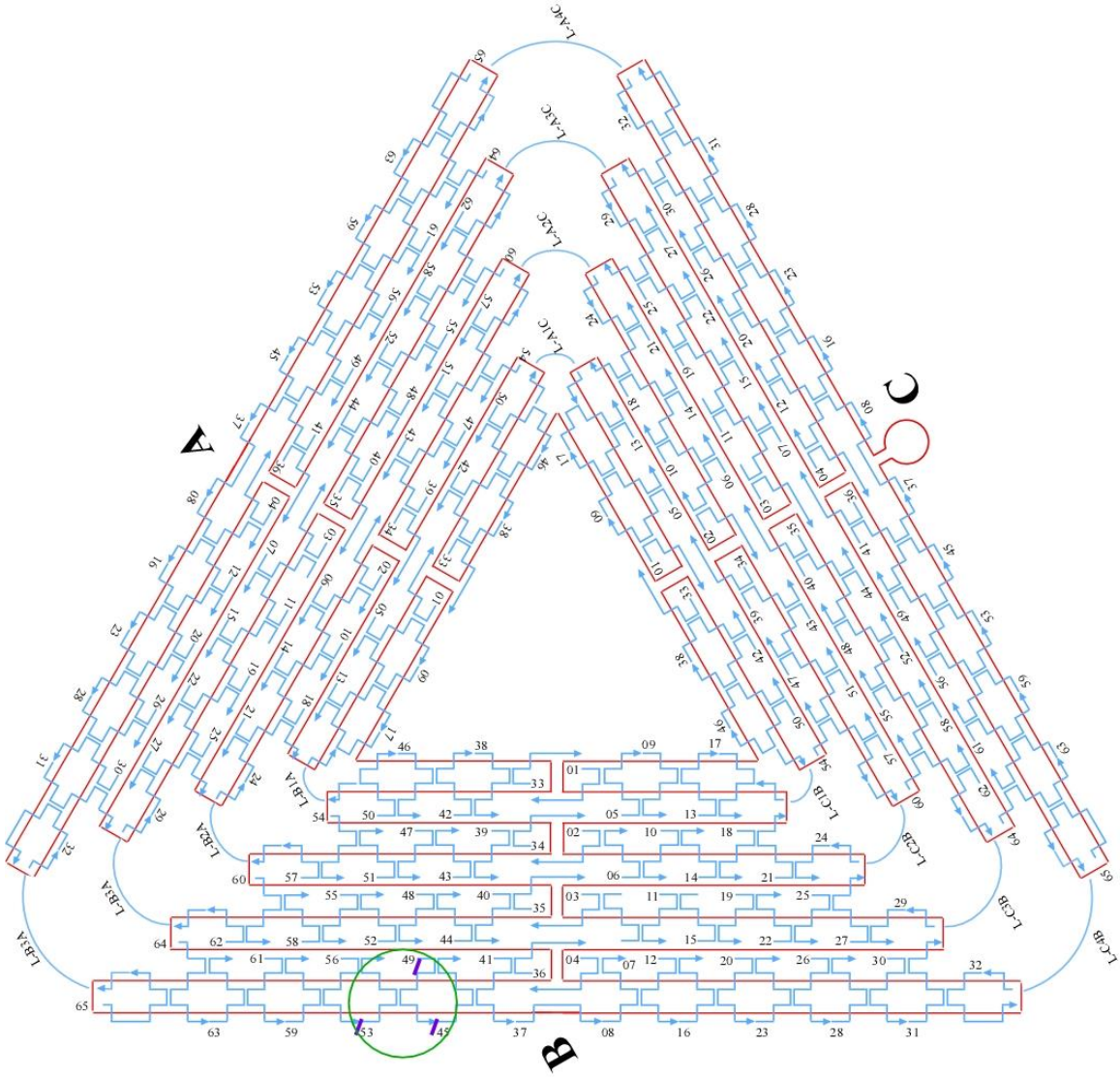

Figure S 7: Schematic design of the triangular DNA origami. The green circles represent the binding sites for the QDs. The short purple lines mark the extension of the A20.

Sequences of the capture strands:

B49-capture:

AAAAAAAAAAAAAAAAAAAATTTTTATCATCGTTGAAAGAGGACAGATGGAAGAAAAATCTACG

B45-capture:

AAAAAAAAAAAAAAAAAAAATTTTTTAATAAAACGAACTAACCGAACTGAC
CAACTCC
B53-capture:

AAAAAAAAAAAAAAAAAAAATTTTACCAGTCAGGACGTTGGAACGGTGTAC

AGACCGAAACAAA

References

1. Deng, Z.T. et al. Aqueous Synthesis of Zinc Blende CdTe/CdS Magic-Core/Thick-Shell Tetrahedral-Shaped Nanocrystals with Emission Tunable to Near-Infrared. *Journal of the American Chemical Society* **132**, 5592-5593 (2010).

2. Yu, W.W., Qu, L.H., Guo, W.Z. & Peng, X.G. Experimental determination of the extinction coefficient of CdTe, CdSe, and CdS nanocrystals. *Chem. Mater.* **15**, 2854-2860 (2003).

3. Smith, A.M., Mohs, A.M. & Nie, S. Tuning the optical and electronic properties of colloidal nanocrystals by lattice strain. *Nature Nanotechnol.* **4**, 56-63 (2009).

4. http://www.horiba.com/us/en/scientific/products/fluorescence-spectroscopy/application-notes/quantum-yields/

5. Deng, Z., Cao, L., Tang, F. & Zou, B. A new route to zinc-blende CdSe nanocrystals: Mechanism and synthesis. *Journal of Physical Chemistry B* **109**, 16671-16675 (2005).

6. Deng, Z.T. et al. Water-Based Route to Ligand-Selective Synthesis of ZnSe and Cd-Doped ZnSe Quantum Dots with Tunable Ultraviolet A to Blue Photoluminescence. *Langmuir* **25**, 434-442 (2009).

7. Deng, Z.T., Yan, H. & Liu, Y. Band Gap Engineering of Quaternary-Alloyed ZnCdSSe Quantum Dots via a Facile Phosphine-Free Colloidal Method. *Journal of the American Chemical Society* **131**, 17744-17745 (2009).

8 Rothemund, P.W.K. Folding DNA to create nanoscale shapes and patterns. *Nature* **440**, 297-302 (2006).

APPENDIX C

SUPPLEMENTAL INFORMATION FOR CHAPTER 3

Supplementary figures:

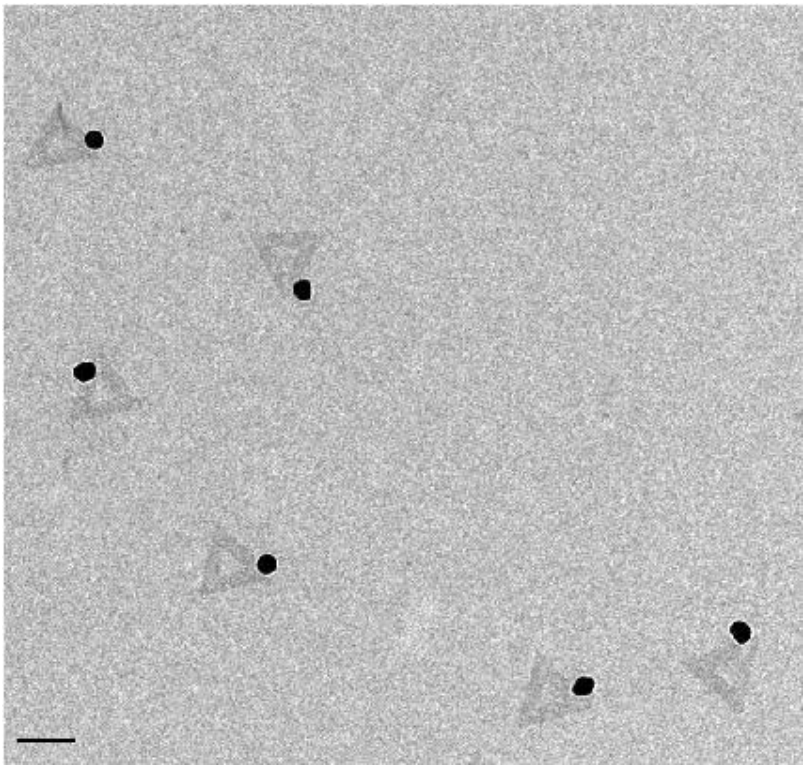

Figure S1: TEM image of the purified DNA origami linked with one 30 nm AuNP. Scale bar 100 nm.

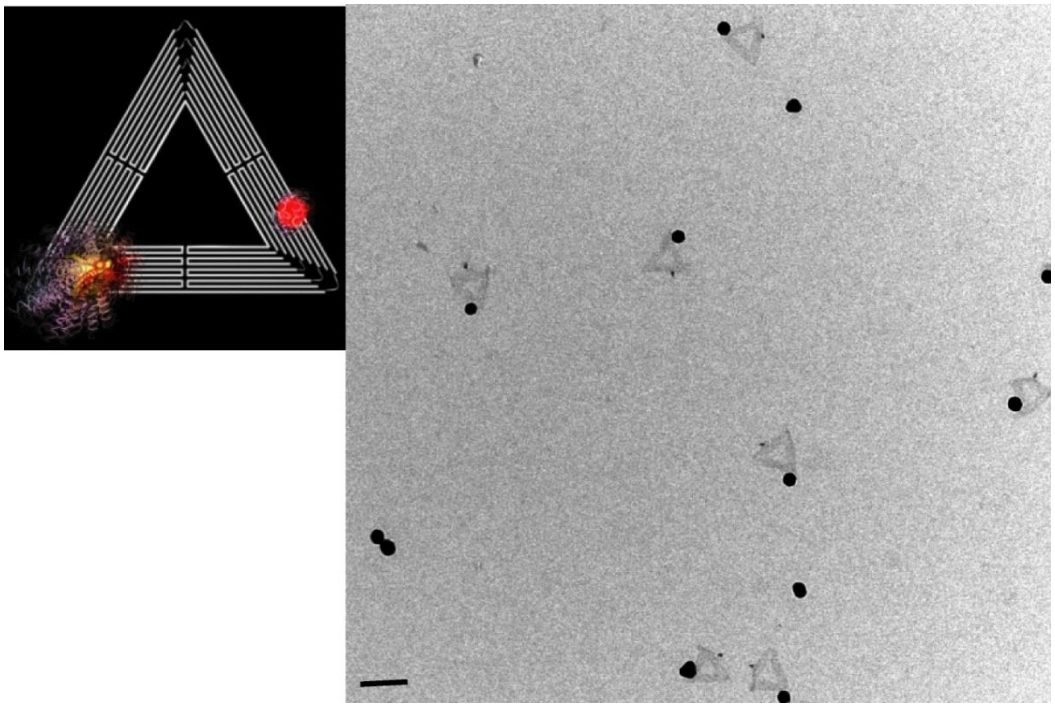

Figure S2: TEM image of the construct 1. Scale bar 100 nm. The average inter-particle distance is ~ 70nm.

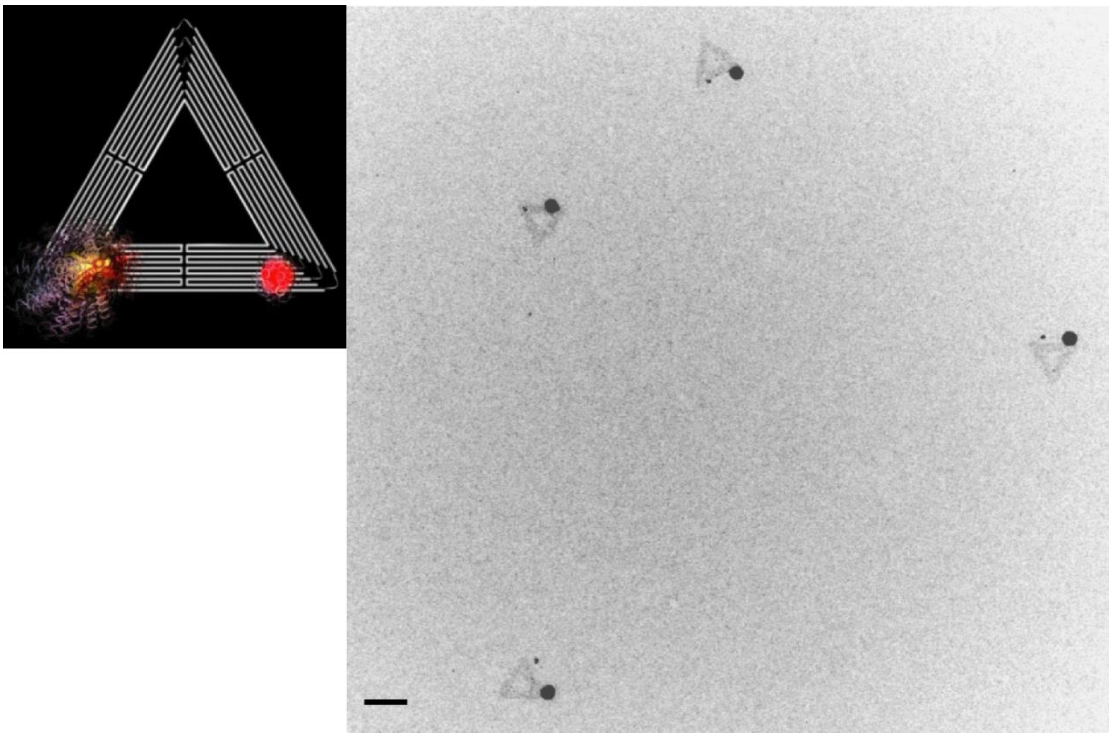

Figure S3: TEM image of the construct (ii). Scale bar 100 nm. The average inter-particle distance is ~ 55 nm.

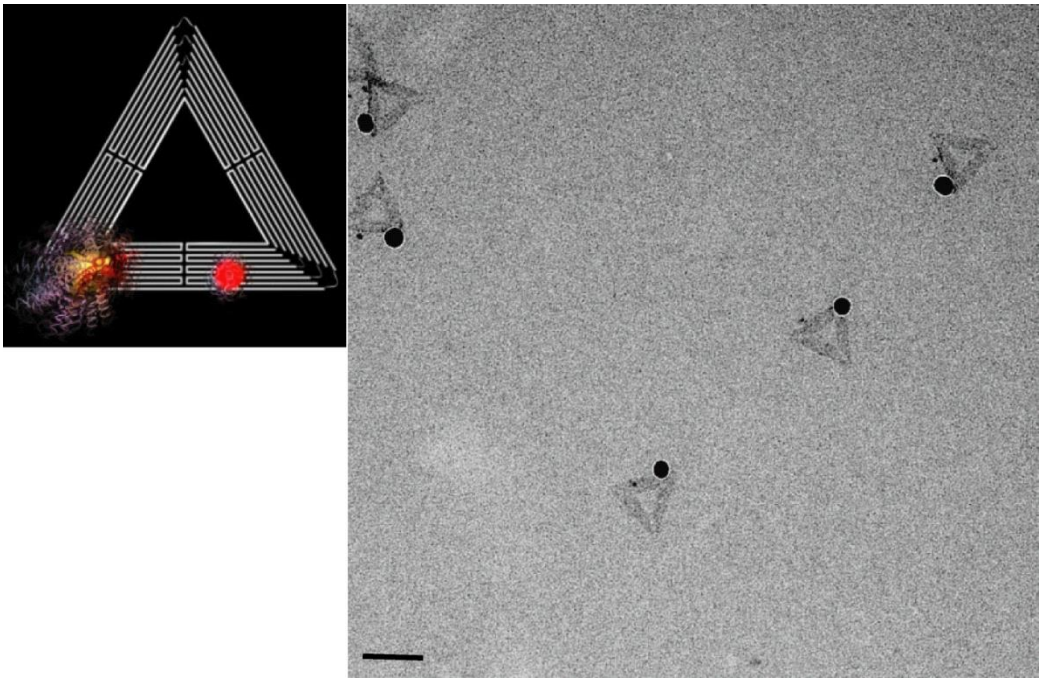

Figure S4: TEM image of the construct (iii). Scale bar 100 nm. The average inter-particle distance is ~ 40 nm.

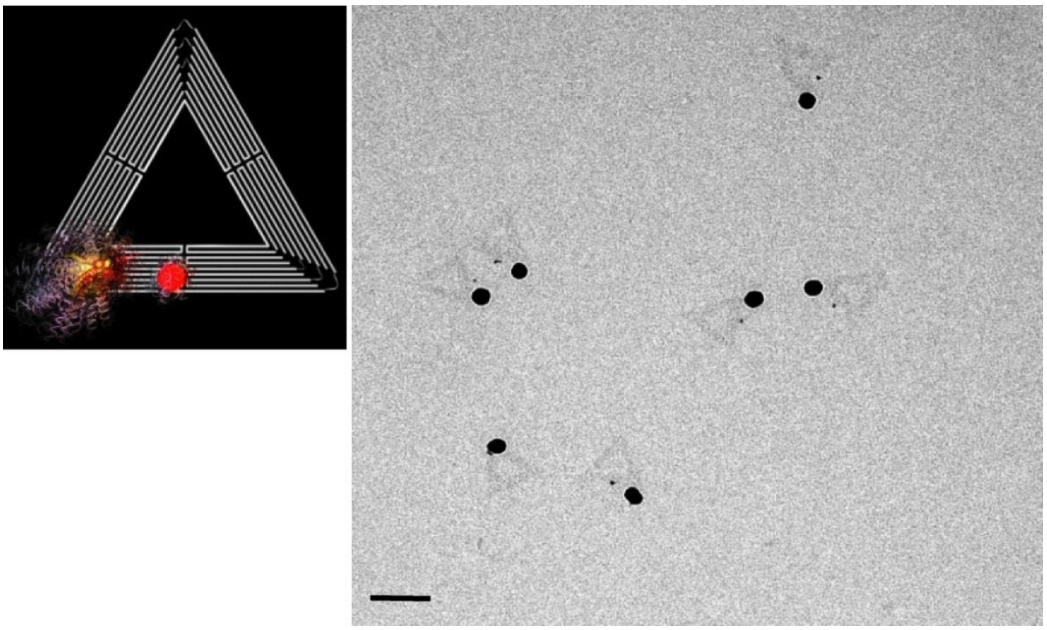

Figure S5: TEM image of the construct (iv). Scale bar 100 nm. The average inter-particle distance is ~ 30 nm.

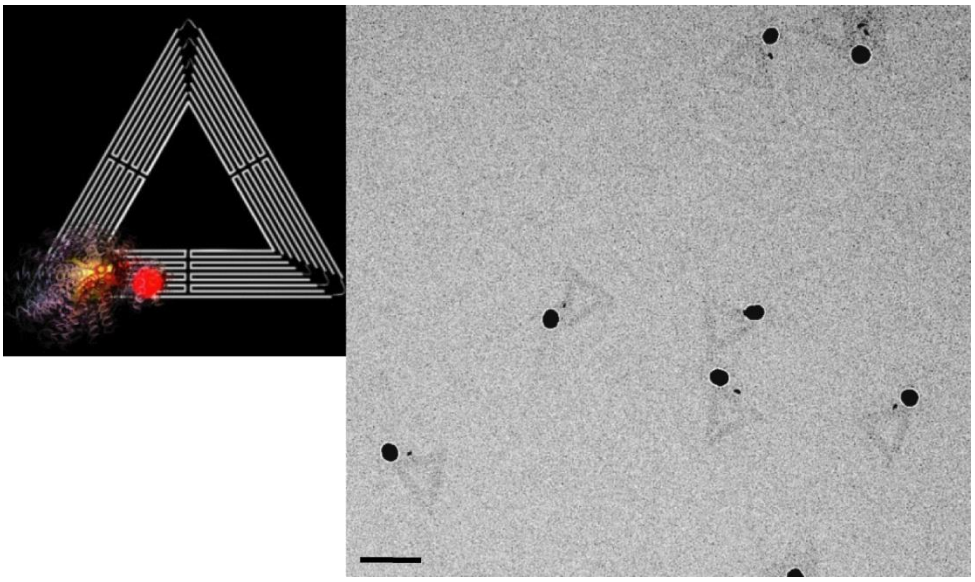

Figure S6: TEM image of the construct (v). Scale bar 100 nm. The average inter-particle distance is ~ 15 nm.

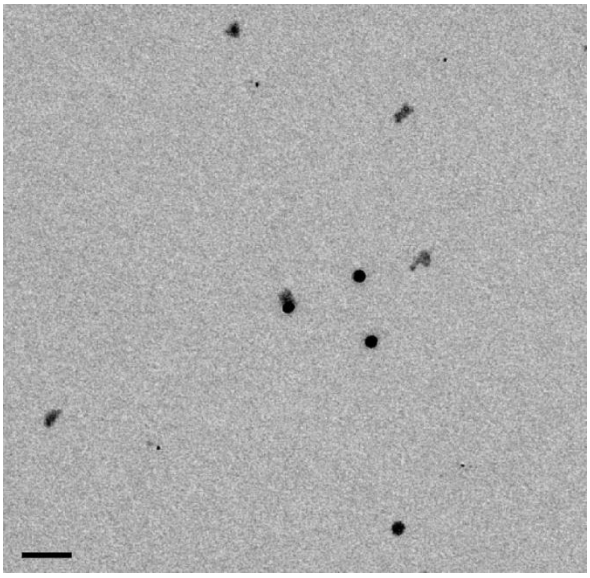

Figure S7: TEM image of the control sample. Origami is destroyed and the unbound AuNPs and QDs are seen in the background.

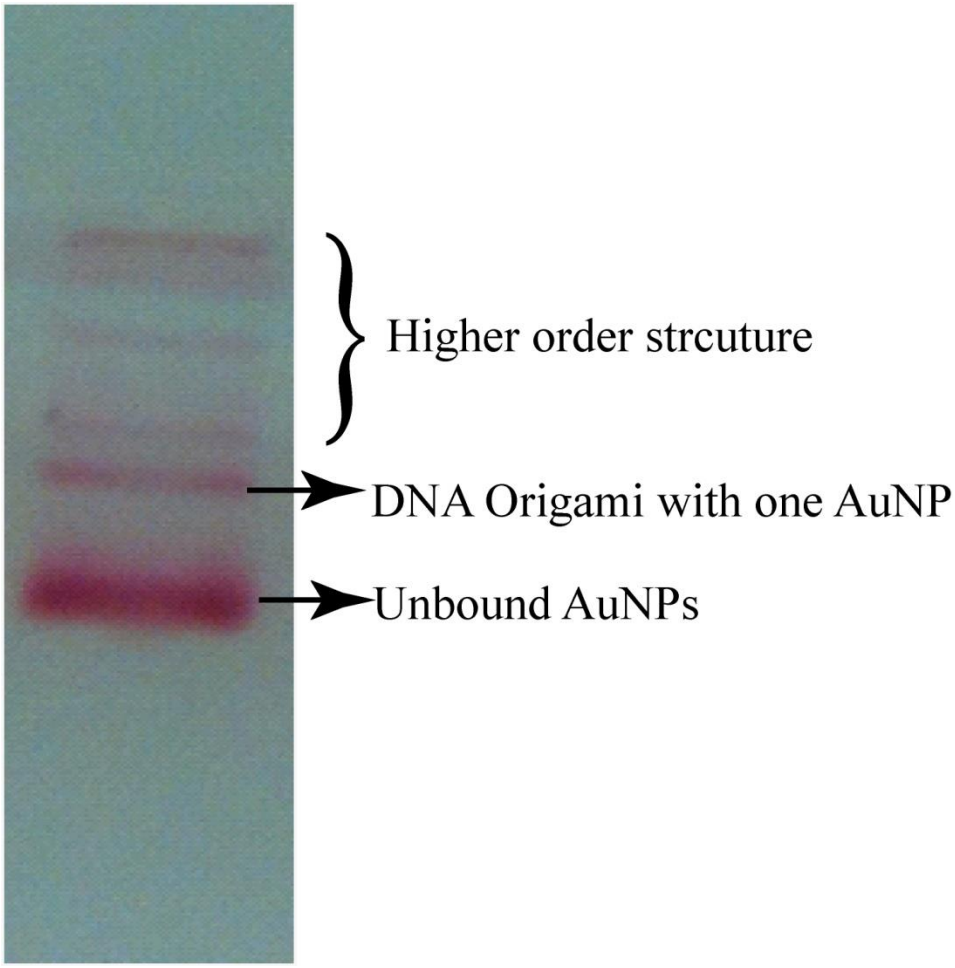

Figure S8: Agarose gel electrophoresis purification of the DNA origami bearing one gold nanoparticle. (1% agarose gel, in 0.5X TAE-Mg buffer, at 10V/cm for 1.5 hours)

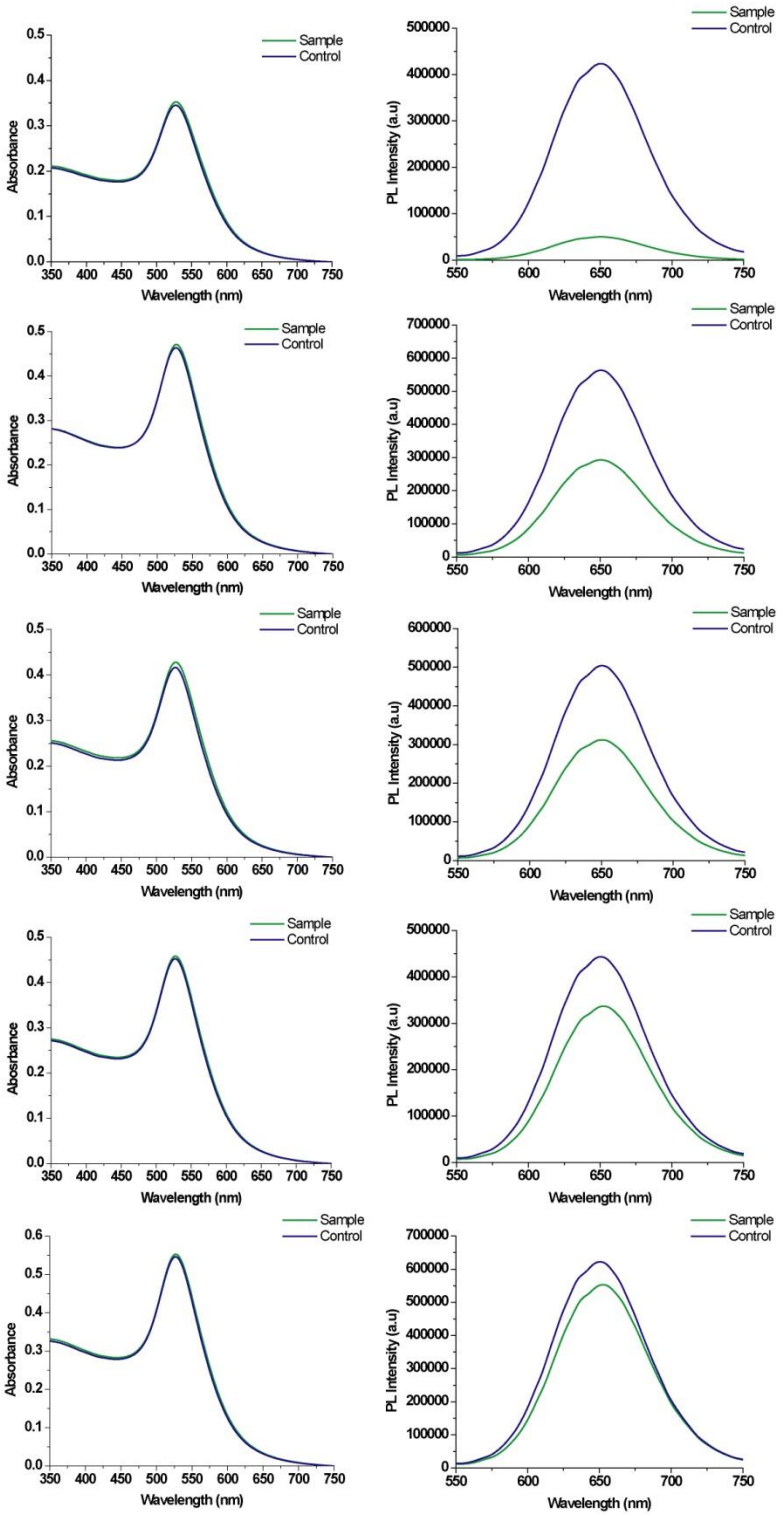

Figure S9: First set of UV-Vis and corresponding PL emission spectra obtained from steady state measurement. Constructs (v) to (i) are plotted from top to bottom.

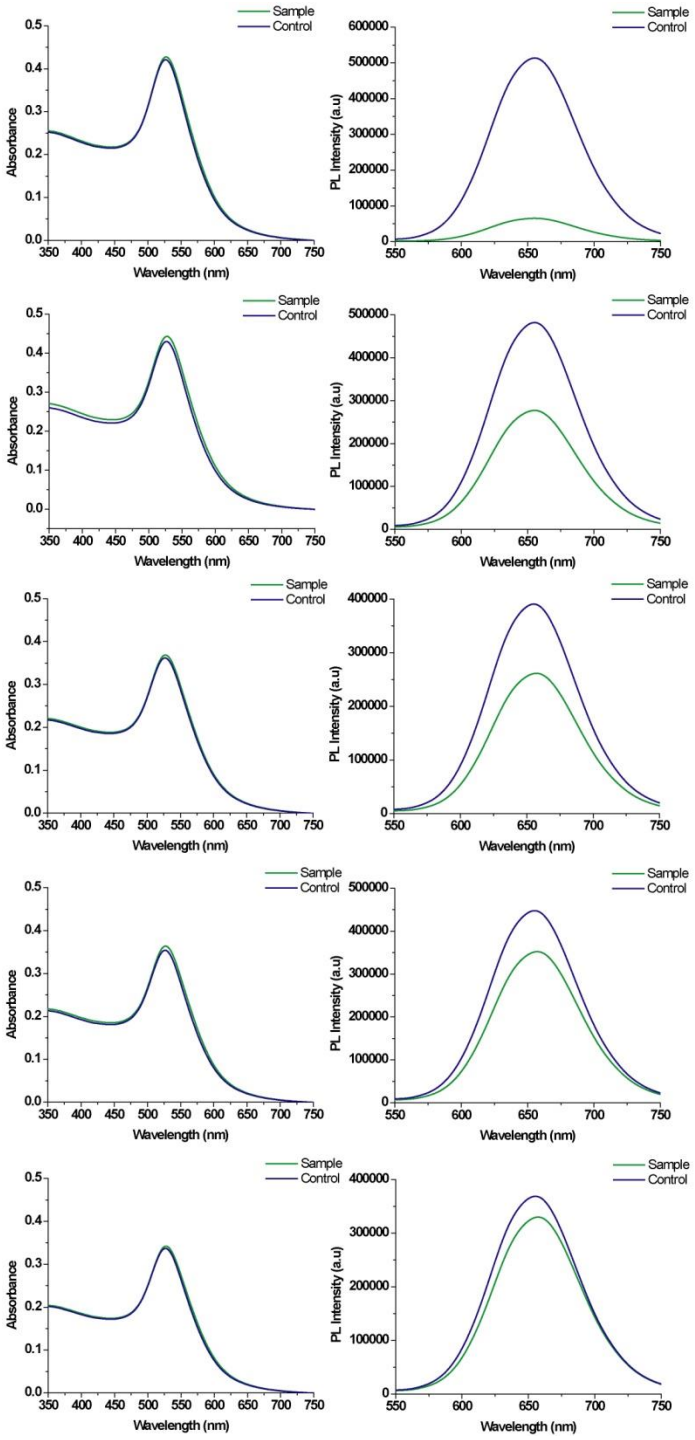

Figure S10: Second set of UV-Vis and corresponding PL emission spectra obtained from steady state measurement. Constructs (v) to (i) are plotted from top to bottom.

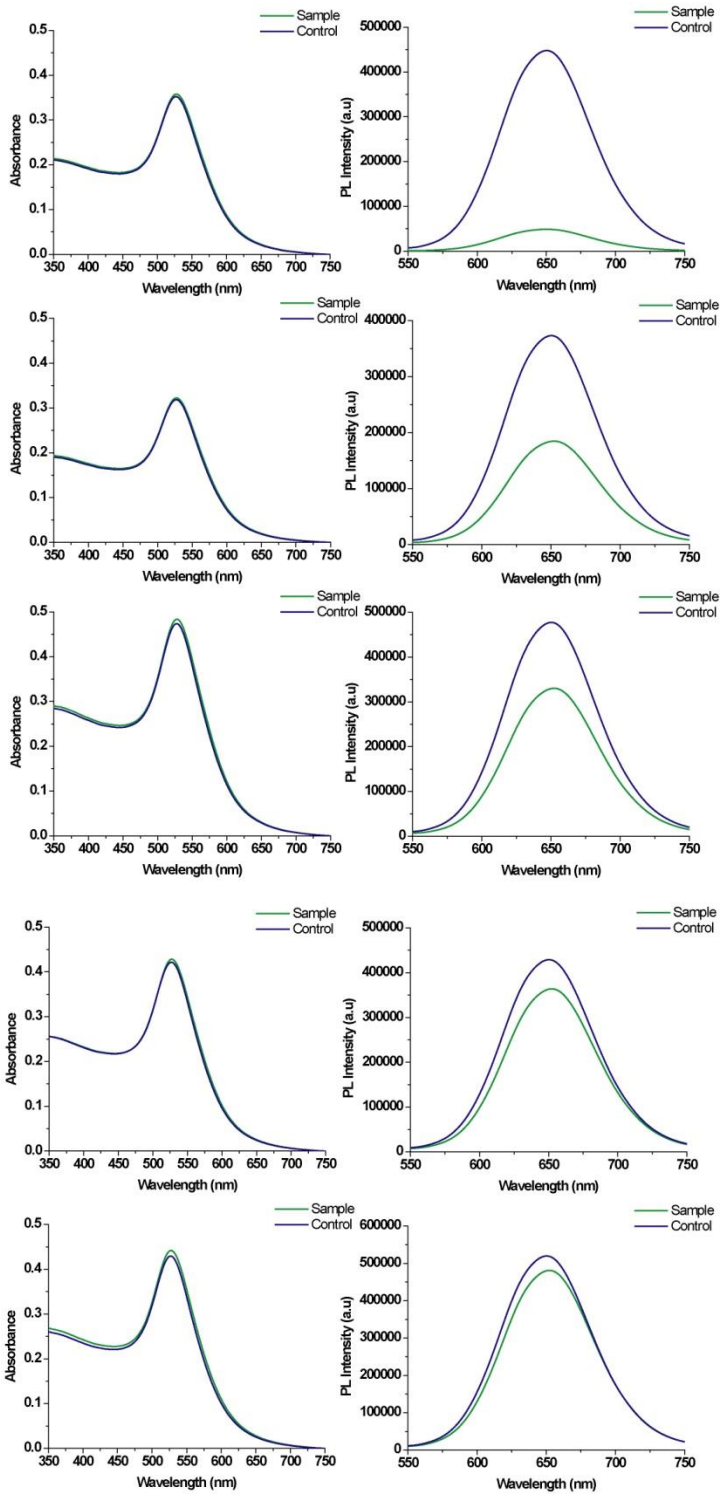

Figure S11: Third set of UV-Vis and corresponding PL emission spectra obtained from steady state measurement. Constructs (v) to (i) are plotted from top to bottom.